Modular information processing in the cerebellar cortex

Ludovic Spaeth

UNIVERSITÉ DE STRASBOURG

ÉCOLE DOCTORALE DES SCIENCES DE LA VIE ET DE LA SANTÉ

INCI CNRS UPR 3212

THÈSE présentée par :

Ludovic SPAETH

soutenue le : **27 septembre 2019**

pour obtenir le grade de : **Docteur de l'université de Strasbourg**

Discipline/ Spécialité : Neurosciences

Traitement modulaire de l'information dans le cortex cérébelleux

Vers la causalité entre l'organisation synaptique fonctionnelle et le comportement moteur

THÈSE dirigée par :

M. ISOPE Philippe	Directeur de recherche, université de Strasbourg

RAPPORTEURS :

Mme CAREY Megan	Directeur de recherche, Champalimaud Foundation
M. LENA Clément	Directeur de recherche, école normale supérieure

AUTRES MEMBRES DU JURY :

M. SCHONEWILLE Martijn	Directeur de recherche, Erasmus University Medical Center
M. GOUTAGNY Romain	Chargé de recherche - HdR, université de Strasbourg

Outline

Acknowledgments / Remerciements

First and foremost, I would like to thank the jury members: **Dr. Megan Carey**, **Dr. Clément Léna**, **Dr. Martijn Schonewille** and **Dr. Romain Goutagny**. They kindly accepted to sacrifice a bit of their precious time to evaluate my work, therefore I am really grateful to them.

I would like to thank **Javier Medina, Megan Carey, Daniela Popa** and **Roy Sillitoe** who had the titanesque task of organizing the last Cerebellum GRC. It was a real success, both on the scientific and the human side. The worldwide cerebellar community is full of amazing and brilliant people who gave me the will to continue my career in this field.

Afin de raconter une histoire intelligible, j'ai dû me creuser la tête pour trouver un plan et organiser mes idées dans la suite ce manuscrit. Du coup, et pour cette partie seulement, je vais prendre le luxe de remercier tout le monde dans un ordre auquel j'apporte peu d'importance. Toutes les personnes citées ci-dessous (et bien évidemment au-dessus aussi) ont eu, de près ou de loin, une influence que j'estime positive sur la réalisation de mon travail de thèse. Je vais probablement oublier de citer pas mal de monde, je m'en excuse avec une pirouette : il serait quelque peu incongru que les remerciements soient plus longs que le reste du manuscrit.

Merci au 3 cavaliers de l'apocalypse, les *sub-zeros* : Théo "*Michelangelo*" Rossi, Charlotte "*Carlota*" Bichara et *Frédérique Laurène-Francine* (Federica, de son vrai nom).
Théo[1], ne change surtout pas tu es sur la bonne voie, ne freine jamais ta curiosité et continue tes facéties. Si les deux autres te tapent sur le système, tu les em*** et tu rentres à ta maison à bord du *7-turdy-7* en claquant des doigts.
Charlotte, le monde est bien petit, mais si bien foutu tout de même. On pourrait en faire une histoire intéressante, genre les jumeaux maléfiques séparés dans leur jeunesse qui se retrouvent à l'âge adulte pour dominer le monde (avec l'accord de maman bien sûr). Sacré blockbuster en perspective.
Fede, thank you for… yourself. Just being yourself, in any situation. Atmosphere in the office turned to something better since you're there. You're funny, authentic and brilliant (even if you refuse to admit it). You'll get the lab keys (and my desk, obviously) after I'm gone.

Merci à ***Kévin***, le seul et l'unique véritable chevalier du métal et du patch clamp, parti trop tôt (à mon goût) découvrir les secrets mystiques du pays du soleil levant. Franchement mec, encore 1 an à respirer les effluves radioactifs du 2e étage et t'avais plus besoin de pipette pour patcher, passer ta main au-dessus de la tranche aurait suffi !

I would like to thank ***Francesca***, the former "*witch of the lab*", who teached me how to perform stereotaxic injections. No one knows how much I miss our patch clamp sessions and your insults toward the set up. I'm almost fluent in italian thanks to them ! You too were gone much too soon from the lab (or I came too late, same deal, but still sad).

Merci à ***Théo[2]***, mon jeune padawan qui a su compenser mon incompétence en tant que mentor par sa pertinence et ton talent. Tu mérites une pinte et ta place au conseil des Jedis.

Merci à ***Jean-Luc***, grâce à qui je suis incollable à la fois sur les cellules de Golgi ainsi que sur la vie des Rolling Stones. Les neurosciences et le rock font vraiment bon ménage.

Merci à ***Didier*** pour la question qui tue à chaque lab meeting. Je n'ai toujours pas digéré la victoire de Rennes en coupe de France, ainsi que la récente déconvenue des parisiens au Roazhon Park mais bon… le flegme breton a du bon tout de même.

Merci à ***Fred*** pour toutes ces blagues graveleuses, elles vont sacrément me manquer. J'en profite pour remercier ***Anne-Marie***, le rossignol du 2e, qui en compagnie de Fred a ramené la coupe du tournoi de pétanque à la maison. J'espère qu'elle y restera derrière les portes rouges pour longtemps.

Merci à ***Bernard*** pour le partage spontané de ses connaissances encyclopédiques (et ce sur à peu près tous les sujets possibles).

Merci à ***Antoine*** d'avoir initié ce fabuleux projet. Et merci pour SynaptiQs qui m'a épargné un temps précieux : j'ai pu analyser mes traces avant de réussir à dompter ce satané Python.

Mention spéciale aux ***membres de l'équipe Gasman/Vitale*** qui s'avèrent être de supers voisins de paliers. ***Steph***, tes mises sur le FC Metz ont trouées mon compte en banque, mais avec ***Marion²*** et ***Audrey*** on aura bien rigolé, et ça, et bien ça n'a pas de prix.

Merci à ***Nathalie***. Merci pour tes doigts de fées qui ont permis le succès de la manip cuff, merci pour ta bonne humeur si communicative et surtout merci pour ce sourire qui ne quitte jamais ton visage, il m'a plusieurs fois évité de passer une journée de merde.

Merci à ***Matthieu*** pour son génie, ses talents de pilote d'avion (qui auront presque réussi à me faire rendre mon petit déjeuner) ainsi que pour sa franche camaraderie et le partage de ses expériences culinaires pour le moins incongrues (ça se prononce *p-a-i-n-a-u-c-h-o-c-o-l-a-t*).

Si certains ont eu la chance de voir Mozart composer, j'ai eu le privilège de voir ***Sam Garcia*** coder. Merci à toi camarade, sans toi j'aurai eu du mal à tordre le cou de ce maudit serpent. Je vous ai dit qu'il était champion du monde de *spike sorting* ?

Un immense merci aux ***Mygales***. ***Pierre, Emeline, Tando, Fanny, Alex, Nono, Pierrick, Sarah, Marine, Sylvain*** et ***Baptou*** vous êtes de vrais rockstars. Vous avez le mérite d'avoir supporté mes obscénités et mes fausses notes sans broncher (le sol bécarre ça sonne jazz). Les répets, le Chariot, les concerts, les virées en Baptruck… je n'ai pas les mots, c'était fantastique et j'espère que ça continuera. J'ai déjà dit que les neurosciences et le rock ça faisait bon ménage ?
J'enchaîne en remerciant ***Noureddine et l'équipe du Chariot*** pour toutes ces pintes et ces barres de rire.

Je veux remercier le gang des Parisiens. Il y a d'abord les Drôles de Dames, ou plutôt trio infernal, composé d'***Aurélie***, ***Béré*** et ***Hind***. Je ne vais pas évoquer les détails du GDR à Stras, par manque de place et on sait jamais des fois que des enfants veuillent lire ce pavé. Il y'a aussi ***Thibaut***, ***Willou*** et ***Inès***. Tous ensemble ils ont cassé les barrières sociales qui séparent la capitale de la province.

Merci à l'ensemble du collectif ***Doctoneuro***. Je n'ai jamais été fervent défenseur du monde associatif, et ces gens-là ont réussi à me faire changer d'avis. Petite aparté pour ***Max***, aussi appelé le Sheitan, qui au-delà d'un éminent président fût également l'une des plus belles rencontres que j'ai pu faire durant ma thèse.

Gros big up à ***TB***, le renard des surfaces, dont j'ai pu partager les facéties depuis nos débuts en licence… t'avais pas de poils au menton et j'avais 20 kg de moins, c'est dire à quel point ça remonte. On n'a pas vu tel duo depuis Wenger et Arsenal (les Invincibles !!!). L'équipe s'est sérieusement étoffée après le recrutement de ***LPV***, venu pour 100 balles et un mars de l'AS Canton Vert, signant au passage le transfert le plus cher du Grand Est. A l'instar de Paris, vous êtes magiques, merci les fratés.

Merci à ***Géraldine*** pour son tact assumé, une véritable bouffée d'air frais presque quotidienne. Merci à ***Damien*** pour ses mots magiques, comme quoi l'Alsace c'est comme la Bretagne, il manque juste l'océan.

Merci à ***Ben***, aussi appelé Léonard, pour son esprit brillant, son flegme légendaire et sa capacité à enchaîner les Ricard comme si chaque verre était le dernier. J'en profite pour remercier le général ***Shani Folschweiller***, dont le passage au labo fût (trop) bref mais tellement agréable. Les allemands ont recruté une vraie pépite.

Il y a deux ***Aline*** que j'aimerais remercier. La première partage notre bureau, et s'assure quotidiennement de la survie de l'alsacien entre ces murs (on est en minorité quel comble…). La deuxième m'a patiemment supporté pendant mes années Master, et m'a poussé à découvrir le monde de la recherche en allant directement sur le terrain.

Merci à la Dream Team, formée dans les années Master : ***David, Nico, Etienne*** et ***Ivan***. Tous plus brillants et attachants les uns que les autres, vous avez su donner une saveur particulière à toutes ces nuits blanches et vous avez rendu les bancs de la fac beaucoup plus agréables.

Un grand merci à ***Elaine*** (alias Satan), qui veille sans relâche sur les enfers et qui dans son temps libre trouve toujours le moyen de mettre mes nerfs à rude épreuve, ça me fait me sentir humain. Un exercice dans lequel ***Léa*** (alias Lucifer) excelle également.

Merci à ***Edouard*** (alias Doudou) et ***Bruno***, les deux zootechs les plus cools de l'univers, les poses clopes avec vous c'est un autre délire. Je veux remercier ***Noémie*** aussi, qui a su traiter mes souris au mieux (elles me l'ont confessé elles-mêmes). Merci également à ***Dominique*** et ***Sophie***, responsables du Chronobiotron, qui se démènent au quotidien pour qu'on puisse réaliser nos manips.

Je tiens à remercier ceux qui étaient présents avant la thèse : ***Thibaut***, ***Boris***, ***Val***, ***Gauthier***, ***Xavier*** et ***Jerry***. Je suis comblé de savoir qu'ils sont toujours là aujourd'hui. Les copains d'abord, viennent ensuite leurs compagnes : ***Marion***, ***Anne***, ***Morgane***, ***Claire*** et ***Delphine***. Parce que oui, il y a heureusement une vie en dehors du labo (enfin ça dépend des jours), et j'ai la chance d'avoir des copains formidables qui entretiennent ma santé mentale au détriment de mes fonctions hépatiques. Quoique l'avenir me réserve, je sais que ceux-là ne seront jamais bien loin.

Merci à ***mes parents***. J'ai hérité de l'abnégation et de la détermination de mon père ainsi que de la curiosité et du grain de folie de ma mère, des atouts indispensables pour réussir dans ce monde fou qu'est la recherche (on croirait presque le titre d'un ouvrage de Marcel Pagnol). Merci à ma sœur, ***Léa*** qui prend un malin plaisir à me rendre euphorique pour mieux me taper sur les nerfs la seconde d'après : un ascenseur émotionnel dont je ne suis pas près de me lasser. Merci à ma grand-mère, ***Marlène***, chez qui je vais allègrement m'échapper pour oublier la pression du quotidien. Enfin, merci à ma (belle) famille, ***Nathalie***, ***Pascal*** et ***Florian*** qui supportent mon exubérance assumée depuis bientôt 10 ans.
J'ai dit plus haut que j'accordais peu d'importance à l'ordre : j'ai menti. Les deux personnes ci-dessous sont au centre de mes attentions et cristallisent ma gratitude (mais vu qu'ils n'aiment pas être sur le devant la scène, seuls les plus courageux lecteurs pourront apprécier leur rôle, ce qui j'imagine, suffira à pleinement satisfaire les doléances des deux intéressés).

Merci à ***Philippe***, capitaine de cette formidable aventure. Merci pour ta curiosité, presque enfantine et tellement communicative, ton optimisme sans faille et ta pédagogie à toute épreuve. Je pense pouvoir compter sur une main seulement les fois où je t'ai vu perdre ton calme, et je n'ai pas assez de doigts ni d'orteils pour compter les fois où tu as su raviver ma confiance. Tu m'as envoyé à 2 Gordons, tu m'as donné ton temps, ta patience, et surtout une envie presque permanente de me surpasser, au travers de ton humilité et de ta curiosité. Deux valeurs qui te résument à elle seules, et qui, selon moi, me seront indispensables pour réussir dans la science mais aussi dans ma vie personnelle.

Les Stones ont Angie, les Doors ont Gloria, Clapton a Layla, et moi j'ai la chance d'avoir ***Marjorie***. Celle qui a autant (voire même plus ?) flippé que moi à l'approche de l'échéance. Merci pour absolument tout. Mon cerveau a souvent été ailleurs, mais je pense (j'espère) que tu sais que mon coeur n'était jamais très loin. Désolé pour tous les coups de gueules, les sautes d'humeurs, ces nuits blanches et ces week ends passés au labo, les oublis répétés, les tirades à la Sheldon Cooper, la liste est encore longue… Quoiqu'il en soit, merci pour ton empathie et ton amour inconditionnel qui m'ont permis d'aller au bout de cette aventure et qui, j'en suis convaincu, me seront indispensables pour aller plus loin encore.

List of Figures

List of abbreviations

Am : Medial A cerebellar zone
AMPA : alpha-amino-3-hydroxy-5-methyl-4-isoxazolepropionic
AI : Lateral cerebellar A zone
CF : Climbing Fiber
cMAO : caudal nucleus of the Medial Accessory Olive
CoN : Commissural Neurons
CPG : Central Pattern Generators
DAO : Dorsal Accessory Olive
DSCT : Dorsal Spinocerebellar Tract
EAAT4 : Excitatory Amino Acide Transporter type 4
GABA : gamma-aminobutyric acid
GC : Granule cell
GC-PC : Granule cell to Purkinje cell
KS : Kolmogorov-Smirnov
LRN : Lateral Reticular Nucleus
LTP : Long Term Potentiation
LVN : Lateral Vestibular Nucleus
M1 : Primary motor cortex
MAD : Median Absolute Deviation
MAO : Medial Accessory Olive
MF : Mossy Fiber
mGluR1 : metabotropic Glutamate Receptor type 1
MLI : Molecular Layer Interneurons
MLR : Mesencephalic Locomotor Region
PC : Purkinje Cell
PF : Parallel Fiber
PF-PC : Parallel Fiber to Purkinje Cell
PKC : Protein Kinase C
PLC : Phospholipase
PO : Principal Olive
PP2B : Protein Phosphatase 2B
PPN : Pedunculopontine tegmental nucleus
PrC : Principal Component
S1 : Primary somatosensory cortex
SD : Standard Deviation
VOR : Vestibulo-Ocular Reflex
VSCT : Ventral Spinocerebellar Tract
ZII : Zebrin II

« Dans les champs de l'observation, le hasard ne favorise que les esprits préparés »

Louis Pasteur

Preamble

Disclaimer

Science has no boundaries: experts in the cerebellar field are (fortunately) not all French, hence the reason of choosing the language of Shakespeare to write my thesis. As a non-native English speaker, I would like to apologize (especially to Megan and Martijn) for the possible (almost certain) mistakes regarding spelling/grammar/conjugation and vocabulary scattered in this manuscript.

Objectives and research questions

During my PhD I had the chance to be involved in three projects that will be described in this manuscript. Since my teenage years, I've never really enjoyed focusing on the same thing again and again, I am more likely to touch everything at once, especially towards unexpected or unpopular directions. My friends and family can imagine the hard work I had to do on myself when the time had come to sit in front of my desk to focus on a single task: write this manuscript.

The cerebellum is involved in movement coordination, motor learning and many other tasks (*detailed in section 1*). To do so, it receives contextual and pre-integrated information from the whole body and other brain regions (*detailed in section 2.1*). These signals are integrated by several neuronal types within the cerebellar cortex and the cerebellar nuclei to compute efficient motor output (*detailed in section 2.2; 2.3 and 2.4*). Developmentally driven topographical relationships between inputs and outputs of the cerebellum (*detailed in section 2.5*) define cerebellar modules and microzones, the latter being functional units of information processing (*detailed in section 3*). The work I did during my thesis is a follow up of a project initiated by Antoine Valera and Philippe Isope: they aimed at understanding the role of the parallel fibers and the way cerebellar modules are linked together. This work ended in a brilliant thesis for Antoine and an elegant story for the lab (*detailed in section 3.3.3*). Briefly, they showed that parallel fibers were able to spread information through different and adjacent cerebellar modules. Surprisingly, the location of the granule cell inputs to a given subset of Purkinje cells are remarkably conserved across different mice. This might sound as a paradox : the orthogonal orientation of Purkinje cells to parallel fibers provides a wealth of possibilities for functional wiring, yet in the anterior vermis it turns out that some inputs are preferentially

selected (Valera et al., 2016). As many of these inputs come from neighboring microzones, their results support the functional inter-modular communication within the cerebellar cortex.

Considering the information above, my PhD project aims at understanding the synaptic functional relationships between cerebellar modules in the anterior vermis. It follows the statements of Valera and colleagues who postulated that the functional microzones are stereotyped from one animal to another (Valera et al., 2016), yet the question of innate vs acquired remains: are granular inputs to Purkinje cells selected under genetic or functional rules?
Valera and colleagues brought the beginning of an answer, as they could alter the synaptic maps *in vitro* by application of synaptic plasticity induction protocols (Valera et al., 2016). My thesis tried to determine the physiological correlates of their results, i.e. to what extent granule cells to Purkinje cells connectivity maps are sensitive to relevant physiological stimuli (i.e. sensorimotor incoming information). The data from the lab combined to the cerebellar litterature led to an appealing hypothesis: the coordination of muscles involved in the execution of a movement should require the coordination of cerebellar modules in charge of these muscles. According to this hypothesis and as Purkinje cells from the anterior vermis are involved in locomotion (*detailed in section 4*) they should select relevant inputs for locomotor behavior. Therefore, different individuals who evolve in the same environment may adopt similar strategies to develop an efficient and functional locomotion yielding similar input patterns to the considered Purkinje cells.

Thus, my thesis aims at investigating the synaptic rules that govern the establishment of inter-modular communication in the lobule III and IV of the cerebellar cortex through two main questions (and concomitant projects) :

(1) How does the intermodular communication takes place within the anterior vermis?
(2) Is their causal relationship between granule cell to Purkinje cell connectivity maps and motor control/adaptation?

To answer the first question, I took advantage of the postnatal development of the cerebellar cortex (*detailed in section 2.5*). I could perform *in vitro* patch clamp experiments coupled to glutamate uncaging (*detailed in section 5.5 to 5.9*) in order to evaluate the functional connectivity between cerebellar modules in pups, juvenile, and adult mice (*detailed in section 6.1*).

The second question involved patch clamp recordings and photo stimulation as well as behavioral quantifications in mice during perturbed or enriched locomotor adaptation (*detailed in section 6.2*). As locomotion is a well-coordinated, cerebellar sensitive motor behavior (*detailed in section 4*) we tried to evaluate how synaptic maps in the anterior vermis could be related to locomotor adaptation.

These two first project are based on the establishment of synaptic maps and thus evaluate the spatial distribution of granule cell inputs to Purkinje cells. The second project showed that inhibition and excitation pathways in the cerebellar cortex can be spatially segregated (*see section 6.3.1*). I was involved in a third project which studied the temporal dissociation of mossy fiber-mediated excitatory and inhibitory inputs to Purkinje cells. Patch clamp recordings combined with optogenetic activation of mossy fibers revealed decorrelated inhibition/excitation sequences in Purkinje cells that support inputs spatial segregation shown in project 2 (*detailed in section 6.3.2*). This work was done in collaboration with Francesca Binda, a former post doc of the lab. Some information and data from this study are part of the present manuscript although the whole story is available in the joined draft manuscript (*see Appendix 5, Binda et al, in prep*).

Since I began studying Neurosciences, one recurrent concept was always something like : the brain is the most flexible structure of the human body, synapses are subject to and selected by functional changes through long term and short term plasticity to adapt to every situation. Neural networks are the biological substrate of highly personal experiences, such as emotions and memories. I like to call these statements *textbook dogmas* : I will not dare to question if they are true or not, because there are a wealth of data to support them, but in this ocean of knowledge there must be at least one counterexample. I found it in Philippe’s lab, where I started my master’s degree internship, through Antoine’s story : I was hooked. This is how started this intense and exciting cerebellar journey that kept on tickling my curiosity days after days.

1. General Introduction

1.1 A (brief) history of cerebellar physiology

Nowadays, if asked to pinpoint the biological location of consciousness and will, one would without a doubt answer the brain. This has however never been so clear as in ancient times the heart was considered as the support for emotions and soul. Aristotle (384B.C. – 322B.C.) considered the brain as a secondary organ, in charge of cooling down the heart, but nonetheless thought that the brain was the container for the common sense. He also described the cerebellum as the *paracephalon*, because of its location at the back of the brain. The Roman physician Galen (129A.D. – 210A.D.) described the bovine cerebellum with more details, showing the major division between the central part (later called the *vermis*) and the hemispheres.

1.1.1 First reports on the cerebellum

The earliest anatomical descriptions of the cerebellum and the hindbrain emerged almost 15 centuries later, during the Renaissance, with the development of dissections on human corpses. The Flemish anatomist Andreas Vesalius (1514-1564) in his famous manuscript *De humani corporis fabrica* (On the Fabric of the Human Body) provided the first illustration of the surface of the human cerebellum. In the next century, the Italian biologist Marcello Malpighi (1628-1694) investigated the inner disposition of the cerebellum, mentioning the cerebellar cortex for the first time, *"delicately placed […] as a free leaf"* (Glickstein et al., 2009) on the top of fibers coming from the spinal cord. Two French physicians and anatomists, Raymond de Vieussens (1641-1716) and Felix Vicq d'Azyr (1746-1794) thereafter reported the first observations of the cerebellar nuclei, especially the *corpus rhomboideum*, renamed *corps dentelé* by Vicq d'Azyr. The other nuclei were labeled as *emboliform*, *globose* and *fastigial* by the German surgeon Benedict Stilling (1810-1879) in 1864. During the 18th century, the Italian surgeon Vincenzo Malacarne (1744-1816) published the first work entirely devoted to the cerebellum (Glickstein et al., 2009) soberly entitled "*Il Cervelleto"*, in which, amongst others, he identified cerebellar subdivisions.

1.1.2 Understanding the cerebellar functions: historical clues

Malacarne also suggested for the first time that the cerebellum might be involved in plastic changes (Glickstein et al., 2009). As a physician, he reported a decrease in the number of cerebellar folia in people suffering from cretinism. The expansion of animal experimentation in the 19th century allowed Luigi Rolando (1773-1831) to observe that a cerebellar lesion led to specific motor symptoms, but not to sensory or intellectual impairments. Pierre Flourens (1794-1867) suggested that the cerebellum is involved in movement coordination rather than production: movement persists after an ablation of the cerebellum in rabbits, but it severely lacks regularity and coordination. Luigi Luciani (1842-1919) described in 1891 in "*Il Cervelletto: nuovi studi di fisiologia normale e patologica"* the triad symptoms associated to cerebellar pathologies: *atonia* (lack of normal muscle tone), *asthenia* (weakness in the limbs) and *astasia*. He described this last symptom by head and trunk oscillations but also tremor during movement in hemicerebellectomized dogs and monkeys. Later, he described a 4th symptom: *dysmetria*, or errors in the metric of movement.

In 1917, Gordon Holmes (1876-1965), a British neurologist, could observe all symptoms described by Luciani in soldiers who survived gunshots in the cerebellum during World War I (Holmes, 1918). He also reported dyskinesia and tremors, and later developed the concept of ataxia. However, Luciani claimed that all cerebellar diseases could be described by his triad of symptoms, denying cerebellar involvement in movement coordination and the existence of a functional localization within the cerebellum(Manni and Petrosini, 1997). The work of the French physician Joseph Babinski (1857-1932) in the next century brought crucial accuracy to cerebellar symptoms and fine functions (Babinski, 1902). He described that patients suffering from cerebellar injuries are unable to coordinate groups of muscle in complex movements (*asynergia*) or to perform rapid sequences of movements (*dysdiadochokinesis*). This brings strong evidence for a major cerebellar involvement in the coordination and execution of voluntary and complex movements.

1.1.3 A century of milestones

At dawn of the 20th century, clinical observations and animal experimentation highlighted the major role of the cerebellum in movement control. Researchers could benefit from the development of microscopy to investigate the cellular architecture of the cerebellar cortex. Lugaro described his eponym cell in 1884. Cajal (1899, 1911) provided worldwide-known drawings of cerebellar neurons, including some of the most beautiful neuron in the central

nervous system and sole output of the cerebellar cortex, the Purkinje cell (PC, originally discovered in 1837 by the Czech anatomist Jan Evangelista Purkyne) (***Figure 1***).
The cerebellar cortex has since been investigated by numerous anatomists. Sanford L. Palay and Victoria Chan-Palay wrote the referenced textbook for cerebellar anatomy describing the cerebellar cortex cytoarchitecture (Palay and Chan-Palay, 1974). Constantino Sotelo and Joseph Altman provided extended work regarding the development of cortical structures and neural migration in the cerebellum (*see section 2.5 for detailed description*).
In the following decades, understanding of cerebellar circuitry has been linked to the development and refinement of electrophysiology. Indeed, the use of microelectrodes allowed Eccles, Llinas and Sasaki to reveal the unique synaptic influence of the climbing fibers (CF) originating in the inferior olive on PCs (Eccles et al., 1966). Masao Ito's group reached a cornerstone in the understating of cerebellar circuits within the cerebellum in showing the monosynaptic inhibition of cerebellar nuclei by PCs in the cat (Ito et al., 1964). Since then, researchers kept on trying to understand the operating rules of neural communication in the cerebellum. With Masanobu Kano, Ito reported for the first-time long-term depression at the granule cell (GC) to PCs (GC-PC) synapse (Ito and Kano, 1982). Scott brought first evidences supporting the modular organization within the cerebellar cortex (Scott, 1965). This cerebellar sophisticated compartmentalization was later discovered by Jan Voogd and Olov Oscarsson (Miller et al., 1969a, 1969b; Voogd, 2011). Richard Hawkes identified neurochemical markers, the Zebrin family, that allowed precise targeting of cerebellar modules (Hawkes et al., 1985).
The cerebellum also provided an interesting source of brainstorming for computational neuroscience : David Marr (Marr, 1969) and James Albus (Albus, 1971) modelled the cerebellar cortex as a perceptron and speculated on cerebellar learning rules that are still debated (Ito, 2006).

1.1.4. The Cerebellum today

Neurons in the cerebellar cortex are regularly arranged as repeated units with a basic circuitry. The structure of the cerebellar cortex was often described as "*crystalline*" in the literature. A common idea in the cerebellar community was that repeated circuits should lead to similar operation processing within the cerebellum. Specificity is then associated to inputs and outputs. In the last decade, many labs showed strong evidences to rule out this idea. Technical improvements in anatomical tracing, electrophysiology, imaging and genetically engineered mutants allowed researchers to show unheard-of molecular and functional heterogeneity in the circuits of the cerebellar cortex (partially reviewed in (Cerminara et al., 2015). The

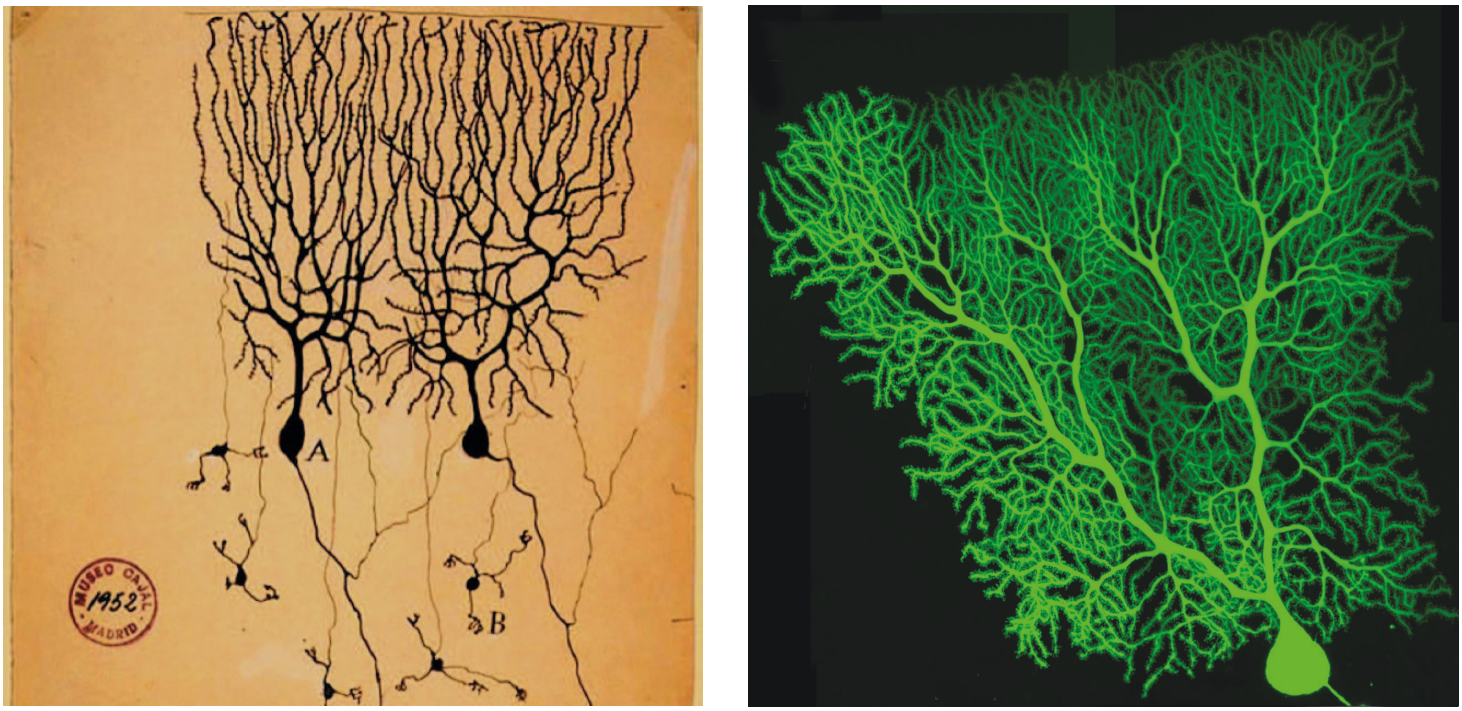

Figure 1 : A century of observation : the Purkinje cell

(left) Drawing of Purkinje cells (*A*) and granule cells (*B*) from pigeon cerebellum by Santiago Ramon y Cajal, 1899. ***Instituto Santiago Ramon y Cajal, Madrid, Spain***.

(right) Two-photon imaging of a sagittal Purkinje cell filled with a green-fluorescent dye. ***Image credit : Boris Barbour, IBENS.***

cerebellum displays heterogeneous functional regionalization in its canonical function, sensorimotor integration, as in example shown by *in situ* calcium imaging of the whole cerebellum in zebra fishes (Knogler et al., 2017). Rules for induction of long term depression at GC-PC synapses, an anti-Hebbian plasticity, have been extended as they depend on regional discrepancies within the cerebellar cortex (Wadiche and Jahr, 2005; Suvrathan et al., 2016). Some other groups extended the repertoire of cerebellar functions. Cerebellar involvement in motor control and learning is possible because the cerebellum integrates sensory motor and contextual information, processing predictions and rewards in many behaviors (Popa and Ebner, 2019).

If the cerebellar contribution to motor tasks is still a source of interest for the cerebellar community, the involvement of the cerebellum in cognitive functions has been extensively studied in the last decades (D'Angelo and Casali, 2012; Xiao and Scheiffele, 2018). In particular, cerebellar impact on fear and anxiety (Apps and Strata, 2015), expectation of reward (Wagner et al., 2017), social behaviors (Carta et al., 2019) and non-motor disorders such as autism spectrum disorders (Wang et al., 2014) have been demonstrated.

Despite an increasing effort of researchers in the cerebellar field, many questions still lack answers. How the system does segregate and compute relevant synaptic information? How is learning stored in synapses? By plasticity or intrinsic modification of neuronal properties, or both? Why do GCs in the cerebellar cortex represent more than 50% of the neurons in the central nervous system? How can the cerebellum perform so many tasks, despite its apparent weak cellular diversity? All these questions, amongst others, promise an exciting and hard-working future for the cerebellar research community.

1.2 Overview: anatomy and histology of the cerebellum

The cerebellum, Latin for "*little brain*" is a structure of the central nervous system historically dedicated to sensorimotor integration. It is involved in numerous motor aspects, such as the control of gait, balance and gaze but also the adaptation and execution of smooth complex voluntary (i.e. locomotion) and fine (i.e. reaching, grasping) movements. It is essential for efficient and accurate motor learning. In this purpose, the cerebellum communicates with several other neural regions, including the spinal cord (Matsushita et al., 1979), the brainstem (Voogd and Ruigrok, 2004) and the thalamocortical pathway (Allen and Tsukahara, 1974).

1.2.1 Evolution of the cerebellum

The cerebellum is present and conserved across almost all vertebrate. It appears first in evolution in jawless fishes such as lampreys (*Petromyzon sp.*, ***Figure 2A***) although limited to the *flocculonodular* lobe. Nonetheless in some species like the electro-receptive Mormyrid fish, the cerebellum reaches gigantic proportions, and becomes larger than the rest of the brain (***Figure 2A***). In fishes and reptiles, the cerebellum usually displays a smooth surface and tends to be rather small compared to the rest of the encephalon. In birds and mammals, it becomes larger and foliated (***Figure 2B***) (Hodos, 2009).
Size, shape and foliation of the cerebellum do vary across evolution, but its general organization is conserved. The cerebellar main body (*corpus cerebelli*) and the auricle (also named *flocculus* in tetrapodes) are present in fishes (except lamprey that lack the *corpus*), amphibian, reptiles and birds (***Figure 2B***) (Voogd and Glickstein, 1998). In mammals, the *corpus cerebelli* shrinks in a narrow worm-shaped medial structure called *vermis*, allowing significant space for the development of bilateral hemispheres, also called *neo-cerebellum* (***Figure 2B***).

1.2.2 Gross organization of the cerebellum

The cerebellum is in the cranial *fossa*, at the caudal extremity of the brain, both in mice and humans (***Figure 3A, 3B***). It overhangs the brainstem and is connected to the dorsal part of the brain via three bilateral pairs of tracts, called inferior (*restiform body*), middle (*brachium pontis*) and superior (*brachium conjunctivum*) cerebellar peduncles.

The cerebellum is composed of two main parts. The cerebellar surface is highly foliated in mice (***Figure 3B***), even more in humans (***Figure 3A***) and represents the first part: the three-layered cerebellar cortex. It projects to the second part and output stage of the cerebellum: 4 bilateral cerebellar nuclei. They are named as following (according to the mediolateral axis): the median nucleus, the anterior and posterior interposed nuclei and the lateral nucleus in mice. In humans, analogues nuclei are found as the fastigial nucleus, the emboliform nucleus, the globose nucleus and the dentate nucleus. In addition, some regions of the cerebellar cortex project directly to the vestibular nuclei, that are localised below the cerebellum in the brainstem (***Figure 4D***). Nomenclature may vary across species, thereby for clarity, and as mice were chosen as the study model, in absence of precision the following parts will consider the murine nomenclature and anatomy rather than the human or feline one.

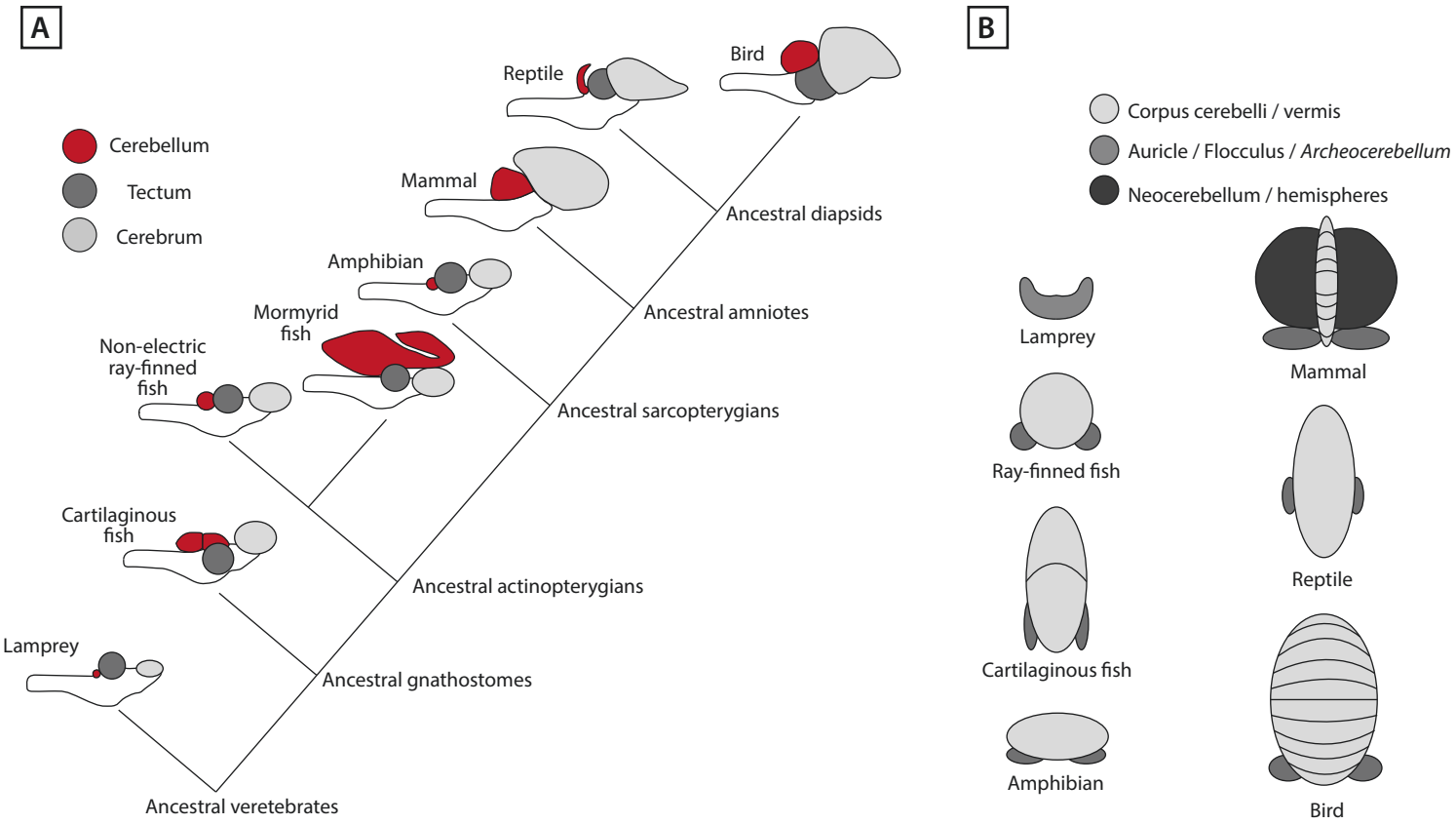

Figure 2 : Evolution of the cerebellum in vertebrate

(A) A cladogram of vertebrate evolution showing variation in shape and size of the cerebellum. All the representations have been scaled between species.

(B) Diagram of cerebellum in vertebrate classes showing the conserved cerebellar disposition across fishes, amphibian, reptile and birds and the emergence of the neocerebellum in mammals.

From Hodos W. (2009) Evolution of Cerebellum. In Binder M.D., Hirokawa N., Windhorst U. (eds). Encyclopedia of Neuroscience. Springer, Berlin, Heidelberg.

1.2.2.1 Segmentation based on anatomy: anteroposterior and mediolateral axis

Many rifts cross the cerebellum in the transverse axis, thus dividing the cerebellar surface in several lobes, or zones. The anterior, posterior and flocculonodular lobes are defined by two major cleavages, the primary and the posterolateral fissures, respectively (***Figure 4A***). The anterior lobe and the flocculonodular lobes are also described as the anterior and nodular zones, whereas the posterior lobe can be separated in a central and posterior zone (***Figure 4A, 4B***).
Smaller fissures delimit the cerebellar lobules, showing a finer level of organization. In mice, ten lobules have been described along the anteroposterior axis (***Figure 4A, 4B***). Nonetheless this number and/or arrangement may vary across species. For instance, in mice, lobules IV and V are fused whereas completely segregated in rats.

The disposition of the lobules allows a second cerebellar segmentation along the perpendicular axis. Thus, the medial part of the cerebellum is called vermis, surrounded by bilateral hemispheres. In between, one can find an intermediate region called paravermis. (***Figure 4C***)

1.2.2.2 Anatomo-functional segmentation of the cerebellum

The compartmentalization of cerebellar functions and input/output projection patterns segregate the cerebellum in another manner. This third organization partially overlaps with the mediolateral organization mentioned above and is linked to the phylogenetic order of emergence of the different cerebellar structures. Three major cerebellar parts can be described, each of them projecting to a specific cerebellar nucleus.

1.2.2.2.1 The vestibulocerebellum

This cerebellar area appears first during evolution and is also called *archeocerebellum* (***Figure 2***). It corresponds in higher vertebrates to the flocculonodular lobe (lobule X) and often the lobule IX that ensures similar functions in balance and adaptation of eye movements (***Figure 4C***). For instance, it has been demonstrated that the flocculonodular lobe is required to control the gain of the vestibulo-ocular reflex (VOR) (Ito, 1984). This reflex allows one to keep gaze on a target while the head is turning: a head rotation will trigger a compensatory eye movement in the opposite direction. To perform this behavior, the cortical part of the vestibulocerebellum receives inputs from the primary vestibular afferents carrying information from the semicircular canals and the otolith organs, dedicated to sense head motion and position. Moreover, the flocculonodular lobe receives strong visual inputs from the superior colliculus and pontine

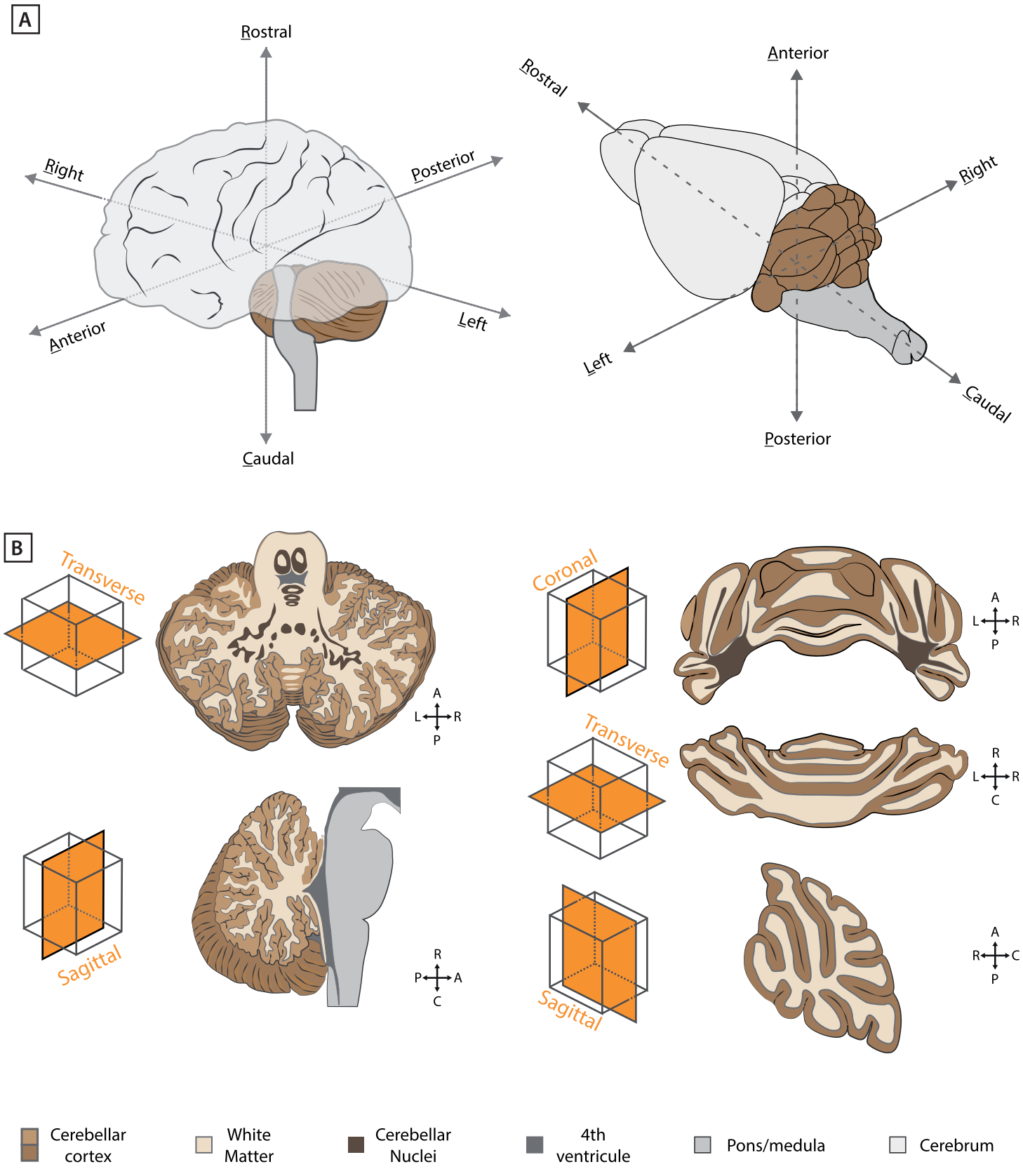

Figure 3 : Spatial orientation of the human and murine cerebellum

(A) Isometric views of the human (*left*) and murine (*right*) encephalon. The cerebellum is in brown.

(B) Corresponding orthogonal sections. Coronal, transverse and sagittal sections in mice are commonly used to prepare acute cerebellar slices.

projections relaying information from the striate cortex. Lobules IX and X then send direct outputs to the vestibular nuclei in the brainstem (***Figure 4D, 5C***).

1.2.2.2.2 The spinocerebellum

The vermis and the paravermis appeared later in evolution (***Figure 2A, 2B***). They represent the cortical part of the spinocerebellum (***Figure 4C***) as they receive numerous direct and indirect somatotopic inputs from the spinal cord through the dorsal and ventral spinocerebellar pathways and the dorsal column nuclei (such as the gracile and cuneate nuclei) (Matsushita et al., 1979; Yaginuma and Matsushita, 1989). Such inputs convey proprioceptive and tactile information from the head, the neck, the proximal body and limb muscles.

The spinocerebellum regulates several motor aspects via the control of body and limb movements, including head, neck, tail and proximal limbs. Thereby the vermal and paravermal region of the cerebellum are essential for the control and adaptation of balance and locomotion via several pathways. Neurons from the vermis project to the medial cerebellar nuclei (***Figure 4D***), the latter targeting brainstem structures involved in locomotion (e.g. the ventromedial reticular formation) and balance (e.g. vestibular nuclei) (***Figure 5C***). The paravermis sends projection to the anterior interposed nuclei (***Figure 4D***) that contacts both the red nucleus in the brainstem and the ventrolateral part of the thalamus, last relay before the primary motor cortex (***Figure 5C***). Ultimately, the intermediate region of the cerebellum has effect on body muscles through the rubrospinal tract and the corticospinal tract.

1.2.2.2.3 The cerebrocerebellum

The most recent step of cerebellar development was marked by the apparition of the cerebellar hemispheres (***Figure 2A, 2B***). While discrete in birds, the *neocerebellum* expanded more than the vermal/paravermal region in mammals (***Figure 2B***).

The cortical part (i.e. the cerebellar hemispheres) project to the bilateral dentate nuclei and the posterior interposed nucleus (***Figure 4D***). Contrary to the spinocerebellum, the cerebrocerebellum receives inputs exclusively from the neocortex via a relay in the pontine nuclei (***Figure 5A***): the pons projects mostly to the contralateral dentate nucleus and hemisphere (***Figure 9A***). In return, the dentate nuclei send projections to many contralateral thalamic nuclei (Allen and Tsukahara, 1974), later projecting to primary and premotor cortical areas. In addition, the cerebrocerebellum targets the parvocellular region of the red nucleus (Allen and Tsukahara, 1974) (***Figure 5C***).

This tight connectivity between the dentate/interposed nuclei and the thalamocortical/rubrospinal pathway suggest a preponderant role of the cerebrocerebellum in

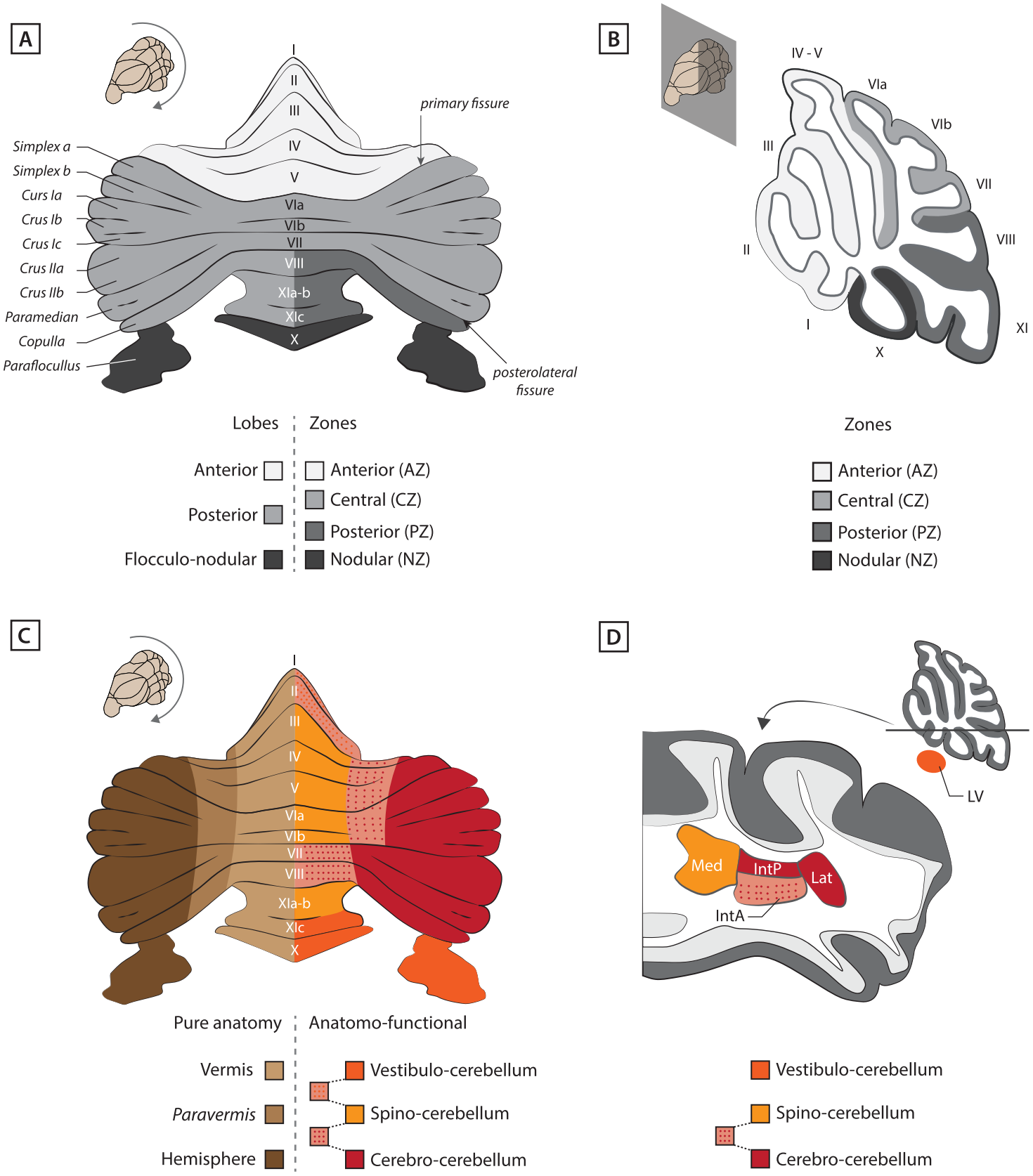

Figure 4 : Anatomy vs function : multiple cerebellar segmentations

(A) Unfolded representation of the cerebellar surface, showing antero-posterior subdivisions according to external scissures.

(B) Sagittal section of the cerebellum and corresponding cortical zones.

(C) Comparison of pure anatomical and anatomo-functional segmentation of the cerebellar cortex (*unfolded view*).

(D) Anatomo-functional subdivision of the cortical outputs : cerebellar nuclei *(down)* and vestibular nuclei *(top)*.

*Abbreviations : **I to X** : cerebellar lobules. **Med / IntP / IntA / Lat** : Medial / Interposed Posterior / Interposed Anterior / Lateral deep cerebellar nucleus. **LV** : Lateral Vestibular Nucleus*

motor preparation. The group of Kazuo Sasaki addressed this question with a functional approach : transient inactivation of the dentate nucleus with a cooling probe increases reaction time and clumsiness in a grasping task in monkeys (Tsujimoto et al., 1993) concomitant with disturbed field potentials in the motor cortex. This link has been confirmed and extended by recent work, as the cerebellar granule cells (GCs) and neurons in layer 5 of the neocortex share encoding dynamics in a motor task (Wagner et al., 2019). Tracing studies revealed anatomical loops between the cerebellum and motor/prefrontal cortex (Kelly and Strick, 2003). Cortical sensory and motor information converge at the cellular level in the cerebellar cortex and cerebellar nuclei (Proville et al., 2014). Premotor cortex and the dentate nuclei are functionally associated, as the cerebellum allows maintenance of preparatory activity in the premotor cortex during learned, goal directed behavior (Chabrol et al., 2019). However these cerebro-cerebellar loops are not restricted to the lateral cerebellar nuclei only, as suppressing the action of the medial cerebellar (i.e. fastigial) nuclei prevents maintenance of preparatory activity in the anterior lateral motor cortex, disrupting motor task success but not movement execution (Gao et al., 2018).

1.3 Cerebellar roles and functions

The cerebellum plays a central role in motor coordination, in the control of gait and balance, and in learning new motor skills through a dialogue with other brain structures, including the spinal cord, the brainstem and the thalamocortical pathway. From grabbing a cup of coffee to play an insane guitar solo, the cerebellum is involved in almost every movement one could perform in a single day.

Moreover, recent evidences show that cerebellar skills may extend to numerous non-motor related tasks (D'Angelo and Casali, 2012) highlighting a role for the cerebellum in many cognitive functions (Ito, 2006; Ramnani, 2006) and disorders (Schmahmann, 2019). Functional imaging revealed cerebellar activation, and thus involvement, in cognitive tasks such as language, explicit memory retrieval and sequence learning (Desmond and Fiez, 1998).

However, as my project was dedicated to study sensorimotor adaptation, cognitive involvement of the cerebellum will not be further discussed.

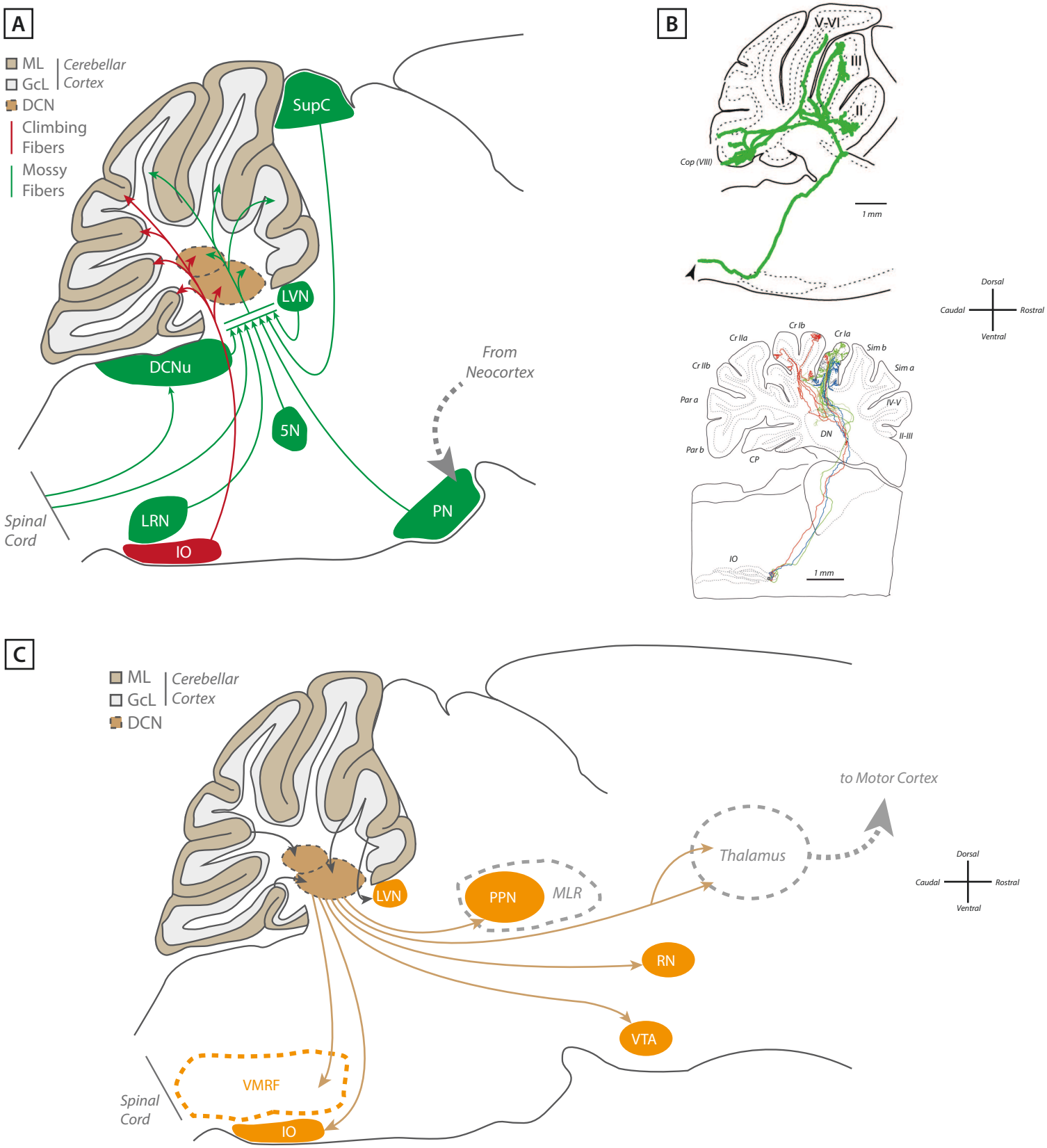

Figure 5 : In and outs of the cerebellum

(A) Major inputs to the cerebellum (*sagittal view*). The inferior olive sends climbing fibers to DCN and cerebellar cortex. Mossy fibers originate from various nuclei in the medulla and the brainstem, often called pre-cerebellar nuclei.

(B, top) Labeling of a single mossy fiber from the spinocerebellar tract (thoracic) shows numerous collaterals. ***Adapted from Luo et al, 2017***. *(B, down)* Labeling of three olivary neurons and related climbing fibers. ***Adapted from Sugihara et al, 2001***.

(C) Direct targets of cerebellar projections.

Abbreviations : ***II to VII:*** *cerebellar lobules* ***5N:*** *Trigeminal Nuclei* ***CP:*** *Copula.* ***CrI/II:*** *Crus I/II* ***DCNu:*** *Dorsal Column Nuclei* ***IO:*** *Inferior Olive* ***LRN:*** *Lateral Reticular Nucleus* ***LVN:*** *Lateral Vestibular Nucleus.* ***MLR*** *: Mesencephalic locomotor region.* ***Par:*** *Paramedian lobule.* ***PN:*** *Pontine Nuclei.* ***PPN*** *: Pedunculopontine Tegmental Nucleus.* ***RN:*** *Red Nucleus* ***Sim a/b:*** *Simplex lobule a/b* ***SupC:*** *Superior Colliculus* ***VMRF:*** *Ventro Medial Reticular Formation ,* ***VTA:*** *Ventral Tegmental Area.*

1.3.1 What does the cerebellum do?

The cerebellum is dedicated to sensorimotor integration, and can adapt or control gesture execution in both non-voluntary and voluntary movements.

1.3.1.1 Cerebellar involvement in non-voluntary movements

The cerebellum is involved in many unconscious movements. The vestibulo-ocular reflex (VOR) allows visual pursuit of a fixed target while the head is moving: when the head turns in one direction, eyes moves in the opposite direction in a compensatory range. The cerebellum controls the gain of this reflex (Miles and Lisberger, 1981; Ito, 2006). Synaptic plasticities within the cerebellar cortex are crucial for an efficient gain control : disruption of synaptic potentiation (Schonewille et al., 2010) and depression (Boyden et al., 2006) impairs VOR adaptation.
The cerebellar cortex plays a key role in the modulation of cutaneously-induced reflexes during stepping (Pijpers et al., 2008) as well as in the adjustment of balance and locomotion (Morton and Bastian, 2004) (*for locomotion see section 4*).

1.3.1.2 Cerebellar control of voluntary movements

The cerebellum is required to perform smooth and accurate goal-directed voluntary movements (Thach et al., 1992; Cerminara et al., 2015). Voluntary movements execution requires motor planification in order to perform smooth and accurate gesture. However, fast and coordinated arm movements for instance cannot be executed under pure feedback control because biological feedback loops are both too slow and have small gains (Wolpert et al., 1998). Neural networks, including the cerebellum, are nonetheless able to overcome this delay using predictive strategies and internal models (Wolpert et al., 1998; Doya, 1999; Bastian, 2006). The cerebellum has been proposed to be composed of multiple paired forward and inverse internal models: a forward dynamic model of the arm, for example, predicts the next state (e.g. position and velocity) of the system given the current state and the motor command. In contrast, inverse models invert the system by providing the motor command that will cause a desired change in state (Wolpert et al., 1998 ; Doya, 1999).

Sensory information (e.g. skin pressure or muscle stretch) from the entire body are conveyed to the cerebellum, as well as visual, auditory and somesthetic information. In addition to real-time sensory information, a copy of the motor command sent to the spinal cord from the

neocortex is provided to the cerebellum, hence named efferent copy (Wolpert et al., 1998, Bastian, 2006).
The cerebellum is then thought to compute real-time movement correction as it learns to predict the output of an action (i.e. forward internal model) and compares it with the actual sensory feedback to ensure motor correction if needed (i.e. inverse model, Wolpert et al., 1998 ; Doya, 1999 ; Bastian, 2006) through projections on motor structures (e.g. motor cortex via the thalamus or the red nucleus, Allen and Tsukahara, 1974). One could ask about the problem of the sensory feedback provided by the execution of self-generated movements : the cerebellum is able to cancel this feedback in order to sort only relevant sensory information (Blakemore et al., 1998; Cullen, 2011; Cullen and Brooks, 2015).

1.3.2 What if the cerebellum gets a nervous breakdown?

A large amount of clinical observations showed how hard life can get in case of cerebellar lesions (*see section 1.1.2*). If cerebellar damage does not cause a loss of movement, it triggers clear and consistent movement impairments, including lack of coordination, increased variability, tremor, and poor accuracy. Notably, cerebellar damages induce greater impairments to movements that require predictive control (i.e. feedforward movements) versus those that require reactive control (i.e. feedback movements) (Morton and Bastian, 2006; Pisotta and Molinari, 2014).

Ataxia is defined as impaired coordination of voluntary muscle movement, usually caused by cerebellar dysfunction or impaired vestibular or proprioceptive afferent input to the cerebellum (Ashizawa and Xia, 2016). Those symptoms can have acute onset after cerebellar injuries or insidious onset with a chronic and slowly progressive clinical course such as in spinocerebellar ataxias of genetic origin (Ashizaway and Xia, 2016). Spinocerebellar ataxias have been linked to dominant mutations of more than 30 different genes, that in any case ultimately lead to functional alteration (Walter et al., 2006) and loss of PCs in the cerebellar cortex (Meera et al., 2016).

The phenotype associated with cerebellar lesions depends on their localization. Lesions in the flocculonodular lobe lead to nystagmus (Patel and Zee, 2015). Cerebellar lesions can be the result of tumors, strokes or degenerative diseases, triggering ataxic phenotype (such as gait and balance impairments in patients when occurring within the vermis) (Sierra et al., 2015) as well as disruption of interlimb coordination and movement sequencing. Dystonia is one of the most common forms of tremor and movement disorder caused by co-contraction of antagonist

muscles. It was historically linked to impairment of the basal ganglia, but numerous studies reported its onset following cerebellar localized lesions(Calderon et al., 2011; Fung and Peall, 2019; Nikolov et al., 2019).
In addition, the cerebellum has been identified as a very important actor in the onset of autistic spectrum disorders (Wang et al., 2014).

2. Histology and physiology of the vermal cerebellum

From the histological point of view, the cerebellum is segregated in two main parts: the cerebellar cortex and the cerebellar nuclei (***Figure 6A***). The histology part of this section will gather brief descriptions of the major inputs to the cerebellum (*section 2.1*), as well as the cytoarchitecture of the cerebellar cortex (*section 2.2*) and the cerebellar nuclei (*section 2.3*). Review of cerebellar fine anatomy will provide substantial support to describe functional concepts that occur in the cerebellar cortex to ensure synaptic integration and information processing (*section 2.4*). Lastly, as some of my experiments were performed in the developing cerebellum, I will review the general steps of embryonic and postnatal cerebellar development (*section 2.5*).

2.1 Inputs to the cerebellum

Two major excitatory inputs reach the cerebellar cortex and the cerebellar nuclei: (1) the mossy fibers (MF) and (2) CFs (***Figure 5B, 6A, 6B, 6C***). As it will be detailed in section *2.4*, these two pathways have different cellular targets within the cerebellum: understanding how these pathways are integrated and combined is a major challenge for the cerebellar community

The cerebellum also receives projections from catecholaminergic fibers originating in the reticular formation and the locus coeruleus, providing respectively serotoninergic and noradrenergic modulatory inputs (Dieudonné, 2001; Carey and Regehr, 2009). Despite their role in plastic phenomenon, these non-glutamatergic pathways will not be further described in this manuscript.

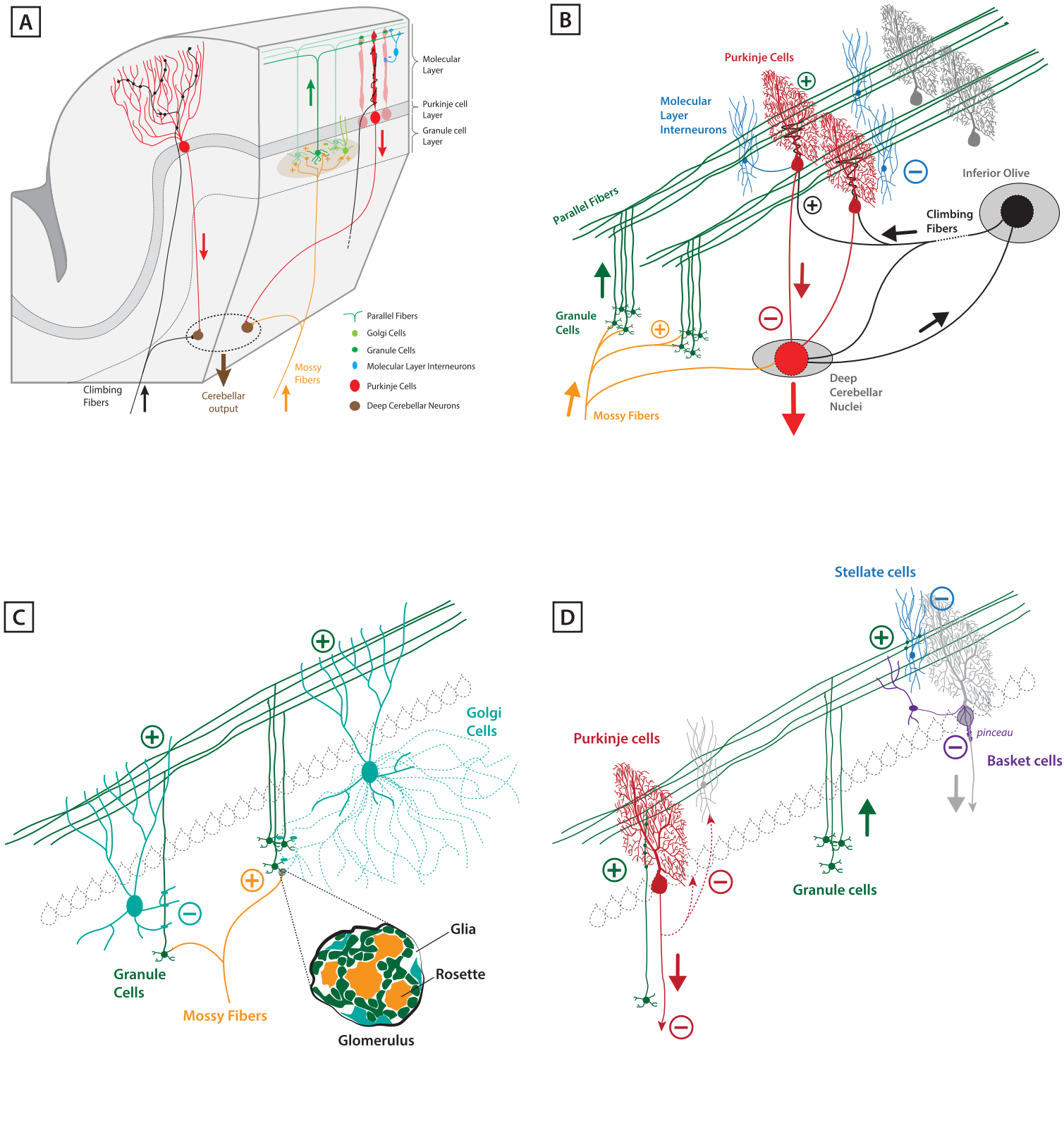

Figure 6 : Architecture and information pathway in the cerebellar cortex

(A) Section of the cerebellum with its major cell types and projection pathways. Climbing and mossy fiber project in the cerebellar cortex and the deep cerebellar nuclei.

(B) Excitatory inputs converge to the Purkinje cells. Climbing fibers project directly onto Purkinje cells while mossy fibers project via the granule cell - molecular layer interneurons - Purkinje cell pathway.

(C) Synaptic integration in the granule cell layer. Mossy fiber terminals (*rosette*), granule cell dendrite and golgi cell axons (*dashed projections*) are packed in the glomerulus, allowing Golgi cells to gait synaptic inputs on granule cells. ***Adapted from Eccles, 1967***.

(D) Synaptic integration in the molecular layer. Purkinje cells, the sole output of the cerebellar cortex, receive direct excitatory inputs from granule cells or indirect feed-forward inhibition from stellate cells and basket cells. Purkinje cells project out of the cerebellar cortex, and on neighboring Purkinje cells and molecular layer interneurons via collaterals.

2.1.1 The MF pathway

MFs carry different types of modalities, such as visual, somatosensory, proprioceptive, auditory and vestibular information to the cerebellar cortex and the deep cerebellar nuclei. They can be described depending on their origin: (1) from the spinal cord or (2) from nuclei in the brainstem and medulla, also called pre-cerebellar nuclei. They target the GC layer in the cerebellar cortex and often send collaterals to the cerebellar nuclei (***Figure 6A, 6B***). Specific MFs inputs to the lobule III/IV of the cerebellar cortex will be further detailed in section *4.2.1.2*.

2.1.1.1 MFs from the spinal cord

The spinocerebellar pathway gathers MFs originating in the spinal cord (***Figure 5A***) It carries proprioceptive and sensory information from muscles spindles (i.e. change in muscle length), Golgi tendon apparatus (i.e. muscle stretch) and cutaneous information (i.e. exteroceptive inputs) from the periphery.

The spinocerebellar tract has multiple origins from different laminae within the spinal cord (Matsushita et al., 1979; Matsushita and Hosoya, 1982) and can be divided into 4 anatomical pathways (Mendoza, 2011; Voogd and Ruigrok, 2012) :

- *(1) The dorsal (or posterior) spinocerebellar tract (DSCT)* conveys information from the caudal ipsilateral part of the body. It derives from axonal fibers generated in the Clarke's column nuclei in the spinal cord.
- *(2) The ventral (or anterior) spinocerebellar tract (VSCT)* also originates in the caudal ipsilateral part of the body, but undergoes decussation within the spinal cord. It ends in the ipsilateral part of the cerebellum, as MFs from the VSCT cross the midline one more time within the cerebellum (Stecina et al., 2013).
- (3) The cuneocerebellar tract projects to the cerebellum after a relay in the cuneate and the external cuneate nuclei (i.e. dorsal column nuclei) and (4) The spino-reticulocerebellar (or rostral) tract. These pathways are thought to represent the respective equivalents of the dorsal and ventral spinocerebellar tracts for the upper extremities (Mendoza, 2011).

2.1.1.2 MFs from the pre-cerebellar nuclei

Numerous MFs originate in nuclei located in the brainstem, hence called pre-cerebellar nuclei. They convey motor and sensory information from the cerebral cortex and the rest of the body (Voogd and Ruigrok, 2012).

MFs from the trigeminocerebellar pathway originate in the trigeminal nuclei (***Figure 5A***) and convey sensorimotor information from the face via cranial nerves.

MFs originating in the pontine nuclei are a major input to the cerebellum (***Figure 5A***) (Serapide et al., 2001; Biswas et al., 2019). In primates, they represent the strongest input to the cerebellum, beside all other types of MFs (Voogd and Ruigrok, 2012). Pontocerebellar MFs relay sensorimotor and visual information from the cerebral cortex as well as information from associative cortical areas and auditory signals. Thus, information carried by pontocerebellar MFs have been pre-processed by the neocortex (Schmahmann and Pandya, 1997).

The lateral reticular nucleus (LRN) sends MFs to the whole cerebellar cortex (***Figure 5A***), except the flocculonodular lobe, as well as systemic collaterals in the cerebellar nuclei (Wu et al., 1999). The LRN relays motor information from the spinal cord (i.e. from the spino-reticulocerebellar tract) and from other brain regions such as the red nucleus (Kitai et al., 1974).

The vestibular nuclei project to the cerebellum (***Figure 5A***). Vestibular MFs projection terminate in the lobule IX (*uvula*) and X (*nodulus*) and secondary vestibular afferents end in the flocculus and paraflocculus (Voogd and Ruigrok, 2012). Vestibular projections can also be found in the anterior vermis, where they overlap with inputs from the cervical part of the spinocerebellar tract (Matsushita and Wang, 1987). Vestibular nuclei encode information relative to equilibrium and balance, as well as head movement kinetic (Merchant, 2011). Anatomical relationships between the vestibular nuclei and the cerebellar cortex are further described in section *4.2.1*.

2.1.2 The CF pathway

CFs originate from the inferior olive, located in the ventral part of the medulla (***Figure 5A***). The inferior olive in mammals can be subdivided in 3 main nuclei: the principal olive (PO), the dorsal accessory olive (DAO) and the medial accessory olive (MAO) (Kooy, 1916). MAO can

be divided in rostral and caudal part (Voogd and Ruigrok, 2012). Each of these nuclei send topographical CF projections to the cerebellar cortex. They are the anatomical basis for modular organization within the cerebellum (***Figure 8B***, *see section 3.1 for a detailed description*). CFs target both the cerebellar cortex and the cerebellar nuclei via collaterals.

The inferior olive receives (mostly ipsilateral) inputs from numerous brain regions such as the reticular formation, the somatosensory cortex, the red nucleus, the periaqueductal grey and (mostly contralateral) inputs from the dorsal column nuclei and the spinal cord (Brown et al., 1977). CF inputs are considered as *"teaching signals"* allowing supervised learning (*see section 2.4.2 for detailed description*) (Medina et al., 2002; Raymond and Medina, 2018) and gate synaptic plasticity of PC synapses (*see section 2.4.3 for detailed description*).

2.2 The cerebellar cortex

The cortical part of the cerebellum is divided in three layers (from external to internal): the molecular layer, the PC layer and the GC layer (***Figure 3, 6A***) surrounding a dense layer of white matter that gathers numerous myelinated axons from (e.g. PC axons). Each layer contains different types of neurons and glial cells that will be described in the following sections.

2.2.1 Cell types in the cerebellar cortex

The cerebellar cortex contains a few types of neurons that are directly or indirectly targeted by the MFs and CFs.

2.2.1.1 The Purkinje Cell

PCs are in a central position within the cerebellar cortex: they are directly targeted by CFs (*see section 2.1.1.2* and ***Figure 6B***) and indirectly by MFs (*see section 2.1.1.2* and ***Figure 6B***). They are spontaneously active around 50Hz (Thach, 1968; Häusser and Clark, 1997; Raman and Bean, 1999) and the final computational stage, sole output of the cerebellar cortex. Therefore, understanding how PCs encode CFs and MFs inputs is crucial to unravel information processing rules within the cerebellum.

2.2.1.1.1 Morphology and inputs

PC somas have a diameter of approximately 20µm in mice and form a monolayer in the cerebellar cortex, the PC layer (***Figure 6***). At adulthood, PCs in the vermis display a characteristic tree-shaped dendritic tree (***Figure 1***) oriented in the parasagittal plane, covering a 100x120µm surface in mice (Nedelescu and Abdelhack, 2013). In general, this dendritic tree starts from the soma in a single (in rare cases two) primary dendrites, that ramified into several secondary dendrites and tertiary branchlets.

Thorny spines located on PCs smooth dendrites (i.e. primary and secondary dendrites) receive hundreds of excitatory inputs from a single CF (***Figure 6A, 6B***) (Palay and Chan-Palay, 1974).

2.2.1.1.2 Targets

PCs are inhibitory neurons that release GABA and target other neurons both in the cerebellar cortex and the cerebellar nuclei (***Figure 6D***). Most of PCs target neurons of the cerebellar nuclei (***Figure 5C, 6A***) although PCs from the flocculus (lobule IX) and the nodulus (lobule X) send a myelinated axon to the vestibular nuclei (***Figure 4C, 5C***) (Tan et al., 1995). In addition, some PCs located in the anterior vermis (lobules I, II, III & IV) also project directly to the medial and lateral parts of the vestibular nuclei (*see section 4.2.1.3* and ***Figure 13***) (VOOGD et al., 1996; Voogd, 2016).

PCs target other neurons within the cerebellar cortex. In adult mice, they display axon collaterals in the parasagittal plane (Hawkes and Leclerc, 1989) that contact other PCs, Lugaro cells and molecular layer interneurons (MLI) (***Figure 6D***) (Palay and Chan-Palay, 1974; de Solages et al., 2008). These collaterals allow cerebellar output to regulate processing in parasagittal zones and to maintain local oscillatory activity of PC networks (de Solages et al., 2008; Witter et al., 2016).

2.2.1.2 The Granule cells

GCs are the only excitatory neurons in the anterior cerebellum (unipolar brush cells are found only in the posterior cerebellum, see Cerminara et al., 2015). They represent the major input stage in the cerebellar cortex, and the most numerous neurons in the mouse brain : almost to 60% of the total neurons in the central nervous system (Harvey and Napper, 1988).

2.2.1.2.1 Morphology and inputs

At the adult stage, GCs are in the GC layer (***Figure 6A***). These neurons are the smallest neurons of the central nervous system (with and average somatic size of 4.82µm) (Harvey and Napper, 1991) and are densely packed ($1.92.10^6$ cells/mm^3 in Harvey & Napper, 1988 and $2.85.10^6$ cells/mm^3 in Palkovits et al., 1971). GCs display 4 to 5 short dendrites that each expand 15-20µm from the soma to end up in a "claw-like" appendage in the glomerulus (***Figure 6C***), therefore receiving one synaptic input from MF (a *rosette*) (***Figure 6C***) (Palay and Chan-Palay, 1974; Tran-Van-Minh et al., 2016) (Palay and Chan-Palay, 1974; Cathala et al., 2003; Lackey et al., 2018). In most cases, GCs receive contacts from MFs carrying different modalities (Bengtsson and Jorntell, 2009; Huang et al., 2013; Chabrol et al., 2015; Powell et al., 2015).

2.2.1.2.2 Targets

GCs send their axon up to the molecular layer (***Figure 6***). It can be divided in 2 parts: (1) the ascending axon and (2) the parallel fiber (PF).

(1) The ascending axon is the initial part of the GC axon, projecting vertically in the molecular layer, parallel to PCs dendritic tree (***Figure 6C,6D***). It makes several synapses with surrounding elements such as PCs (Harvey and Napper, 1988), Golgi cells (Hamori, 1981; Cesana et al., 2013) and MLIs (***Figure 6C, 6D***) (Sultan and Bower, 1998).

(2) In the molecular layer, the ascending axon splits in a T-shape fashion forming two branches running in opposite direction in the mediolateral axis: PFs (***Figure 6***). They are unmyelinated and realize *en passant* synapses on PCs, MLIs and Golgi cells (***Fig 6C, 6D***). A PF crossing the dendritic tree of a PC will make a synapse on a dendritic spine located on the tertiary branchlets only (***Figure 6B, 6D***) (Palay and Chan-Palay, 1974) with a probability of 50% (Harvey and Napper, 1988). In rodents, a single PC can receive up to 175 000 physical PF inputs (Harvey and Napper, 1988), however most of them (~85%) have been described as functionally uneffective (i.e. silent synapses) (Ekerot and Jörntell, 2001; Isope and Barbour, 2002). PFs can travel up to several millimeters in the mouse vermis (Pichitpornchai et al., 1994; Lackey et al., 2018), crossing the dendrites of hundreds of PCs and MLIs along the mediolateral axis (***Figure 6B***) (Harvey and Napper, 1991).

GCs and PFs represent the sole excitatory inputs of PCs and MLIs, providing both monosynaptic excitation and disynaptic feed-forward inhibition on PCs (*see section 2.4.1.2* and ***Figure 6D***).

2.2.1.3 Molecular Layer Interneurons

MLIs are GABAergic neurons and are the only cell-type having their soma located within the molecular layer (***Figure 6A***). Two classes of MLIs are classically distinguished in the literature depending on their location and morphology: (1) stellate cells, are located in the ⅔ upper part of the molecular layer, and (2) basket cells, located in the lower part of this layer, close to PC somas (***Figure 6D***). Based on a quantitative study of the axonal plexus, Sultan & Bower concluded that stellate and basket belong to a continuum rather than to two distinct populations (Sultan and Bower, 1998). In both cases, MLI dendritic and axonal projections are mostly restricted to the parasagittal plane.

2.2.1.3.1 Morphology and inputs

MLIs receive hundreds of excitatory inputs from PFs (Palay and Chan-Palay, 1974). A single MLI can also receive up to 20 inhibitory synaptic inputs from other surrounding MLIs (Lemkey-Johnston and Larramendi, 1968; Llano and Gerschenfeld, 1993; Häusser and Clark, 1997). In addition to these chemical inputs, MLIs are synchronized together by electric gap-junctions (Mann-Metzerand and Yarom, 2000; Alcami and Marty, 2013). They also receive synaptic inhibition from the PCs collaterals (***Figure 6D***) (Witter et al., 2016) and non-synaptic excitation through glutamatergic spillover from CFs (Szapiro and Barbour, 2007).

2.2.1.3.2 Targets

Unlike PFs, MLIs make inhibitory synapses on PCs dendritic shaft (O'Brien and Unwin, 2006; Goodlett and Mittleman, 2017). A single PC is contacted by 6 to 10 MLIs in rodents (***Figure 6B, 6D***) (Palay and Chan-Palay, 1974; Häusser and Clark, 1997).

Stellate cells make chemical synapses onto PCs dendritic trees located in the sagittal plane (*see section 2.2.1.1.1*). Basket cells axonal plexus form a basket-shaped terminal around the cell body of PCs, with a very specialized terminal called *pinceau* (***Figure 6D***). It is devoid of any kind of synapses (Iwakura et al., 2012) and regulates the timing of action potentials in the PCs via ephaptic transmission (Blot and Barbour, 2014): a release of positive charges around to the PC soma that provides extremely fast inhibition as it prevents the generation of action potentials.

2.2.1.4 Other neurons in the granule cell layer

Amongst the numerous GCs, the GC layer contains several types of inhibitory interneurons: the Golgi cells, the Lugaro cells, the Globular cells and the unipolar brush cells. This last type of neuron is found in the posterior cerebellum only and therefore will not be further detailed.

2.2.1.4.1 The Golgi cells

Golgi cells represent most of the inhibitory interneurons in the GC layer and act as an interplay between the molecular and the GC layer (***Figure 6C***). Indeed, they display a dendritic tree orientated in the parasagittal plane (Sillitoe et al., 2008) divided in two parts: basal dendrites remain in the GC layer and are contacted by MF terminals and the ascending GC axon (Cesana et al., 2013), while apical dendrite project up to the molecular layer and are contacted by neighboring GCs (***Figure 6C***) (Valera et al., 2016) via PFs (Dieudonné, 1998; Kanichay and Silver, 2008). The axonal plexus of Golgi cell targets GCs in an extensive fashion, displaying hundreds of contacts (***Figure 6C***) (Palay and Chan Palay, 1974).

Golgi cells, which gate information transfer within the GC layer via a feedback inhibition on GCs, are coupled by electrical gap junction and play an important role for the coordination of cerebellar sensorimotor integration through oscillatory activity (Dugué et al., 2009). Simat et colleagues have identified several subtypes of Golgi cells based on their molecular and morphologic characteristics (Simat et al., 2007). Golgi cells can release either GABA or glycine yet 70% of them release both neurotransmitters. Golgi cells can be sorted according to morphological discrepancies, and differential metabotropic glutamate receptors expression. In the glomerulus, MFs provide axo-axonal excitation on Golgi cells that in return modulates GCs synaptic integration (***Figure 6C***). Moreover, Golgi cells are not contacted by PCs nor MLIs as electric or optogenetic activation of these neurons failed to elicit any post synaptic currents (Hull and Regehr, 2012; Witter et al., 2016).

2.2.1.4.2 The Lugaro & Globular cells

Lugaro cells are mixed GABA/Glycinergic neurons found in the GC layer, close to PC somas (Palay and Chan-Palay, 1974). They receive inputs from PC collaterals (Witter et al., 2016) and from serotonergic fibers (Dieudonné and Dumoulin, 2000). Their dendrites are orientated in a diagonal plane. They display two axonal plexuses : one along their dendrites that targets surrounding MLIs (Lainé and Axelrad, 1998) and a second that expands in the mediolateral axis (Valera et al., 2016) targeting Golgi cells (Dieudonné and Dumoulin, 2000) and PCs (Dean et al., 2003).

Globular cells receive monosynaptic inhibition from PCs in addition with monoaminergic excitation (Hirono et al., 2012). They display a globular-shape soma (Lainé and Axelrad,

1998). Together, Lugaro and Globular cells represent 15% of the interneurons in the GC layer (Simat et al., 2007).

2.2.1.5 The Bergmann Glia

The Bergmann glial cells are specialized astrocytes localized in the PC layer, surrounding PC somas. They emit projections in the parasagittal plane named radial fibers, that wrap around PC somas and dendrites forming microdomains around excitatory and inhibitory synapses on PCs (Palay and Chan-Palay, 1974).

Bergmann glial cells are Aldolase-C positive (Fujita et al., 2014), participate in non-synaptic transmission through glutamate reuptake, express GABA receptors and tonically release GABA (Lee et al., 2010). These findings suggest that Bergmann glial cells should actively be involved in synaptic transmission modulation within the cerebellar cortex (De Zeeuw and Hoogland, 2015).

2.3 The Vestibular Nuclei and the Deep Cerebellar Nuclei

PCs from the cerebellar cortex project directly on two different structures: the vestibular nuclei in the brainstem and the cerebellar nuclei, located in the cerebellum (***Figure 4D***). Both nuclei represent the major output stage of the cerebellum and project to other motor (Allen and Tsukahara, 1974; Schmahmann and Pandya, 1997; Kelly and Strick, 2003; Glickstein et al., 2011) or non-motor (Apps and Strata, 2015) regions of the brain (***Figure 5C***).

2.3.1 The Vestibular Nuclei

The Vestibular nuclei oversee the maintenance of equilibrium and posture, the perception of head motion and acceleration and are involved in muscle tone (Merchant, 2011). They are divided in four nuclei: *medial*, *superior*, *inferior* and *lateral vestibular nuclei*. The medial vestibular nuclei receive inputs from the semicircular canals (Merchant, 2011) in the inner ear, from PCs located in the lobules IX and X of the cerebellar cortex and from a subset of PCs in the anterior vermis (*see details in section 4.2.1.3* and ***Figure 6D, 13***) (Tan et al., 1995; VOOGD et al., 1996). It sends projections through the medial vestibulospinal tract to motor neurons in the cervical region of the spinal cord, hence mediating reflexive movements of the neck that help stabilize the position of the head in space (Merchant, 2011).

Some PCs from the vermal region in lobules I, II, III & IV project to the vestibular nuclei (*see section 4.2.1.3 for a detailed description*) (Voogd, 2016). In addition, it receives inputs from the semicircular canals, utricle, and the inferior olive through CFs collaterals (Ruigrok, 1997). It projects through the spinal cord in the medial parts of the ventral horn of the spinal gray. Tonic excitation of this pathway affects motor neurons that innervates gravity-opposing muscles in the limbs (Merchant, 2011).

2.3.2 The Cerebellar Nuclei

In mice, there are 4 cerebellar nuclei: medial, anterior interposed, posterior interposed and lateral (***Figure 4D***). The lateral part of the medial nuclei and the medial part of the posterior interposed nuclei overlap in a region named *interstitial cell group* (Voogd and Ruigrok, 2004). The cerebellar nuclei compute the output signal from the cerebellum as they integrate inhibitory information from PCs and excitatory inputs from MFs and CFs collaterals (***Figure 6A, 6B***) (Gauck and Jaeger, 2000; Rowland and Jaeger, 2005; Bengtsson et al., 2011; Steuber and Jaeger, 2013; Bengtsson and Jörntell, 2014).

Neurons in the cerebellar nuclei have been classified in six groups that are either projections neurons or local interneurons : glutamatergic, GABAergic nucleo-olivary and glycinergic projection neurons, and local GABAergic and/or glycinergic cells (Czubayko et al., 2001; Uusisaari and Knöpfel, 2008, 2011; Alviña et al., 2009; Bagnall et al., 2009; Tadayonnejad et al., 2010; Zheng and Raman, 2010; Blenkinsop and Lang, 2011; Bengtsson and Jörntell, 2014; Husson et al., 2014). Most of these neuronal types have been described and classified according to their intrinsic biophysical properties (i.e. spike width, after hyperpolarization kinematics and spiking rate) (Uusisaari et al., 2007; Uusisaari and Knöpfel, 2008, 2011; Bagnall et al., 2009; Ankri et al., 2015; Najac and Raman, 2015; Canto et al., 2016).

The cerebellar nuclei project to the motor cortex through the thalamus, the tectum and the red-nucleus (***Figure 5C***) (Allen and Tsukahara, 1974; Schmahmann and Pandya, 1997; Kelly and Strick, 2003; Glickstein et al., 2011).

2.4 Functional connectivity in the cerebellar cortex

The cerebellar cortex integrates numerous types of information to compute efficient motor output. As seen previously (*section 2.1.1*) MFs carry sensorimotor messages to GCs (i.e. input stage) that target PCs (i.e. output stage) with a high degree of convergence. PC synaptic integration of GC inputs are respectively modulated by Golgi cells and MLIs (Ito, 2006). As it will be detailed later (*section 2.4.2*), the selection of relevant GC inputs by PCs is under the control of CF inputs. Despite a wealth of anatomical PF-PC synapses, most of them remain silent (Ekerot and Jörntell, 2001; Isope and Barbour, 2002). Understanding how GC inputs are selected is a major challenge in the cerebellar community and a question I tried to address in my PhD project.

After brief explanation of information flow within the cerebellar cortex (*section 2.4.1*), I will go through functional concepts that provide hypotheses about supporting rules for GC input selection: The Marr-Albus-Ito model for supervised learning (*section 2.4.2*), long term plasticity at PF-PC synapses (*section 2.4.3*) and silent synapses (*section 2.4.4*). Short-term plasticity occurs at PF-PC synapses too, but as they take place in shorter time scales (milliseconds to minutes), they go beyond the scope allowed by the timescale of my results. Therefore, they will not be furthered describe in this manuscript.

2.4.1 Flow of information in the cerebellar cortex

2.4.1.1 Information processing in the granule cell layer

MFs convey vestibular (Arenz et al., 2008), somatosensory (Chadderton et al., 2004; Jorntell and Ekerot, 2006), proprioceptive (Bengtsson and Jorntell, 2009) and tactile (Jorntell and Ekerot, 2006; Bengtsson and Jorntell, 2009) information to GCs (***Figure 6C***) at a wide range of frequencies, from a few Hz (i.e. proprioceptive information) up to 1 kHz (tactile stimuli) (Bengtsson and Jörntell, 2009). MF-GC synapses are contained in the glomerulus (***Figure 6C***) that favors glutamate spillover and synaptic transmission via alpha-amino-3-hydroxy-5-methyl-4-isoxazolepropionic acid (AMPA) receptors activation (DiGregorio et al., 2002). Slow and fast MF discharge patterns are reliably transmitted to GCs (Rancz et al., 2007; Schwartz et al., 2012). In most cases, GCs receive contacts from MFs carrying different modalities (Huang et al., 2013; Chabrol et al., 2015). MF inputs have distinct synaptic properties and shape GC output using a temporal signature: minimal electric stimulation of MFs from the

vestibular nuclei showed that MF combinations are encoded by the first spike latency onset to the stimulation (Chabrol et al., 2015).

2.4.1.2 Information processing in the molecular layer

Some studies have shown that GCs are able to discharge action potentials in a wide range of frequencies, up to 1kHz (Chadderton et al., 2004; Jorntell and Ekerot, 2006; Ritzau-Jost et al., 2014) that can be reliably transmitted to PCs via PFs (***Figure 6D***) (Valera et al., 2012). Thus, PFs can relay MFs information to PCs with a high temporal precision and fidelity, raising the question of signal modulation by GCs. Following PF or GC stimulation, MLIs provide reliable feed-forward inhibition (i.e. a sequence composed of excitation followed by inhibition within 5ms) onto PCs allowing modulation of GC inputs synaptic integration and therefore PCs discharge (Brunel et al., 2004; Mittmann et al., 2005; Grangeray-Vilmint et al., 2018). In addition, recent findings from the lab showed that MLIs are more than synaptic modulators, as their inhibitory influence expands PC dynamic range (Grangeray-Vilmint et al., 2018; Dorgans et al., 2019).

Thanks to MF-GC and MF-GC-MLI mediated inputs, PCs encode several and important aspects of the movement, for instance locomotion kinetics (Powell et al., 2015; Sarnaik and Raman, 2018) or the position of whiskers during voluntary movements (Chen et al., 2016). As PCs are spontaneously active any relevant information should significantly affect their discharge and the output message of the cerebellar cortex. Selection of reliable inputs by PCs is under the control of CFs signals that gate, amongst other, plasticity af PF-PC synapses (*see section 2.4.3*).

2.4.2 The Marr-Albus-Ito cerebellar perceptron for supervised learning

The cerebellar functional microcircuit has been described for the first time by Eccles, Ito and Szentágothai (Ito, 2006). Little after, David Marr proposed the following theory: the cerebellum acts as a supervised learning machine (Marr, 1969) based on a perceptron (***Figure 7***). The perceptron is an algorithm proposed to model neural networks and described by Frank Rosenblatt (Rosenblatt, 1958): several input cells are converging to the output cells in a feedforward manner (***Figure 7***). Each input cell has a given weight, and the linear sum of the weights codes for the general incoming flow of information (i.e. context or pattern). If the good combination of inputs occurs (i.e. pattern of activated PFs) at the good time, the linear sum will reach a given threshold, triggering output cell firing and propagation of the information to the next stage. In addition, the system is able to learn: individual weights can be potentiated or depressed by the action of an external signal. The cerebellar cortex provides a striking

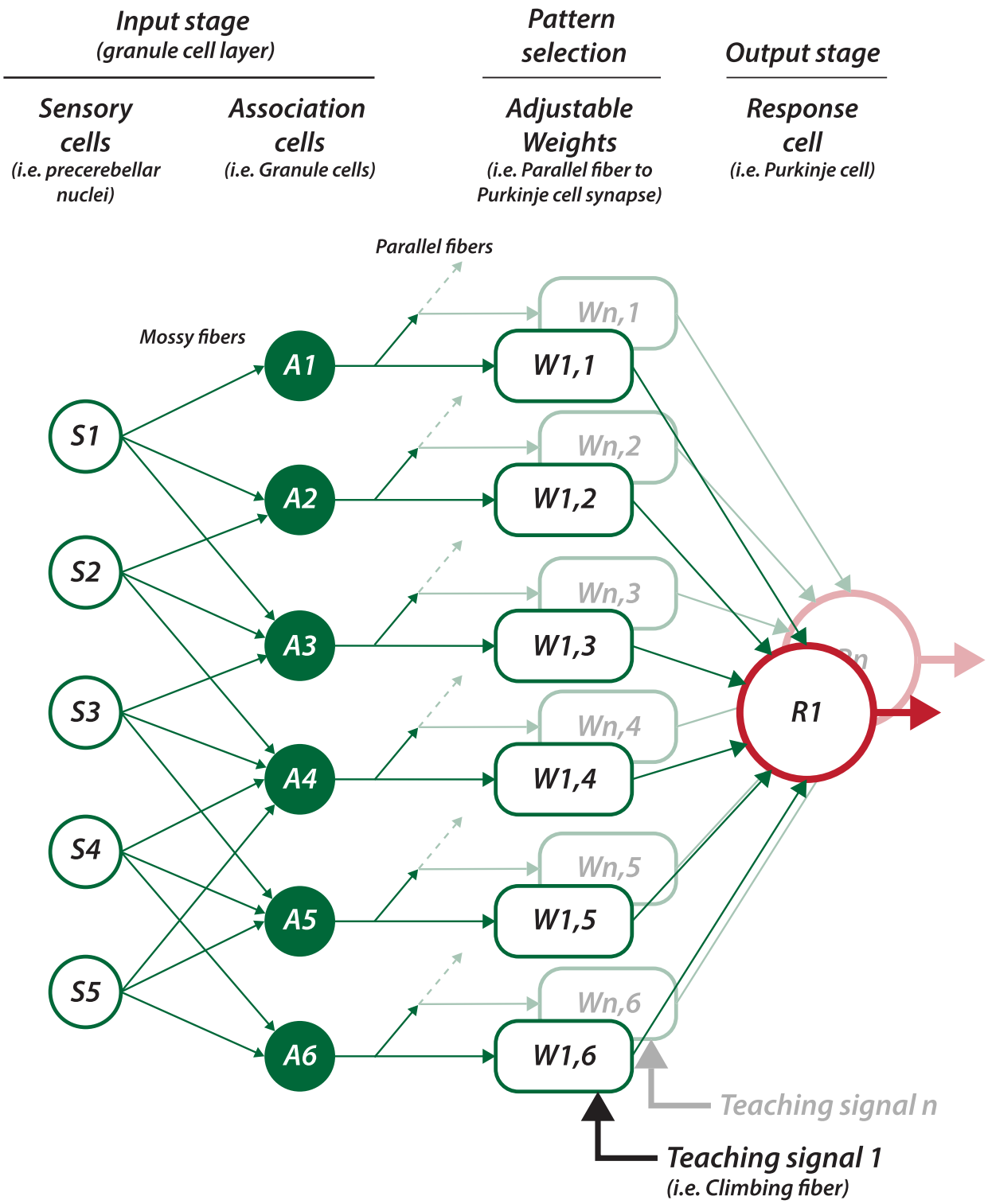

Figure 7 : The Marr-Albus-Ito model for supervised learning

Illustrated pattern-discrimination algorithm applied to the cerebellar cortex. Mossy fibers coming from various precerebellar nuclei (S1 to S5) scatter somatosensory information between several granule cells (A1 to A6) that associate modalities. Both of these elements constitute the input stage of the system, located in the granule cell layer of the cerebellar cortex, acting as a pattern classification device. The Purkinje cell (R1 to Rn) is the sole output of the cerebellar cortex. Parallel fibers to Purkinje cells synapses are tunable under the control of the climbing fiber (teaching signal) : relevant patterns are thus selected. Finally, the Purkinje cell will fire only under a specific sensorimotor context (i.e. pattern discrimination). ***Adapted from Albus, 1971***

support for this algorithm. In Marr's model, the input cells are GCs, PF-PC synapses are weighted and PCs are the output cells (***Figure 7***). PF-PC synapses weights are gated by CFs signals (Marr, 1969).

However, Marr thought that CFs were potentiating PF-PC synapses, which has been refuted by James Albus: conjunctive activation of CFs and PFs on a given PC should depress the PF-PC synapses (Albus, 1971). A decade later, the group of Masao Ito described the plasticity predicted by Albus in rabbits, known as long term depression (LTD) at PF-PC synapses (Ito and Kano, 1982; Ito et al., 1982; Ito, 2001). The Marr-Albus-Ito perceptron algorithm for supervised learning has since been extended and physiologically supported by other groups (Dean et al., 2010; Carey, 2011; Raymond and Medina, 2018). In this cerebellar model, PCs integrate sensorimotor context provided by PFs. The relevance of an input (i.e. a pattern of activated PF) is determined by (1) the activated GC population and (2) the weights or strength of PF-PC synapses.

In supervised learning, the selection of relevant input pattern is under the control of a teaching signal: the CF input (***Figure 7***). Here comes the notion of cerebellar adaptive filter (Dean et al., 2010): the weights of the individual input connections (i.e. PF-PC synapses) can be adjusted at will by an *error* signal provided by the CFs. In other words, CF teaching signals trigger the selection of specific input patterns (***Figure 7***) (Raymond and Medina, 2018; i.e. the group of activated GC firing at the same time): if it is relevant, synaptic weights at the given synapses are reinforced.
In the cerebellum it has been suggested that reinforcement required for motor learning would be a depression of PC-PC synapses (Ito, 2006), but in recent studies potentiation has also been demonstrated (Gutierrez-Castellanos et al., 2017). In addition, the role of CFs has been extended as teaching signal can result from both expected and unexpected stimuli during a learning task (Ohmae and Medina, 2015; Kostadinov et al., 2019).

Recently, Yamazaki and Lennon proposed an extension to the Marr-Albus-Ito model: the cerebellar cortex should be able to perform reinforcement learning in addition to supervised learning. In this learning paradigm, there is no more need for an explicit teaching signal (CFs), instead, learning can occur through responses from an evaluative feedback provided by the MLIs (Yamazaki and Lennon, 2019). The involvement of MLIs in the consolidation of motor learning has already been demonstrated (Wulff et al., 2009).

2.4.3 Long term plasticity at the PF-PC synapses

Synaptic plasticity occur at PF-PC synapses (Jörntell and Hansel, 2006; Gao et al., 2012) and in other synapses within the cerebellar cortex. Both Long-Term Potentiation (LTP) and Long-Term Depression (LTD) have been described and involved in motor learning (Ito, 1984; Coesmans et al., 2004; Jörntell and Hansel, 2006; Carey, 2011; Gutierrez-Castellanos et al., 2017). As PF-PC synapses are a major site of information storage in the cerebellar cortex (Ito, 1984, 2001; Coesmans et al., 2004; Jörntell & Hansel, 2006), unraveling the rules that govern LTP or LTD induction has been a major challenge in the cerebellar community for many years as well as mandatory to understand information processing and selection in the cerebellar cortex.

2.4.3.1 Long term depression

LTD has been the first cerebellar postsynaptic plasticity discovered *in vivo* (Ito and Kano, 1982; Ito et al., 1982) and has been historically studied in the cerebellar-dependent eyeblink conditioning (YEO, 1991; Shibuki et al., 1996; Medina et al., 2002). In this associative learning, the CF input conveys information related to an unconditioned stimulus (e.g. an air puff), while the PF inputs convey information related to the conditioned stimulus (e.g. a sound) (Mauk and Donegan, n.d.; Chen et al., 1996; Yeo and Hesslow, 1998; Carey and Lisberger, 2002).
Concomitant activation of CF and PFs on the same PC leads to depression of PF-PC synapses (Wang et al., 2000; Ito, 2001; Safo and Regehr, 2008). CF inputs induce strong depolarization of PCs yielding significant calcium signaling by (1) calcium influx through voltage-gated calcium channels (opened by the CF/PF inputs) and (2) internal release of calcium through the Phospholipase C (PLC) - Inositol triphosphate (IP3) - Diacylglycerol (DAG) signaling. This second calcium increase is at first triggered by activation of post synaptic mGluR1 receptors (Takechi et al., 1998; Wang et al., 2000). Both IP3/DAG- and voltage-gated channel induced calcium transients will finally activate de Protein Kinase C (PKCα) pathway resulting in internalization of postsynaptic AMPA receptors (Wang and Linden, 2000). LTD at PF-PC synapses can be induced in acute cerebellar slices with multiple stimulation protocols that usually involve high (Piochon et al., 2010) or low (Yamaguchi et al., 2016) stimulation frequency of PF beam coupled with concomitant CF activation in presence of synaptic inhibition antagonists (Jörntell and Hansel, 2006). Other studies nonetheless extended these protocols, highlighting differential results in LTD induction according to the timing between CF and PF stimulation (Suvrathan et al., 2016) and in presence of physiological calcium concentration and synaptic inhibition (Bouvier et al., 2018) or with strong PF stimulation (Hartell, 1996).

2.4.3.2 Long term potentiation

Unlike LTD, LTP at parallel fiber to PF-PC synapses is triggered by PF stimulation only (Coesmans et al., 2004, Jörntell and Hansel., 2006). In this case, membrane depolarization by AMPA receptors opens voltage-gated calcium channels that induce calcium influx through T-type voltage dependant calcium channels (Cav3.1) (Isope and Murphy, 2005; Isope et al., 2012; Ly et al., 2013; Binda et al., 2016) and activate the calcium/calmodulin-activated Protein Phosphatase 2B (PP2B) pathway (Carey and Regehr, 2010). Dephosphorylation of free AMPA receptors should promote their insertion within the postsynaptic membrane. Recently, it has been shown that MLIs would play a major role in LTP establishment, as they would promote potentiation of PF-PC synapses by de-inactivating T-type calcium channels (Binda et al., 2016). In cerebellar slices, LTP of GC-PC synapses can be induced by repetitive high frequency burst of stimulation in PFs (Coesmans et al., 2004) or GCs (Valera et al., 2016).

2.4.3.3 Plasticities interplay

Both LTP and LTD are involved in a wide range of cerebellar-dependent behaviors. LTD is involved in the control of vestibulo-ocular reflex (VOR) gain (Ito, 1982, 1984) and eyelid conditioning (Medina et al, 2002). LTP at PF-PC synapses is also mandatory for proper motor learning and VOR adaptation (Schonewille et al., 2010; Gutierrez-Castellanos et al., 2017).

Studies based on manipulation of sensory receptive fields (Jörntell and Ekerot, 2003; Apps and Garwicz, 2005) predicted behavioral consequences of LTD and LTP in global motor adaptation and learning. In a given cortical column, concomitant activation of PFs and CFs have reciprocal effect on PFs cutaneous receptive field: PF-PC receptive fields are narrowed (i.e. synapses are depressed or silenced) while PF-MLI-PC receptive fields are increased (i.e. synapses are potentiated) (Jörntell and Ekerot, 2002, 2003).

However, genetically preventing LTD induction in mice does not necessarily lead to motor troubles : genetic invalidation of AMPA receptors does not impair VOR adaptation nor eyeblink and locomotor conditioning (Schonewille et al., 2011). As several forms of long term plasticity (both LTP and LTD) coexist at the PF-PC synapse, it has been proposed that they act in synergic fashion, thus impairing one type of LTP/LTD may not necessarily lead to motor learning deficits as it could be compensated by other forms of plasticity (Gao et al., 2012). LTD could nonetheless be established in the mutants described above using different induction protocols *in vitro* (Yamaguchi et al., 2016).

2.4.4 Silent PF-PC synapses

2.4.4.1 Most of PF-PC synapses are silent

The Marr-Albus-Ito model suggest that patterns of GC inputs are detected by PCs, and that the corresponding synapses are selected (or not) under the control of CFs (***Figure 7***). In 2001, Ekerot & Jörntell recorded PC activity in anesthetized cats in response to tactile stimulation and demonstrated that neighboring PCs have different receptive fields for PFs (Ekerot and Jörntell, 2001). Then the effective PF input to a Purkinje can only correspond to a few per cent of the total number of cutaneously activated PFs making synaptic contact with the cell. They concluded that most of the PF-PC synapses do not elicit measurable responses, they are silent. These findings were first quantified *in vitro* by Isope & Barbour (Isope and Barbour., 2002; Brunel et al., Neuron 2004) who recorded GC-PC pairs in rats : they estimated that ~85% of PF-PC synapses are silent. Indeed, when stimulating GCs 40µm away from the PC dendritic axis, the probability to find an active synapse drops below 10% (Isope and Barbour, 2002). Active unitary synapses showed an average response in PCs of 8.4 ± 7.1 pA, while large unitary responses (~60pA) were only found for local GCs (Isope and Barbour, 2002).

Silent synapses can rely on two mechanisms: the synapse can either be *mute* (no presynaptic release) or *deaf* (no postsynaptic receptors). Current experiments in the laboratory are performed in order to determine which mechanism is involved at the GC-PC synapses.

2.4.4.2 Evaluating the role of PFs: controversies in the litterature

Whether local or distant GC inputs would drive a single PC has been debated in the litterature. Ekerot and Jörntell claimed that PCs were actively driven by GCs located away from the PC somas (Ekerot and Jörntell, 2001; Jörntell and Ekerot, 2002). Other groups suggested the opposite idea : functional GC inputs are located within the PC dendritic axis (Brown and Bower, 2001; Isope and Barbour, 2002). But if GC inputs are only locally distributed, why would PFs run on long distances to cross hundreds of PCs? (Harvey and Napper, 1991). Glutamate uncaging on acute cerebellar slices nonetheless revealed that PCs are functionally contacted by local and distant GCs at the same time, suggesting that both type of inputs are relevant and should be considered for PCs synaptic integration (Walter et al., 2009; Valera et al., 2016).

The anatomy of PFs leads to another controversy in the litterature: the beam vs the patch hypothesis. The beam hypothesis was originally proposed by Braintenberg & Atwood (Braitenberg and Atwood, 1958; Eccles et al., 1967). In this theory, excitatory GC inputs would depolarize every PC they cross inducing a depolarising tidal wave (hence the *beam* excitation). However, experiments showing that PFs do not make synapse on every PC they cross (probability ≈ 0.5 according to Napper & Harvey, 1989) and that most of GC-PC synapses are silent (Ekerot and Jörntell, 2001, Isope and Barbour, 2002) explain why the beam hypothesis could not be physiologically observed *in vivo*.

The patch hypothesis results from functional observations: peripheral stimuli (i.e. cutaneous or nociceptive) elicit significant discharge in PCs, MLIs and GCs located in the same location (Shambes et al., 1978; Bower and Woolston, 1983; Brown and Bower, 2001) within a restricted column-wise orientated portion of the cerebellar cortex. This theory is linked to the following idea : the ascending axon from GCs would have a specific properties leading to PC preferential integration of signal originating in GCs located in the same microzone (see *section 7.3.4 for discussion*) (Gundappa-Sulur et al., 1999).

2.5 Development of the cerebellar cortex

This section reviews the main stages of embryonic and postnatal development of cerebellar inputs, neurons and patterning in rodents. The development of the cerebellar cortex starts at the embryonic stage and terminates within the first weeks of life in mice. In humans as well, neural cells start to colonize the future cerebellum at around 10 weeks of gestation, and histological changes have been reported up to 13 months after birth (Friede, 1973). A wealth of the information relative to the development of cerebellar neurons come from the extensive work and literature provided by Joseph Altman (Altman, 1972a, 1972b, 1972c, 1982; Altman and Bayer, 1985, 1987) and Constantino Sotelo (Nunes and Sotelo, 1985; Nunes et al., 1988; Bourrat and Sotelo, 1991; Chedotal and Sotelo, 1993).

2.5.1 Development of cerebellar afferents

CF & MF pathways are developed at different time scales: CFs start developing earlier, and still undergoes morphological and wiring maturation while the adult topography of MF inputs seems to be established after 1 week of life in mice.

2.5.1.1 Development of the CF pathway

Olivary neurons are amongst the first neurons of the olivo-cerebellar system to be generated, around embryonic day 12 to 13 (E12-E13) (Altman, 1982; Bourrat and Sotelo, 1991). Their axons extend through the brainstem and invade the cerebellar cortical plate by E17 to contact PCs (Chedotal and Sotelo, 1993). These projections are already broadly organized in a topographical fashion: PCs express molecular cues along the anteroposterior and rostro caudal axis that guide the incoming CFs (Chédotal et al., 1997). At embryonic stage, CFs contact PCs from E20, suggesting a very early influence of the inferior olive in the cerebellar cortex (Chedotal and Sotelo, 1993).

At the postnatal stage, CFs undergo 5 critical steps of development (***Figure 8B***) (Hashimoto and Kano, 2005; Leto et al., 2016) :

- (1) *the creeper stage (**Figure 8B**)* : CFs start to creep onto PCs transient arborescence, establishing peri somatic but functional synaptic contacts (Crepel et al., 1976). Most of the CFs make contacts with several adjacent PCs, hence starts the multi-innervative CF process (Crepel et al., 1976; Chedotal and Sotelo, 1993).
- (2) *the pericellular nest stage:* around postnatal day 5 (P5), CFs establish nests around PC somas (Chedotal and Sotelo, 1993). On average, 3.5 CFs establish synaptic contacts on PC peri somatic processes (Mariani and Changeux, 1980; Chedotal and Sotelo, 1993).
- (3) *the capuchon stage:* around P9, CFs terminals switch from the soma to the PC primary dendrites (somatodendritic translocation). Multi-innervation on several PCs is decreased by 50% (Crepel et al., 1976; Chedotal and Sotelo, 1993).
- (4) *the immature stage:* between P10 and P14 the final synaptic translocation occurs, transients CFs degenerate to reach the 1:1 CF/PC ratio know in the adult (Mariani and Changeux 1980; Chedotal and Sotelo, 1993). During this period, CFs display either weak or very strong synaptic inputs. The CF with the most dominant synaptic contact is selected and innervates the PC during the adult stage (Hashimoto and Kano, 2005).
- (5) *the adult stage:* a single CF provides hundreds of functional synaptic contacts on the PC dendritic tree (Hashimoto and Kano, 2005).

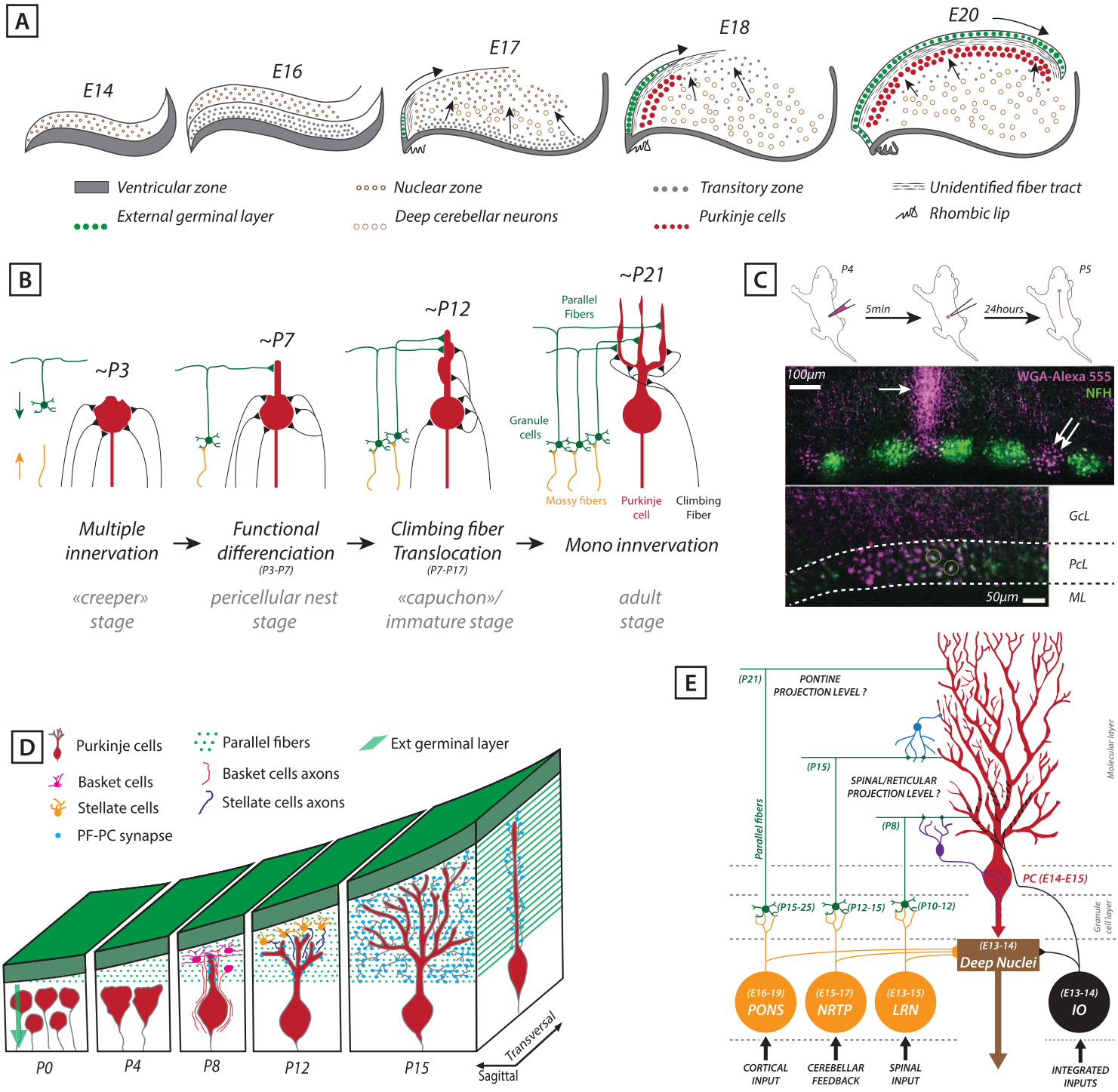

Figure 8 : Embryonic and postnatal development of the rodent cerebellar cortex

(A) Summary diagram of the major steps in the prenatal development of the cerebellum. The deep nuclei neurons are postulated to derive from the earlier generated and differentiating nuclear zone. The Purkinje cells are initially gathered in a transitory zone and then migrate to the surface beneath the spreading ext. germinal layer to form the primitive cortex. ***Adapted from Altman, 1982.***

(B) Diagram showing postnatal development of CF-PC synapse. Until P3, synaptic strengths of multiply-innervating CFs are relatively uniform. From P3 to P7, one CF is selectively strengthened, which is termed the phase of functional differentiation. From P9 on, the strongest (*winner*)CF undergoes translocation to growing dendrites (the phase of CF translocation). On the other hand, weaker (*loser*) CFs remain around the soma and are eventually eliminated in two distinct phases (the early and late phases of CF elimination). ***Adapted from Leto et al, 2016.***

(C top) Schematic illustrating the injection of WGA-Alexa 555 into the spinal cord of a pup. *(C down)* WGA-Alexa 555 tracing of spinocerebellar mossy fibers (arrow) and transsynaptic tracing of neuronal somata (double arrow) in the anterior cerebellum. NFH staining revealed a pattern of zones that was complementary to a subset of traced Purkinje cells. Some of the WGA-Alexa 555-traced neuronal somata were co-labeled with NFH, a marker for Purkinje cells (yellow circles). ***From Sillitoe, 2015.***

(D) Postnatal development of PCs dendrites. Granule cells migrate from the ext germinal layer (green arrow), spreading parallel fibers while basket and stellate cells help to form the dendritic tree. PF-PC synaptogenesis starts at P7. ***Adapted From Altman, 1982.***

(E) Summary diagram of the temporal relationships between the cytogenesis of some precerebellar nuclei (the external cuneate nucleus not included) and the cerebellum. The dates are based on the studies described in the text; the selective connections of parallel fibers of the upper and lower molecular layer with mossy fi bers of different origins are hypothetical. ***Adapted from Altman, 1982.***

BC : *basket cells,* ***CF :*** *climbing fiber,* ***E# :*** *embryonic day #,* ***GcL :*** *Granule cell layer,* ***IO :*** *Inferior olive,* ***LRN :*** *lateral reticular nucleus,* ***ML :*** *molecular layer,* ***NRTP :*** *nucleus reticularis tegmenti pontis,* ***P# :*** *postnatal day #,* ***PC :*** *Purkinje cell,* ***PcL :*** *Purkinje cell layer,* ***PF :*** *parallel fibers,* ***SC :*** *Stellate cells*

GCs and PFs are highly involved in the CF degeneration. Indeed, the development of functional GC-PC synapses helps to regulate the elimination of the transient CFs (***Figure 8B***) (Mariani and Changeux, 1980; Sugihara et al., 2000; Hashimoto and Kano, 2005).

2.5.1.2 Development of the MF pathway

Little is known about the development of MFs during the embryonic stage. However, Altman established the date of birth of several precerebellar nuclei: reticular and dorsal column nuclei neurons are born between E12 and E15, while pontine nuclei neurons start to be generated strictly after E15 and settled in their final location within E20-E22 (***Figure 8E***) (Altman, 1982). Nunes & Sotelo studied the postnatal development of the spinocerebellar tract in rodents (Nunes and Sotelo, 1985). They reported 4 stages of progression in the anterior vermis :

- (1) At P1, MFs from the spinocerebellar pathway reach the white matter within the cerebellum.
- (2) In what the authors call a *waiting phase*, between P1 and P3, MFs become denser in the anterior and posterior vermis but do not reach the grey matter (inner granule cell layer).
- (3) Between P3 and P5 occurs the *proto columnar stage*, in which MFs migrate into the inner granule cell layer, forming rough parasagittal bands. At this stage, the inner granule cell layer is not completely formed, few GCs are present, and MFs realize transient contacts with PCs (Altman, 1982b). PCs organization was proposed to guide the distribution of incoming MFs (Ji and Hawkes, 1995). Electronic microscopy revealed mature synapses ultrastructure between MF terminals and GCs at the end of this stage, although Altman and Bayer reported biochemical matureness of those synapses around P15 (Altman and Bayer, 1987).
- (4) Between P5 and P7 the rough column-wise organization of MF projections gets refined, leading to the pattern known in the adult, correlated with the appearance of mature *rosettes* that connect to GCs (***Figure 8B, 8C***) (Leto et al., 2016)

Thus, the adult projection pattern of the spinocerebellar tract is reached as soon as P7 (Nunes and Sotelo, 1985). This has been later confirmed by Roy Sillitoe (***Figure 8C***) who suggested that, as for CFs, PCs may generate a zonal wiring by using molecular cues, neuronal activity and/or synaptic contact (Sillitoe, 2015).

2.5.2 Development of neurons in the cerebellar cortex

Cerebellar cortical neurons are derived from two germinal zones. Inhibitory neurons such as PCs, Golgi cells and MLIs are born within the ventricular zone : the neuroepithelium that will

in the end form the roof of the 4th ventricle (***Figure 8A***) (Butts et al., 2014; Rahimi-Balaei et al., 2018). On the other hand, the rostral rhombic lip located at the dorsal edge of the cerebellar primordium generates the external germinal layer, that gives birth to excitatory neurons of the cerebellum: GCs and unipolar brush cells (***Figure 8A***) (REF Rahimi-Balaei et al, 2018).

2.5.2.1 Embryonic and postnatal development of PCs

PCs start migrating from the ventricular zone at E13 (***Figure 8A***) (Altman, 1975). They reach the cerebellar cortical plate through radial migration (Rahimi-Balaei et al., 2018) at E20, passing through the immature cerebellar nuclei (***Figure 8A***), establishing synaptic contacts with nuclear neurons and growing up their axons (Leto et al., 2016).

At birth (P0), most of PCs are installed in the cerebellar cortex but forming a 6 to 12 cells-stacked layer (Altman and Bayer, 1987). Based on optic and electronic microscopy and histological stainings, Joseph Altman described 5 phases of PC postnatal development (***Figure 8D***, Altman, 1972b):

- (1) from P0 to ~P4: **PCs progressively form a monolayer.** Their soma is shaped to favor a stationary position rather than a migrating one: the apical pole starts to grow.
- (2) from ~P4 to ~P8: **PCs grow a transient apical cone and peri somatic processes**. Transient parallel fibers synapses are established on the apical cone, as in the adult they branch on tertiary branchlets spines only. CFs establish transient contacts with PCs peri somatic processes (this corresponds to the *pericellular nest stage described in 2.5.1.1*).
- (3) from ~P8 to ~P12: **the synaptic domain of PC soma enters maturation**. Indeed, many synapses from basket cells are observed, as well as significant glial wrapping. The transient apical cone shows maximal enlargement, coupled with the outgrowth of primary dendrites and a few smooth branchlets, but PF-PC synapses remain quite rare.
- (4) from ~P12 to ~P15: **maturation of the lower synaptic domain**. At this stage, it is possible to discriminate between the upper and the lower part of PC synaptic trees. PFs and lower stellate cells are contacting this latter part of the dendritic tree.
- (5) from ~P15 to P21: **maturation of the upper portion of PC dendrites**. Many PFs and stellate cells synapses contact the upper part of PC dendritic tree.

PCs undergo massive morphological changes during postnatal development and reach their famous mature dendritic arborization after 3 weeks of life (***Figure 8E***). They acquire pacemaker firing activity within the first days of life, although at a lower firing rate than in adults which progressively reach adult firing rate at ~4 weeks old in rodents (Jayabal and Watt, 2019).

2.5.2.2 Embryonic and postnatal development of GCs & PFs

During embryonic development, GC progenitors are located within a transient layer, formed around E20 (***Figure 8A***): the *external germinal layer*, located at the surface of the cerebellar cortex (***Figure 8D***). In the literature, the term *external granule cell layer* can be found, but has been judged inappropriate and misleading by Altman (Altman, 1972a) as this layer remains transitory and generates other cell types than the GCs. This layer can be subdivided in two parts: (1) the proliferative zone, located externally, that contains mitotic neurons progenitors and stem cells and (2) the premigratory zone, located internally, that packs the PFs forming the future molecular layer (***Figure 8D***) (Altman, 1972a).

At birth, once post-mitotic GCs have been generated within the proliferative zone, they start radial migration along Bergmann glial cells processes through the premigratory zone, piling up underneath PCs (Altman, 1982). As they cross the premigratory zone/molecular layer, GC axons start growing along the mediolateral axis: PFs are born. The soma continues to migrate radially to reach the GC layer, growing what will be the future ascending axon. PFs get stacked as the premigratory zone/molecular layer expands in thickness, and PC dendritic trees grow up (***Figure 8D***) (Altman 1972a). The date of birth/migration of GCs determines their position in the molecular layer: early born GCs will have their PFs in the lower part of the molecular layer (***Figure 8E***) (Altman, 1982). Molecular layer expansion and GC migration occur up to P21, and the external germinal layer has fully disappeared at P30 (Altman, 1982; Rahimi-Balaei et al., 2016). Functional PF-PC synapses have been reported as early as P7 (Scelfo and Strata, 2005).

Based on precerebellar neurons birth date and MF migration in the GC layer, Altman speculated and predicted the topography of precerebellar modalities on PC dendritic trees. According to him, spinocerebellar and reticular MFs should connect GCs that project in the lower part of PC dendrites, while pontocerebellar MFs should project in the upper part of the molecular layer (***Figure 8E***) (Altman, 1982).

2.5.2.3 Postnatal development of MLIs

Precursors of stellate and basket cells are born in the ventricular zone. Thereafter they migrate to the cerebellar white matter postnatally, while undergoing cell division (Rahimi-Balaei et al., 2018). Then they migrate radially and get stacked to the transient molecular layer (a.k.a. the premigratory zone described in 4.2.2) (REF Altman 1972a; Rahimi-Balaei et al., 2018). Stellate

and basket are thought to have distinct role in the development of the PC dendritic tree. Perpendicular outgrowth of the primary PC dendrites is promoted by basket cells providing a channel through the bed of PFs. Stellate cells help to the expansion and growth of secondary smooth branches (***Figure 8D***) (Altman, 1982).

2.5.3 Development of modular patterning in the cerebellar cortex

Ontogeny recapitulates phylogeny was Haeckel's answer to the link between species. The cerebellum displays modular compartmentalization (*see section 3 for detailed description*) conserved across birds and mammals (Sillitoe et al., 2005). This modular organization relies on the topography of CFs inputs, forming parasagittal bands in the cerebellar cortex (Apps and Hawkes, 2009; Voogd, 2011). One could ask if CFs topography are developmentally driven. Indeed, olivo-cerebellar projection are already organized in para-sagittal bands in neonatal rodents (Sotelo et al., 1984).

When looking at Zebrin II (ZII) (*see section 3.2.1*) expression in PCs during development, Hashimoto & Mikoshiba found that two different clusters of post mitotic PCs were generated in the ventricular zone (Hashimoto and Mikoshiba, 2003). Indeed, the birthdate of PCs determine their ZII identity: early-born cells (E10 to E11.5) will be ZII-positive while late-born cells (E11.5-E13) will be ZII-negative cells. These embryonic clusters get dispersed up to P5 (Apps and Hawkes, 2009). Moreover, in the vermis, PCs acquire their definitive position once they migrated in the cerebellar cortex: they maintain their original mediolateral position in adulthood (Sgaier et al., 2005). Thus, PC spatial location helps for the selection of CF inputs. The molecular identity of the postsynaptic neuron is important to guide and select migrating CF inputs (Sotelo, 2004).

It seems that PCs are important for proper MF wiring too : for example, in mutants that lack ZII+ PCs, aberrant spinocerebellar projections have been observed in the vermis (Nunes et al., 1988; Chédotal et al., 1997; Sotelo, 2004). Indeed, PCs may guide incoming MFs through transient synaptic contacts (Altman, 1982 ; Sillitoe, 2005).

Taken together, this information supports an input-specific driven model: PCs may be responsible for the development of modular organization and projection maps within the cerebellar cortex. They may fulfil this role through molecular, functional or synaptic cues that yet have not been described (Leto et al., 2016).

3. Modular organization of the cerebellum

The cerebellum is described as the repetition of microcircuits associated in parallel, the cerebellar modules (***Figure 9A***). They are thought to be functional units for information processing (Apps and Garwicz, 2005 ; Voogd, 2011). As seen in section 2, the cerebellar cortex is composed of a few cell types, which would at first sight support weak anatomical or functional diversity. However, studies in the last decades showed numerous architectonic variations (reviewed in Cerminara et al., 2015) and striking functional discrepancies within cerebellar circuitry (Wadiche and Jahr, 2005; Xiao et al., 2014; Zhou et al., 2014; Valera et al., 2016).

My project was dedicated to the understanding of communication rules between cerebellar modules within the cerebellar cortex. When I started to study the cerebellum in 2015, the definition of the cerebellar module was not really clear in the literature, I could often read the following terms: *modules*, *micromodules*, microzones, *zones* or even *multizonal microcomplex* (this last item sounds absolutely barbaric to me). Because the somatotopic organization of the cerebellum has been studied at different scales by different groups, several terms were defined. Richard Apps & Richard Hawkes wrote an article in 2009 to propose a unified modular framework within the cerebellum (Apps and Hawkes, 2009). At the end of 2018 under the initiative of Tom Ruigrok, Richard Apps & Richard Hawkes, we wrote a consensus paper gathering current views and evidence in the literature, in order to clarify the nomenclature and concepts relative to the cerebellar modular organization (Apps et al., 2018). I had the privilege to contribute to this exciting and interesting topic (*see Appendix 5*).

3.1 Modules, zones and microzones in the cerebellum

In this section I will describe the different scales and terminology available in the literature referring to the modular organization of the cerebellum. The cerebellar modules have been identified both with anatomical (i.e. with tracing studies) and functional (i.e. with electrophysiology) approaches.

3.1.1 The cerebellar module

The cerebellar modules are thought to be the functional processing units of the cerebellum (Oscarsson, 1979; Apps and Garwicz, 2005; Apps and Hawkes, 2009; Apps et al., 2018) : they receive spatially segregated inputs, and they target a precise location, hence they are dedicated to a given task (Ruigrok, 2011). Indeed, the definition of the anatomical cerebellar modules is given by to the topography of the inputs and the outputs. It involves three interconnected networks (***Figure 9A***) (Apps and Hawkes, 2009 ; Apps et al., 2018):

- (1) **the inferior olive**: a subset of olivary neurons synchronized by gap junctions send **CFs** to
- (2) longitudinal clusters of **PCs in the cerebellar cortex** targeting
- (3) **clusters of neurons within the cerebellar nuclei or vestibular nuclei** that send collaterals to the olivary neurons mentioned in (1) (***Figure 9A***).

The first report for a topographical projection between the inferior olive, the cerebellar cortex and the cerebellar nuclei date from the 40s, with the work of Brodal and Jansen (as written by Jan Voogd in Apps et al., 2018). They described the projections from the accessory olive to the paravermis that project to the interposed nucleus in monkeys (Jansen and Brodal, 1940). This was the first demonstration of a somatotopic organization within the cerebellum. It has been confirmed that the modular organization follows the macroscopic subdivisions of the cerebellum : sub-nuclei of the olive project in a somatotopic fashion to the medial/lateral vermis, the paravermis and the hemispheres which project respectively to the medial cerebellar nuclei, the lateral vestibular nucleus the interposed nuclei and the lateral nuclei (Voogd and Ruigrok, 2004; Apps et al., 2018). Jan Voogd defined the first nomenclature : zones were named A, B, C & D along the mediolateral axis of the cerebellum (***Figure 9A***) (Groenewegen and Voogd, 1977; Ruigrok, 2011). Modules are task-related units based on their inputs/outputs relationships (Cerminara and Apps, 2011). The selective disruption or lesions of one of them lead to focal and motor deficits in rodents (Pijpers et al., 2008) and humans (Delmaire et al., 2007).

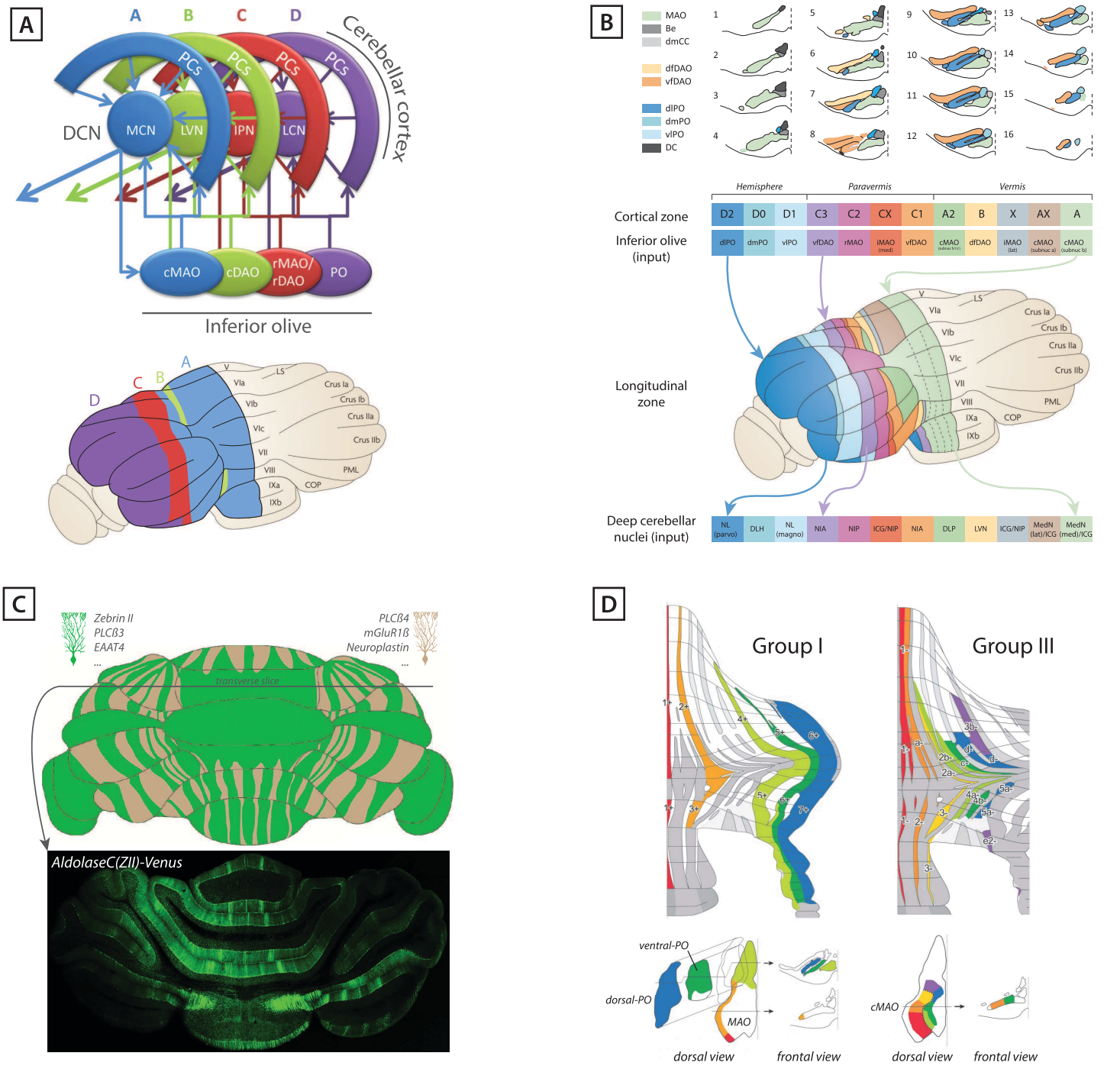

Figure 9 : Modular organization in the cerebellum

(A top) The cerebellar module or olivo-cortico-nuclear loop. The topographical relationship between nuclei of the interior olive, the cerebellar cortex and the deep cerebellar nuclei (*DCN*) defines 4 cerebellar modules. *(A down)* Corresponding cerebellar surface. ***Adapted from Apps et al, 2018 and Apps & Hawkes, 2009.*** *(B top)* Frontal sections of the rodent inferior olive, highlighting the olivary subnuclei. Slices go from rostral (1) to caudal (16). *(B down)* The longitudinal cerebellar zones, as named by Jan Voogd, and corresponding anatomical olivary inputs and outputs (deep cerebellar nuclei). ***Adapted from Apps & Hawkes, 2009.*** *(C top)* Zebrin band patterns and corresponding molecules. ***Adapted from Cerminara et al, 2015***. *(C down)* Transverse slice of ALDOC-Venus mouse cerebellar cortex, revealing ZII+ Purkinje cells (*in green*). ***Adapted from Apps & Hawkes, 2009*** *(D)* Zebrin bands as markers of longitudinal zones boundaries. Unfolded view of projecting climbing fibers (*top*) and corresponding injection sites in the inferior olive (*down*). Climbing fibers from the group I project to ZII+ Purkinje cells, while group III climbing fibers project to ZII- Purkinje cells. ***Adapted from Sugihara & Shinoda, 2004.***

I to X: *cerebellar lobules.* ***1/1+ to 7/7+*** *: Zebrin positive bands.* ***r/cMAO/DAO*** *: rostral/caudal Medial/Dorsal Accessory Olive,* ***PO*** *: Principal Olive,* ***MCN*** *: Medial Cerebellar Nuclei,* ***LVN*** *: Lateral Vestibular Nucleus,* ***LCN*** *: Lateral Cerebellar Nuclei,* ***IPN*** *: Interposed Nuclei,* ***cMAO*** *(subnuc a), subnucleus a of caudal medial accessory olive;* ***cMAO*** *(subnuc b), subnucleus b of caudal medial accessory olive;* ***cMAO*** *(subnuc b1/c), subnucleus b1 and c of caudal medial accessory olive;* ***COP****, copula pyramidis;* ***dfDAO****, dorsal fold of dorsal accessory olive;* ***DLH****, dorsolateral hump;* ***DLP****, dorsolateral protuberance of medial nucleus;* ***dlPO****, dorsal lamella of the principal olive;* ***dmPO****, dorsomedial subnucleus of the principal olive;* ***EAAT4*** *: excitatory amino-acid transporter type 4;* ***ICG****, interstitial cell group;* ***iMAO*** *(lat), lateral part of intermediate medial accessory olive;* ***iMAO*** *(med), medial part of intermediate medial accessory olive;* ***LVN****, lateral vestibular nucleus;* ***LS****, lobulus simplex;* ***MedN (lat)****, lateral part of medial nucleus;* ***MedN (med)****, medial part of medial nucleus;* ***mGluR1ß*** *: metabotropic glutamate receptor type 1ß,* ***NIA****, nucleus interpositus anterior;* ***NIP****, nucleus interpositus posterior;* ***NL (magno)****, magnocellular part of lateral nucleus.* ***NL (parvo)****, parvocellular part of lateral nucleus;* ***PLCß3/4*** *: Phospholipase Cß3/4;* ***PML****, paramedian lobule;* ***rMAO****, rostral medial accessory olive;* ***vfDAO****, ventral fold of dorsal accessory olive;* ***vlPO****, ventral lamella of the principal olive*

3.1.2 CF zones and microzones

Cerebellar modules combine neurons and projections from the inferior olive, the cerebellar cortex and the cerebellar nuclei. They were the first concept relative to modular organization in the cerebellum. Using anatomical tracing, and fine study of the myelo architectural structure in the cerebellar cortex, Jan Voogd defined this modular organization and described seven parasagittal zones in the ferret (Voogd, 1967) and in the cat (Voogd et al., 1969). These fine olivo-cerebellar projections have since been established in rodents (***Figure 9B***) (Sugihara and Shinoda, 2004; Voogd and Ruigrok, 2004) and in mice (Schonewille et al., 2006; Sugihara and Quy, 2007): CFs from olivary nuclei target multiple lobules within the parasagittal plane.

This longitudinal topography suggests a parasagittal information processing : a single olivary neuron sends multiple CF collaterals (van der Want et al., 1989) to PCs through different lobules in the anteroposterior axis (***Figure 5B***). CF inputs topography tends to support parallel information processing, however associative processing (i.e. that involves neighboring zones) has been observed. In some cases the olivary projections spread information across zones, as in the paravermis : where adjacent zones share the same CF inputs (Voogd et al., 2003). Very precise injections to label few olivary neurons at once resulted in narrow parasagittal bands in rodents (***Figure 9D***) (Sugihara and Shinoda, 2004) and in mice (Quy et al., 2011). Parasagittal (or longitudinal) zones refer to the cortical part of the cerebellar modules only: longitudinal PC stripes receive inputs from a given subset of olivary neurons, and project to subregions of the cerebellar nuclei. The zones identified by the group of Izumi Sugihara are more discrete (i.e. narrower) than longitudinal zones previously established, suggesting that parasagittal zones may be divided in smaller units: anatomical microzones.

In the 70s, Olov Oscarsson predicted this refinement: anatomical zones could be subdivided, but by functional considerations (Oscarsson, 1979). His group recorded PC activity in cats, while mapping cutaneous CF receptive fields. Thus, they could for instance segregate the B zone in smaller regions (Andersson and Oscarsson, 1978a) : the classical subdivision of the inferior olive can be refined to distinguish smaller functional units, hence introducing the concept of functional microzone. This confirmed the previous results (Armstrong et al., 1974) and has since been largely studied by other groups (Ekerot et al., 1995; Garwicz et al., 1998b; Trott et al., 1998a, 1998b; Ekerot and Jörntell, 2001) using electrophysiological mappings and/or neuronal tracings in cats and rats. These findings have since been reported in mice using two-photon calcium imaging (Ozden et al., 2009; Schultz et al., 2009; Tsutsumi et al., 2015).

Nowadays, by combining data from anatomical tracings and electrophysiological mappings, 12 different parasagittal zones have been identified, named from medial to lateral: *A, AX, X, B, A2, C1, C2, CX, C3, D1, D0* and *D2* zones (***Figure 9B***) (Sugihara and Shinoda 2004 ; REF Apps and Garwicz 2005 ; REF Apps and Hawkes, 2009). As a consensus, microzones are defined by zones of PCs that share similar olivary receptive fields (Apps et al., 2018).

3.1.3 The functional olivo-cortico-nuclear closed loop

Cerebellar modules and zones are defined by strict topographical relationships between the inferior olive, the cerebellar cortex and the deep cerebellar nuclei (***Figure 9A***). Olivary neurons are electrically coupled via gap junctions (Sotelo et al., 1974; Van Der Giessen et al., 2006) and display oscillatory synchronisation (Lefler et al., 2014). Little is known about the extension of functional oscillatory behaviors within the olive and thus in what extent olivary neurons could synchronize different cerebellar modules.

Many studies highlighted the fact that cerebellar nuclei neurons project back to the inferior olive in a functional and efficient way (Ekerot and Larson, 1979; Garwicz and Ekerot, 1994; Uusisaari and De Schutter, 2011; Lefler et al., 2014; Najac and Raman, 2015), illustrating the concept of functional olivo-cortico-nuclear loop.
Chaumont and colleagues brought an ultimate step in the comprehension of this loop: they optogenetically synchronized PCs firing while recording the cerebellar cortex and the targeted cerebellar nuclei (Chaumont et al., 2013). They could observe light-induced inhibition in the cerebellar nuclei, followed by a ~100ms delayed CF response in the PCs: the olivo-cortico-nuclear loop is therefore a closed loop (***Figure 9A***).

3.2 Molecular stripes in the cerebellum

The cerebellum shows another form of compartmentalization based on differential expression of neurochemical markers essentially in PCs. An alternate expression defines striped patterns at the surface of the cerebellar cortex (***Figure 9C***). The first evidence of such patterns was published by Scott in the 60s : 5'-nucleotidase staining shows parasagittal bands in the molecular layer (Scott, 1965). In the following decades, other molecules were found to show a differential expression in several cell types: PCs, GCs, Bergmann glia, MFs, unipolar brush

cells and Golgi cells (Cerminara et al., 2015). One question remains: do these molecular markers spatially overlap and define a combinatorial code or do they show singular expression? More important, how can they be related to the anatomo-functional organization of the cerebellar modules?

3.2.1 PCs molecular clusters: The Zebrin bands

The discovery of the stripped pattern of 5'-nucleotidase has been followed by the identification of several other markers. More than 10 markers have been highlighted, including heat shock protein 25; cocaine and amphetamine regulated transcript, metabotropic glutamate receptors (mGluRs), excitatory amino acid transporter (EAAT4), phospholipase C beta 3 and 4 (PLCβ3,PLCβ4), type 1 inositol 1,4,5-trisphosphate receptor, protein kinase C (PKC), neuroplastin, GABA receptors, acetylcholinesterase, neurogranin and various other transgenes (for original papers and review see Cerminara et al., 2015). All these markers are involved in different physiological processes but they all share one equivalent feature: they are differentially expressed by subsets of neighboring PCs, dividing the cerebellar cortex into array of rostrocaudally oriented bands or stripes (***Figure 9C***, Cerminara et al., 2015 ; Apps and Hawkes, 2009).

The most studied member of these markers is the Zebrin II (ZII) (***Figure 9C***) (Apps and Hawkes, 2009). It has been discovered by Richard Hawkes (Hawkes et al., 1985) who gave the name Zebrin to this family of molecular markers, due to the zebra-aspect of a whole mounted cerebellum after immunostaining (***Figure 9C***). Later, the ZII has been subsequently identified as Aldolase C (Ahn et al., 1994), a respiratory enzyme implicated in fructose metabolism. The cerebellar cortex shows a canonic array of alternated ZII+ (PCs expressing ZII) and ZII- (PCs lacking ZII) rostrocaudally orientated bands along the mediolateral axis (***Figure 9C***). Zebrin bands have been named depending on their location from the midline : the first band (on the midline) is ZII positive, hence named P1+, the second band, named P1- , is negative, the third band is the second positive band from the midline, hence name P2+ and so on up to P7+ in the hemispheres (***Figure 9C, 9D***) (Hawkes and Herrup, 1995; Sugihara and Shinoda, 2004; Sugihara and Quy, 2007).

The AldolaseC/ZII pattern is remarkably conserved over species from fishes to primates (although some minor differences, and exception for amphibians, Sillitoe et al., 2005 ; Apps and Hawkes, 2009). Moreover, other Zebrins such as PKC, PLCβ3 or EAAT4 share the exact

same pattern than AldolaseC/ZII, while for instance PLCβ4 or mGluR1β display an opposite pattern (***Figure 9C***) (Cerminara et al., 2015).

3.2.2 Anatomo-functional relevance of the Zebrin band pattern

Congruence of CFs and MFs with the Zebrin band pattern have been reported in the *copula pyramidis* and the paramedian lobule (Voogd et al., 2003). The group of Izumi Sugihara showed that this statement could be extended to the entire cerebellar cortex for the CFs, highlighting a tight relationship between olivo-cerebellar projections and the Zebrin bands (***Figure 9D***) (Sugihara and Shinoda, 2004 ; Sugihara and Quy, 2007 ; Apps and Hawkes, 2009).

PCs molecular identity seem to be related to the topography of CF afferences. Boundaries of specific groups of CF projecting to longitudinal bands of PCs remarkably match the Zebrin band pattern. This feature is at the base of Sugihara and Shinoda's description of 5 groups of olivary neurons projecting to specific zebrin bands (Sugihara and Shinoda, 2004). Some groups of olivary neurons project to ZI+ PCs only, with a preference for the anterior (***Figure 9D***, Group I) or the posterior cerebellar cortex (***Figure 9D***, Group II). Group III olivary neurons project only to ZII- PCs, and Group IV consists of mixed ZII+/ZII- mixed projections restricted to the paravermis and hemispheres (Sugihara and Shinoda, 2004).

Thus, Zebrin bands are a reliable tool to identify the cerebellar modules and zones. This explains the choice of the Aldoc-Venus transgenic mouse line (*see section 5.2*) (Fujita et al., 2014) for my experiments: the expression of an Aldolase C-Venus fluorescent protein allowed me to target cerebellar modules *in situ* (***Figure 9C, 14A***).

ZII compartmentalization was also correlated with functional discrepancies between PCs (reviewed in Cerminara et al., 2015 ; Apps et al., 2018). Notably, zonal differences in plasticity induction (Wadiche and Jahr, 2005) and CF glutamate release (Paukert et al., 2010) have been described. Zhou et al reported that intrinsic firing properties of PCs *in vivo* were different depending on their molecular identity (Zhou et al., 2014). They showed that ZII+ PCs simple spike firing rate is slower (~60Hz) than in ZII- PCs (~95Hz). Neighboring ZII+/ZII- PCs exhibit the same discrepancy, hence ruling out the link of regional variation or different parallel fiber inputs (Zhou et al., 2014) as adjacent PCs share common GCs inputs (Valera et al., 2016). Difference in firing rate seems to be linked to the expression of TRPC3, a nonspecific cation ion channel, (Zhou et al., 2014). Moreover, they report modular variation in olivary discharge in awake mice: complex spike rate is higher in ZII- PCs (Zhou et al., 2014).

Beyond intrinsic properties, Zebrin patterning is also correlated with differences in synaptic plasticity (Apps et al., 2018). EAAT4 (Dehnes et al., 1998), a glutamate transporter, and mGluR1β are differentially expressed by PCs, respectively following or mirroring the Zebrin II pattern (***Figure 9C***) (Cerminara et al., 2015). For instance, LTD in lobule X of rodents could not be induced (Wadiche and Jahr, 2005) with classical protocols: this lobule uniformly expresses Zebrin II (Apps and Hawkes, 2009) and increased levels of EAAT4 providing high level of glutamate clearance in synaptic cleft of ZII+ PCs. For LTP, Wang et al reported that patches of long latency responses to theta burst stimulation of parallel fibers were potentiated in ZII+ bands that express mGluR1β & PLCβ4 contrary to ZII- PCs (Wang et al., 2011).

3.3 Mossy fiber modular projections and functional microzone

Although the definition of the cerebellar modules relies on the topography of CF inputs, MF projections are also topographically organized.

3.3.1 Distribution of mossy fiber terminals

Unlike olivary projections that project to one or two parasagittal zones, a single MF tend to project bilaterally in multiple zones (Apps and Hawkes, 2009) hence sending dozens of collaterals through the whole cerebellar cortex in different lobules (***Figure 5A, 10A***) (Wu et al., 1999; Luo et al., 2017; Biswas et al., 2019). Thus, it is not surprising to find MFs carrying different modalities converging onto a single GC (Huang et al., 2013; Chabrol et al., 2015).

In the vermis, MFs arising from the spinal cord and dorsal column nuclei seem to project in a modular fashion : anatomical tracing revealed that terminals from the spinocerebellar and cuneocerebellar tract end up in parasagittal bands in lobule III & IV of the cerebellar cortex (***Figure 10B***) (Ji and Hawkes, 1994; Sillitoe, 2015; Valera et al., 2016). However, this projection patterns do not necessarily overlap perfectly with the zebrin band pattern (***Figure 10B***) (Valera et al., 2016). As for CFs, the group of Izumi Sugihara performed unitary labeling of MFs from the thoracic and lumbar spinal cord. They demonstrate that MF *rosettes* terminate either in ZII+ or ZII- parasagittal bands (REF Luo et al., 2017). However, when studying MFs originating in the pontine nuclei, they found collaterals that project mostly to ZII+ zones in the anterior vermis and the *copula pyramidis* (***Figure 10A***) (Biswas et al., 2019) in mice.

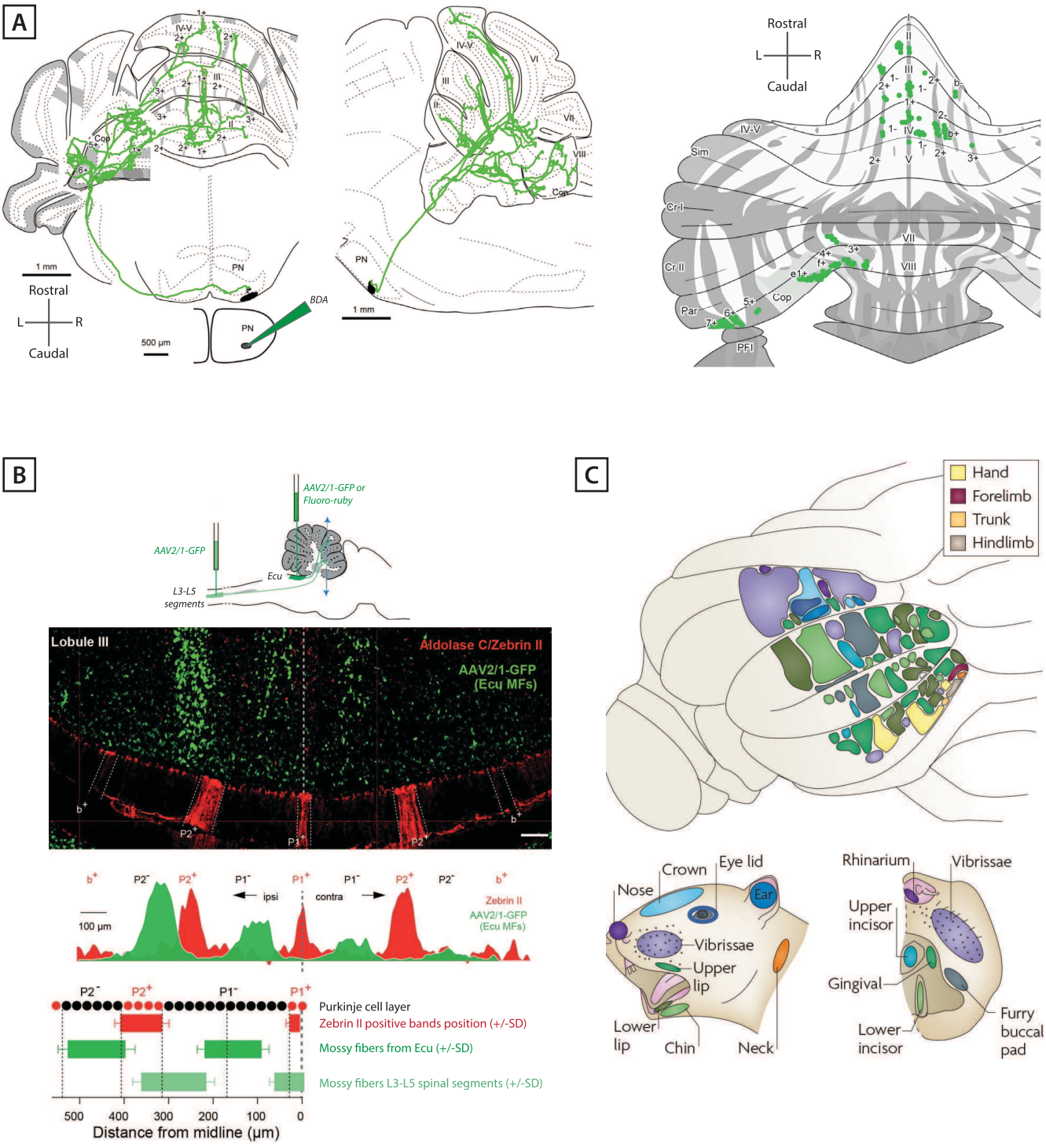

Figure 10 : Modular projections of pontine, spinal and cuneate mossy fibers & fractured somatotopy

(A left) Mossy fiber projections are redundant and bilateral. Frontal and sagittal slices of mouse cerebellum/brainstem showing single fiber reconstruction (*in green*) after injection of anterograde Biotyn Dextran Amin (*BDA*) in the pontine nucleus (*PN*). ***Adapted from Biswas et al, 2019.***

(A right) Some mossy fibers from the pontine nucleus project preferentially in ZII+ bands. Unfolded view of the cerebellar cortex. Mossy fiber rosettes are represented by green dots. ***Adapted from Biswas et al, 2019.***

(B) Mossy fibers project in a column-wise, modular fashion. Anterograde neuronal tracers were injected in the L3-L5 spinal segments or in the external cuneate nucleus (*Ecu*). Mossy fiber projections clusters (*green*) are input specific, and do not necessarily overlap with climbing fiber projections (represented by AldolaceC/ZII immunostaining, *in red*). ***Adapted from Valera et al, 2016.***

(B down) The longitudinal cerebellar zones, as named by Jan Voogd, and corresponding anatomical olivary inputs and outputs (deep cerebellar nuclei). ***Adapted from Apps & Hawkes, 2009.***

(C) Fractured somatotopy : mossy fibers receptive fields are organized as patches. Dorso-posterior view of the left hand side of the rat cerebellum showing the spatial distribution of receptive fields recorded in the granular layer in response to mechanical stimulation of different body parts. Note the multiple representations of the same body parts to produce a 'fractured somatotopical' mosaic pattern of variable sized patches. ***From Apps & Hawkes, 2009***.

Redundancy of MF inputs expands the combinatorial code of incoming modalities (i.e. pattern discrimination by GCs).

3.3.2 The fractured somatotopy

MF receptive fields in the granule cell layer also revealed complexity. The group of W. Welker performed electrophysiological micro mappings of tactile receptive fields in the GC layer of Crus I, Crus II and paramedian lobules in rodents (Shambes et al., 1978). They established multiple sensory representation of body parts in a *mosaic* or *patchy* fashion, hence called *fractured somatotopy* (***Figure 10C***) (Shambes et al., 1978 ; Apps and Hawkes 2009 ; Apps et al., 2018). These early findings are in accordance with anatomical redundancy of mossy fiber projections which project in patches (the terms "*bleb*" or "*patches*" can also be found in the literature) throughout the GC layer of multiple lobules and zones (*see section 3.3.1*).
Woolston's group confirmed this fractured somatotopy in the cerebellar hemispheres, especially in the lobule simplex, paramedian lobule, Crus I and Crus II (**Figure 10C**), (Bower and Woolston, 1983). In cats, Garwicz, Jörntell & Ekerot performed similar mappings in C1 and C3 regions that receive sensory MF inputs from the forelimbs (Garwicz et al., 1998b, 1998a; Ekerot and Jörntell, 2001). As far as I know, such micro mappings for MF receptive fields were not performed in the vermal part of lobules III & IV, the region I focused on, although CF inputs were mapped in rats (Jörntell et al., 2000).

With tactile stimulations, correspondence between CF and MF receptive field could be observed (Brown and Bower, 2001) or not (Garwicz et al., 1998a, 1998b ; Ekerot and Jörntell, 2001). Micro mappings experiments allowed Brown & Bower to investigate the topographical relationships between CF and MF inputs. They discovered that tactile stimulation on face skin of anaesthetized rats elicited (1) complex spikes in Crus II PCs (i.e. revealing CF receptive fields) but also activation of GC layer localized directly underneath (i.e. highlighting MF receptive fields) (Brown and Bower, 2001). This shows a strong overlap (*congruence*) between MF and CF projections (anatomically confirmed by Pijpers et al., 2006). Although congruence can be observed in most case, some experiments reported *patchy* MF inputs instead (i.e. no overlap between CF and MF receptive fields, Ekerot and Jörntell, 2001, 2003). Since these two group of experiments were not performed within the same location (mostly Crus I/II vs C1/C3 zone), the different results can be explained by different operational rules within distinct regions of the cerebellar cortex (Valera et al., 2016).

Most of PCs located in the anterior vermis receive local GC inputs (Valera et al., 2016). CF would thus carry pre-integrated somatosensory information and MF would bring raw sensorimotor information from the same region of the body to PCs within a microzone, hence the concept of cerebellar functional unit, or functional microzone (Apps & Garwicz, 2005 ; Apps and Hawkes, 2009).

3.3.3 Functional clusters of PCs

CF and MF projections in the cerebellar cortex display a spatial paradox. On the first hand, CF projections are well organized along the parasagittal axis, synchronizing arrays of PCs with precise pre-integrated sensory motor information and dedicating them to given tasks (*see section 3.1* and ***Figure 9***). On the other hand, MF receptive fields are fractured and redundant: the same information is brought to multiple location within the cerebellar cortex with a blurry organization as opposed to the CF pathway (*see sections 3.3.1, 3.3.2* and ***Figure 9***). Both inputs converge to a unique target: PCs (***Figure 6B***). A burning question is: how does a single PC computes this jungle of incoming inputs? A starting point is given by the Marr-Albus-Ito model: PCs select relevant inputs under the supervision of CF activity (Ito, 2000). In other words, GCs and PFs provide a wealth of combinatory inputs, yet preferential pattern or inputs (i.e. PF-PC synapses) are selected at will through network activity and learning (***Figure 7***).

Valera and colleagues studied the functional connectivity between GCs and PCs: patch clamp recordings of PCs in acute cerebellar slices coupled to photostimulation of caged glutamate in the GC layer allowed them to establish synaptic maps (Valera et al., 2016). They showed that (1) PCs in the anterior vermis receive local (i.e. in the GC layer underneath PC soma) as well as distal functional GC excitatory inputs and (2) neighboring PCs share common spatial GC input patterns (***Figure 11A***). Synaptic maps from different groups of neighboring PCs recorded in different mice are similar, yielding conserved GC inputs to PCs across individuals (Valera et al., 2016).
Thus, four functional PC clusters in the A/AX zones could be identified, each of them having its own granular inputs (Valera et al., 2016). My project was focalized on the PC cluster located in a 0 to 120µm range from the midline in the A zone (***Figure 11B*** corresponding to cluster #1 in Valera et al., 2016).

While MFs and CFs are hardwired during development (Apps et al. 2018), PCs can choose relevant PF-PC synapses depending on the task they have to fulfill under CF supervision, resulting in the selection preferential GC inputs. Hence the concept of functional PC clusters,

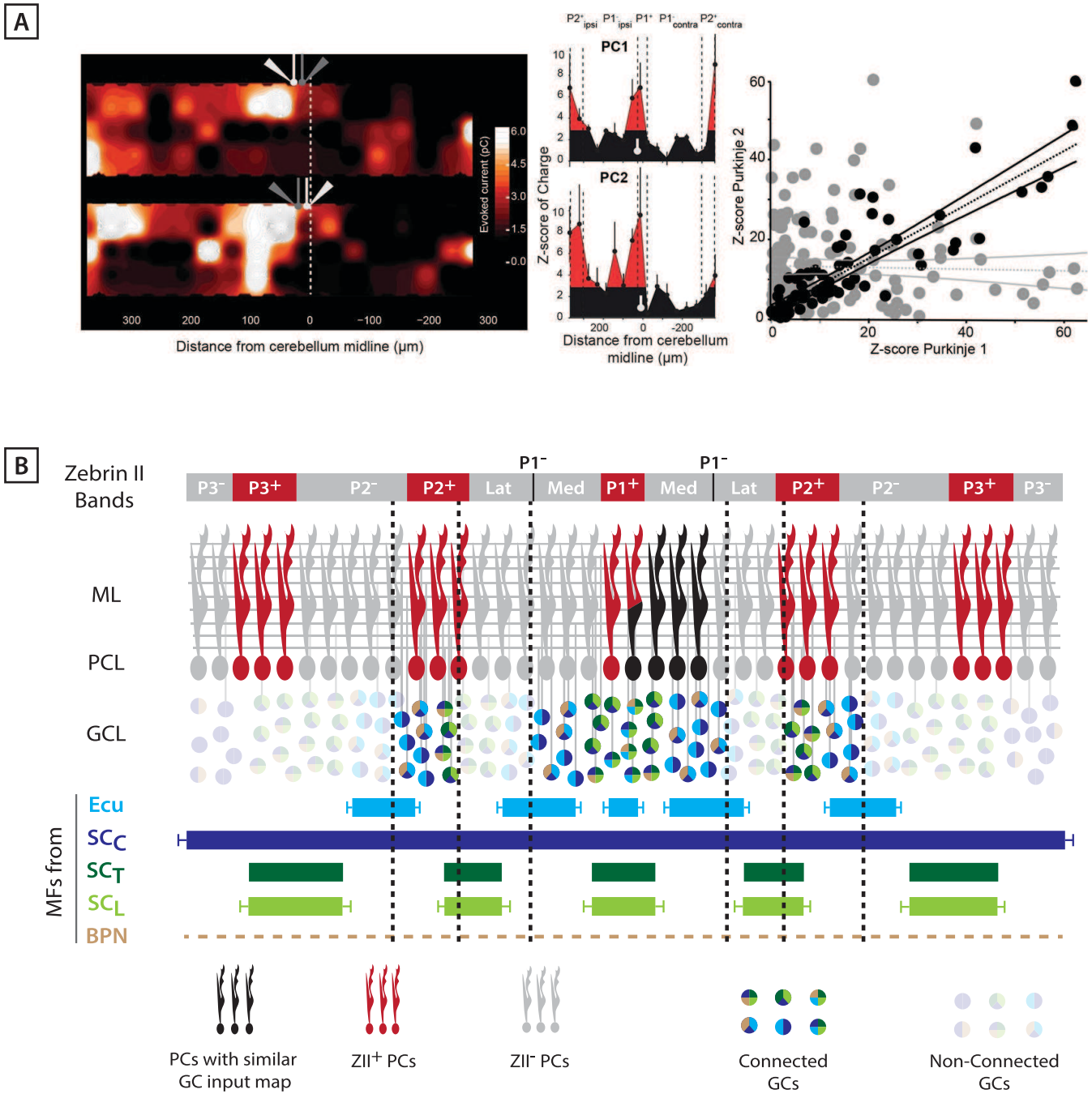

Figure 11 : The mossy fiber-granule cells inputs on Purkinje cells define functional clusters in the cerebellar cortex.

(A) Neighboring Purkinje cells share similar granule cell input patterns. Two neighboring Purkinje cells (PCs) were simultaneously recorded and caged-glutamate was systematically uncaged. (Left) Map of the recorded synaptic charge measured in PC1 (white cell, top) and PC2 (white cell, bottom). Most of the responding and silent sites were observed at the same location or close by, although a few differences can be observed. (Middle) Corresponding mediolateral granule cell (GC) connectivity pattern to PC1 (top panel) and PC2 (bottom panel) expressed as a Z- score of the synaptic charge. PC positions are indicated in white. (Right) Site by site correlation of GC connectivity patterns between neighboring PC pairs (black dots, r = 0.74 ± 0.14; n = 8 pairs). Shuffled pairs showed no correlation (gray dots, r = 0.02 ± 0.09). ***From Valera et al, 2016.***

(B) The functional PC cluster #1. GC clusters belonging to different microzones (identified by the zebrin band pattern in red and grey) communicate with specific groups of PCs (one example in black). In this example, a group of PCs (120 µm width spanning $P1^-$ and $P1^+$ zebrin bands) close to the midline receives GC inputs from ipsi and contralateral $P2^+$, ipsi and contralateral median $P1^-$ and $P1^+$ microzones. This organization is conserved across mice. Each GC cluster receives specific MF inputs from different precerebellar nuclei and modalities (identified by the color in the GC pie chart). MFs projections in the GCL are complex and redundant. The other GCs remain silent or unconnected (shaded pie chart). This functional PC cluster does not necessarily fit with the anatomical boundaries given by the CF and MF inputs. ***From Apps et al, 2018.***

***ML** : Molecular Layer, **PCL** : Purkinje Cell Layer, **GCL** : Granule Cell Layer, **MFs** : Mossy Fibers, **Ecu** : External Cuneate, **SC_L** : Lumbar part of the Spinocerebellar Tract, **SC_T** : Thoracic part of the Spinocerebellar Tract, **SC_C** : Cervical part of the Spinocerebellar Tract, **BPN** : Basal Pontine Nuclei, **CFs** : Climbing Fibers, **MFs** : Mossy Fibers, **PCs** : Purkinje Cells, **GCs** : Granule Cells.*

demonstrated by Valera et al : clusters of neighboring PCs in the anterior vermis display similar functional GC inputs (***Figure 11B***) (Valera et al., 2016, Apps et al., 2018). Moreover, some of these GC inputs come from distant, non-neighboring microzones, ruling out pure parallel processing in the cerebellar cortex and establishing functional inter-modular communication via PFs in the cerebellar cortex (***Figure 10A, 10B***) (Valera et al., 2016 ; Apps et al., 2018). In other words, PCs within a microzone sharing similar CF identity can select relevant MF inputs from adjacent or distant modules.

Unlike functional microzones, PCs functional clusters are thus defined by the combination of GC impinging on PCs at a given time rather than local MF inputs (***Figure 10B***). PCs select relevant MF inputs that are not present within their own microzone (because MF collaterals are not randomly distributed nor project in every location of the cerebellar cortex) and synaptic plasticities at PF-PC synapses allow input maps to evolve (as expected by modulation of MF receptive fields in Jörntell and Ekerot, 2002 and demonstrated *in vitro* by Valera et al., 2016). This adds another dynamic layer of possibilities for signal processing in the cerebellar cortex: PFs multiplex modules could be involved in specific tasks (Apps et al., 2018).

4. Cerebellar involvement in locomotion

Locomotion in vertebrates is a basic motor behavior allowing animals to interact with their environment. It allows fishes to swim, birds to fly, mice to break free from the experimenter and apes to climb in trees. This behavior is also the final common pathway for many complex tasks computed by the brain such as exploration, predation or escape. Although locomotion can be automatic behavior, it involves the precise coordination of tens of muscles in the body. Moreover, depending the requested task, different regime of movement should be possible with the same muscles and limb primary anatomical organization. For instance, in mice, locomotion can be segregated in four distinct behaviors: walk, trot, bound and gallop (***Figure 12B***). These locomotor outputs rely on proper kinematics, speed ranges and limb alternance (Bellardita and Kiehn, 2015).

Therefore, vertebrates must adjust muscle contractions based on somatosensory information (i.e. proprioceptive and vestibular) and in combination with implicit or voluntary motor programs. Ultimately, locomotion should adapt to any perturbation from the external world such as obstacles and to any alteration of body integrity (i.e. growth, fatigue or lesions). In

vertebrates like rodents, locomotion results in a characteristic alternance of limb kinematics cycles, such as swing, stance and stride (***Figure 12A***) (Mendes et al., 2015).
In this section, I briefly review the involvement of several central nervous system areas in locomotion: the spinal execution of locomotion, then the supraspinal control of locomotor activity. Lastly, I emphasize the role of the cerebellum in locomotor control and adaptation.

4.1 Neural substrate of locomotion

Planification and initiation of locomotion requires the concerted activation of several brain structures such as the cerebral cortex, the basal ganglia, the cerebellum, the midbrain and the hindbrain (Kiehn, 2016). Locomotion may appear as a simple behavior, nonetheless it requires patterns and precisely timed sequences of alternate excitation and inhibition that are generated in very specific neural networks within the spinal cord (Kiehn, 2016; Côté et al., 2018).

4.1.1 Spinal-dependent locomotor activity

Muscles that allow body movement are directly controlled by motor neurons and indirectly affected by local interneurons localized in the ventral/medial/dorsal spinal cord. These latter interneurons can be classified according to their role in reflex pathways, or by morphological or genetic markers (***Figure 12C***) (Côté et al., 2018). These spinal interneurons are assembled in modular networks that control a given subset of motoneurons. They are dedicated to generating rhythmic motor activity in absence of descending (from supraspinal structure) or sensory-related inputs, hence their name of *Central Pattern Generators* (CPGs) (***Figure 12C***) (Grillner and Jessell, 2009; Côté et al., 2018).
CPGs directly drive motor neurons (***Figure 12C***). Moreover, CPGs and motor neurons are locally interconnected to generate activity patterns to coordinate intralimb flexion and extension movements: agonist and antagonist muscles are contracted and released alternatively (Kiehn 2016 ; Côté et al., 2018) (***Figure 12C***). While walking, when a group of flexor motor neurons around a joint is inhibited, the corresponding extensor motor neurons around the same joint are excited, and vice versa (Kiehn, 2016).
In addition, and to avoid aberrant agonist/antagonist muscles activation, a local sensory-driven mechanism is present. Some inhibitory dorsal spinal cord interneurons, expressing Retinoid-related Orphan Nuclear Receptor are thought to apply a synaptic gating on motor neurons.

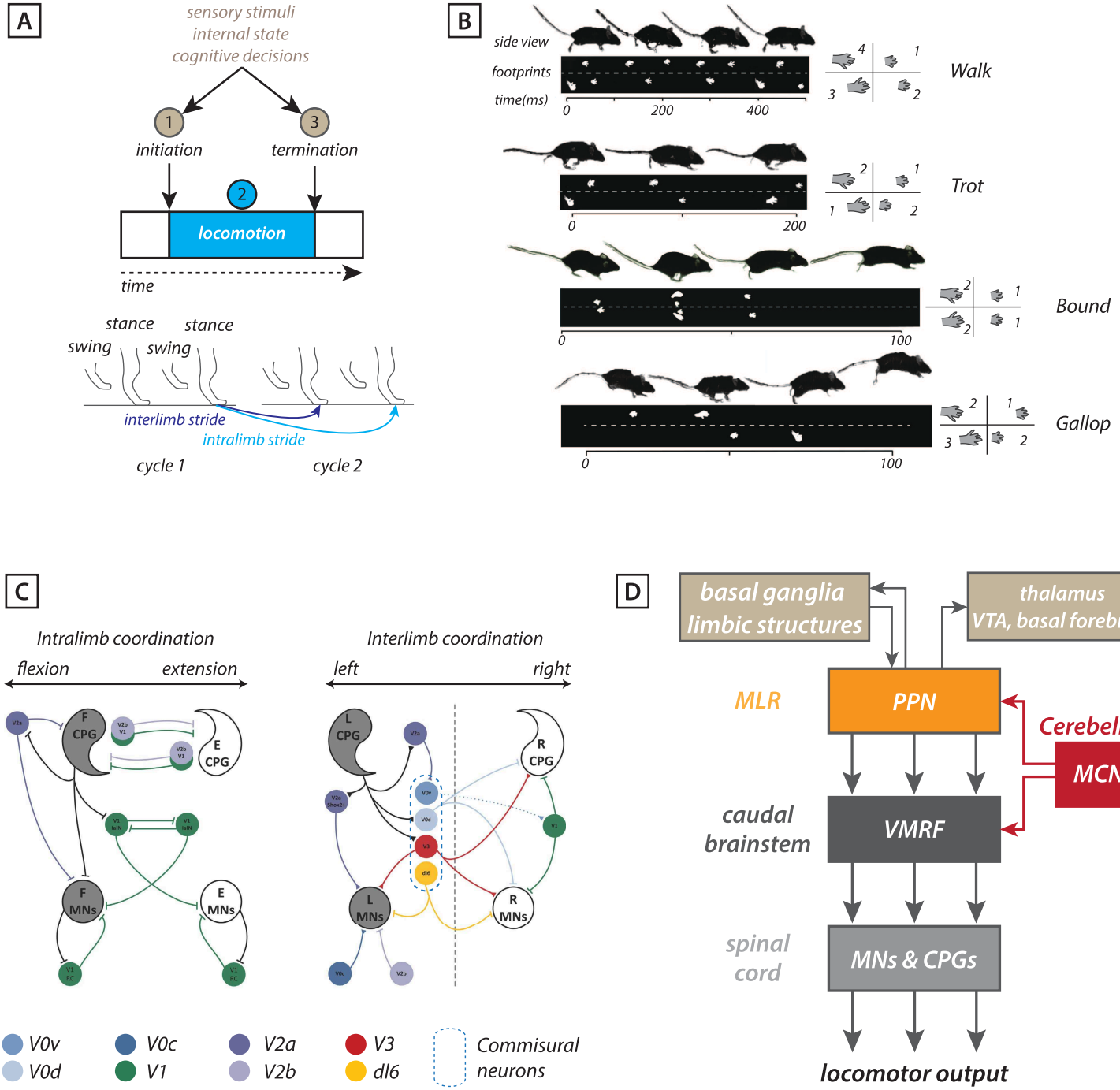

Figure 12 : Neural substrate for the control of locomotion

(A top) Division of the locomotor process in three behavioral phases. *(A down)* Cyclic events measured to evaluate and quantify locomotion in rodents. Swing is the time when the paw is in the air, while stance represents the time it touches the ground. Stride is the time between two consecutive stance of the same paw (i.e. intra) or opposite paw (i.e. inter). ***Adapted from Ferreira-Pinto et al, 2016***

(B) Locomotor behaviors in mice. Side views and corresponding footprints and limbs alternance order for walk, trot, bound and gallop. ***Adapted from Bellardita et al, 2015***

(C) Genetically identified spinal interneurons contributing to locomotion. Schematic of the synaptic connectivity of genetically identified populations of interneurons developing from the ventral spinal cord and involved in (*left*) intralimb and (*right*) interlimb coordination during locomotion. Experimentally demonstrated projections are illustrated by a solid line and predicted connectivity with a dashed line. ***Adapted from Côté et al, 2018***

(D) Cerebellar location in the neural system for locomotion. The MLR is the crossroad between supraspinal structures (i.e. decision and initiation/stop) and medullary/spinal (i.e. effector) structures. The cerebellum acts on both MLR and medullary regions. ***Adapted from Ferreira-Pinto et al, 2016 with data from Takakusaki et al, 2016 and Teune et al, 2010.***

CPG : *central pattern generator,* ***E :*** *extensor ,* ***F :*** *flexor,* ***L :*** *left,* ***MCN :*** *medial cerebellar nuclei,* ***MNs :*** *motor neurons,* ***PPN :*** *pedunculopontine tegmental nucleus,* ***R:*** *right,* ***VMRF :*** *ventromedian reticular formation,* ***VTA :*** *ventral tegmental area*

Based on sensory feedback from agonist (i.e. flexor) muscles, they prevent simultaneous contraction of antagonist muscles (i.e. extensor) (Ferreira-Pinto et al., 2018).

In limbed animals, intralimb coordination is essential for proper locomotion, as well as inter-limb dialogue: left-right and forelimb-hindlimb movements have to be synchronized. Different rhythms between limbs allow different locomotor behavior such as walking, trot, gallop ou bound (Bellardita and Kiehn, 2015). Forelimb-hindlimb may involve long range, longitudinal communication between cervical, thoracic and lumbar segment of the spinal cord (Côté et al., 2018). Left-right balance and synchrony is locally ensured by a network of interneurons localized near the spinal cord midline, hence named commissural neurons (CoN) (***Figure 12C***) (Grillner and Jessel, 2009 ; Kiehn, 2016 ; Côté et al., 2018). Their role is to send and receive synaptic inputs from the contralateral motor neurons and CPGs. Briefly, left CoNs receive inputs from right CoNs, and vice versa. CoNs act on both side CPGs in order to synchronize left-right limb movements (***Figure 12C***). CoNs and CPGs are associated in a modular fashion, and are individually recruited depending on the behavior: walk, gallop and bound in mice are the outcome of 3 different spinal modules (Bellardita and Kiehn, 2015).

4.1.2 Supraspinal control of locomotion

Although CPGs are quite autonomous, locomotion can be either triggered or stopped, accelerated or slowed down by the action of supraspinal structures (***Figure 12A***) (Grillner and Jessel, 2009 ; Kiehn, 2016 ; Ferreira-Pinto et al., 2018).
One specific region of the brainstem is considered as a key in the supraspinal orchestration of locomotion: the *Mesencephalic Locomotor Region* (MLR) (Ferreira-Pinto et al., 2018). It is subdivided in two nuclei, the cuneiform nucleus and pedunculopontine tegmental nucleus (PPN) both located in the pontomedullary reticular formation (Takakusaki et al., 2016; Takakusaki, 2017). Shik & Orlovsky electrically stimulated the MLR in cats : they were able to elicit a wide range of locomotor activities correlated with the frequency and intensity of the delivered stimulation (Shik and Orlovsky, 1976). Anatomically, the MLR is at the heart of locomotion networks (***Figure 11D***), connecting upstream regions such as basal ganglia and thalamus with downstream effector in the medulla such as the magno- and gigantocellular lateral reticular formation (Ferreira-Pinto et al., 2018) that later project on spinal motor-neurons and CPGs (***Figure 11D)*** (Esposito et al., 2014). Basal ganglia require the action of MLR

excitatory neurons to induce locomotion (Roseberry et al., 2016). Optogenetic activation of nuclei within the reticular formation elicits a wide range of locomotor behavior (reviewed in Ferreira-Pinto et al., 2018).

The medial cerebellar nuclei project to both stages of hindbrain/midbrain locomotor controls (***Figure 12D***): the pontomedullary reticular formation (Teune et al., 2000; Takahashi et al., 2014) and the ventromedial reticular formation (Teune et al., 2010). Principal glutamatergic deep cerebellar neurons from the medial cerebellar nuclei establish functional synapses on the PPN (Hazrati and Parent, 1992; Takakusaki et al., 2016). These functional inputs on MLR and the caudal brainstem may directly or indirectly be the neural substrate of the cerebellar control for locomotion.

4.1.3 Effect of enriched environment in the central nervous system

Enriched environment for rodents has been defined as the use of housing conditions that offer enhanced sensory, motor, and cognitive stimulation of brain neuronal systems in comparison with standard housing (Toth et al., 2011). Environmental enrichment of laboratory animals influences brain plasticity, stimulates neurogenesis, increases neurotrophic factor expression, and protects against the effects of brain insult (Fares et al., 2013).

Rodents training in running wheels or treadmills allow the performance of natural motivated behaviors such as gallop and bound. Therefore, we postulate that such locomotor behavior may also enriched housing conditions in laboratory. For instance, acute and prolonged training of mice on treadmills showed significant neuronal activation (measured with fosB-ΔfosB staining) in several motor-related brain regions such as the cerebral cortex (S1/M1), basal ganglia and the anterior cerebellar vermis (Tsai et al., 2019) compared to standard-housed mice.

The group of Stefan Hallermann recently described functional refinement of granule cell electrophysiological properties in cerebellar slices from enriched mice (Eshra et al., 2019). In their conditions, enriched mice were housed in large cohorts (~9 individuals/cage) in presence of toys to ensure social, cognitive and motor learning. After enrichment, GCs in the lobule IX displayed faster action potential and increased maximum firing rate. Moreover, mice raised in enriched environment showed significant improved performance on Rotarod task compared to controls (Eshra et al., 2019). These behavioral and functional changes are likely the reflect of behavioral adaptation such as inter-limb coordination and new sensory-motor experiences. These modifications within brain areas have been studied *ex-vivo*, however recent evidence show that *in vivo* cerebellar learning is positively modulated during locomotion (and by

optogenetic activation of MFs, mimicking incoming contextual information) (Albergaria et al., 2018; Raymond, 2018). Counterintuitively, adding noise in the system seems to increase cerebellar-dependent learning performance.

4.2 Adaptation and control of voluntary locomotion: here comes the cerebellum

Several supraspinal structures are involved in the direct establishment of locomotion kinematics (Ferreira-Pinto et al., 2018), including the cerebellum (Kiehn, 2016). Indeed, one of the major symptoms reported in cerebellar patients are walking ataxias (Morton and Bastian, 2004). Electrical stimulation of the medial cerebellar white matter in decerebrated cats triggers locomotion, mimicking the result of MLR stimulations (Mori et al., 1999). Previous experiments had revealed increase of PCs and nuclear neurons firing rate during locomotion (Armstrong and Edgley, 1984, 1988). The cerebellum would however not be physiologically responsible of locomotion initiation or stop but rather be involved in indirect control of body gait and balance but also in correction of limb movements, resulting in adaptation of locomotion and learning of new locomotor strategies (Morton and Bastian, 2004, 2006; Darmohray et al., 2019). Moreover, extensive study of cerebellar micro-circuits fine anatomy revealed a central position for the anterior vermis in the control of axial and proximal body muscles, suggesting a preponderant, nonetheless complex, role of the anterior cerebellum in locomotion.

4.2.1 Locomotion-related input/output relationships in the anterior vermis

This section will focus on locomotor-related inputs and outputs in the medial part of the lobules III and IV, as I recorded PCs in this area. It involves the cerebellar A, AX and B zone, corresponding to $P1^+$, $P1^-$, $P2^+$ and P2- Zebrin bands (***Figure 13***). For clarity, the A zone can be subdivided in two equal parts: the medial A zone (Am, close the P1+ Zebrin band) and the lateral A zone (Al, close to the $P2^+$ Zebrin band).

4.2.1.1 CF inputs to A/AX/B zones in lobules III/IV

The cutaneous CF receptive fields to the A and B zone in the anterior vermis have been electrophysiologically mapped in cats (Miller et al., 1969a, 1969b; Andersson and Oscarsson,

1978b) and in rats (Jörntell et al., 2000). CF inputs to the Am zone were discharging when tactile stimulation was applied to the ipsilateral face, proximal part of the tail and proximal fore- and hind limbs, summarized as *"ipsilateral mixed proximal inputs"* (Jörntell et al., 2000) or following electrical stimulation of the midbrain and the spinal cord (Miller et al., 1969a). In the Al zone, responses were elicited by stimulation of both proximal and distal hindlimbs (Jörntell et al., 2000).

CF targeting A and AX zones arise from the caudal part of the medial accessory inferior olive (cMAO) (Apps and Hawkes, 2009; Quy et al., 2011). Horn and colleagues selectively inactivated the cMAO in freely moving cats using precise acute injections of CNQX (antagonist of AMPA receptors) (Horn et al., 2010). They reported mild to severe imbalance during walking, characterized by lateropulsion away from the side of injection, and aberrant, clumsy walking patterns. Most affected cats were not able to perform more than 1 or 2 steps in the first minutes following the cMAO inactivation (Horn et al., 2010).

The B zone is targeted by CFs coming from the DAO (Apps and Hawkes, 2009). After DAO inactivation, cats displayed increased errors in reaching-grasping tasks, in addition with mild limping and waddling during locomotion resulting from uncoordinated forelimb movements (Horn et al., 2010). Taken together, these functional and behavioral results show a major involvement of the A and B zone in the coordination of locomotion.

4.2.1.2 Fine mossy fiber inputs to the A/AX/B zones in lobules III/IV

A and B zones receive MFs from various locomotor-related locations, embracing inputs from effectors (i.e. muscles) as well as controllers (i.e. supraspinal structures). Forelimb and hindlimb sensorimotor information target the A/AX/B zone trough projection from the ventral spinocerebellar tract, dorsal column nuclei and the lateral reticular nucleus (***Figure 13***) (Matsushita et al., 1979; Ji and Hawkes, 1994; Wu et al., 1999; Quy et al., 2011; Valera et al., 2016).

In addition, MFs from the pontine nuclei project strictly in the ZI+ parts of A and AX zone: $P1^+$ and $P2^+$ (***Figure 13***) (Biswas et al., 2019). The pontine neurons that generate these MFs are localized in the region receiving information from the forelimb somatosensory cortex area (Kratochwil et al., 2017). We can then speculate that $P1^+/P2^+$ bands receive cortical-integrated information relative to the forelimb movements.

4.2.1.3 Outputs from A/AX/B zones in lobules III/IV

PCs target cerebellar nuclei, that project on mid and hindbrain regions involved in locomotion. Ultimately, they control precise locomotor effective motor units such as axial or distal limb

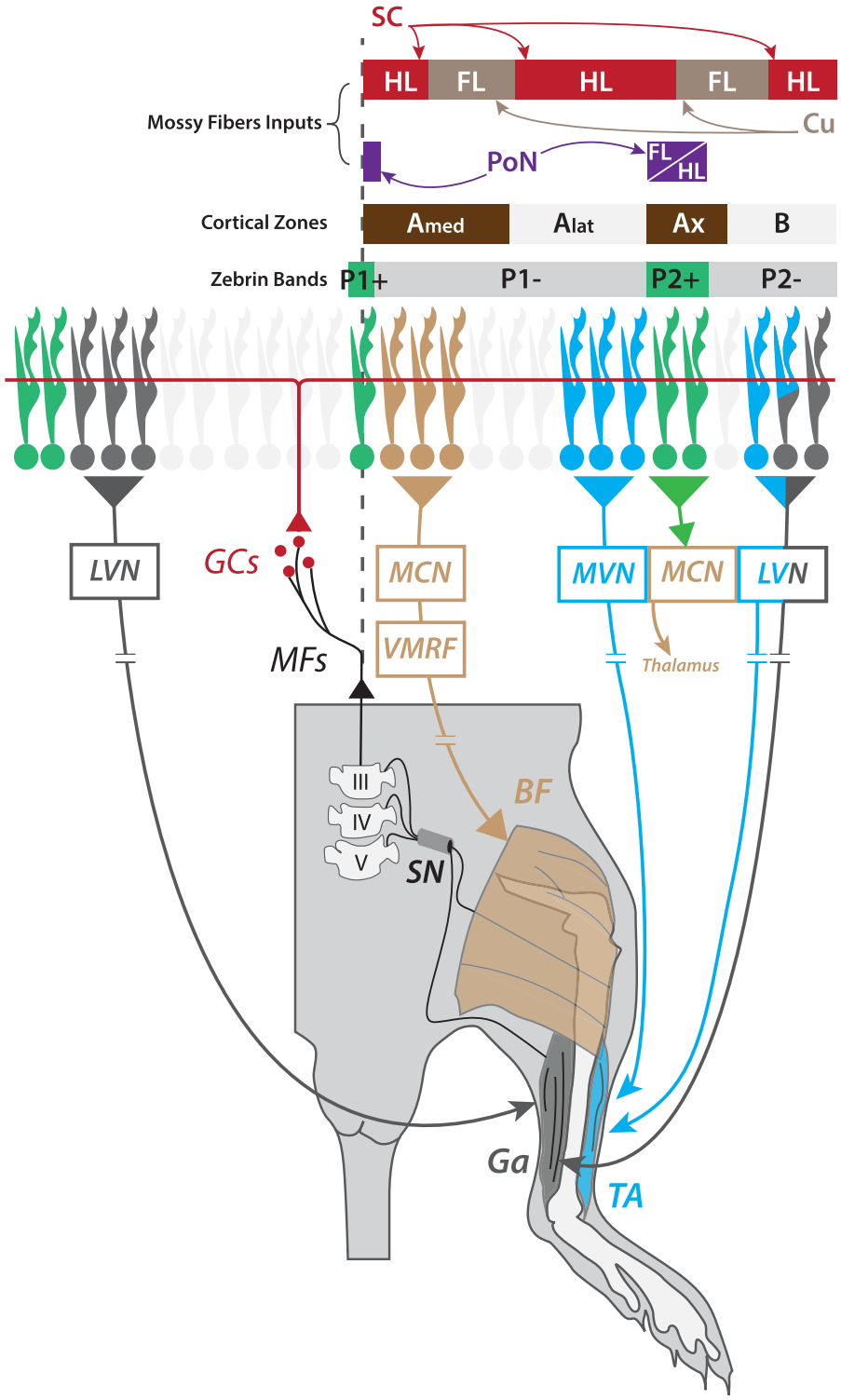

Figure 13 : Locomotor-related inputs and outputs to the anterior vermis

Fine projections of precerebellar nuclei to the anterior microzones of the cerebellar cortex. These microzones targets precise brainstem nuclei and ultimately some muscles in the hindlimbs.

The cerebellar cortex gets sensory-motor information from hindlimb muscles via mossy fibers originating from L3 to L5 lumbar segment and from forelimb muscles through the cuneate nucleus. Mossy fibers relay on Granule Cells (in red), that send the parallel fibers (*in red*) through the transverse plane of the molecular layer, contacting hundreds Purkinje cells. Neighboring Purkinje cells send indirect motor output to specific muscles from the hindlimb, with relays in the deep cerebellar nuclei and midbrain/hindbrain locomotor related structures. ***This figure has been built combining data from Ji & Hawkes, 1994; Ruigrok et al, 2008; Valera et al, 2016: Voogd et al, 2016 & Biswas et al, 2019.***

***III/IV/V** : lumbar segments, **BF** : biceps femoralis, **FL/HL** : forelimbs/hindlimbs, **Ga** : gastrocnemius, **MCN** : medial cerebellar nuclei, **MVN** : medial vestibular nuclei, **LVN** : lateral vestibular nuclei, **PoN** : pontine nuclei, **SC** : spinal cord, **SN** : sciatic nerve, **TA** : tibialis anterior, **VMRF** : ventro median reticular formation.*

muscles. Ruigrok & colleagues performed transsynaptic retrograde labeling in rodents : they injected rabies viruses in hindlimb muscles and highlighted a fine modular compartmentalization of PCs projections (Ruigrok et al., 2008) (summarized in ***Figure 13***). Thus, PCs from the A/AX/B control several muscles of the hindlimbs, such as the *biceps femoralis*, the *gastrocnemius* and the *tibialis anterior* (***Figure 13***). Projection are indirect, as cerebellar output neurons do not directly contact motor neurons in the spinal cord. For instance, PCs in the Am zone project to the medial cerebellar nuclei, that project to the ventromedial reticular formation (gigantocellular part, Teune et al., 2000) and the pontomedullary reticulospinal neurons (Takahashi et al., 2014) before reaching the spinal cord (***Figure 13***) and ultimately the ipsilateral *biceps femoralis*. However, PCs from the B zone project to the lateral vestibular nucleus (Voogd, 2016), that can directly target motoneurons controlling the ipsilateral *gastrocnemius* and *tibialis anterior* (but also through indirect projections via the pontine reticular nucleus, see Murray et al., 2018). Finally, PCs from the $P2^{+}$ Zebrin band project to the lateral medial nuclei (Sugihara et al., 2011) that projects to the ipsilateral lateral vestibular nucleus, contralateral vestibulospinal nucleus and the ventromedial thalamus (***Figure 13***) (Teune et al., 2010). This last projection consolidates the preferential relationship with cortical inputs/outputs of ZII+ vermal regions.
These fine tracing studies show direct and/or indirect control of PCs from the A/AX/B zone on proximal and distal forelimb/hindlimb muscles involved in locomotion.

4.2.2 Functional cerebellar impact on locomotion

In addition to the fine locomotor-related anatomy described earlier, several physiological evidences suggest a preponderant role for the cerebellum in the execution and adaptation of voluntary locomotion.
Powell et al performed patch clamp recording of GCs in the lobule V while mice were walking or resting on a treadmill (Powell et al., 2015). They showed that (1) GCs encode locomotor behavior, as they fire when mice are running but not resting and (2) walking patterns can be predicted by the GC discharge motifs. Thus, GCs reliably encode locomotor related MF sensorimotor information (Powell et al., 2015). GC information is then transmitted to PCs that requires balanced representation of incoming excitation and inhibition to compute a proper locomotor output. Indeed, optogenetic silencing of MLIs in running mice triggers unidirectional (positive) modulation of PCs and disrupted locomotor behavior (Jelitai et al., 2016). With rhythmic incoming locomotor-related information, PCs encode locomotion kinematics (i.e. steps or speed, Muzzu et al., 2018) and provide cyclic modulation of nuclear neurons, that is essential for the smooth execution of well-trained, voluntary locomotion in mice (Sarnaik and

Raman, 2018). Taken together these findings show that the cerebellum encodes locomotion kinematics, and efficient voluntary locomotion requires an accurate cerebellar motor output.

Beside its involvement in ongoing locomotion, the cerebellum plays a key role in locomotor adaptation. This has been evaluated in healthy humans and cerebellar patients on a split-belt adaptation tasks (Morton and Bastian, 2006). Briefly, patients are walking on a two-sided treadmill, allowing modulation of speed in each hindlimbs independently. The speed of one side of the treadmill is then accelerated, with predictive (feedforward) clues or not (reactive feedback), and patients must overcome the perturbation in adapting their walking behavior in order to keep stable balance. Results showed that cerebellar patient were able to adapt in reactive feedback fashion (i.e. when one side of the treadmill suddenly accelerate without any prior cues), but not in feedforward situation (i.e. when they were aware of the incoming perturbation). This highlights that the cerebellum seems to play an essential role in predictive but not reactive locomotor adjustments (Morton and Bastian, 2006; Pisotta and Molinari, 2014). In order to investigate the physiology of cerebellar contribution in predictive locomotor adjustments, the group of Megan Carey transposed the split belt tasks from humans to mice (Darmohray et al., 2019). They could demonstrate that split-belt adaptation was purely cerebellar dependent (i.e. it does not require the cerebral cortex). In addition they were able to refine the cerebellar region involved in this behavior : chemogenetic inactivation of the interposed cerebellar nuclei abolish locomotor adaptation and cerebellar learning on the split belt task. Moreover, unilateral chemogenetic manipulations in this region differentially impairs spatial and temporal adaptation (Darmohray et al., 2019).

5. Material & Methods

During my PhD thesis, I was involved in 3 main projects: (1) the study of the development of inter-modular communication in the cerebellar cortex, (2) the investigation of the synaptic rules for locomotion adaptation in the cerebellar cortex and (3) to decipher the temporal inhibitory/excitatory balance from MF to PCs. The next paragraphs will explain the experimental approach for projects 1 and 2. The methods for project 3 are available in Appendix 5 (*Binda et al, submitted version*).

5.1 Ethics

All experiments were conducted in accordance with the guidelines of the *Ministère de l'Education Supérieure et de la Recherche* and the local ethical committee, the *Comité Régional En Matière d'Expérimentation Animale de Strasbourg* (CREMEAS) under the referral procedure n° A67-2018-38 (delivered on the 10th of December, 2013 to the Chronobiotron UMS3415).

5.2 Mice

Two strains of mice were used for the experiments : the AldolaseC-Venus (ALDOC, gift from Pr. Izumi Sugihara, for ref see Fujita et al., 2014) and the Thy1-Cop4-CHR2-eYFP (Thy1, The Jackson Laboratory, stock #007612) mutants. Both lines are established at the Chronobiotron (UMS3415) under the CD1 outbred background.
Only male mice aged from P9 to P90 have been used. Mice were housed by 3 or 4 littermates per cage, in conditions required to fulfil their ethogram with food and water *ad libitum* in a 12/12 light/dark cycle.

5.3 Surgeries

5.3.1 Cuffed mice

ALDOC male mice were anesthetized by inhalation of isoflurane (Verflurane, Virbac, France, 4% for induction then 1-2% for the surgery). Mice were then lay at rest on the left side of the body to expose the right hindlimb. A mix of lidocaïn/bupivacaïne (2 mg/kg each) was subcutaneously injected prior to incision. A 0.5 cm incision was made parallel to the femur to expose leg muscles. Muscles were gently separated using sterilized wooden sticks to expose the main branch of the sciatic nerve. The nerve was pulled out and a sterile 2 mm section of split PE-20 polyethylene tubing (cuff), 0.38 mm ID / 1.09 mm OD, was wrapped around the nerve with the help of a pointed steel stick and a bulldog clamp (***Figure 19A***). The nerve was then pushed back under the muscle fascia, and skin was sutured (Yalcin et al., 2014). For ***sham mice***, the same procedure was followed except that no cuff was implanted. After surgeries mice received an intraperitoneal injection of non steroidal anti inflammatory drug (NSAID ; Metacam, 2 mg/kg) and were left at rest for 24h minimum before behavioral assessment (see section 5.11). In cuffed animals, the plastic cuff remained around the sciatic nerve until the sacrifice of the animals.

5.3.2 Pre-cerebellar nuclei rAAVs-mediated transduction

This section comes from *Binda et al, in prep* (*see Appendix 5*).

In vivo stereotaxic injections of rAVVs viral particles were performed as previously described (Valera et al., 2016). CD1 male mice (P21) were anesthetized by a brief exposure to isoflurane 4 % and anesthesia was maintained by intraperitoneal injections of a mixture of ketamine (131 mg/kg), medetomidine (1 mg/kg) and acepromazine (3 mg/kg). rAAVs 9/2 particles carrying the cDNA for ChRd2(H134R)-YFP under the hSyn promoter (3.38 10^{13} GC/ml; Penn Vector Core, Pennsylvania) were unilaterally injected in the cuneate nucleus at an approximate speed of 250 nl/min via a graduated pipette equipped with a piston for manual injections. A final volume of 1.5 µl was delivered by two injections (0.75 µl/injection) separated by 0.2 mm in the anteroposterior direction; after that half of the virus volume was delivered, the pipette was raised up 0.2 mm and maintained in place until the end of the injection. For effective virus diffusion, the pipette was left in place at least 5 minutes following injection. Injections coordinates were determined from The Mouse Brain Atlas (Franklin and Paxinos, 2007) and corrections based on tissue markers were applied to counterbalance the variability of the CD1 outbred background (from lambda, starting point: AP 2.73 ± 0.14, Lat 1.36 ± 0.08, DV: 5.1 ±

142 0.09, mean ± SEM). At the end of the injection, antipamezole (1 mg/kg) were administered to the mice via intraperitoneal injection to favor recovery from anesthesia

5.1.3 Di-I injections

P8-P9 CD1 pups were placed in crushed ice for 2-3 minutes to be anesthetized. A small incision was rapidly made over the cerebellum and .5 to 1µL fluorescent dye (Vybrant DiI cell labeling solution, Thermo Fisher) was injected at the midline of lobules IV/V of the cerebellar cortex using a glass pipette and a pressure pump (Picospritzer III, Parker, USA). Location and depth of the injection were determined by eye using visual cues. After injection, the opened skin was closed with a drop a biocompatible glue (Vetbond, 3M, USA) and pups were placed on a heat pad a few minutes' prior return to the mother in the homecage.

P30 CD1 mice were anesthetized by inhalation of isoflurane (Verflurane, Virbac, France, 4% for induction then 1-2% for the surgery) and mounted on a stereotaxic frame (Model 68526, RWD Life Science). Body temperature was monitored all along the surgery using a rectal probe and a heat pad. A mix of lidocaïn/bupivacaïne (2 mg/kg each) was subcutaneously injected over the skull prior to incision, followed by an intraperitoneal injection of NSAID (Metacam, 2 mg/kg). A parasagittal incision was made over the skull to expose lambda and bregma landmarks. The skull was cleaned using cotton sticks soaked in sterile 0.9% NaCl solution (saline). A 0.5 mm diameter hole was drilled at AP =-2mm, ML = 0 (from Lambda) to expose lobules IV/V. DiI was injected as described for pups. Skin was sutured after injection and animals were put back in their home cage

5.4 Locomotor enrichment

ALDOC mice had access to a running wheel for 1h/day during 21 consecutives days. For each session, mice were removed from their housing cage and individually placed in a another cage equipped with a vertical running wheel without any access restriction to the wheel. Locomotor activity was monitored using a piezoelectric sensor counting the amount of wheel turns during each session.

5.5 Slice Preparation

Slices were prepared from P9–P90 male CD1 ALDOC or ThyOne Cop4 mice. P12 to P90 Mice were anesthetized by inhalation of isoflurane 4% (Verflurane, Virbac, France) and then killed by decapitation. P9 and P10 pups were sedated by hypothermia prior to decapitation. The cerebellum was rapidly dissected out and placed in ice-cold (<4°C) artificial cerebrospinal fluid (ACSF) bubbled with carbogen (95% O2, 5% CO2), containing (in mM): NaCl 120, KCl 3, NaHCO3 26, NaH2PO4 1.25, CaCl2 2.5, MgCl2 2, glucose 10 and minocycline 0.00005 (Sigma- Aldrich, USA). Then 300 mm-thick transverse acute cerebellar slices were prepared (Microm HM 650V, Microm, Germany) (***Figure 14A***) in ice-cold (>4°C) N-methyl-D-aspartate (NMDG) based solution containing (in mM) : NMDG (93), KCl (2.5), NaH2PO4 (1,2), NaHCO3 (30), HEPES (20), Glucose (25), sodium ascorbate (5), Thiourea (2), sodium pyruvate (3), N-acetylcysteine (1), Kynurenic acid (1), MgSO47H20 (10), CaCL2.2H2O (0.5). After cutting, slices were maintained in a water bath at 34°C for 45 min in bubbled ACSF.

5.6 Patch clamp recordings

Whole-cell patch-clamp recordings in voltage-clamp mode were obtained using a Multiclamp 700B amplifier (Molecular Devices, USA) and acquired with WinWCP 4.2.2 freeware (John Dempster, SIPBS, University of Strathclyde, UK). Patch pipettes (3-4MΩ) were pulled with borosilicate capillaries (Warner instruments) using a gravitational puller (model PC12, Narishige, Japan). Series resistance was monitored and compensated (70%–80% typically) in all experiments, and cells were held at -60 mV to isolate excitatory postsynaptic currents (EPSCs) or 0 mV to isolate inhibitory postsynaptic currents (IPSCs). The internal pipette solution contained (in mM): CsMeSO4 135, NaCl 6, HEPES 10, MgATP 4 and Na2GTP 0.4. pH was adjusted to 7.3 with KOH and osmolarity was set at 300 mOsm. Biocytin (Sigma Aldrich) or neurobiotin (Vector Laboratories, USA) were added (1 mg/ml each) for cell reconstruction. Voltages were not corrected for the liquid junction potential, which was calculated to be 9 mV (i.e. the membrane potential was 9 mV more hyperpolarized than reported). We accepted recordings for which the inward current at -60 mV did not exceed 1 nA. Synaptic currents in PCs were low-pass filtered at 2.4-2.6 kHz, then sampled at 20–50 kHz. All recorded cells were located in lobule III or IV. All experiments were performed at room temperature using the same bubbled ACSF than for dissection. We systematically blocked NMDA, adenosine, CB1, GABAB and mGluR1 receptors to limit the modulation of EPSCs/IPSCs amplitude by activity-dependent activation of these receptors. They were

respectively blocked using (in mM): D-AP5 0.05 (Ascent Scientific, Abcam Inc), DPCPX 0.0005, AM251 0.001, CGP 52432 0.001 and JNJ16259685 0.002 (Tocris-Cookson, UK). For excitatory maps only, inhibitory transmission was blocked with Picrotoxin (0.1mM).

5.7 Loose-cell attached recordings

Loose cell-attached recordings on GCs in voltage clamp were obtained using a Multiclamp 700B amplifier (Molecular Devices, USA) and acquired with WinWCP 4.2.1 freeware (John Dempster, SIPBS, University of Strathclyde, UK). Rosettes were recorded with 5 MΩ glass pipettes (borosilicate) and potential was held at 0 mV for all recordings. The internal pipette solution contained (in mM): NaCl 120, KCl 3, HEPES 10, NaH_2PO_4 1.25, $CaCl_2$ 2, $MgCl_2$ 1 and glucose 10 (Sigma- Aldrich, USA). Osmolarity and pH were respectively set at 295 mOsm and 7.3. Recordings were low-pass filtered at 2.6 kHz then sampled at 20-50 kHz. All experiments were performed at room temperature (23°C) using the same bubbled aCSF than for slices preparation.

5.8 Photostimulation

Uncaging experiments were performed by bath-application of the recording chamber with 100µM of RuBi-Glutamate (Tocris-Cookson, UK). To map GC to PC connections, the slices were placed according the horizontal plane in the recording chamber. In ALDOC, Venus fluorescence allowed precise targeting of the medial A zone. In Thy1 mice, the A zone was located by an estimation of the midline position. A micromirror DMD device (Mosaïc, Andor Technology, Belfast, Ireland) mounted on an optic microscope (Olympus BX51, Japan) allowed systematic photostimulation of 20*20µm or 40*40µm squared granular layer regions with LED-blue light (460nm, Prizmatix, Israel) through a 40X objective (Zeiss, Germany). For uncaging and optogenetic stimulation, EPSCs/IPSCs were elicited by 30ms steady illumination. Prior to mappings, the patched PC is centered in the field of view (40X) and a photostimulation virtual grid is displayed under the PC layer, covering underneath GC layer (***Figure 14C, 14D***). In the developmental dataset (***see section 6.1***) a low-resolution grid is used, containing XX sites (41*41µm per site) while synaptic maps after motor adaptation (*see section 6.2*) were obtained with a high-resolution photostimulation grid (20*20µm per site). In both resolutions the photostimulation grid covers 320 µm of the GC layer in the mediolateral axis and the whole anteroposterior axis. Once mapping is complete, the field of view is

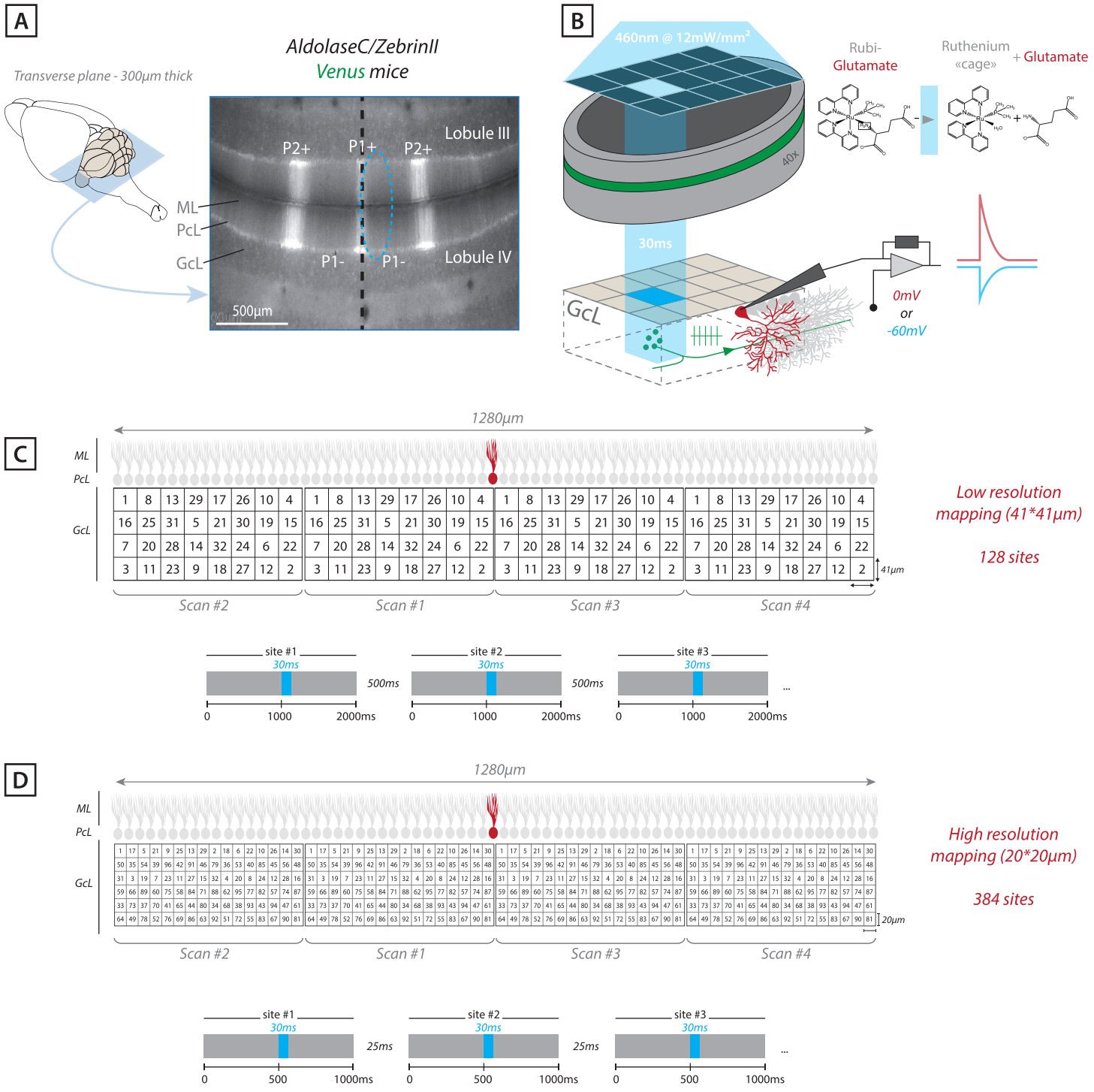

Figure 14 : mapping of granule cells to Purkinje cells functional connectivity

(A) Slice preparation. 300µm thick transverse cerebellar slice are prepared from ALDOC-Venus CD1 mice. The fusion protein allows direct visualisation of the zebrin bands. All Purkinje cells were recorded in the P1- medial zone (dashed blue circle) in lobules III/IV.

(B) Photostimulation in acute slices. A micromirror DMD device (Mosaic, Andor Technology) allows targeting of squared region of the granule cell layer. Flashed granule cells are triggered by blue light that release circulant RuBi GLutamate, EPSCs in Purkinje cells are recorded at Vh = -60mv and IPSCs are recorded at Vh=0mV.

(C) Low and *(D)* high resolution stimulation grids and corresponding stimulation protocols. The patched Purkinje cell (in red) is placed on the right side of the field of view prior to first mapping (scan #1). When first scan is complete, the field of view is dragged to the left to perform scan#2, and so on. A complete mapping is compose of 2 to 4 scans, each scan is made from 6 to 10 photostimulations (460nm, 30ms at 12mW/mm^2) of individual sites.

(D) Measures and Z-score calculation. For a given site, evoked synaptic charge Qstim (or amplitude, Astim) is measured in a 200ms window following onset of stimulation. Corresponding background noise (Qnoise or Anoise) is measured outside the stimulation period. Every noise measures for a whole map are averaged to get the AVGnoise value. The σnoise value is the half width at half maximum of the gaussian fit computed over noise values distribution.

displaced along the field of view to extend the photostimulated GC layer. Typically, 3 to 4 field of views and consequent mappings are done for each experiments, covering a GC layer zone of 1230 µm wide in the mediolateral axis. Two stimulations of the same granular site were separated by 60 seconds minimum. For each experiment, a single site of the granular layer was photostimulated between 5 and 10 times in total (yielding 5 to 10 recordings for averaging and analysis).

5.9 Immunohistochemistry & map/pattern reconstruction

5.9.1 Slice reconstruction

After recordings, the patch pipette was gently removed from the recorded PC and the slice was immediately transferred from the recording chamber to 4% paraformaldehyde (Electron Microscopy Sciences) in ACSF for a maximum of 24h (4°C) to allow fixation and slice reconstruction. Zebrin bands were identified using venus fluorescence or monoclonal antibody against Aldolase C (1/50 to 1/200, 3 hours at room temperature, gift from R. Hawkes, Calgary, Brochu et al., 1990). Recorded cells were labeled using Alexa 555-Streptavidin (Thermo-Fisher, 1/1000, 3 hours at room temperature). Ipsi- and contralateral P1+, P1-, P2+ and P2- Zebrin bands and distance between recorded PC and the midline (P1+) were measured in each experiments. In adult CD1 mice, averaged Zebrin band lengths in lobule III/IV were (in µm±SD) : *P2- contralateral* 416.6±70.72; *P2+ contralateral* 71.56±24.59; *P1- contralateral* 320.516±62.94; *P1+* 34.63±16.18; *P1- ipsilateral* 320.46±60.54; *P2+ ipsilateral* 69.75±22.53; *P2- ipsilateral* 438.04±64.25. Recorded PCs (n=133 in total) were located at 52.42±29.8 µm from the midline of lobules III/IV, corresponding to the cluster 1 defined by Valera and colleagues (Valera et al., 2016) (*see section 3.3.3*).

5.9.2 Reconstruction of connectivity map for a single experiment

After current leak subtraction, the average synaptic charge (eQstim for EPSCs and iQstim for IPSCs) or the average minimum/maximum amplitude (eAstim for EPSCs / iAstim for IPSCs) for each site of photostimulation were computed on 200 ms time window from the onset of each photostimulation (***Figure 15A, 15B***). Charge or Amplitude of the noise (Qnoise or Anoise, i.e. charge or amplitude due to spontaneous activity in the slices) was calculated in a similar 200ms time window but before or after photostimulation (***Figure 15A, 15B***). Qnoise or Anoise histogram was fitted with gaussian yielding standard deviation (σnoise) (***Figure 25C***). For each photostimulation site, **synaptic charge Z-score** value was calculated as follows:

$$Z\ score\ =\ \frac{Q_{stim}\ -\ \underline{x}}{\sigma_{noise}}$$

$$Q_{stim}\ =\ average\ synaptic\ charge\ of\ the\ site$$
$$\underline{x}\ =\ average\ Qnoise\ value\ in\ the\ whole\ experiment$$
$$\sigma_{noise} = gaussian - fitted\ standard\ deviation\ of\ Qnoise\ distribution$$

For each photostimulation site, **synaptic amplitude Z-score** value was calculated as follows:

$$Z\ score\ =\ \frac{A_{stim}\ -\ \underline{x}}{\sigma_{noise}}$$

$$A_{stim}\ =\ average\ maximum\ synaptic\ amplitude\ of\ the\ site$$
$$\underline{x}\ =\ average\ Anoise\ value\ in\ the\ whole\ experiment$$
$$\sigma_{noise} = gaussian - fitted\ standard\ deviation\ of\ Anoise\ distribution$$

Z-scores of 1.96 and 3.09 corresponding to a significance level of respectively 0.023 and 0.001 were chosen to define significant and silent sites.

5.9.3 Individual and median GC input patterns:

In each mediolateral position of the GC layer, the site with the maximum Z-score value was used to build spatial patterns for each experiment (***Figure 15D***). In order to pool z scores between mice, distance and position values in each experiments were normalized to the length of the P1- ipsilateral Zebrin band, yielding following positions in adult CD1 mice (% of P1- ±SD): *P2- contralateral* -267,52±36,76; *P2+ contralateral* -134,38±14,92; *P1- contralateral* -110,52±12,61; *P1+* -10,83±5,17; *P1- ipsilateral* 100; *P2+ ipsilateral* 122,94±6,85; *P2- ipsilateral* 256,92±33,43. Thus negative %P1- positions correspond to z scores located on the contralateral side from recorded PCs and positive %P1- positions correspond to ipsilateral z scores. Recorded PCs were located on average at 17.98±10.18 %P1-.

Median input pattern (i.e. group data) were built as follows: z scores from input pattern of several experiments were sorted according to their normalized mediolateral position in the GC layer and median values were computed in bins of 8 to 12%P1-. The bin size was chosen in order to ensure a minimum of 5 z scores values for median calculation.

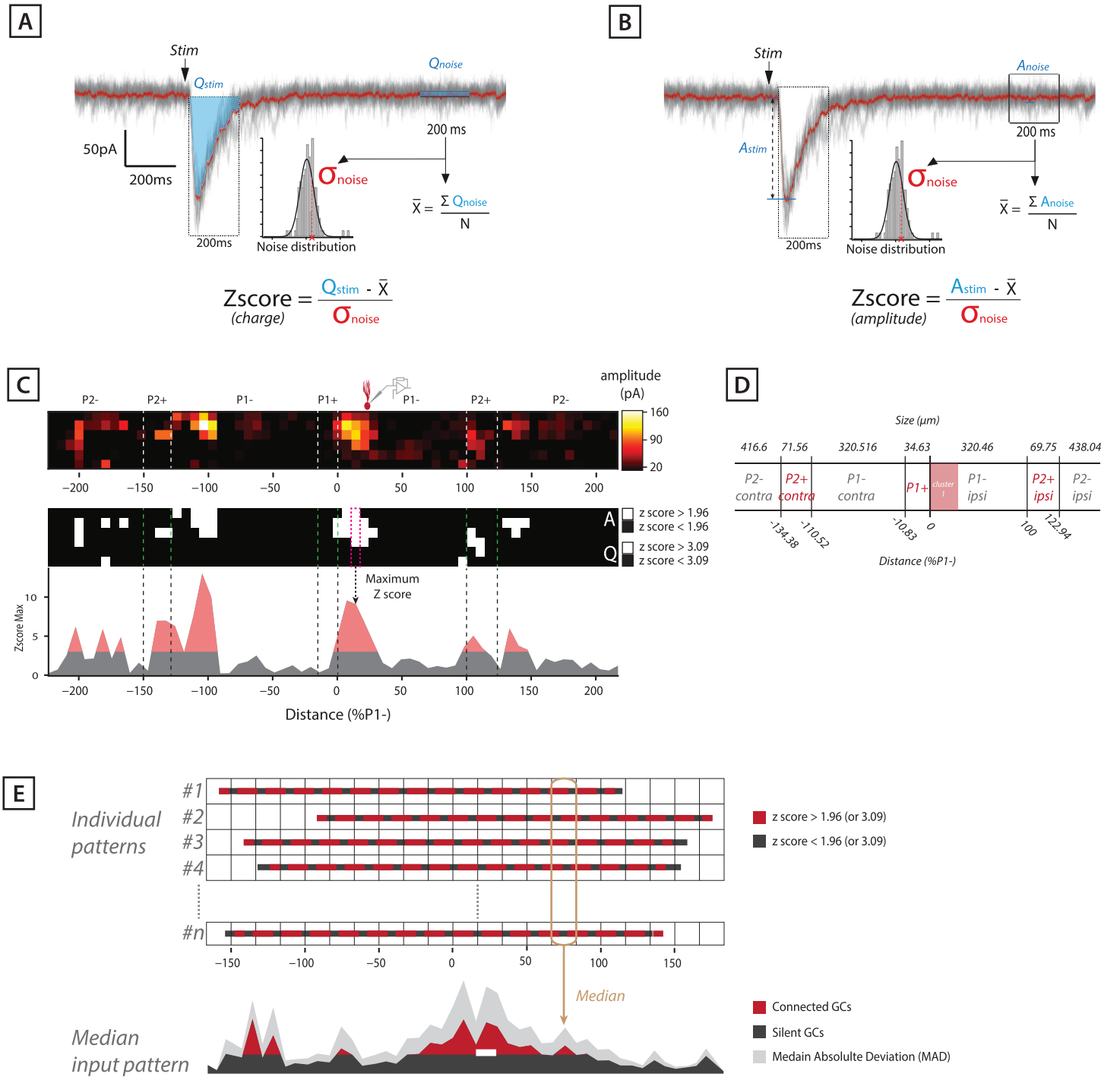

Figure 15 : Z score computation and reconstruction of individual synaptic maps, individual and median patterns

(A) Measures of synaptic charge and associated Z-score. For a given site, evoked synaptic charge Qstim is measured in a 200ms window following onset of stimulation. Corresponding background noise (Qnoise) is measured in a 200ms time window outside the stimulation period. Every noise measures for a whole map are averaged to get the X value. Standard deviation σnoise value is computed by gaussian fit of noise distribution.

(B) Measures of synaptic amplitude and associated Z-score. For a given site, maximum evoked synaptic amplitude Astim is measured in a 200ms window following onset of stimulation. Corresponding background noise (Anoise) is measured in a 200ms time window outside the stimulation period. Every noise measures for a whole map are averaged to get the X value. Standard deviation σnoise value is computed by gaussian fit of noise distribution.

(C top) Evoked amplitudes are positioned according to the spatial position of associated photostimulation site. *(C middle)* Binary Z-score map established with synaptic map located above. GC eliciting significant synaptic amplitudes (i.e. z-score > 1.96) to recorded PC (in red) are shown in red; while non connected GCs (i.e. z-score < 1.96) are shown in black. For analysis of significant charges, z-score cut off is 3.09. *(C down)* The maximum z-score value is extracted in each column of GC layer in order to build individual GC-PC input pattern. Significant zscores are in red, non significant zscores are in black.

(D) Correspondence between Zebrin bands size and normalized referential (averaged values). In order to pool z scores between mice, distance and position values in each experiments were normalized to the length of the P1- ipsilateral Zebrin band. Functional cluster 1 defined by Valera et al., 2016 is represented by the red-filled box (0-120µm from midline, corresponding to 0 - 33% P1-). All recorded PCs were located in this cluster.

(E) Schematic method for the establishment of median input patterns. Individual patterns are spatially positioned and stacked within a global matrix. Zscore median is computed across patterns in order to establish median input pattern between several individual patterns yielding spatial distribution of median connected GCs (in red), non connected GCs (in black) to recorded Purkinje cells within functional cluster 1 (white bar). Light gray filled curve represents median absolute deviation.

5.9.4 Variance to median pattern

In order to evaluate the dispersion of synaptic maps, individual synaptic patterns were compared to the median pattern. In each condition, individual z scores were compared to median z score of the same spatial bin as follow:

$$Vmed = \frac{1}{n}\sum_{i=1}^{n}(Xi - Xm)^2$$

$$V_{med} = variance\ to\ median, n = sample\ size\ (number\ of\ patterns)$$
$$X_i = individual\ z\ score, X_m = median\ z\ score$$

5.10 Analysis of MF stimulation recordings

EPSC and IPSC average traces from MF optogenetic stimulation were obtained and synaptic charges were calculated for a 150 201 ms window. The latency was defined as the crossing point between the baseline and the linear fit of the MFs-induced response calculated between the 20 % and 80 % of the rising phase. Statistics are indicated in the text. For the ΔLat measurement following direct GC stimulation, the dataset recorded for this experiment has been combined with the dataset from Grangeray-Vilmint et al., (2018).

5.11 Catwalk & balance assessment

To assess and quantify cuff-induced gait and balance impairments, we built a pressure-sensor catwalk device. Mice were trained to walk in a 80 cm long corridor covered with two parallel ribbon pressure sensors (force-sensing-resistors, Interlink 408, Adafruit) on each side (***Figure 19B***). Pressure and video acquisition were triggered by a Raspberry Pi microcomputer when the mouse enters the corridor and cross an IR-barrier. Pressure from the left/right part of the body was then monitored during locomotion before (baseline) and after cuff or sham surgery. Pressure signals for left and right side of the body were acquired simultaneously with WinWCP 4.2.2 freeware (John Dempster, SIPBS, University of Strathclyde, UK). Recordings were digitized at 15-20 kHz. For technical details (i.e. apparatus dimensions, scripts and wiring diagrams) see Appendix 4.

5.12 Analytic tools

Most of the analysis and statistics were performed on electrophysiological and behavioral data (catwalk) using homemade scripts and routines written in Python 3.6 available at : https://github.com/ludo67100/GC-PC_maps.

Recordings were stored on local SQL database and preprocessed if needed with python-based open source software for electrophysiological analysis and handling :

- *OpenElectrophy* : http://neuralensemble.org/OpenElectrophy/ (Garcia and Fourcaud-Trocmé, 2009)
- *SynaptiQs*: https://synaptiqs.wixsite.com/synaptiqs (Antoine Valera)

Principal components analysis and clustering were performed with python- or R-based open source software:

- *Orange Data Mining* (University of Ljubljana): https://orange.biolab.si/ (Demsar et al., 2013)
- *FactoMineR* package for R : http://factominer.free.fr/index_fr.html, (Lê et al., 2008)

6. Results

This section will describe the experimental results I obtained to answer the two questions addressed in the preamble. First part of the results will be dedicated to the developmental dataset, i.e. GC-PC functional mappings performed in P9 to P30 mice (section 6.1). The second part describes mappings and behavioral data that investigates the adaptation of functional PC clusters to locomotor impairment or training (6.2).
In the third part we looked at the spatial and temporal segregation of excitatory and inhibitory GC inputs to PCs. Results are shown in section 6.3.

6.1 Postnatal development of GC-PC connectivity maps in the anterior vermis

Stereotyped GC inputs showed by Valera and colleagues (*see section 3.3.3*) (Valera et al., 2016) raised a fundamental question: how are established GC-PC synaptic maps? In other words, do distant cerebellar microzones communicate during development?

To address this question, PCs of lobules III/IV within functional cluster 1 (*see section 3.3.3*) were recorded in voltage clamp configuration (***Figure 14A, 14B***) and Rubi-Glutamate was systematically uncaged in 41*41µm squared areas of the GC layer (*see methods 5.6, 5.8*). Synaptic inhibition was blocked by picrotoxin (*see methods 5.6*) and evoked excitatory postsynaptic currents (eEPSCs) were recorded in acute cerebellar slices from mice aged between P9 and P40.

6.1.1 Local GC inputs are larger than distant inputs, except between P14 and P18

In order to investigate the functional relationship between cerebellar microzones, significant synaptic charges (eQ, z score > 3.09, *see methods 5.9.2*) elicited by the photostimulation were segregated in 2 categories: (1) local eQs (i.e. elicited by GCs belonging to the same functional microzone, *see section 3.3.3*) and (2) distant eQs (i.e. elicited by GCs from every other positions within the GC layer, ***Figure 16A***).

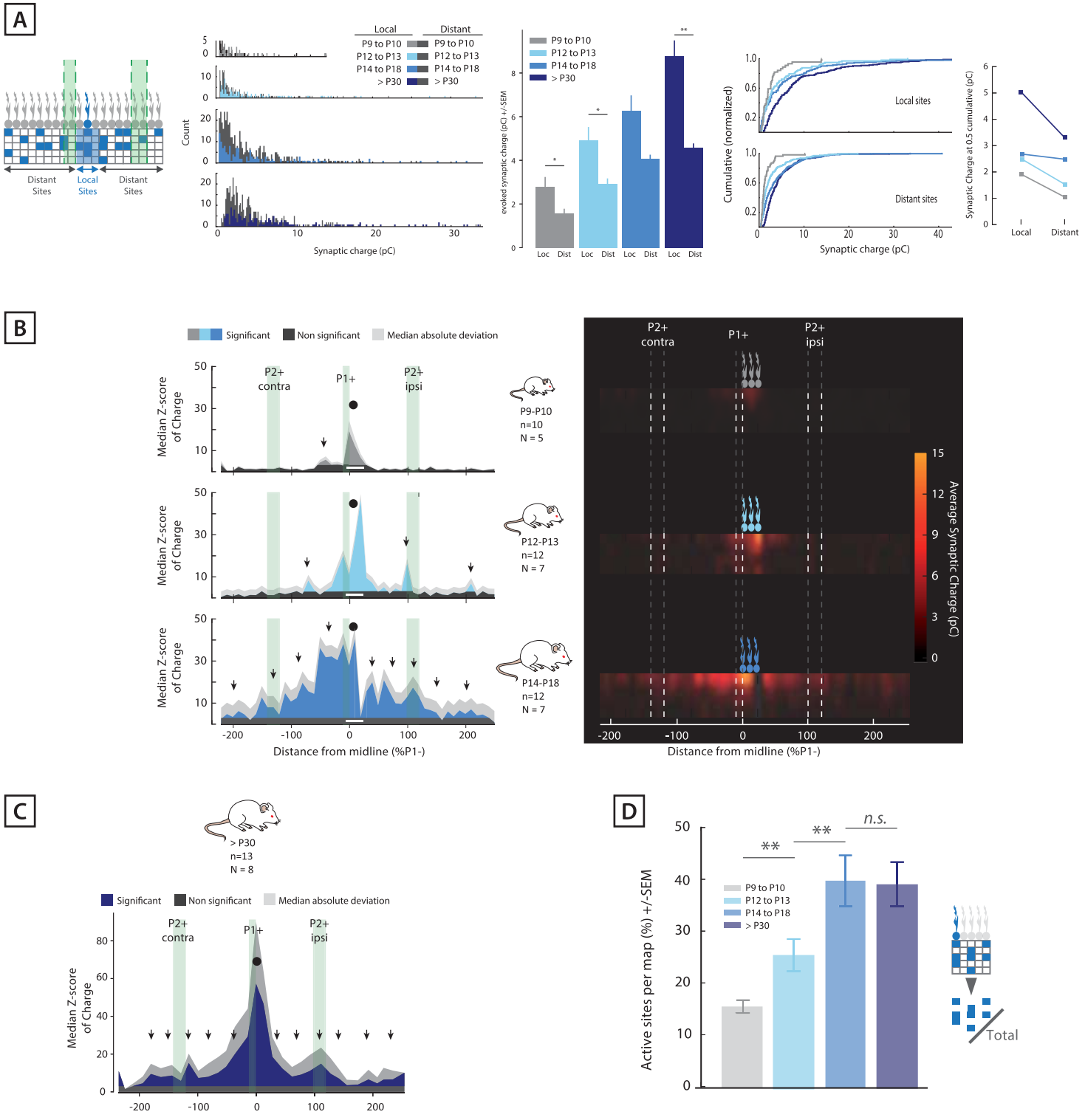

Figure 16: Development of the inter-modular communication within the cerebellar cortex

(A, from left to right) Sorting local and distant granule cell inputs : Local inputs belong the functional microzone of interest, i.e. granule cells located underneath the recorded Purkinje cells while distant inputs are located in other microzones. Distributions of synaptic charges evoked by photostimulation of local and distant granule cells. Average evoked synaptic charge +/- SEM (* : p<0.001; ** : p<0.000001, two-sided Mann Whitney test). Normalized cumulative distributions of synaptic charge evoked by photostimulation and synaptic charges at p=0.5 of occurrence for local and distant granule cells.

(B, left) Median GC input patterns to PCs within functional cluster 1 (=0-33%P1-, white bar) recorded in P9-P10, P12-P13 or P14-P18 mice. Non connected GCs are represented in black. Shades of blues curves represent functionally connected granule cells (i.e. Z-score > 3.09). Light gray curve represent median absolute deviation. Local cluster is observed in every conditions (black dot), while distant clusters mentioned in text (black arrows) appear as the animal grow up. *(B, right)* Corresponding spatial maps representing average evoked synaptic charge according to the position of the granule cells photostimulation sites.

(C) Median GC input patterns to PCs within functional cluster 1 (=0-33%P1-, white bar) recorded in adult mice. Non connected granule cells are represented in black. Dark blue curve represents functionally connected granule cells (i.e. Z-score > 3.09). Light gray curve represent median absolute deviation. The local granule input is represented by a black dot. Black arrows show distant inputs.

(D) Proportion of active vs silent granule cell photostimulation sites per mice age (** : p<0.01, n.s. : non significant, two-sided Mann Whitney test).

In adult mice, glutamate uncaging evoked local eEPSCs with an average synaptic charge of 8.78 ± 9.39 pC. GCs belonging to other microzones elicited significantly smaller eEPSCs, with an average synaptic charge of 4.5 ± 4.01 pC ($p=1.001^{-8}$, two-sided Mann Whitney test, n=13 (***Figure 16A***). This trend for higher local eEPSCs vs distant eEPSCs was confirmed in mice pups P9 and P10 (2.79 ± 2.9 pC vs 1.57 ± 1.55 pC on average, p=0.0027, n=10) and between P12 and P13 (4.09+/-6.04pC vs 2.92+/-3.46 on average, p=0.00039, n=12, ***Figure 16A***). In mice aged between P14 and P18, average synaptic charge of local eEPSCs does not differ from charge elicited by distant GCs (6.27 ± 8.65 vs 4.05 ± 4.29 pC on average, p=0.144, n=12). This was confirmed by an evaluation of the cumulative distributions of local and distant synaptic charges: at 0.5 cumulative, local and distal GCs induce similar synaptic charges (2.82 vs 2.71 pC, ***Figure 16A***) in P14-P18 mice.

6.1.2. GC inputs at P9 are observed only in the local microzone

GC-PC connectivity maps have been built from glutamate uncaging experiments in order to identify the spatial origin of the granular inputs. Microzone identity was determined after slice reconstruction using the Zebrin band patterning (*see methods 5.9* and ***Figure 16B, 16C***).

PCs in cluster 1 were recorded in slices from P9-P10 mice (n=10, N=5) and median input patterns were built (*see methods 5.9* and ***Figure 16B***). Connected GCs were found underneath the recorded PCs (from 0 to 32 %P1-, z score max = 19.7 ± 11.57, median ± MAD) and in a narrow contralateral band (10 to 30%P1-, z score max = 7.65 ± 3.75, median ± MAD) (***Figure 16B***). These functional inputs are located within the upper half of the GC layer (***Figure 16B***). Both input locations correspond to the Am zone.

Strikingly, the median input pattern does not reveal any other functionally connected GC regions (z score < 3.09, ***Figure 16B***) i.e. originating in neighboring microzones. However, discrete distant GC inputs could be observed occasionally (in 2 out of 10 synaptic maps, ***Figure 18A***). Significant sites in the median input pattern shows positions of the GC layer that are conserved between individuals, (i.e. in which GC inputs have a high probability of occurrence).
Our results showed that distant GC inputs in P9-P10 mice are (1) extremely rare and (2) their spatial position is not conserved between individuals (***Figure 16B***).

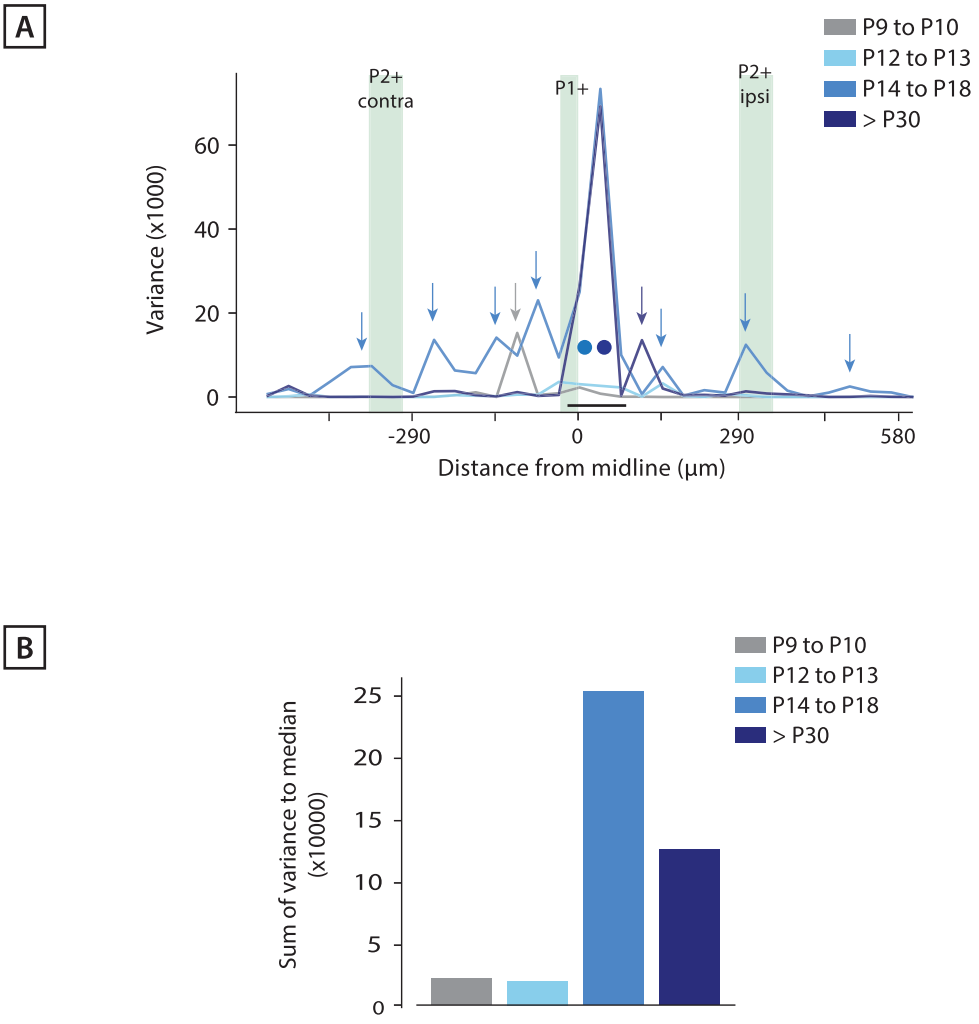

Figure 17: Toward a critical period in developing cerebellar networks

(A) Variance to median pattern according to the mediolateral axis. Squared distance computed in panel A were divided by √(n-1) in each condition. Local variance is represented by colored dots, distant variance hotspots are represented by colored arrows. Purkinje cell positions is shown by the black horizontal bar.
(B) Corresponding variance to median pattern : each colored bar represents the sum of equivalently-coloured curve in panel A.

6.1.3 PFs cross the entire vermis at P8

As the molecular and GC layer undergo maturation at P9-P10 (*see section 2.5*), the absence of distal GC inputs at P9-P10 could be explained by a lack of fully grown PFs within the anterior vermis. To address this question, Di-I was injected (*see methods 5.1.3*) in the lobules IV/V at P8, and individual parallel fibers were reconstructed using confocal imaging and measured from the injection point (***Figure 18B***). Fully grown PFs are present as soon as P8 and travel along the entire vermis (up to 800µm from injection site, ***Figure 18B***). Thus, the presence of local inputs only is likely due to a lack of functional synapses from distant sites rather than undeveloped PFs.

6.1.4 PF mediated communication between microzones starts at P12

Synaptic maps established in P12-P13 animals revealed local (z score max = 44.65 ± 16.5; median ± MAD) and distant GC inputs (***Figure 16B***). Local GC inputs are located at all depths of the GC layer (***Figure 16B***). Distant GC hotspots can be observed in the ipsilateral $P2^+$ Zebrin band (100%P1-, z score max = 17.5 ± 6.47, median ± MAD) and in ipsilateral $P2^-$ Zebrin band (210%P1-, z score max = 6.89 ± 3.15, median ± MAD, ***Figure 16B***). These results illustrate the first steps of intermodular communication within the anterior vermis. Most of distant GC inputs to PCs from functional cluster 1 belong to neighboring ipsilateral zones.

6.1.5 Synaptic connectivity maps expand between P14 and P18

In P14-18 mice, significant GC inputs are localized within the whole photostimulated GC layer, providing inputs from ipsi and contralateral A, AX and B zones (i.e. $P1^-$, $P2^+$ and $P2^-$ zebrin bands, ***Figure 16B***).

In order to quantify the expansion of GC inputs, the proportion of significant eEPSCs has been determined in each synaptic maps (***Figure 16D***). Between P12/P13, 24.94±8.9% (mean ± SD) of the photostimulated GC layer elicited significant eEPSCs in PCs located in functional cluster 1 (***Figure 16B, 16D***). A two-fold increase in functionally connected photostimulated was observed in P14/P18 mice (40.72±13.1%; mean ± SD, p=0.00704, two-sided Mann-Whitney test on distribution). The increase of connected GCs was more important between P12/P13 and P14/18 than between P9/P10 (15.5 ± 3.18% in P9/P10 vs 24.94 ± 8.9%; mean ± SD in P12/P13 mice, ***Figure 16D***), suggesting faster functional synaptogenesis in adolescent mice rather than pups.

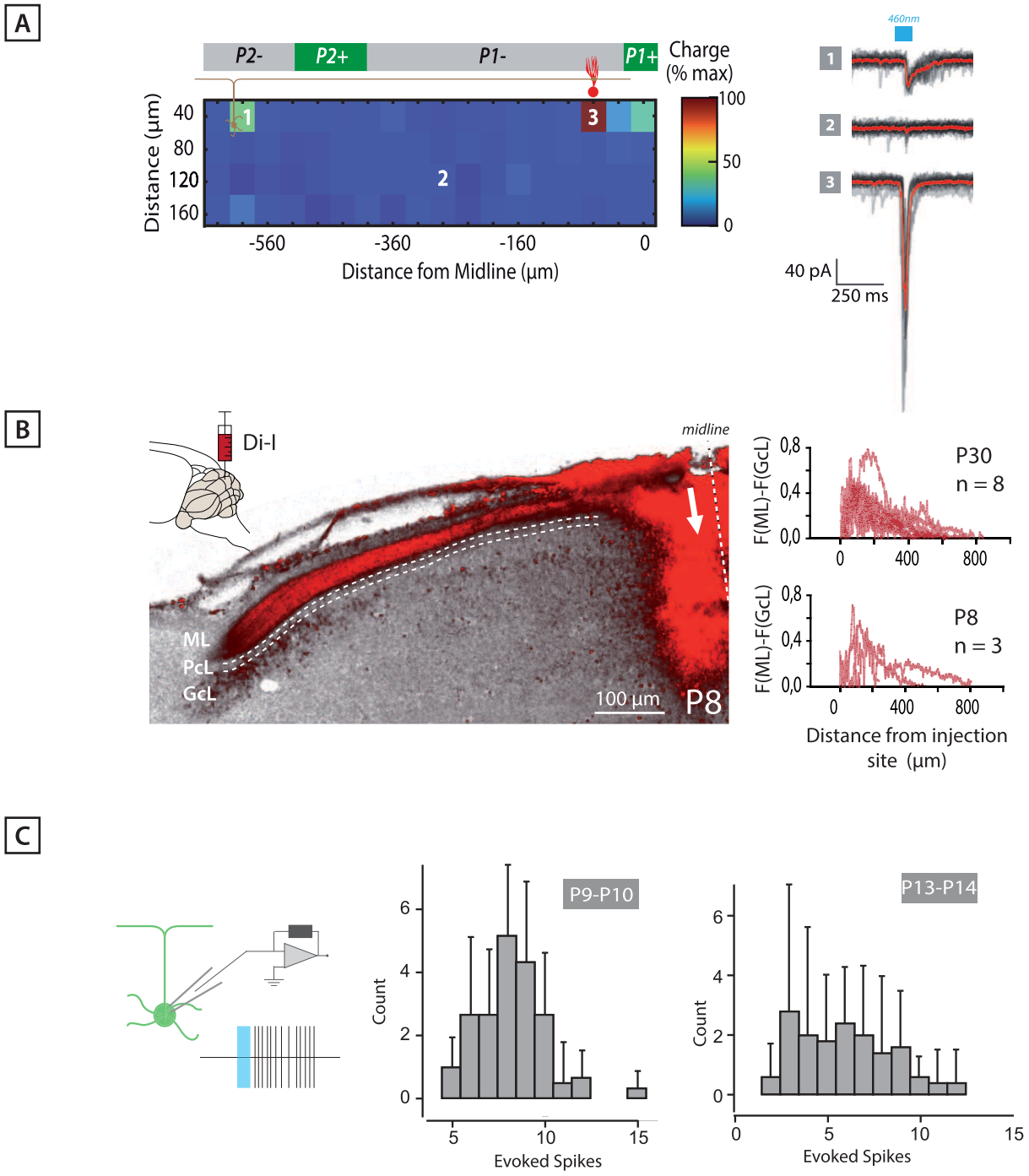

Figure 18: Postnatal growth of parallel fibers and granule cell excitability in the anterior vermis

(A) Example of synaptic input map at P9 (*left*) and recorded EPSCs (*right*). Local input is present underneath the recorded Purkinje cell (*3, in red*). Majority of photostimulated granule cells are silent (*2*), yet occasional single distal sites could be observed (*1*). Raw recordings are superimposed in light gray, red traces correspond to average.

(B) Parallel fibers travel along the whole vermis at P8. Rarity of distant inputs at P9-P10 is not due to a lack of parallel fibers. Example of Di-I injection in the vermis at P8 (*white arrow*) and fluorescence ratio between the molecular and the granule cell layer. ***ML** : molecular layer; **PcL** : Purkinje cell layer; **GcL** : granule cell layer.*

(C) Postnatal granule cell are equivalently sensitive to Rubi-glutamate. Granule cells firing rate has been recorded in loose-cell attached configuration during glutamate uncaging. Light-evoked spike distributions do not differ between P9/P10 and P13/P14 (p=0.29, independent samples t-test on distribution).

6.1.6 Critical period for the establishment of synaptic maps

Synaptic maps established in adult mice (>P30, n=13, N=8) revealed similar median input pattern (***Figure 16D***) than P14/P18 mice (***Figure 16B***). In addition, both conditions display similar amount of GC inputs (40.72 ± 13.1% in P14/P18 vs 39.51 ± 15.51% in adults, mean ± SD, p=0.247, two-sided Mann-Whitney test on distributions, ***Figure 16D***).

In order to evaluate the variance in synaptic maps, individual synaptic z score patterns were compared to the median pattern for each condition (*see methods 5.9.4* and ***Figure 17A, 17B***). P14/P18 mice showed higher interindividual variance than either younger or adult mice ($251.854.10^3$ vs $125.1943.10^3$, ***Figure 17B***). Variance observed in adult mice was mostly explained by the local inputs (i.e. inputs in the medial A zone, corresponding to $P1^+$ and ipsilateral $P1^-$ zebrin bands, ***Figure 17A***). Local inputs in P14-P18 mice were equivalently variable (maximum variance $73.395.10^3$ vs $69.212.10^3$, ***Figure 17A***) however distant GC inputs displayed higher variance as well, especially in the ipsilateral $P2^+$ band and contralateral $P1^-$ and $P2^+$ zebrin bands (***Figure 17A***). While local GC inputs to cluster 1 PCs are conserved in P14/P18 mice and adults, distal inputs are highly variable between adolescent mice, suggesting potential functional rearrangements of GC to PC inputs at this age.

Taken together, these results show that stereotyped GC-PC clusters defined by Valera and colleagues (Valera et al., 2016) appear progressively throughout postnatal development of the cerebellar cortex. Communication between microzones via PFs starts at the end of second week of life, mostly between ipsilateral microzones, then gets exacerbated during adolescence prior to stabilization at adulthood.

6.2 Toward a causal link between locomotor adaptation and synaptic maps in the anterior vermis

Valera and colleagues identified stereotyped spatial distributions of GC inputs to clusters of PCs within the anterior vermis (Valera et al., 2016). As GC-PC synapses can be adjusted via synaptic plasticity (*see section 2.4.2*) they investigated whether connectivity maps could be altered *in vitro*. Electric PFs stimulation at 1 Hz or repeated glutamate uncaging in GC layer modified the GC-PC synaptic maps (Valera et al., 2016). These results suggest that conserved GC inputs across individuals could be the consequence of synaptic plasticities and cerebellar learning that occurred during the life of mice, notably during locomotor adaptation (Valera et al., 2016, Apps & Garwicz., 2005; Dean et al., 2010).
We then hypothesized that different behavioral conditions should involve differential learning strategies resulting in differential synaptic maps and microzones combinations. Since lobules III & IV are largely involved in forelimb and hindlimb coordination as well as locomotor adaptation (*see section 4.2*) mice underwent procedures to improve or impair their locomotor abilities (*see methods 5.3.1, 5.4*). PCs within functional cluster 1 (*see section 3.3.3*) were recorded in voltage clamp configuration and Rubi-Glutamate was systematically uncaged in 20*20µm squared areas of the GC layer in order to establish GC-PC synaptic maps resulting from different behavioral conditions (*see methods 5.6, 5.8* and ***Figure 14A, 14B***).

6.2.1 The cuff model triggers severe but transitory locomotor impairment

Adult ALDOC male mice were cuffed (N=10) on the right sciatic nerve (*see methods 5.3.1*). First, their locomotor behavior was monitored in a modified catwalk behavioral assay (*see methods 5.11 and appendix 4*): animal balance was measured using pressure sensor during locomotion in a corridor (***Figure 19B***). For each trial, the pressure signal from the left side is summed to the negative pressure signal of the right side, in order to obtain a sinusoïd curve representing left/right limb alternance (***Figure 19C***). Integral of this signal represents balance asymmetry, hence named balance index. Therefore, balance index ≈ 0 means that animals are well balanced (i.e. they used both side of their body equally as expected in healthy condition). Positive and negative indexes represent balance asymmetry toward left and right of the body respectively (***Figure 19C***).

Before surgery mice displayed normal left/right balance: no asymmetry could be observed in the pressure profile (baseline balance index = -0.08 ± 0.32, mean±SD, (***Figure 19D***). Mice use both side of the body to walk, without any preference from trial to trial. After surgery, cuffed

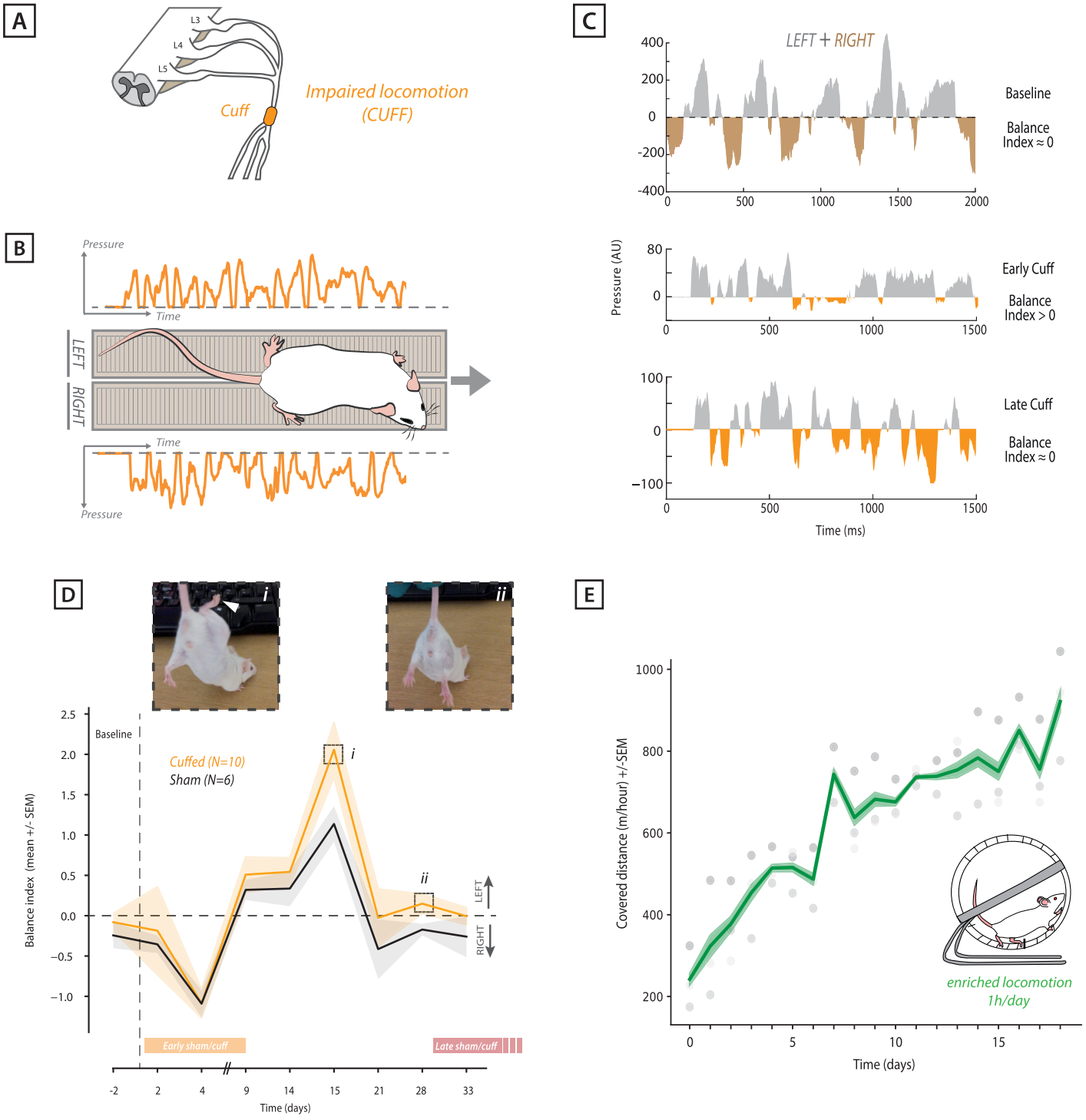

Figure 19 : impaired or enhanced locomotor activity in mice

(A) The cuff model involves a small plastic piece wrapped around the main branch of the right sciatic nerve (see Yalcin et al, 2015).

(B) Catwalk assay for locomotion performance assessment: mice are trained to run on pressure sensors to evaluate left/right balance (left panel).

(C) For each trial, the pressure signal from the left side is summed to the negative pressure signal of the right side, in order to obtain a sinusoïd curve representing left/right limb alternance. Integral of this signal represents balance asymmetry, hence named balance index. Therefore balance index ≈ 0 means that animals are well balanced (e.g. in control and after balance recovery in cuffed mice, top and bottom plots). Positive index balance (e.g. after cuff implementation, middle plot) yields balance deficit and asymmetry towards the left side of the body.

(D) Temporal course of locomotor impairement in SHAM and cuffed mice. The cuff surgery induces severe, nonetheless transitory balance impairment. Mice limp on the cuffed side up to 9 days after surgery, then switch side to reach maximum impairment and display right hindlimb extenstion reflex (*inset i*). Mice recover normal balance 3 weeks after surgery, and lose the extension reflexe (*inset ii*). SHAM mice display mild balance impairment in comparaison. The dashed line represents surgery day (*t=0*). Synaptic maps recorded during transitory right-based asymmetry (t<9 days) are classified as early cuff/sham while maps obtained after full recovery (*t>30 days*) are classified as late cuff/sham.

(C) Model for locomotor enrichment. Mice had free access to a running wheel (one wheel/mouse) for 1h a day for 20 days prior to synaptic maps recording.

mice were tested on the catwalk for 33 days (***Figure 19D***). All mice showed altered balance after cuff: they limped on the cuffed side (i.e. right side, balance index = -1.08±0.54, mean±SD, ***Figure 19D***). We named this transitory phase (between day 2 to day 9) "*early cuffed*" phase in the following paragraphs.

After 9 days, a progressive switch of the limping side was observed (***Figure 19B***). In 11 days, the right-based asymmetry (-1.08±0.54, mean±SD at day 4) switched to a left-based asymmetry (balance index = 2.05±1.06, mean±SD at day 15, ***Figure 19B***), highlighting the progressive compensation of right hindlimb impairment by the other side of the body (i.e non-cuffed side). 3 weeks after the cuff, all mice completely resumed normal balance and showed a balance index equivalent to values observed in baseline (t=21 days, balance index = -0.028 ± 1.1, mean±SD, ***Figure 19D***). This phase will be qualified as *"late cuff"* phase in the following paragraphs.

6.2.2 Sham animals display mild locomotor impairment

As opposed to cuffed animals, SHAM animals (N=6 mice) lack the plastic cylinder (cuff) but underwent the same surgery process (*see methods 5.3.1*). SHAM mice also displayed a transitory phase (early SHAM) with limping on the right side (balance index = -1.09 ± 0.38, mean±SD, ***Figure 19D***) then a compensation by the left side (t=15 days after cuff, balance index = 1.13 ± 0.49, mean±SD, ***Figure 19D***). They recovered an efficient balance at 21 days after surgery, just like the cuffed animals (balance index = -0.41 ± 0.82, mean±SD, ***Figure 19D***). If the time course of the balance was the same between SHAM and cuffed animals, the degree of asymmetry is smaller in SHAM mice in the compensatory phase (1.13±0.49, mean±SD for SHAM vs 2.05±1.06, mean±SD for cuffed at day 15, ***Figure 19D***). These results suggest stronger maximum impairment in cuffed mice compared to SHAM mice, although no statistical difference could be found (p=0.061, Mann-Whitney test) and further experiments would be required in order to increase the sample size.

The cuff model provides a "*2 in 1"* model for locomotor impairment: cuffed and SHAM animals show transitory limping from right to left side within the same time course, although limping phenotype tend to be amplified in cuffed mice.

6.2.2 The cuff model increases synaptic connectivity in the anterior vermis

Excitatory synaptic GC-PC maps were recorded (*as described in methods 5.6,5.8,5.9* and ***Figure 14B, 15***) in control (i.e. naïve, raised in standard conditions, n=14), early cuff/SHAM (n=7, n=21) and late cuff/SHAM (n=13, n=17) conditions mice (***Figure 20B***).

In order to quantify the changes in GC inputs in the different conditions, we first determined the proportion of significant eEPSCs (i.e. amplitude z score > 1.96, *see methods 5.9*) in each synaptic maps (***Figure 20C, 20D***). Synaptic amplitudes were summed in each map and the total excitatory inputs to PCs within cluster 1 was estimated (***Figure 20C***). The total evoked synaptic amplitude increased in early and late cuffs compared to controls (total amplitude (nA) = 75.8 ± 44.7; 56.9 ± 33.3 vs 26.2 ± 14.6; mean ± SD, p=0.0012, p=0.013 respectively, two-sided Mann Whitney test on distributions, ***Figure 20C***) and sham conditions (total amplitude (nA) = 23.7 ± 12.2 vs 75.8 ± 44.7 and 16.2 ± 9. vs 56.9 ± 33.3, mean±SD, p=0.0026, p=0.0016 respectively, two-sided Mann Whitney test on distributions). In addition, we determined the proportion of the photostimulated GC layer eliciting significant eEPSCs in recorded PCs (***Figure 19D***). The amount of active GC sites increased in both early (21.85 ± 10.87%, mean±SD) and late cuffed mice (25.0 ± 11.77%, mean±SD) when compared to control mice (15.1 ± 8.18%, mean±SD; p-values = 0.0304 and 0.0065 respectively, one-sided Mann Whitney test on distributions, ***Figure 19D***).
Taken together these results highlight a striking increase of the global functional GC-PC synaptic connectivity in cuffed mice.

6.2.3 Locomotor adaptation tunes synaptic maps and inter modular communication in the anterior vermis

Functional GC-PC maps of PCs located within the functional cluster 1 in lobules III/IV were recorded and median input patterns were built from control, enriched, early SHAM/cuffed and late SHAM/cuffed animals. We then addressed whether connectivity maps have changed in impaired/improved locomotor conditions vs control mice.

6.2.3.1 Control condition

Control mice (n=14 maps, N=10 mice) were raised in standard conditions (*see methods 5.2*). Median input pattern revealed local GC connections in the medial A zone (from -60 to 70% $P1^{-}$, z score = 5.62 ± 3.94, median ± MAD, at 18% $P1^{-}$, ***Figure 21A***) Distant GC hotspots were

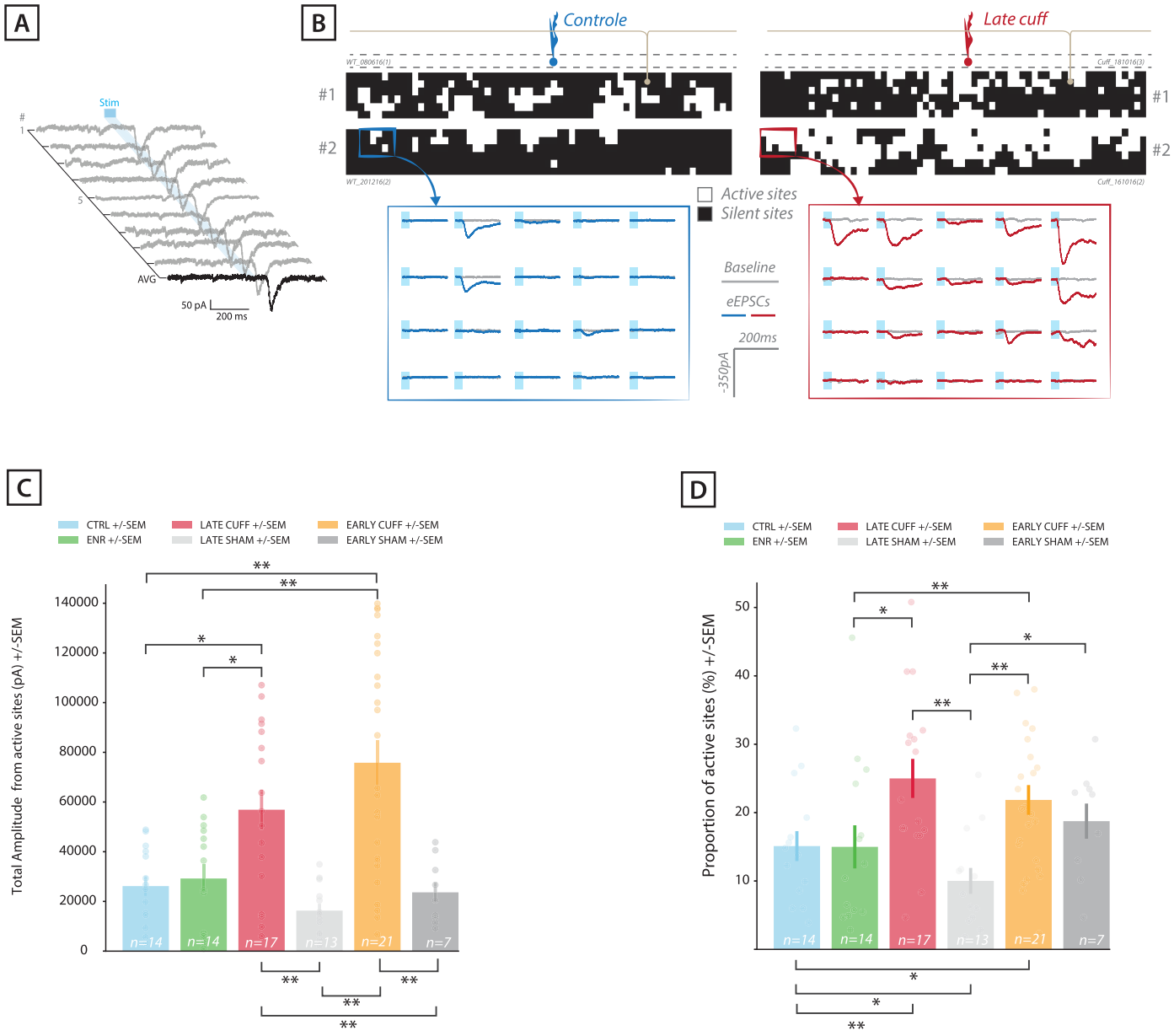

Figure 20 : The cuff model increases synaptic connectivity and variance in the anterior vermis

(A) Example of eEPSCs obtained after 9 consecutives photostimulation on the same site of the granule cell layer (*light gray trace*) and corresponding average (*black trace*).

(B) Example of synaptic maps obtained in controle (*left*) and late cuff (*right*) mice and corresponding averaged eEPSCs. Active sites (i.e. amplitude z-score >= 2.0) are shown in white, while silent sites (i.e. amplitude z-score < 2.0) are shown in black.

(C) Average total synaptic amplitude evoked by RuBi glutamate uncaging. In each conditions, significant synaptic amplitudes (i.e. z-score >= 2.0) have been summed (*colored dots*). Colorbar represent average +/- SEM (*: p<0.05; **: p<0.01,two-sided Mann Whitney test on distribution).

(D) Proportion of active sites per maps. In each conditions the amount of significant synaptic amplitudes (i.e. z-score >= 2.0) has been evaluated (*colored dots*). Colorbar represent average +/- SEM (*: p<0.05; **: p<0.01, one-sided Mann Whitney test on distribution).

observed in both ipsilateral (z score = 3.07 ± 1.97 , median ± MAD, at 102% P1) and contralateral $P2^+$ (z score = 2.75 ± 2.43, median ± MAD, at -137% $P1^-$) Zebrin bands (***Figure 21A***). A GC hotspot was observed in the contralateral (z score = 5.98 ± 2.09, median ± MAD, at -232% $P1^-$) but not in the ipsilateral B zone (z score = 1.94 ± 0.8, median ± MAD) suggesting contralateral lateralization of the pattern (***Figure 21A***) in control mice.

6.2.3.2 Enriched condition

Enriched mice (n=14, N=7) were raised in similar housing conditions than control mice (i.e. cage size, number of individuals per cage, type of litter and food) except voluntary training 1h/day for 3 weeks in a running wheel (*see methods 5.4*). We assessed the locomotor activity by measuring the covered distance in each session (***Figure 19E***). Low activity in the running wheel (covered distance (meter/hour) = 242.19 ± 61.84, mean ± SD) was observed at day 0. Mice continuously increased locomotor activity from session to session (covered distance (meter/hour) = 682.42 ± 73.44a t day 10 and 921.27 ± 110.06 at day 19; mean ± SD) suggesting an efficient adaptation to the running wheel.

After 20 days of training, mice were sacrificed in order to record PCs within functional cluster 1 and establish GC-PC spatial maps (***Figure 21B***). Similar local inputs to control condition were found (from -30 to 77% $P1^-$, z score = 7.45 ± 6.67, median ± MAD, at 6.3%$P1^-$, Figure ***21B***). Unlike in control mice, no significant median GC inputs were found in the contralateral A or B zone (z score = 1.44 ± 1.24, median ± MAD, at -101% $P1^-$, ***Figure 21B***), but distal peaks of connectivity were found in the ipsilateral AX/B zone (z score = 2.76 ± 1.53 and 2.36 ± 1.92, median ± MAD, at respectively 137% $P1^-$ and 162% $P1^-$, ***Figure 21B***). Although contralateral GC hotspots could be occasionally observed in individual maps, locomotor training tends to limit functional inputs from contralateral A and B zones.

6.2.3.3 Early SHAM/cuffed conditions

GC-PC maps were recorded in SHAM (n=7, N=5) and cuffed (n=21, N=14) mice during the early post surgery phase (*see sections 6.2.1 and 6.2.2*). Data from post surgery day 6, 7, 8 and 9 were pooled to build median input patterns in early SHAM (***Figure 21C***) and early cuffed (***Figure 21D***) condition. Early SHAM mice display functional local GC input (z score = 6.66 ± 4.02, median ± MAD, at 18% $P1^-$). Significant GC inputs are spread without discontinuity from -60 (z score = 2.48 ± 1.59, median ± MAD) to 125% $P1^-$ (z score = 1.96 ± 1.24, median ± MAD) covering the contralateral medial A zone and ipsilateral A/AX zone (***Figure 21D***). Similar

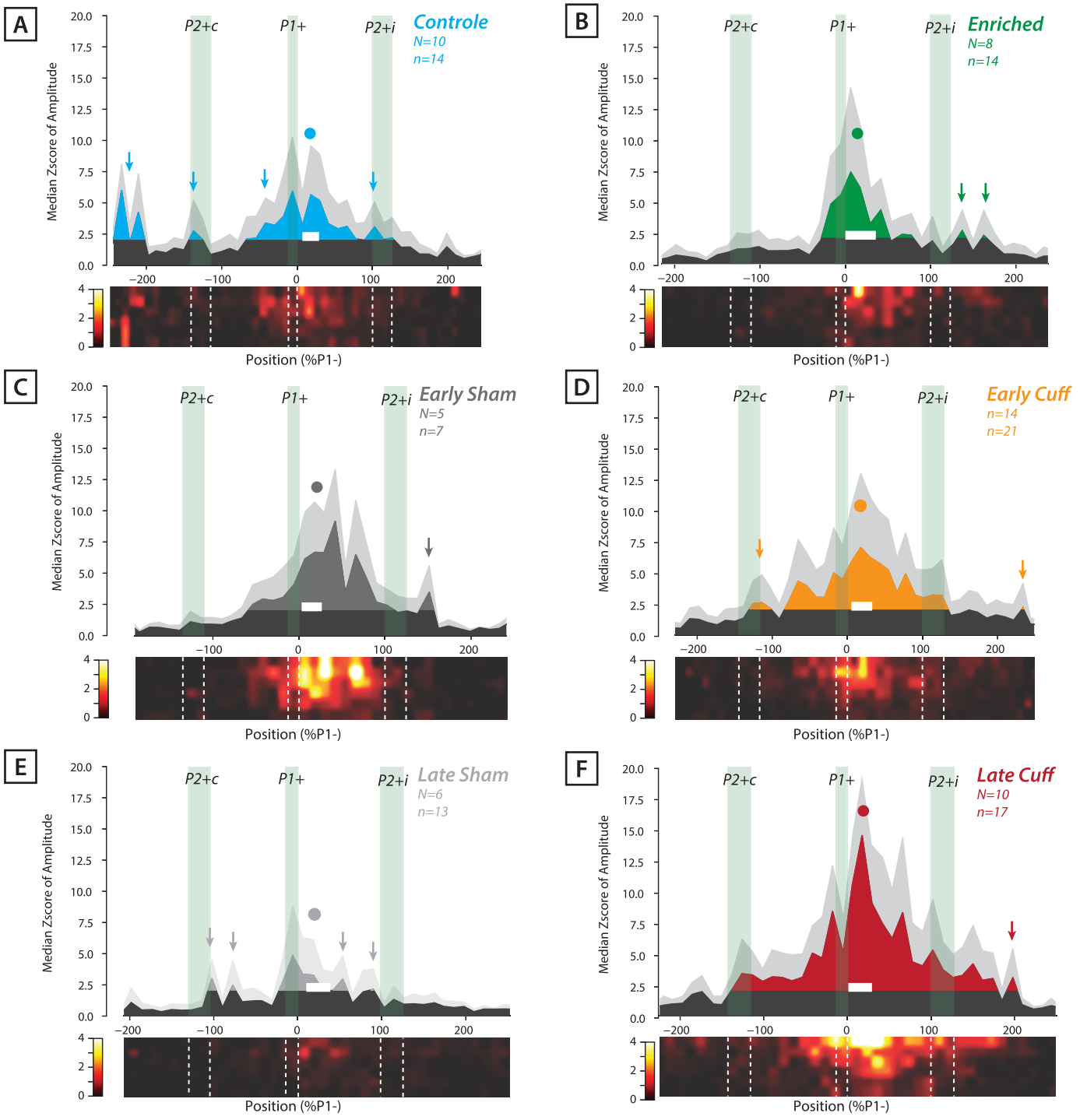

Figure 21 : Locomotor adaptation tunes synaptic maps

Median granule cell input patterns to Purkinje cells located functional cluster 1 (0 to 33%P1-, *white bar, see methods*) recorded in controle *(A)*, enriched *(B)*, early SHAM *(C)*, early cuff *(D)*, late SHAM *(E)* and late cuff *(F)* mice. Non connected granule cells are represented in black. Color-filled curves represent functionally connected granule cells (i.e. Z-score > 1.96). Light gray curve represent median absolute deviation. Local cluster is observed in every conditions (*black dot*) while location of distant clusters is variable (*arrows*).

spatial organisation of the GC inputs were found in early cuffed mice with significant connections continuously spreading from -78% (z score = 2.6 ± 1.74, median ± MAD) to 125% $P1^-$ (z score = 3.16 ± 2.83, median ± MAD) (***Figure 21D***). Contralateral distal GC inputs were found in $P2^+$ Zebrin band in early cuffed mice (z score max = 2.58 ± 2.24, median ± MAD at -133% $P1^-$) but not in corresponding SHAM condition (z score max in $P2^+$ contralateral = 1.09 ± 0.8, median ± MAD). A single ipsilateral distant GC connectivity peak was observed in the $P2^-$ Zebrin band in both early SHAM (z score = 3.45 ± 2.14, median ± MAD at 151%$P1^-$) and early cuffed mice (z score = 2.15 ± 1.97, median ± MAD at 234 %$P1^-$) (***Figure 21C, 21D***). SHAM and cuffed mice display similar motor impairment following surgery (*see section 6.2.2*), GC connections to PCs located within functional cluster 1 originate in the same Zebrin bands, with the exception of connected GCs found in contralateral P2+ band in early cuffed mice but not in early SHAM mice.

6.2.3.3 Late SHAM/cuffed conditions

GC-PC maps were recorded in SHAM (n=13, N=6) and cuffe d (n=17, N=6) mice after complete balance recovery (*see section 6.2.1 and 6.2.2* and ***Figure 19B***). Local GC inputs were found in late cuffed (z score max = 14.46 ± 8.5, median ± MAD at 17 %$P1^-$, ***Figure 21F***) and late SHAM animals (z score = 3.33 ± 2.92, median ± MAD at 6 %$P1^-$, ***Figure 21E***). In late cuffed mice, significant GC input arise from a wide region that includes the $P2^+$ contralateral Zebrin band (z score = 2.14 ± 1.22, median ± MAD at -137 %$P1^-$) to the ipsilateral $P2^-$ Zebrin band (z score = 3.06 ± 2.32, median ± MAD at 198 %$P1^-$) without discontinuity (***Figure 21F***). No significant inputs were found in the contralateral $P2^-$ band (z score max in $P2^-$ = 1.95±1.19, median ± MAD) (***Figure 21F***).

Late sham mice on the other hand displayed distant peaks of connectivity, both in ipsi (i.e. lateral part of $P1^-$, z score = 2.14 ± 1.6) and contralateral side (e.g. in $P2^+$ band, z score = 2.99 ± 1.51, median ± MAD at -102% $P1^-$) (***Figure 21E***).

After balance recovery, PCs from functional cluster 1 in cuffed mice still receive massive GC inputs from almost every photostimulated microzones. In SHAM mice these connections are more discrete highlighting many silent zones, as it was found in control mice (*see section 6.2.3.1*), suggesting that GC-PC network may return to a basal condition (i.e. as it was before impairment).

6.2.4 Median input pattern highlight conserved GC inputs between individuals

Are spatial distributions of GC inputs (*see section 6.2.3* and ***Figure 21***) determined randomly or according to behavioral conditions? To address this question, synaptic amplitudes from significant GC inputs (i.e. corresponding z score > 1.96) of each conditions were grouped and positioned along their position mediolateral axis (***Figure 22A***). Another distribution was then generated: positioned amplitudes were then randomly shuffled *n* times (*n*= number of synaptic maps recorded in each condition) and averaged (purple curves in ***Figure 22A***). Positioned data were then compared to randomly generated data (***Figure 22A***).
In every conditions, positioned data was statistically different than randomly positioned values (Kolmogorov-Smirnov (KS) test on distributions, see individual p values in ***Figure 22A***). These results demonstrate that GC connection peaks observed in median input patterns (*see section 6.2.3* and ***Figure 21***) are due to spatially relevant GC connections in individual maps, therefore input patterns are conserved between animals in their respective conditions.

In order to identify similarities in GC-PC maps recorded in different experimental groups, positioned amplitudes of each condition described earlier in this paragraph were compared one with another (***Figure 22B, 22C***). Synaptic amplitude distribution from control mice differed from enriched mice (p-value = $7.33.10^{-13}$, KS test between distributions), early SHAM (p-value=0.504, KS test between distributions), early cuff (p-value=$2.08.10^{-25}$, KS test between distributions) and late cuff mice (p-value=$2.54.10^{-5}$, KS test between distributions) (***Figure 22C***). Strikingly, synaptic amplitudes from late sham animals (i.e. measured after full locomotor recovery) do not differ from the ones recorded in control mice (p-value=0.112, KS test between distributions) (***Figure 22C***). Therefore, despite transitory mild impairments, sham mice recover an efficient locomotor behavior as well as synaptic inputs in the anterior vermis comparable to control mice.

6.2.5 Increased inter-individual variability in cuffed mice

Median input patterns revealed stereotyped GC connections to PCs located within functional cluster 1 (***Figure 21, 22A***). However, we could not exclude variability in our dataset. For instance, median input patterns from late cuffed mice showed no contralateral GC inputs in the contralateral $P2^{-}$ Zebrin band (***Figure 21F***), however occasional GC inputs could be observed in few individual maps (see example in ***Figure 20B***). Can we evaluate inter individual variability? To address this question, individual synaptic z score patterns were compared to

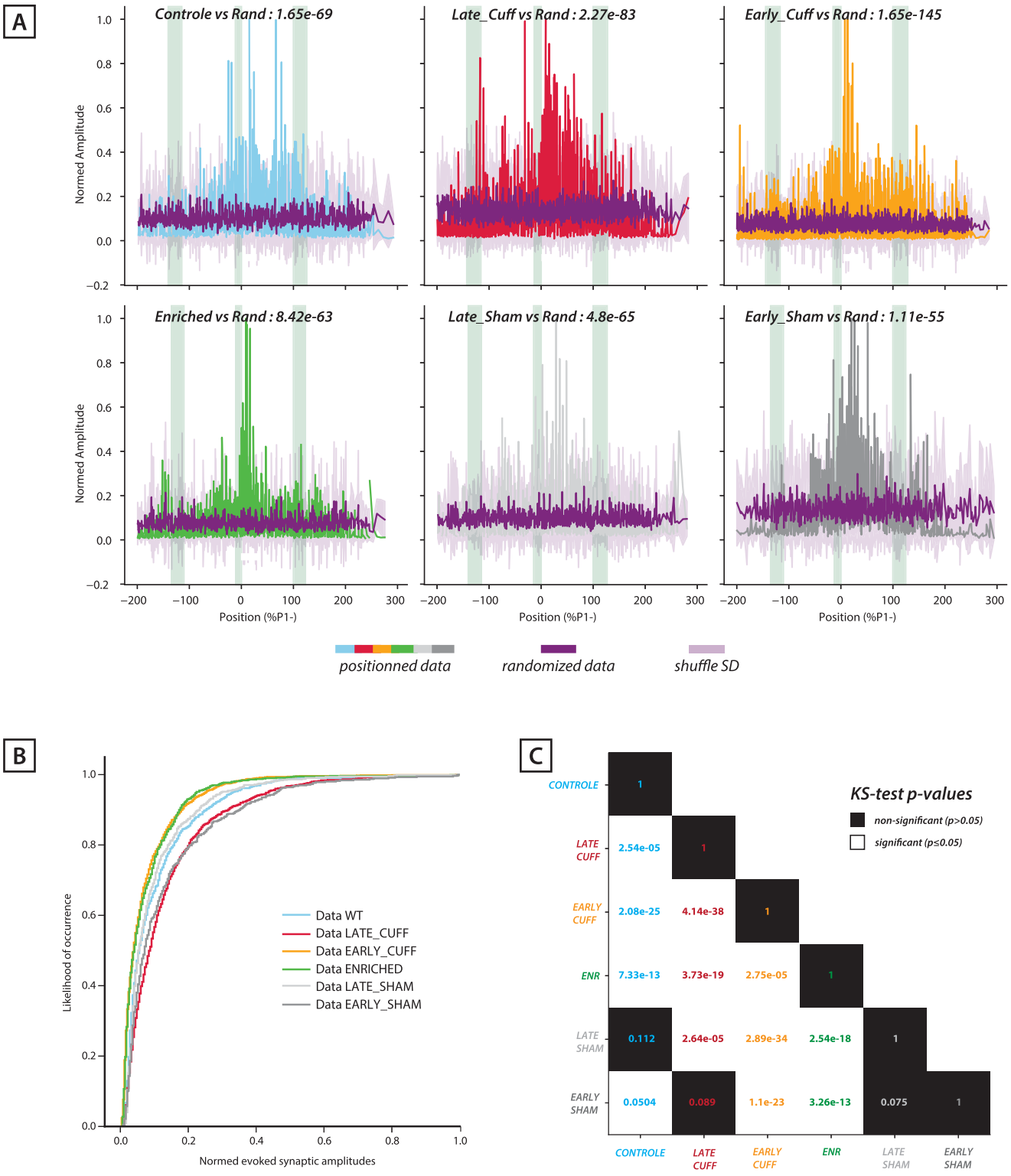

Figure 22 : Synaptic spatial maps are not due to randomness

(A) For each condition, significant evoked synaptic amplitudes (i.e. z-score <= 2.0) have been normalized and sorted along the mediolateral axis (colored curves, according to the position of the granule layer site that actually evoked the eEPSC used to measure synaptic amplitude). The purple curve represents the average pattern after shuffling of the synaptic amplitudes n times (n = number of maps recording for each condition). Shaded purple curve represents the standard deviation of the average random pattern. Statistical discrepancies between sorted and randomized data has been tested with the Kolmogorov-Smirnov test (p-values are indicated on top of each panel).

(B) Cumulative plot of experimental distributions shown in (A).

(C) Results (p-values) of Kolmogorov-Smirnov (KS) test computed between experimental distributions shown in (A).

median input pattern and variance to median pattern was calculated in each condition (*see methods 5.9.4* and ***Figure 25A, 25B***). Early and late cuffed mice display higher interindividual total variance to median input pattern than control (total variance = 11546.11 vs 24472.0 vs 3894.63, ***Figure 25B***) and respective SHAM mice (total variance = 4704.99 vs 11546.11 for early SHAM/cuff and 2759.97 vs 24472.0 for late SHAM/cuff, ***Figure 25B***). In each condition, most of the variance is explained by the local inputs (***Figure 21***). However, in early cuffed mice, the variance to median pattern of distant inputs is increased and this trend is exacerbated in late cuff mice (***Figure 25A***).

To extend this analysis of variability, significant synaptic amplitudes (i.e. corresponding z-score ≥ 2.0) from all mice were sorted and averaged according to their input location within the Zebrin bands (*see Table 1, Appendix 1*) and analyzed with principal component analysis (PCA) (***Figure 23A, 23B***). This analysis allowed us to identify the parameters that account for the highest variance in our dataset. The PCA extracted 11 principal components (PrCs) that cover the total variance between individuals. PrC1 alone explained 61% of the total variance and synaptic amplitudes from the local cluster (i.e. located in medial P1- Zebrin bands / A zone) (***Figure 23A***) are highly correlated to this component (r=0.78) (***Figure 23B***). This results confirms the trend described earlier in this paragraph: the local inputs are highly involved in inter-individual variability of synaptic maps.
The local GC cluster is anti-correlated with PrC2 (r = -0.57) and poorly correlated with other following PrCs (*see Table 2, Appendix 1*). In addition, no distant GC inputs were strongly correlated to any PrCs (*see Table 2, Appendix 1*). As the cumulative PrCs 2 to 11 explain remaining 39% of the total variance, the study of distant GC inputs should bring information about the association of different microzones in a given contextual behavior.

6.2.6 Different behavioral conditions result in specific association between distant microzones

6.2.6.1 Combinations according to Zebrin bands

To evaluate whether specific locations in the median synaptic maps have correlated synaptic inputs, we pooled the significant synaptic amplitudes (i.e. z score > 1.96) elicited by distant GCs (i.e. belonging to any microzone except the medial part of the P1- Zebrin band or A zone) according to the Zebrin bands they originated from. Each group of amplitudes was then averaged and normalized according to the average synaptic amplitude measured in the whole

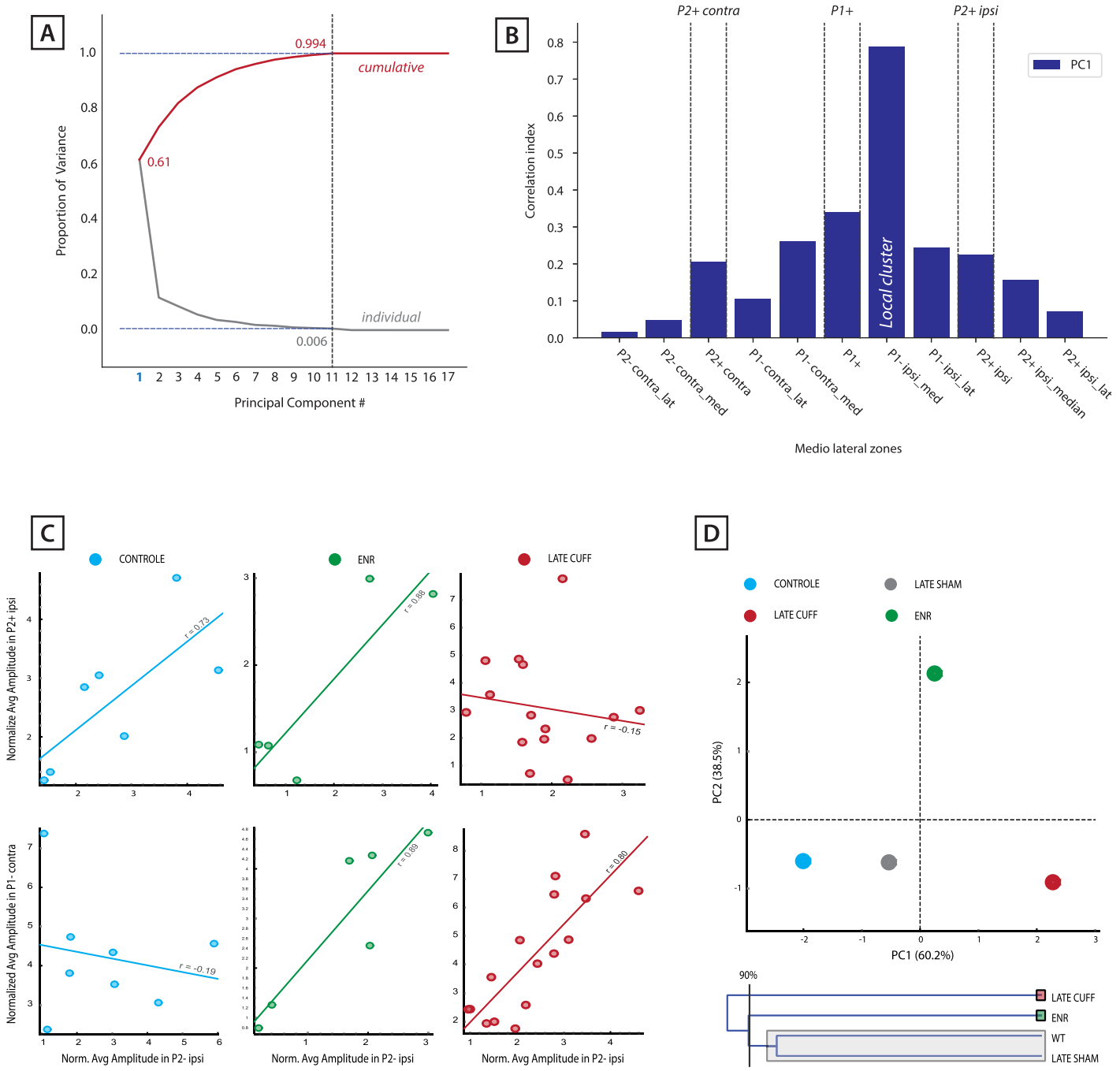

Figure 23 : Distant granule cell inputs rely on behavioral adaptation

(A) Principal component analysis (PCA) has been performed on average synaptic amplitude in each Zebrin band (*see Table 1*) in every conditions. Input data were not normalized (as they belong to the same physical unit). PCA results in 11 principal components that cover the whole variance of the dataset. PC1 covers 61% of the dataset variance.

(B) Correlation indexes in PC1 (*see Table 2*). Amplitudes from the local cluster (i.e. median P1- Zebrin band) are highly correlated to PC1 (0.78), thus most of the variance between individuals rely on local granule cell inputs.

(C) Linear regression between synaptic inputs. Normalized synaptic amplitudes have been compared depending on their spatial location, according to data in panel A and B, inputs from the local cluster have been discarded.

(D) Principal component analysis (*top*) and hierarchical clustering (*down*) on Zebrin bands correlation indexes. Correlation indexes from panel C (see table 3) have been analysed by PCA for the following conditions : controle, enriched, late sham and late cuff animals. PC1 and PC2 cover a total of 98.7% of the dataset variance. 3 clusters could be isolated from hierarchical clustering on resulting components (Ward's method) : controle and late sham animals belong to the same cluster.

synaptic map, yielding one average amplitude value per Zebrin bands in each individual. These values were compared 2 by 2 between individuals in each experimental conditions using linear regressions (***Figure 23C,*** each dot is a couple of values for a given synaptic map). We show in ***Figure 23C*** that synaptic amplitudes from pairs of Zebrin bands, e.g. $P2^+$ ipsilateral vs $P2^-$ ipsilateral, can be correlated in control (r=0.73) and enriched (r=0.88) mice, but not in late cuffed mice (r=-0.15) (***Figure 23C***). On the other hand, synaptic amplitudes from another pair of Zebrin bands, e.g. P1- contralateral vs P2- ipsilateral, are correlated in enriched (r=0.89) and late cuffed (r=0.80) but not in control mice (r=-0.19) (***Figure 23C***).
In order to clarify the possible combinations between experimental conditions, the coefficients of correlation from band to band linear regressions (*Table 3, Appendix 1*) were analyzed with PCA (***Figure 23D***). The sum of resulting principal components PrC1 and PrC2 explains 98.7% of the total variance within the dataset (PrC1 60.2%; PrC2 38.5%, ***Figure 23D***). Variable coordinates in the PrC1/PrC2 plane identified 3 clusters: one for enriched mice, one for late cuffed mice and a last cluster including both control and late SHAM mice (***Figure 23D***), suggesting low inter-group variance between control and late SHAM mice. Clustering was then confirmed by a hierarchical classification (Ward's method, inertia cut off = 90%) on resulting PrC values. The resulting dendrogram reveals 3 independant classes describing enriched, late cuffed and mixed control/late SHAM conditions, suggesting comparable GC-PC functional connectivity between control and late SHAM mice (***Figure 23D***).

6.2.6.2 Combinations according to CF microzones

The analysis has been extended at the study of every synaptic amplitude. Synaptic amplitudes from non significant photostimulated sites (i.e. z score < 1.96) were added to the significant ones (i.e. z score > 1.96) and were sorted, averaged and normalized according to the average synaptic amplitude measured in the whole synaptic map, yielding one average amplitude value per distant microzone in each individuals (***Figure 24A***, *see Table 4, Appendix 1*). As in section *6.2.6.1*, values were compared 2 by 2 using linear regressions in each experimental conditions between microzones. Linear regressions yielded numerous combinations (for correlation indexes see *Table 5, Appendix 1*; for individual plots see *Appendix 2*). Results are summarized in ***Figure 24B, C and D*** showing resulting correlation coefficients in every conditions.
In control mice, 2 pairs of microzones were significantly correlated: AX and B zones from the same side are positively correlated (r=0.792 for contralateral side, r=0.692 for ipsilateral side) (***Figure 24B***). No correlation between contralateral AX/B zones was observed in enriched mice (r=0.307) but correlation was conserved for ip silateral AX and B zones (r=0.82) in addition with new correlated zones (e.g. ipsilateral AX zone with ipsilateral Al zone, ***Figure***

24B). The number of correlated microzones increased in early SHAM and cuffed mice compared to control mice (2 pairs in controle vs 6 in early SHAM and 13 in late cuffed, ***Figure 24C***).
After balance recovery, a single pair of microzones was correlated in late cuffed mice (contralateral Am zone and ipsilateral AI zone, r=0.67, ***Figure 24D***). Contralateral AX and B zones as well as ipsilateral AX and B zones were correlated in late sham mice (***Figure 24D***) as in control mice (***Figure 24B***), confirming that mildly-impaired mice recover similar synaptic maps than naive animals.

Taken together, both analyses highlight the fact distant GCs are not associated randomly: neighboring microzones converge to PCs within functional cluster 1 according to specific rules depending on behavioral adaptation. Moreover, after mild locomotor impairment recovery, synaptic maps resume functional state comparable to what is observed in non impaired mice.

6.3 Positive and negative association of cerebellar microzones

Feed-forward inhibition provided by MLIs plays a key role in temporal integration of GC inputs in PCs (see section 2.4.1.2). Valera and colleagues recorded synaptic maps between GC and MLIs located within the functional cluster 1 (Valera et al., 2016). They found that neighboring MLIs and PCs display GC input maps that do not always overlap, suggesting that PCs may combine separately excitatory and inhibitory synaptic inputs originating from distinct GC clusters located in different microzones. Therefore, we decided to investigate whether excitation and inhibition could be related to the modular distribution of GC inputs, both on a temporal and a spatial point of view.

6.3.1 GC-mediated excitation and inhibition are mostly independent

We studied the spatial organisation of monosynaptic (i.e. GC-PC) and disynaptic (i.e. GC-MLI-PC) pathways in the anterior vermis. This work has been done in collaboration with Théo Gagneux, who recently joined the lab to perform his PhD thesis.

PCs within functional cluster 1 (n=10, N=9) were recorded in voltage clamp configuration at a holding potential of -60 or 0mV and RuBi Glutamate was uncaged in the GC layer in order to

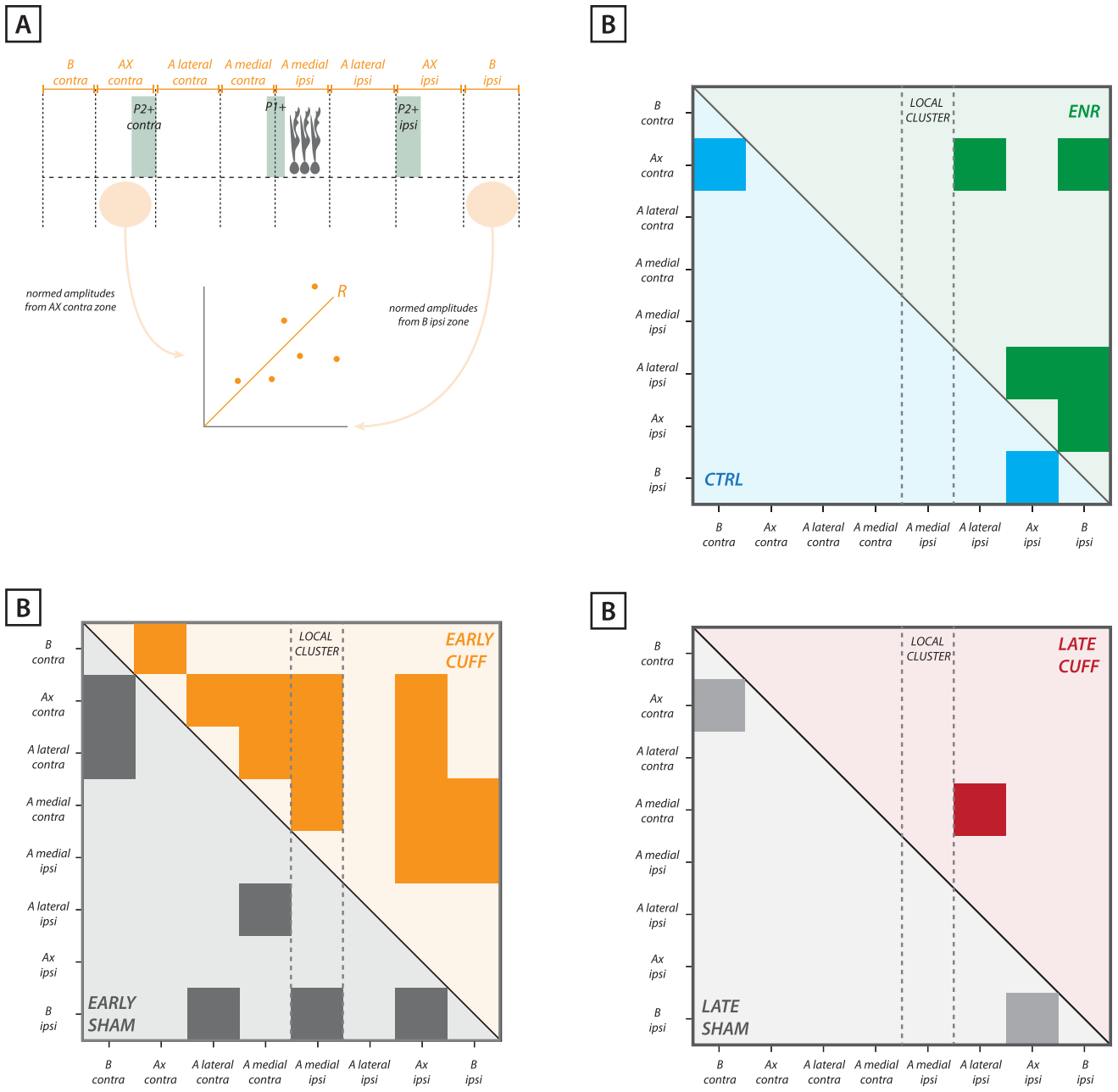

Figure 24 : Patterns of preferentially-associated microzones

(A) Synaptic amplitudes (including corresponding z-score<2.0) were sorted depending on their input location (i.e. according to cerebellar microzones), then have been centered to average. Per individual, an averaged value has been extracted (see table 4) and linear regressions were computed between microzones (*see Appendix 1 for individual regression plots*). Resulting correlation indexes have been reported in boxes *(B)*, *(C)* and *(D)* for control/enriched, early sham/early cuff and late sham/late cuff conditions. For clarity, only correlation indexes > 0.6 are represented by color-filled squares (*see table 5 for individual coefficients*). Dashed vertical lines correspond to amplitudes within the local cluster (medial part of ipsilateral A zone).

establish excitatory and inhibitory synaptic maps (***Figure 26A***). Photostimulation-evoked EPSCs (i.e. holding = -60mV) showed average synaptic amplitude of -29.7 ± 23 pA (mean ± SD), while photostimulation IPSCs (i.e. holding = 0mV) showed average synaptic amplitude of 49.2 ± 56.5 pA (mean ± SD; ***Figure 26A***).

In order to study the overlap between excitatory and inhibitory inputs, GC photostimulation sites were sorted whether they elicited EPSCs or IPSCs, yielding 4 categories of inputs (***Figure 26B***) :

- (1) Pure excitatory inputs (12 ± 8.5%; mean ± SD): photostimulation of a given site induced EPSCs only (i.e. corresponding z score at -60mV > 1.96 and z score at 0mV < 1.96)
- (2) Pure inhibitory inputs (13 ± 11%; mean ± SD): photostimulation of a given site induced IPSCs only (i.e. corresponding z score at -60mV < 1.96 and z score at 0mV > 1.96)
- (3) Mixed excitatory and inhibitory inputs (4 ± 7%; mean ± SD): photostimulation of a given site elicited inward and outward synaptic current (i.e. corresponding z score at -60mV > 1.96 and z score at 0mV > 1.96)
- (4) No significant inputs (71%): glutamate uncaging on a given site did not elicit significant response (i.e. corresponding z score at -60mV < 1.96 and z score at 0mV < 1.96)

Median synaptic input patterns have been established both for excitation and inhibition (*see methods 5.9.3*) (**Figure 26C**). Although local inhibitory (median amplitude z-score = 3.57 ± 2.49; median ± MAD at 16 %$P1^-$) and excitatory (z-score = 4.27 ± 4.01, median ± MAD) were observed, distant inhibitory and excitatory GC inputs do not systematically overlap. For instance, the ipsilateral $P2^+$ band contains GCs that provide both excitation (z-score = 3.32 ± 2.6, median ± MAD at 107 %$P1^-$) and inhibition (max amplitude z-score = 2.5 ± 1.42; median ± MAD) on PCs from functional cluster 1 (***Figure 26C***). On the other hand, GCs within the medial contralateral $P1^-$ Zebrin band are mostly excitatory (z-score = 2.56 ± 1.01 and 2.76 ± 2.01, median ± MAD at -20 %$P1^-$ and -49 %$P1^-$respectively in excitatory input pattern vs z score < 1.96 at corresponding positions in inhibitory pattern, ***Figure 26C***) while the distal ipsilateral A zone is essentially inhibitory (z-score = 3.98 ± 2.12, median ± MAD at 74 %$P1^-$ for inhibition vs z score = 1.82 ± 1.3, median ± MAD at corresponding position in excitatory pattern) (***Figure 26C***).

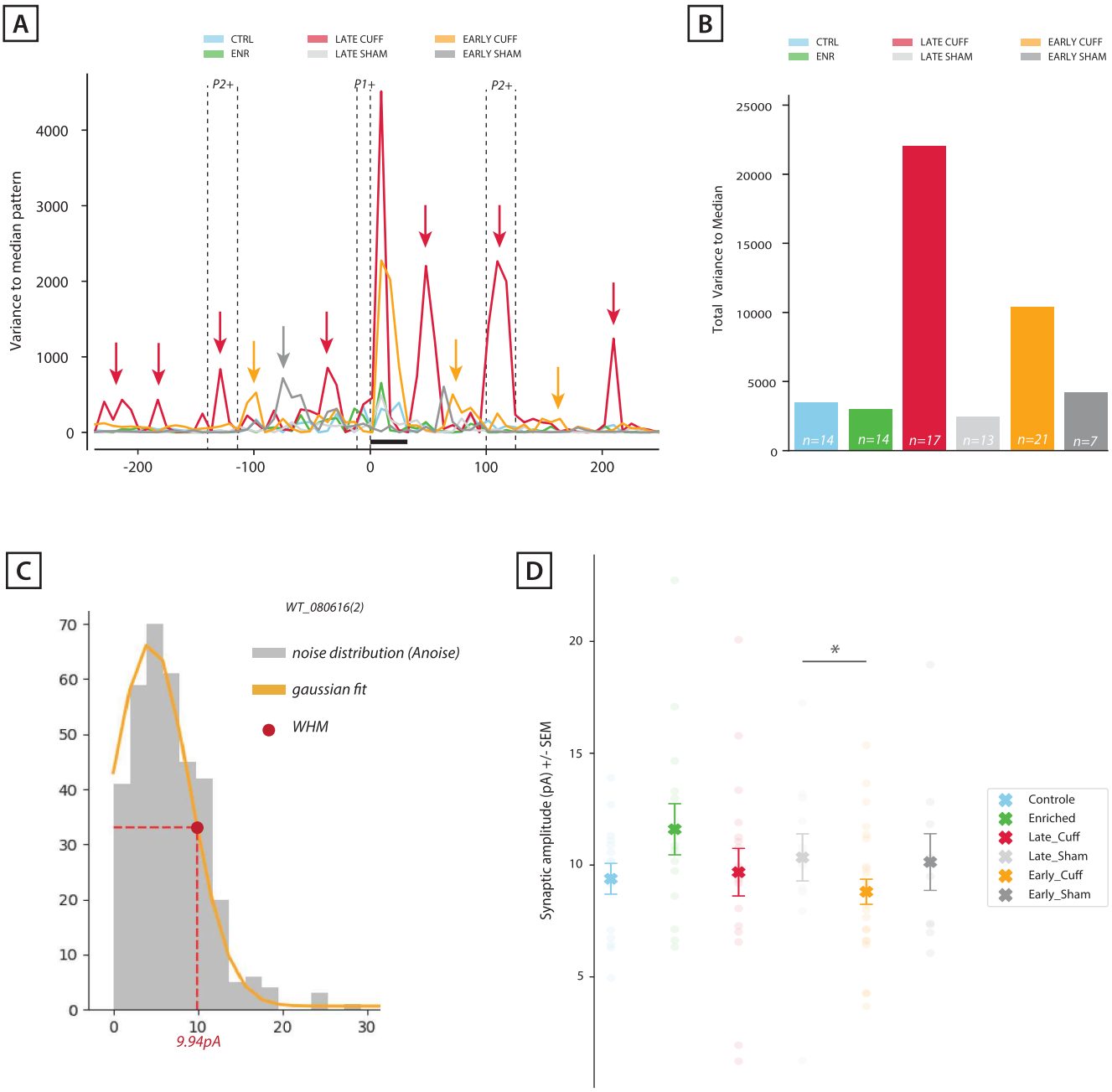

Figure 25 : The cuff model increases variance in synaptic maps, but not background synaptic activity.

(A) Variance to median pattern. In each conditions, individual z-score patterns have been compared to the corresponding median pattern (shown in fig. 21) : for each distance bin, squared differences between individual data and median pattern have been summed then divided the sample size (see Methods 5.9.4). Purkinje cell position is shown by the black horizontal bar. Distal inputs clusters mentionned in the main text are shown by coloured arrows.

(B) Corresponding total squared distance to median pattern : each colored bar represents the sum of equivalently-coloured curve in panel A.

(C) Example of noise distribution from a single mapping experiment. Synaptic amplitude (Anoise) have been measured in a time window out of photostimulation (see fig method 14D), leading to distribution in gray. Gaussian fit to the distribution is then computed (orange curve) to determine width at half-maximum value (WHM; red dot).

(D) Distributions of WHM values recorded in each experiments. No statistical differences were observed, except between late sham and early sham distributions only (*, p-value=0.0247, two-sided Mann Whitney test on distribution).

These results show that GC-PC and GC-MLI-PC pathways can be spatially segregated: PCs may combine excitatory and inhibitory inputs originating in different neighboring microzones as predicted by Valera and colleagues (Valera et al., 2016). In addition, classic feed forward inhibition depicted in the litterature (*see section 2.4.1.2*) might not the only nor the principal configuration for PCs to integrate excitatory and inhibitory inputs.

6.3.2 Temporal dissociation of MF-mediated inhibitory and excitatory inputs

The study of GC-PC and GC-PC-MLI inputs spatial distribution shed light on potential differential integration of excitatory and inhibitory information by PCs. However, maps were established by GC photostimulation, therefore it remains unclear whether PCs can integrate differential excitation/inhibition (E/I) sequences following MF stimulation, the physiological pathway. To address this question we optogenetically stimulated MF originating in the external cuneate in acute cerebellar slices and recorded resulting E/I sequences in PCs within the vermis. The following results belong to a submitted manuscript (see *Binda et al, in prep, Appendix 5*).

6.3.2.1 Optogenetic MF stimulation evokes excitation and inhibition in PCs

To mimic MF natural inputs, we injected rAAV 9/2 in precerebellar nuclei in order to express Channelrhodopsin 2 (ChRd2(H134R)-YFP) in individual MFs (*see methods 5.3.2*). Since different synaptic properties have been described at the MF-GC connection from different origins (Chabrol et al., 2015) we chose to target a unique pre-cerebellar nucleus, the cuneate (number of recordings n= 57, number of cells nc = 15 and number of mice N = 4) which convey proprioceptive and exteroceptive information from the upper limb. Also, several studies have demonstrated that MF originating in the cuneate nucleus send collaterals at different location in the same lobule (Quy et al., 2011 ; Valera et al., 2016). First, we assessed whether individual fluorescent MF rosettes could be photostimulated in acute cerebellar transverse slices. Fluorescent MF rosettes were recorded in loose cell-attached mode (Barbour and Isope, 2000) while pulses (10-100 ms length) of blue light were elicited. In all the fluorescent rosettes, illumination triggered a unique or a short burst of action potentials (mean spike number = 3.967 ± 2.5 n = 6; ***Figure 27A***). Using a confocal-based laser scanning approach, we then systematically illuminated small zones (83 x 83 µm) of the GC layer from a given lobule (Lobule III to VIII) to stimulate MF rosettes while EPSCs and IPSCs were monitored in a PC70 (n=15) recorded in whole cell mode (***Figure 27B***).

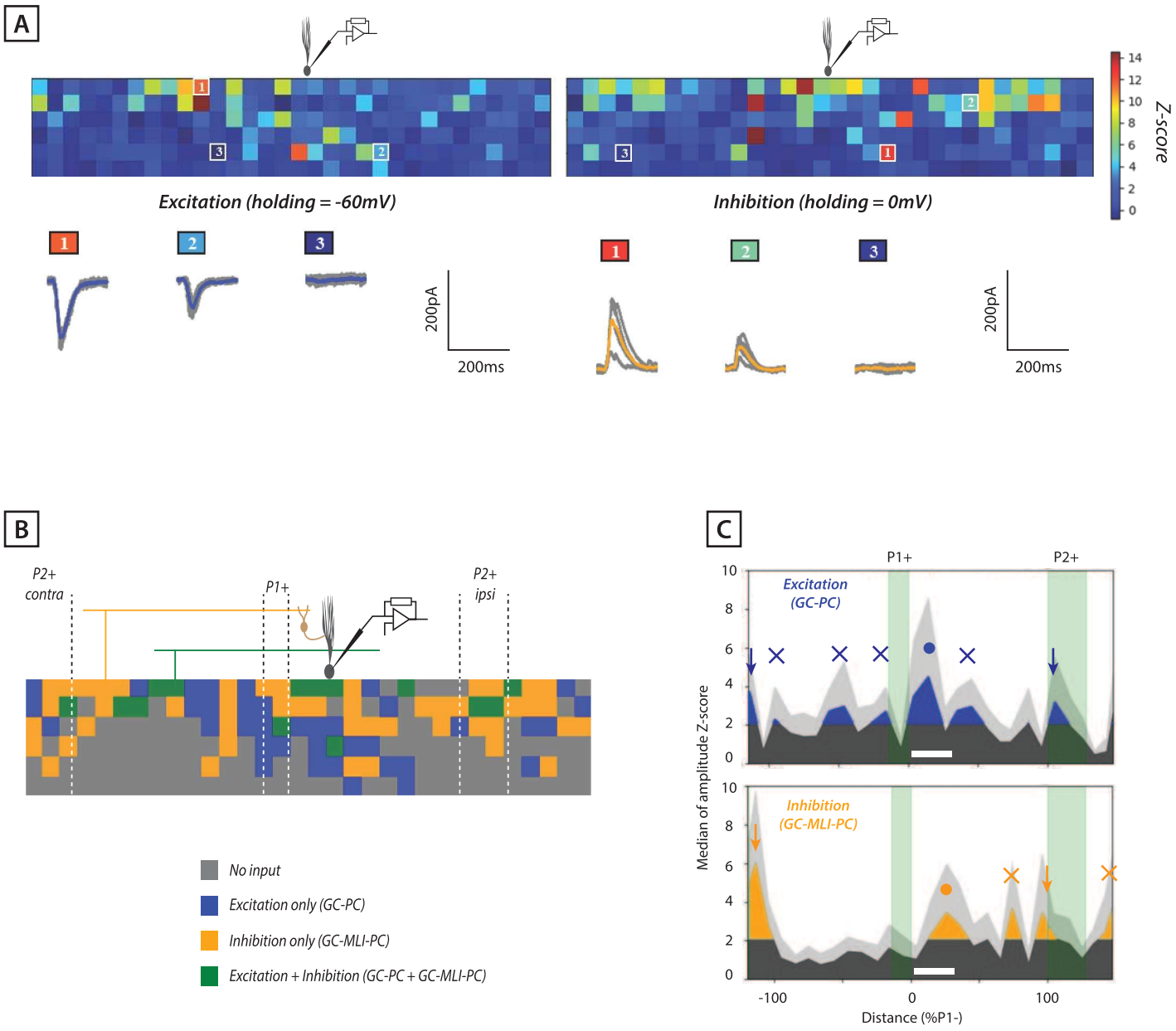

Fi gure 26 : Granule cell mediated inhibition and excitation pathways are independant

(A) Example of a single experiment : a PC located in functional cluster 1 has been recorded at -60mV (left) and 0mV (right). Glutamate uncaging in the GC layer yielded respective excitatory and inhibitory synaptic maps. Example traces shown under each map represent strong, mild and absent synaptic inputs (average is colored, raw records are in gray).

(B) Maps shown in (A) have been superimposed. GC-PC functional connectivity can be segregated in 4 categories : no input (in gray, i.e. z-score for excitation and inhibition < 2.0); excitatory inputs only (in blue, i.e. z-score for excitation > 2.0 but z-score for inhibition < 2.0), inhibitory inputs only (in orange, i.e. z-score for excitation < 2.0 but z-score for inhibition > 2.0) and both inputs (i.e. z-score > 2.0 for excitation and inhibition).

(C) Median excitatory (top) and inhibitory (down) GC input patterns to PCs within functional cluster 1 (=0-33%P1-, N=9 mice, n=10 cells, white horizontal bars) recorded in adult mice raised in standard condition. Non connected granule cells are represented in dark gray. The blue curve represent functional excitatory inputs (i.e. amplitude Z-score > 2.0). The orange curve represent functional inhibitory inputs (i.e. amplitude Z-score > 2.0). Light gray curve represent median absolute deviation. Local cluster is observed in every conditions (blue/orange dots), while distant clusters mentioned in text can overlap (orange/blue arrows) of be independant (orange/blue crosses).

***GC-PC** : granule cells to Purkinje cells monosynaptic pathway; **GC-MLI-PC** : granule cells to molecular layer interneurons to Purkinje cells disynaptic pathway*

6.3.2.1 Stimulating specific MFs induced a wide range of temporal EPSC/IPSC profiles in PCs

EPSCs and IPSCs (or synaptic charges, EPSQ and IPSQ, *see methods 5.10*) elicited in PCs by MFs illumination (50 ms pulses) were recorded at Vm = -60 mV and Vm = 0 mV respectively (***Figure 27B***; EPSQ: - 3.5 ± 3.4 pC; IPSQ: 13.8 ± 11.5 pC, mean ± SD). Although we observed excitation followed by inhibition in 45/57 recordings, in 6/57 inhibition preceded 4 excitations and in 6 recordings only inhibition was observed. Furthermore, we observed a large temporal spread of the onset of excitatory and inhibitory synaptic inputs elicited by MFs from a given area. This temporal spread was quantified by measuring the differences between IPSC and EPSC latencies from the beginning of illumination (ΔLat = latency I – latency E). ΔLat ranged from negative to positive values that can exceed ±5 ms (from – 11.8 to 13.21 ms ; mean = 3.6 ± 4.55 ms, mean ± SD; ***Figure 27C***). We compared this distribution withΔLat measured following direct electrical stimulation of GC clusters (GC_ΔLat; ***Figure 27D***). As opposed to MF stimulation, GC stimulation systematically lead to short ΔLat (mean GC_ΔLat = 2 ± 0.74 ms, mean ± SD, n = 23; ***Figure 27D***) as previously shown (Vincent and Marty, 1996; Brunel et al., 2004; Mittmann et al., 2005; Grangeray-Vilmint et al., 2018). We then used GC_ΔLat as a proxy for the classical FFI in the GC-MLI-PC pathway evoked by one GC cluster. Since in this dataset 0< GC_ΔLat <5 ms (***Figure 27D***), we separated the ΔLat measurement from the MF illumination experiment in two groups (***Figure 27E***): a putative FFI-ΔLat (group 1; n = 27/57; 47.5%) with 0 < ΔLat <5 ms and a second group (group 2; n = 30/57) aggregating the other measurements, including ΔLat > 5ms (31.5%) or negative (10.5%) and MF stimulation eliciting only inhibition (10,5%). These results show that PCs can integrate E/I sequences according multiple scenarii, and not only via feed forward inhibition.

Therefore, the ΔLat spread can solely be explained by a dissociation between a direct GC-evoked excitation and an indirect GC-evoked inhibition mediated by different cluster of GCs, as predicted by spatial maps described in *section 6.3.1*. Thus, these findings suggest that the burst of action potentials elicited by blue light in MF rosettes is propagated in MF collaterals that target different GC clusters in the GC layer, including distant subsets of GCs targeting local MLIs but not PCs.

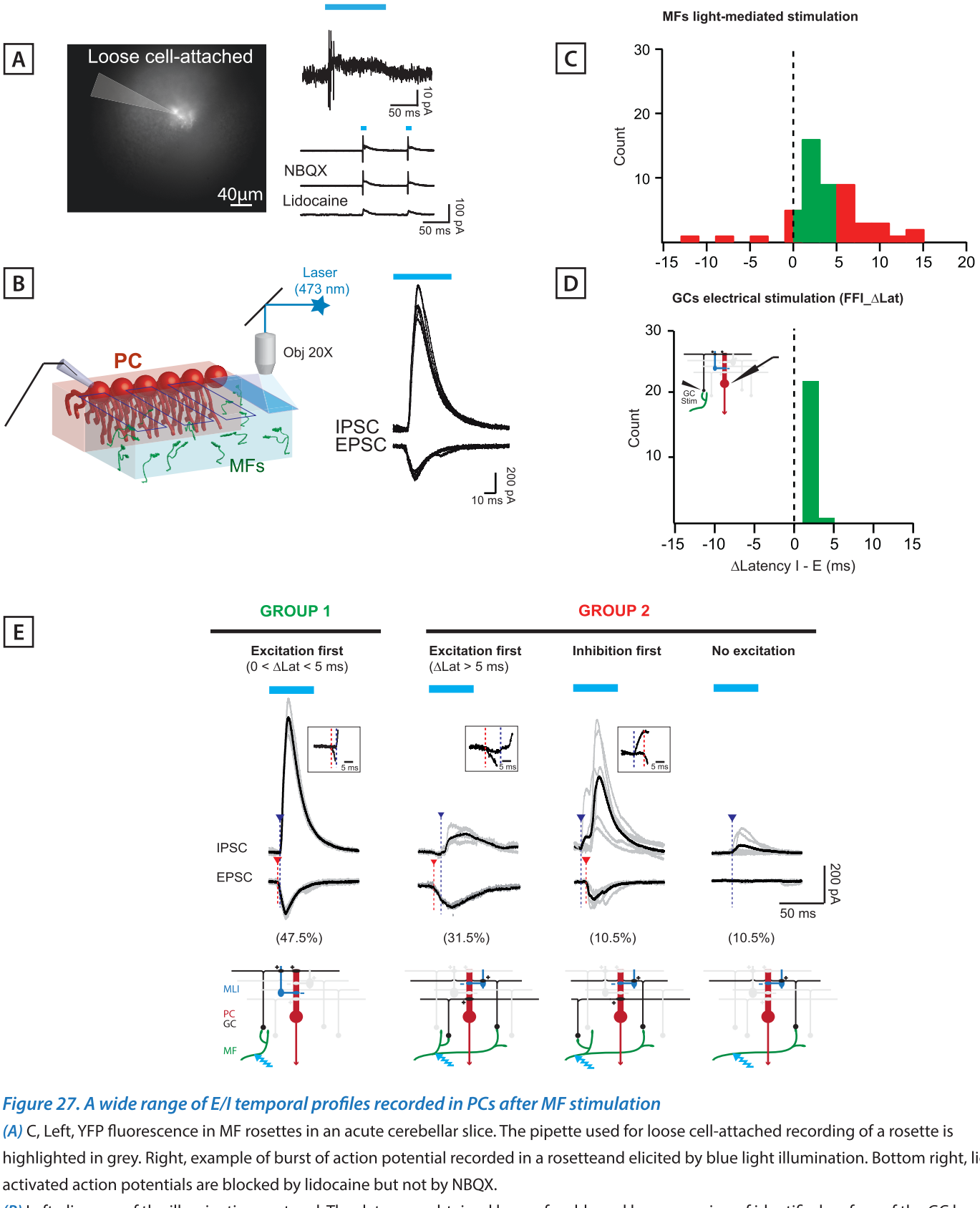

Figure 27. A wide range of E/I temporal profiles recorded in PCs after MF stimulation

(A) C, Left, YFP fluorescence in MF rosettes in an acute cerebellar slice. The pipette used for loose cell-attached recording of a rosette is highlighted in grey. Right, example of burst of action potential recorded in a rosetteand elicited by blue light illumination. Bottom right, light activated action potentials are blocked by lidocaine but not by NBQX.

(B) Left, diagram of the illumination protocol. The data wereobtained by confocal-based laser scanning of identified surface of the GC layer (83x83µm). Left, representative traces of EPSC and IPSC induced by light-mediated stimulation of MFs in one area of the GC layer.

(C) Histogram of the ΔLat following MF illumination.

(D) Histogram of the ΔLat following GC.

electrical stimulation. Inset, diagram illustrating FFI.

(E) Two groups and 4 types of E/I temporal profiles were distinguished during MFs illumination. Group 1 corresponds to 0 < ΔLat < 5 ms. Group 2 correspond to ΔLat < 5 ms, negative (Inhibition first) and GC clusters eliciting only inhibition (No excitation). Red and Blue triangle identify the onset of the excitatory and inhibitory current, respectively. Inset, highlight of the onset of EPSC and IPSC superimposed. Bottom, the 4 potential scenarios explaining the profiles. Excitation first (0 < ΔLat < 5 ms) corresponds to classical FFI, i.e. the same GCs contact both MLIs and PCs. Excitation first (ΔLat < 5 ms) and inhibition first illustrate that several clusters of GC have been excited (two GC clusters are represented in the diagram below) which elicit excitation and inhibition independently. No excitation, only inhibition has been observed.

From Binda et al, in prep.

7. Discussion

My PhD project aimed at understanding the synaptic rules that underlie inter-modular communication within the cerebellar cortex. Using patch clamp recordings and glutamate uncaging on acute cerebellar slices, we could demonstrate for the first time a causal relationship between locomotor adaptation and functional synaptic organization within cerebellar microcircuits. Glutamate uncaging and optogenetic MF stimulation in slice shed light on extended rules for differential PC integration of excitatory and inhibitory inputs from adjacent cerebellar modules.

This work provides new tools for the understanding of movement disorders as identifying the combination of modules involved in a given behavior may lead to the development of specific protocols of compensatory stimulations for movement disorders.

7.1 Critical periods for the establishment of synaptic maps

Synaptic maps have been established during the postnatal development of the cerebellum in mice (*see section 6.1*). Although functional PF-PC synapses appear at P7 (as reported in the litterature Scelfo and Strata 2005), our results demonstrate that at P9-P10 they are mediated by local GCs, (i.e. PC and GCs belong to the same microzone). Only sporadic distant GC inputs could be observed in < 10% of the experiments despite the presence of long PFs. Therefore, the lack of distant inputs may be due to a functional immature state of PF-PC synapses. Further immunohistochemistry would be required to determine the presence of physical synapses and to confirm this hypothesis. Conserved distant GC inputs (i.e. coming from other microzones) occur at P12-13 which coincide with eyes opening (Hoy and Niell, 2015; Shen and Colonnese, 2016). At this time pups stop to waddle around and start to actively explore their homecage, expressing goal-directed body motion, suggesting a potential increase in the number of functional PF-PC synapses due to the expansion of incoming sensory motor inputs.

Between P14 and P18 occurs a significant step in the organisation of functional GC-PC synapses: intermodular communication is exacerbated, synaptic input patterns and the proportion of active GC inputs are similar to what has been observed in adults (***Figure 16***). However, an increased inter-individual variability is observed in these adolescent mice compared to adults. These findings may suggest the existence of a critical period in the cerebellar networks (***Figure 17***) as observed in other brain regions (for review see Hensch,

2005). GC-PC maps variability in this period of age can be explained by developmental cues, as GC-PC synapses compete with CF inputs during CF translocation phase (*see section 2.5.1.1*). Since similar inter-individual variability was also found in adult cuffed mice vs adult control mice (***Figure 25***), the impact of incoming sensory motor input on GC-PC unstability cannot be ruled out.

7.2 Conserved GC-PC synaptic patterns between individuals and mouselines

Valera and colleagues described stereotyped GC input patterns across animals, highlighting specific links between identified regions of the cerebellar cortex (Valera et al., 2016). They nonetheless reported inter-individual discrepancies in the synaptic maps, that also appeared in my dataset (*see paragraph 6.2.5* and ***Figure 23A, 23B, 25A, 25B***). Maps and patterns built from all experimental conditions display a significant level of variance mostly explained by variations in synaptic amplitudes within the local inputs. However, the median synaptic input patterns I obtained in control mice corresponds exactly to the one described by Valera and colleagues (*see Appendix 3*) although it has been established in a different mouse line (EAAT4 vs ALDOC) using different optical systems (confocal-based laser scanning vs DMD-based led stimulation). CD1 mice are outbred mouse lines, and we have no way to quantify nor to control genetic crossovers and mutations. These results highlight the robustness and reliability of GC-PC synaptic maps in the anterior vermis, ruling out genetic selection of GCs clusters towards a source-dependant driven model.

The synaptic pattern obtained with low-resolution mappings in adults (***Figure 16C***) differs from the one obtained with high-resolution glutamate uncaging (***Figure 21A***). Indeed, with small uncaging sites (20x20µm, *see methods 5.8* and ***Figure 14D***) peaks and valleys could be observed, while using low-resolution mappings (41*41µm, *see methods 5.8* and ***Figure 14C***) fully silent GC columns are quite rare to see. This is explained by a wider activation of the GC layer. The difference in the amount of GCs stimulated between 20*20 and 41*41µm zones follows a cubic factor, increasing the probability to observe nonspecific overlap of GC inputs. If we consider a volume of GC layer of *20x20x100µm* (*=40000µm^3 or 4.10-5mm^3*) with a density of *1.92.10^6* GCs per mm^3 (as described by Harvey and Napper, 1988), the photostimulation of this area will activate approximately *4.10^{-5} x 1.92.10^6* = **76.8** GCs. The

stimulation of a 41x41x100µm cubic area would on the other hand activate $2.10^{-4} \times 1.92.10^{6}$ = **384** GCs, yielding a 5-fold factor between the two conditions. Therefore, using low resolution mappings, the probability to find silent GCs is low, leading to a large number of false-positive active sites and underestimation of silent sites. In addition, median patterns are built after selection of the maximum z score value within GC columns, which are composed of 4 vertically stacked photostimulation sites in the low resolution scan. Therefore, in case of 3 silent sites vs 1 active site the whole column is considered as active.

7.3 Inter-modular communication in the anterior vermis rely on sensory-motor adaptation and learning

In order to identify a link between GC-PC synaptic maps and locomotor adaptation, two antagonists strategies were employed: locomotion in mice was either impaired or improved, using the cuff and the enriched model respectively. Both conditions had a significant influence on the synaptic maps and patterns when compared to the control mice, highlighting a causal relationship between cerebellar microcircuits and behavioral adaptation.

7.3.1 Neuropathic pain might influence GC-PC connectivity

The cuff condition, originally dedicated to neuropathic pain modeling (Yalcin et al., 2015) lead to the most important modifications, increasing both synaptic connectivity and variance in synaptic maps. This long lasting effect still occurs days after balance recovery (when compared to the sham condition) and could be explained in three ways. **(1)** The impairment goes beyond the scope of balance evaluation. The catwalk allowed us to measure body balance, but fine alteration of hindlimbs coordination could not be monitored and thus cannot be excluded. Indeed, several studies reported that mechanical allodynia in cuffed hind limbs could last up to 10 weeks after animals were cuffed (Yalcin et al., 2011; Sellmeijer et al., 2018). Therefore, it would be interesting to establish synaptic maps 3 or 4 month after the cuff.
(2) The cerebellum is involved in pain-related motor adaptation (Coombes and Misra, 2016) and is at the heart of anxiety-related circuits (Apps and Strata, 2015). As mechanical allodynia triggers pain-related signals that could potentially participate to the reshaping of GC-PCs synaptic maps. CFs discharge in PCs from lobule V has been recorded in the X zone after nociceptive cutaneous stimulation of the hind limbs (Garwicz et al., 1992). Coombes and

Misra reported activation of cerebellar lobules VI and VIIb (but not in lobules III or IV) in humans when exposing the subject's arm to nociceptive thermal stimulation (Coombes and Misra, 2016).

The cuff has long term effects as it triggers anxiety-related behaviors in mice (Yalcin et al., 2011; Ref Sellmeijer et al., 2018). Although these effects were observed 8 weeks after cuff, they are unlikely to be involved in the alteration of GC-PC maps observed in my experiments.

(3) Since inter individual variance strongly increased in maps from cuffed animals (***Figure 25A, 25B***), mice used different strategies to overcome the sciatic injury. As the cuff is inserted by hand with visual clues only, we cannot rule out some variability in the positioning. Also, each mouse may have found personal strategies to adapt to the cuff, leading to increased variability in synaptic maps.

7.3.2 Pure motor adaptation tunes GC-PCs synaptic maps

The early SHAM mice displayed altered synaptic maps when compared to control mice. Unlike cuffed mice, SHAM mice do not display mechanical allodynia (Yalcin et al., 2011; Medrano et al., 2016; Sellmeijer et al., 2018) and thus no pain-related signal should influence GC-PC maps. Since SHAM mice showed similar impairments albeit attenuated in the time course of balance compared to cuffed mice, the surgical trituration of the sciatic nerve triggers sensorimotor perturbations leading to transitory locomotor impairment. Therefore, we can conclude that pure locomotor impairments can be correlated with the altered synaptic maps and rearrangement of microzones targeting PCs within functional cluster 1. In addition, after SHAM mice recovered efficient locomotion, inter-modular communication in lobules III/IV resumed functional state comparable to the one found in control mice, i.e. in absence of impairment (*see section 6.2.6* and ***Figure 23A, 23B and 24***).

On the other hand, permanent changes in the network were also observed in the enriched condition: locomotor training suppressed most of the contralateral granular inputs to the medial A zone as well as inputs from the $P2^+$ ipsilateral Zebrin band. Some MFs that project to the Zebrin positive bands in lobule III and IV originate from the pontine nuclei (Biswas et al., 2019) that relay processed information from the cerebral cortex. PCs from the $P2^+$ Zebrin bands target the medial cerebellar nuclei, from which some neurons projet the thalamus to finally reach the cerebral cortex (***Figure 13***). Therefore, after locomotor training PCs from the medial A zone may have depressed sensory-motor inputs coming from the cortex. These results are in accordance with recent data showing that locomotor adaptation requires the cerebellum but not the cerebral cortex (Ref Darmohray et al., 2019).

In conclusion, although the data obtained in cuffed animals do not allow us to rule out a synergistic effect of pain and motor adaptation on the alteration of synaptic maps, experiments conducted in SHAM and enriched mice showed a direct causal link between locomotor adaptation and functional connectivity in the cerebellar cortex, in accordance with predictions of previous experiments (Valera et al., 2016). GCs from different origins converge to functional PC clusters in a source-dependent driven model: dynamic, PF-mediated microzones association may be a neural substrate of interlimb coordination at a given time (***Figure 28***).

7.3.3 Plasticities at GC-PC synapses support synaptic map reshaping

As predicted by previous results *in vitro* (Valera et al., 2016), locomotor adaptation induced alteration of GC-PC synaptic maps through potentiation and suppression of GC inputs. Selection of these inputs may be the result of both LTP and LTD mechanisms that occurred during the life of the animals (REF Jörntell and Hansel, 2006, Gao et al., 2012, Valera et al., 2016). Moreover, distant GC inputs were either completely suppressed (e.g. in enriched vs control condition) or selected (e.g. cuffed vs control condition) suggesting the action of respective silencing or awakening of GC-PC synapses. GC-PC synapses awakening has already been demonstrated *in vitro* via sustained optical stimulation of putative silent GCs (Valera et al., 2016).

7.3.4 Influence of local GC inputs

The PCA and the variance analysis revealed that local inputs (i.e. GCs within the same microzone as the recorded PCs) explained most of the inter individual variance. Although the local GC inputs are present in all conditions, recorded synaptic amplitudes from this location were highly variable and stronger than synaptic inputs coming from distant microzones. Reports in the literature already mentioned that local GCs display higher probability of connection than distal inputs (Isope and Barbour, 2002) as well as higher release probability (Sims, 2005). The ascending axon would thus display particular functional properties, although it is still a matter of debate in the community (Gundappa-Sulur et al., 1999; Walter et al., 2009). However, glutamate uncaging experiments on GCs do not allow us to speculate on a preferential role for local GCs at the expense of distal inputs in PC synaptic integration (Walter et al., 2009, Valera et al., 2016). A study from the lab showed that subthreshold GC inputs (i.e. that do no trigger firing in PCs) modulate PCs firing rate (Grangeray-Vilmint et al., 2018).

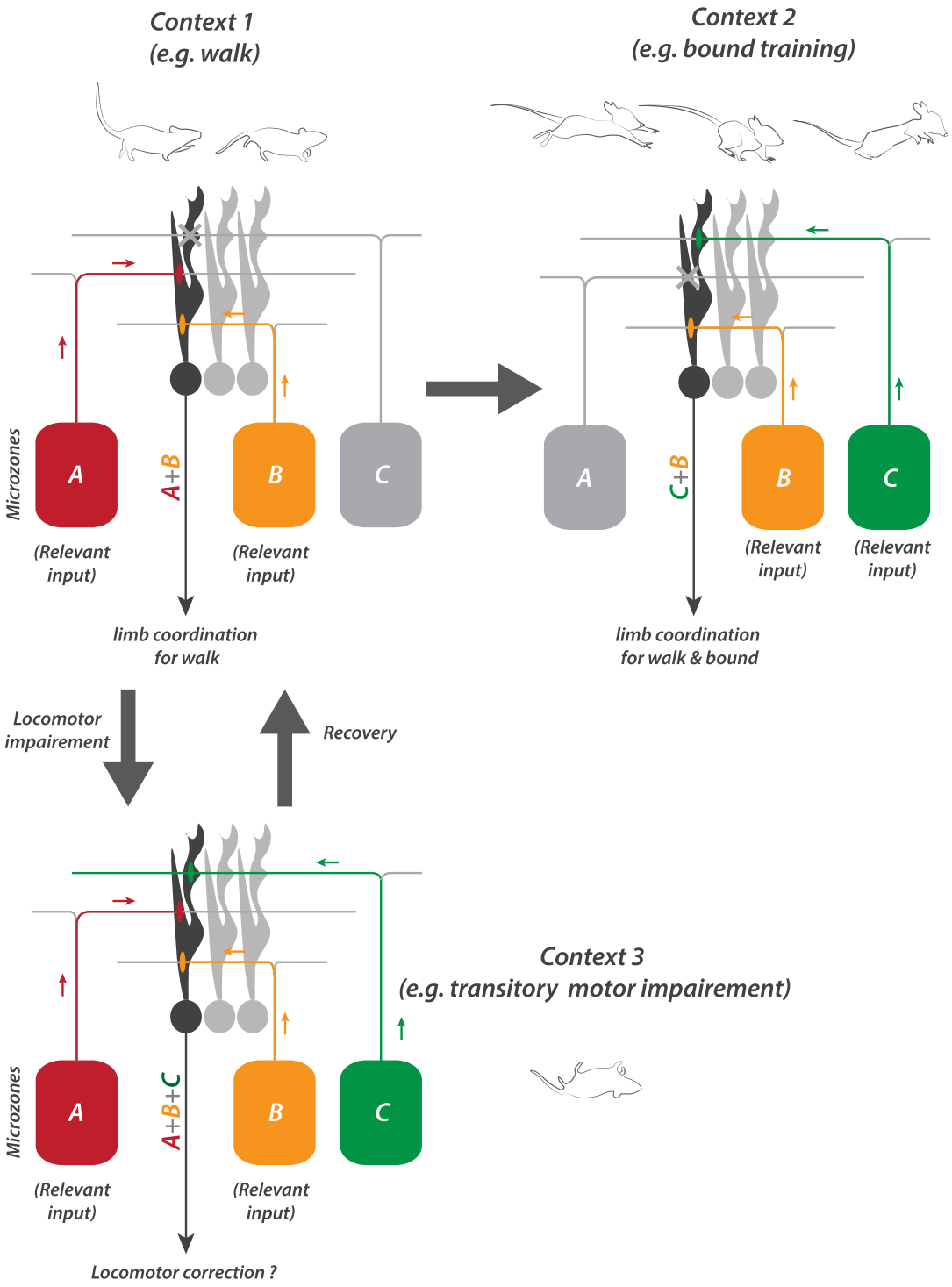

Fi gure 28 : Toward a dynamic source-dependant driven model for inter-modular communication within the cerebellar cortex

Our results highlighted causal relationship between cerebellar microcircuits synaptic organization following locomotor adaptation. Arrays of Purkinje cells can select incoming information through synapses arising from different microzones, depending on their relevance towards ongoing motor learning. Therefore microzones are not associated in a random fashion, prefered associations seem to be induced by the context and the nature of behavioral adaptation.

As PCs are spontaneously active, any significant GC input, no matter how small has significant influence on the output message from the cerebellar cortex.

7.3.5 Relevance of PC cluster 1 in locomotor control

PCs located within the functional cluster 1 target the medial cerebellar nuclei and ultimately the *biceps femoralis*, therefore controlling movements in the ipsilateral hind limb (Ruigrok et al., 2008) (see ***Figure 13***). My data show that the spatial distribution of functional GC inputs to this PC cluster in sensitive the adaptation of locomotor behavior (*see section 6.2*). However, the contribution of the medial vermis to locomotor coordination remains unclear. Although GCs (Powell et al., 2015) and PCs (Jelitai et al., 2016) in vermal lobule V encode locomotion kinematics, locomotor adaptation during a split-belt task is controlled by the paravermal cerebellum (i.e. C zone in the paravermis and interposed nuclei) rather than the medial cerebellum (Darmohray et al., 2019) (*see section 4.2.2*).

Cerebellar regulation of locomotion may therefore follow a modular organisation. The planning and execution of visually guided locomotion depends on the contribution of multiple cortical areas, including the posterior parietal cortex and the motor cortex (Drew and Marigold, 2015). Since cortical sensory and motor information converge to Crus I region (Proville et al., 2014), the lateral cerebellum could be implicated in gait adjustment during goal-directed or goal-initiated locomotion, while temporal and spatial interlimb adaptation rely on the paravermal cerebellum (Darmohray et al., 2019).
The medial part of the cerebellum (i.e vermis and medial cerebellar nuclei) is highly involved in gait and balance control (CHAMBERS, 1955; Morton and Bastian, 2004; Sierra et al., 2015; Takakusaki, 2017) through high connectivity with the vestibular nuclei (VOOGD et al., 1996; Merchant, 2011). Disruption of the vermal modules (A/AX) through cMAO inactivation produces aberrant and uncoordinated walking patterns in cats (Horn et al., 2010). Therefore, PCs within the cerebellar vermis may participate to locomotor adaptation and control through regulation of gait and global balance.

7.4 Excitation and inhibition synaptic pathways are independant

7.4.1 Beyond the scope of feed forward inhibition

Mappings of disynaptic inhibitory inputs also revealed conserved input patterns from surrounding MLIs to PCIs located in the functional cluster 1. Surprisingly, mixed excitatory and inhibitory GC inputs represent a minority of the GC inputs. MF stimulation experiments confirmed that the direct feedforward excitation-inhibition sequence described in the literature (Eccles et al., 1967; Brunel et al., 2004; Mittmann et al., 2005; Grangeray-Vilmint et al., 2018) is not the only way for PCs to integrate excitatory and inhibitory inputs. Feedforward inhibition has been described in the litterature following simulations of beams of PFs (Eccles et al. 1967; Mittman et al., 2005) which increase the probability to recruit both inhibitory and excitatory PF. Other studies however showed that stimulations of GC clusters instead of PFs would be more physiologically accurate, as they expand the range of PCs discharge (Brunel et al., 2004; Grangeray-Vilmint et al., 2018) as well as refine synaptic plasticity induction within cerebellar microcircuits (Bouvier et al., 2018).

7.4.2 Mirrored excitatory and inhibitory patterns

Besides local inputs, the inhibitory input pattern is mostly symmetrical to the monosynaptic excitatory input, confirming findings of Valera and colleagues (Valera et al., 2016). Although they mapped GC inputs to MLIs, our extended inhibitory GC-MLI-PC synaptic patterns are similar to their findings (e.g. inputs are mostly in the ipsilateral side). This can be explained by the fact that PCs are contacted by a few neighboring MLIs only (Palay and Chan-Palay 1974, Häusser & Clark, 1997) that share similar GC input patterns (Valera et al., 2016). The plasticities interplay within cerebellar microcircuits support this mirrored patterns: LTD induction at the PF-PC synapses can induce LTP at PC-MLI synapses, and vice versa (Jörntell and Ekerot, 2002; Coesmans et al., 2004; Rancillac and Crépel, 2004; Gao et al., 2012).

7.4.3 Caged glutamate is a perfectible tool

Glutamate uncaging (with UV or blue light) has been extensively used by researchers to perform neural networks mappings in several brain regions (for review see Shepherd, 2012).

It is an interesting tool as it does not require genetic encoding of light-sensitive ion channels (i.e. ChannelRhodopsin) and thus can be easily applied to acute slices. It allowed us to elicit reliable EPSCs in PCs (***Figure 20A***). However, available caged-glutamate molecules (e.g. RuBi Glutamate or MNI Glutamate) show a major drawback as partially antagonize GABA-A dependent neurotransmission. Indeed, Fino and colleagues reported a 50% decrease of evoked IPSCs amplitudes in the cerebral cortex with bath application of 300µM RuBi Glutamate (Fino et al., 2009). Thus, the interpretation of inhibitory maps is somehow limited as we probably underestimate the strength of GC-PC-MLI disynaptic connections. To limit this effect, we used 3 times less concentrated RuBi Glutamate than Fino and colleagues (100µM vs 300µM). We have planned to perform control experiments in acute cerebellar slices in order to (1) determine the exact antagonist effect in the previous experiments and (2) to evaluate the possibility to find a satisfying compromise between the dose of caged glutamate, the quality of the overall experiment and the antagonist effect on inhibitory neurotransmission.
In addition, the lab has recently started to collaborate with the Team of Chemistry and Molecular Biology (CNRS/Université de Strasbourg UMR 7199, Illkirch, France) leaded by Alexandre Specht & Thomas Grutter to work on the development of new caged-compounds that lack this antagonist effect.

7.5 Perspectives and future directions

My PhD project brought new elements of discussion for the understanding of information processing and integration within cerebellar microcircuits. It raised several questions I will review in this paragraph, as well as experiments that would be interesting to perform in order to answer these questions.

In P14 to P18 mice, a large increase in the probability of connection between distant GCs and PCs in functional cluster 1 occurs with no clear stereotyped organization. However, after P30, the adult GC input map was reliably observed in all the mice. We cannot distinguish developmental from functional effects in the establishment of synaptic maps. Therefore, it would be interesting to perturb, delay or accelerate locomotor learning in juvenile mice in order to uncover potential corresponding influence on synaptic maps in the anterior vermis.

The mappings of inhibitory connections raised questions regarding the real aspect of unitary Gc to PCs connections. Since excitation and inhibition can be spatially and temporally segregated, future studies of cerebellar microcircuits should consider both types of GC inputs.

Once clean caged compounds will be available it would be exciting to perform inhibitory mappings after locomotor adaptation in order to fulfill this dataset. As the balance between excitation and inhibition is crucial for the computation of cerebellar output, I would be curious to see how motor adaptation (where appropriate) would shape the selection of inhibitory inputs.

Since cerebellar microzones are dedicated to the control of specific motor units (Apps and Garwicz., 2005; Ruigrok, 2011), understanding how they compute incoming information is a key point that may lead to development of compensatory stimulation protocols for movement disorders. It would be interesting to perform restricted optogenetic stimulations or silencing of precise cerebellar microzones (i.e. the B zone) in impaired or ataxic mutants in order to see in what extent it may help mice to recover efficient, healthy-like motor coordination.
We started new experiments in the lab that involve *in vivo* MF optogenetic stimulation in mice executing a motor task. Locomotor impairment is assessed with high speed motion capture of hindlimbs kinematics and we plan to evaluate synaptic connectivity within the cerebellar cortex after motor learning. Therefore, we will try to highlight which microzones are precisely involved in the learning of new locomotor strategies.

REFERENCES

Ahn AH, Dziennis S, Hawkes R, Herrup K (1994) The cloning of zebrin II reveals its identity with aldolase C. Development 120:2081–2090 Available at: http://www.ncbi.nlm.nih.gov/pubmed/7925012 [Accessed February 3, 2015].

Albergaria C, Silva NT, Pritchett DL, Carey MR (2018) Locomotor activity modulates associative learning in mouse cerebellum. Nat Neurosci 21:725–735 Available at: http://dx.doi.org/10.1038/s41593-018-0129-x.

Albus JS (1971) A theory of cerebellar function. Math Biosci 10:25–61 Available at: http://linkinghub.elsevier.com/retrieve/pii/0025556471900514.

Alcami P, Marty A (2013) Estimating functional connectivity in an electrically coupled interneuron network. Proc Natl Acad Sci 110:E4798–E4807 Available at: http://www.pnas.org/cgi/doi/10.1073/pnas.1310983110.

Allen GI, Tsukahara N (1974) Cerebrocerebellar communication systems. Physiol Rev 54:957–1006 Available at: http://www.physiology.org/doi/10.1152/physrev.1974.54.4.957.

Altman J (1972a) Postnatal development of the cerebellar cortex in the rat. II. Phases in the maturation of Purkinje cells and of the molecular layer. J Comp Neurol 145:399–463 Available at: http://doi.wiley.com/10.1002/cne.901450402.

Altman J (1972b) Postnatal development of the cerebellar cortex in the rat. I. The external germinal layer and the transitional molecular layer. J Comp Neurol 145:353–397 Available at: http://doi.wiley.com/10.1002/cne.901450305.

Altman J (1972c) Postnatal development of the cerebellar cortex in the rat. III. Maturation of the components of the granular layer. J Comp Neurol 145:353–397 Available at: http://doi.wiley.com/10.1002/cne.901450305.

Altman J (1982) Morphological Development of the Rat Cerebellum and Some of Its Mechanisms. Exp Brain Res (Suppl) 6:8–46.

Altman J, Bayer SA (1985) Embryonic development of the rat cerebellum. I. Delineation of the cerebellar primordium and early cell movements. J Comp Neurol 231:1–26 Available at: http://doi.wiley.com/10.1002/cne.902310103.

Altman J, Bayer SA (1987) Development of the precerebellar nuclei in the rat: IV. The anterior precerebellar extramural migratory stream and the nucleus reticularis tegmenti pontis and the basal pontine gray. J Comp Neurol 257:529–552 Available at: http://doi.wiley.com/10.1002/cne.902570405.

Alviña K, Ellis-Davies G, Khodakhah K (2009) T-type calcium channels mediate rebound firing in intact deep cerebellar neurons. Neuroscience 158:635–641 Available at: http://dx.doi.org/10.1016/j.neuroscience.2008.09.052.

Andersson G, Oscarsson O (1978a) Brain Projections to Lateral Vestibular Nucleus from Cerebellar Climbing Fiber Zones. 564.

Andersson G, Oscarsson O (1978b) Climbing fiber microzones in cerebellar vermis and their projection to different groups of cells in the lateral vestibular nucleus. Exp Brain Res 32:565–579 Available at: http://www.ncbi.nlm.nih.gov/pubmed/689129 [Accessed November 20, 2013].

Ankri L, Husson Z, Pietrajtis K, Proville R, Léna C, Yarom Y, Dieudonné S, Uusisaari MY (2015) A novel inhibitory nucleo-cortical circuit controls cerebellar Golgi cell activity. Elife 4:1–26 Available at: http://www.ncbi.nlm.nih.gov/pubmed/25965178.

Apps R et al. (2018) Cerebellar Modules and Their Role as Operational Cerebellar Processing Units. The Cerebellum 17:654–682 Available at: http://link.springer.com/10.1007/s12311-018-0952-3.

Apps R, Garwicz M (2005) Anatomical and physiological foundations of cerebellar information processing. Nat Rev Neurosci 6:297–311 Available at: http://www.nature.com.scd-rproxy.u-strasbg.fr/nrn/journal/v6/n4/full/nrn1646.html [Accessed February 3, 2015].

Apps R, Hawkes R (2009) Cerebellar cortical organization: a one-map hypothesis. Nat Rev Neurosci 10:670–681 Available at: http://www.ncbi.nlm.nih.gov/pubmed/19693030 [Accessed February 3, 2015].
Apps R, Strata P (2015) Neuronal circuits for fear and anxiety — the missing link. Nat Rev Neurosci 16:642–642 Available at: http://dx.doi.org/10.1038/nrn4028.
Arenz A, Silver RA, Schaefer AT, Margrie TW (2008) The Contribution of Single Synapses to Sensory Representation in Vivo. Science (80-) 321:977–980 Available at: http://www.sciencemag.org/cgi/doi/10.1126/science.1158391.
Armstrong DM, Edgley S a (1984) Discharges of nucleus interpositus neurones during locomotion in the cat. J Physiol 351:411–432 Available at: http://doi.wiley.com/10.1113/jphysiol.1984.sp015253.
Armstrong DM, Edgley SA (1988) Discharges of interpositus and Purkinje cells of the cat cerebellum during locomotion under different conditions. J Physiol 400:425–445 Available at: http://doi.wiley.com/10.1113/jphysiol.1988.sp017130.
Armstrong DM, Harvey RJ, Schild RF (1974) Topographical localization in the olivo-cerebellar projection: An electrophysiological study in the cat. J Comp Neurol 154:287–302 Available at: http://doi.wiley.com/10.1002/cne.901540305.
Arsénio Nunes ML, Sotelo C (1985) Development of the spinocerebellar system in the postnatal rat. J Comp Neurol 237:291–306 Available at: http://www.ncbi.nlm.nih.gov/pubmed/3840179.
Ashizawa T, Xia G (2016) Ataxia. Contin Lifelong Learn Neurol 22:1208–1226 Available at: http://insights.ovid.com/crossref?an=00132979-201608000-00014.
Babinski J (1902) Sur le rôle du cervelet dans les actes volitionnels nécessitant une successionrapide de mouvements (Diadococinésie). Rev Neurol 10:1013–1015.
Bagnall MW, Zingg B, Sakatos A, Moghadam SH, Zeilhofer HU, Lac S d. (2009) Glycinergic Projection Neurons of the Cerebellum. J Neurosci 29:10104–10110 Available at: http://www.jneurosci.org/cgi/doi/10.1523/JNEUROSCI.2087-09.2009.
Bastian AJ (2006) Learning to predict the future: the cerebellum adapts feedforward movement control. Curr Opin Neurobiol 16:645–649 Available at: http://linkinghub.elsevier.com/retrieve/pii/S0959438806001395 [Accessed September 25, 2013].
Bellardita C, Kiehn O (2015) Phenotypic Characterization of Speed-Associated Gait Changes in Mice Reveals Modular Organization of Locomotor Networks. Curr Biol 25:1426–1436 Available at: http://dx.doi.org/10.1016/j.cub.2015.04.005.
Bengtsson F, Ekerot C-F, Jörntell H (2011) In Vivo Analysis of Inhibitory Synaptic Inputs and Rebounds in Deep Cerebellar Nuclear Neurons Tell F, ed. PLoS One 6:e18822 Available at: http://www.pubmedcentral.nih.gov/articlerender.fcgi?artid=3084242&tool=pmcentrez&rendertype=abstract [Accessed November 27, 2012].
Bengtsson F, Jorntell H (2009) Sensory transmission in cerebellar granule cells relies on similarly coded mossy fiber inputs. Proc Natl Acad Sci 106:2389–2394 Available at: http://www.pnas.org/cgi/doi/10.1073/pnas.0808428106.
Bengtsson F, Jörntell H (2014) Specific relationship between excitatory inputs and climbing fiber receptive fields in deep cerebellar nuclear neurons. PLoS One 9:1–9.
Binda F, Dorgans K, Reibel S, Sakimura K, Kano M, Poulain B, Isope P (2016) Inhibition promotes long-term potentiation at cerebellar excitatory synapses. Sci Rep 6:33561 Available at: http://www.nature.com/articles/srep33561.
Biswas MS, Luo Y, Sarpong GA, Sugihara I (2019) Divergent projections of single pontocerebellar axons to multiple cerebellar lobules in the mouse. J Comp Neurol Available at: http://doi.wiley.com/10.1002/cne.24662.
Blakemore S-J, Wolpert DM, Frith CD (1998) Central cancellation of self-produced tickle sensation. Nat Neurosci 1:635–640 Available at: http://www.nature.com/articles/nn1198_635.
Blenkinsop TA, Lang EJ (2011) Synaptic Action of the Olivocerebellar System on Cerebellar Nuclear Spike Activity. J Neurosci 31:14708–14720 Available at:

http://www.jneurosci.org/cgi/doi/10.1523/JNEUROSCI.3323-11.2011.
Blot A, Barbour B (2014) Ultra-rapid axon-axon ephaptic inhibition of cerebellar Purkinje cells by the pinceau. Nat Neurosci 17:289–295 Available at: http://www.ncbi.nlm.nih.gov/pubmed/24413696.
Bourrat F, Sotelo C (1991) Relationships between neuronal birthdates and cytoarchitecture in the rat inferior olivary complex. J Comp Neurol 313:509–521 Available at: http://doi.wiley.com/10.1002/cne.903130311.
Bouvier G, Aljadeff J, Clopath C, Bimbard C, Ranft J, Blot A, Nadal J-P, Brunel N, Hakim V, Barbour B (2018) Cerebellar learning using perturbations. Elife 7:1–45 Available at: https://elifesciences.org/articles/31599.
Bower JM, Woolston DC (1983) Congruence of spatial organization of tactile projections to granule cell and Purkinje cell layers of cerebellar hemispheres of the albino rat: vertical organization of cerebellar cortex. J Neurophysiol 49:745–766 Available at: http://jn.physiology.org.scd-rproxy.u-strasbg.fr/content/49/3/745 [Accessed February 3, 2015].
Boyden ES, Katoh A, Pyle JL, Chatila TA, Tsien RW, Raymond JL (2006) Selective Engagement of Plasticity Mechanisms for Motor Memory Storage. Neuron 51:823–834 Available at: https://linkinghub.elsevier.com/retrieve/pii/S0896627306006726.
Braitenberg V, Atwood RP (1958) Morphological observations on the cerebellar cortex. J Comp Neurol 109:1–33 Available at: http://www.ncbi.nlm.nih.gov/pubmed/13563670.
Brochu G, Maler L, Hawkes R (1990) Zebrin II: A polypeptide antigen expressed selectively by purkinje cells reveals compartments in rat and fish cerebellum. J Comp Neurol 291:538–552 Available at: http://doi.wiley.com/10.1002/cne.902910405.
Brown IE, Bower JM (2001) Congruence of mossy fiber and climbing fiber tactile projections in the lateral hemispheres of the rat cerebellum. J Comp Neurol 429:59–70 Available at: http://www.ncbi.nlm.nih.gov/pubmed/11086289 [Accessed February 3, 2015].
Brown JT, Chan-Palay V, Palay SL (1977) A study of afferent input to the inferior olivary complex in the rat by retrograde axonal transport of horseradish peroxidase. J Comp Neurol 176:1–22.
Brunel N, Hakim V, Isope P, Nadal J-P, Barbour B (2004) Optimal Information Storage and the Distribution of Synaptic Weights. Neuron 43:745–757 Available at: https://linkinghub.elsevier.com/retrieve/pii/S0896627304005288.
Butts T, Green MJ, Wingate RJT (2014) Development of the cerebellum: simple steps to make a “little brain.” Development 141:4031–4041.
Calderon DP, Fremont R, Kraenzlin F, Khodakhah K (2011) The neural substrates of rapid-onset Dystonia-Parkinsonism. Nat Neurosci 14:357–365 Available at: http://www.nature.com/neuro/journal/v14/n3/full/nn.2753.html [Accessed May 21, 2015].
Canto CB, Witter L, De Zeeuw CI (2016) Whole-Cell Properties of Cerebellar Nuclei Neurons In Vivo Charpier S, ed. PLoS One 11:e0165887 Available at: http://dx.plos.org/10.1371/journal.pone.0165887.
Carey MR (2011) Synaptic mechanisms of sensorimotor learning in the cerebellum. Curr Opin Neurobiol 21:609–615 Available at: http://dx.doi.org/10.1016/j.conb.2011.06.011.
Carey MR, Lisberger SG (2002) Embarrassed, but Not Depressed : eye opening lessons for cerebellar learning. Neuron 35:223–226 Available at: https://linkinghub.elsevier.com/retrieve/pii/S0896627302007717.
Carey MR, Regehr WG (2009) Noradrenergic Control of Associative Synaptic Plasticity by Selective Modulation of Instructive Signals. Neuron 62:112–122 Available at: http://dx.doi.org/10.1016/j.neuron.2009.02.022.
Carey MR, Regehr WG (2010) Phosphatase Activity Controls the Ups and Downs of Cerebellar Learning. Neuron 67:525–526 Available at: http://dx.doi.org/10.1016/j.neuron.2010.08.015.
Carta I, Chen CH, Schott AL, Dorizan S, Khodakhah K (2019) Cerebellar modulation of the reward circuitry and social behavior. Science (80-) 363.
Cathala L, Brickley S, Cull-Candy S, Farrant M (2003) Maturation of EPSCs and Intrinsic Membrane Properties Enhances Precision at a Cerebellar Synapse. J Neurosci

23:6074–6085 Available at: http://www.jneurosci.org/lookup/doi/10.1523/JNEUROSCI.23-14-06074.2003.
Cerminara NL, Apps R (2011) Behavioural Significance of Cerebellar Modules. The Cerebellum 10:484–494 Available at: http://link.springer.com/10.1007/s12311-010-0209-2.
Cerminara NL, Lang EJ, Sillitoe R V., Apps R (2015) Redefining the cerebellar cortex as an assembly of non-uniform Purkinje cell microcircuits. Nat Rev Neurosci 16:79–93 Available at: http://www.nature.com/doifinder/10.1038/nrn3886 [Accessed January 20, 2015].
Cesana E, Pietrajtis K, Bidoret C, Isope P, D'Angelo E, Dieudonne S, Forti L (2013) Granule Cell Ascending Axon Excitatory Synapses onto Golgi Cells Implement a Potent Feedback Circuit in the Cerebellar Granular Layer. J Neurosci 33:12430–12446 Available at: http://www.jneurosci.org/cgi/doi/10.1523/JNEUROSCI.4897-11.2013.
Chabrol FP, Arenz A, Wiechert MT, Margrie TW, DiGregorio DA (2015) Synaptic diversity enables temporal coding of coincident multisensory inputs in single neurons. Nat Neurosci 18:718–727 Available at: http://www.nature.com/articles/nn.3974.
Chabrol FP, Blot A, Mrsic-Flogel TD (2019) Cerebellar Contribution to Preparatory Activity in Motor Neocortex. Neuron 103:506-519.e4 Available at: https://doi.org/10.1016/j.neuron.2019.05.022.
Chadderton P, Margrie TW, Häusser M (2004) Integration of quanta in cerebellar granule cells during sensory processing. Nature 428:856–860 Available at: http://www.nature.com/articles/nature02442.
CHAMBERS WW (1955) Functional Localization in the Cerebellum. AMA Arch Neurol Psychiatry 74:653 Available at: http://archneurpsyc.jamanetwork.com/article.aspx?doi=10.1001/archneurpsyc.1955.02330180071008.
Chaumont J, Guyon N, Valera AM, Dugué GP, Popa D, Marcaggi P, Gautheron V, Reibel-Foisset S, Dieudonné S, Stephan A, Barrot M, Cassel J-C, Dupont J-L, Doussau F, Poulain B, Selimi F, Léna C, Isope P (2013) Clusters of cerebellar Purkinje cells control their afferent climbing fiber discharge. Proc Natl Acad Sci U S A 110:16223–16228 Available at: http://www.pnas.org/cgi/content/long/1302310110v1.
Chédotal A, Bloch-Gallego E, Sotelo C (1997) The embryonic cerebellum contains topographic cues that guide developing inferior olivary axons. Development 124:861–870 Available at: http://www.ncbi.nlm.nih.gov/pubmed/9043067 [Accessed May 20, 2015].
Chedotal A, Sotelo C (1993) The "creeper stage" in cerebellar climbing fiber synaptogenesis precedes the "pericellular nest" - ultrastructural evidence with parvalbumin immunocytochemistry. Dev Brain Res 76:207–220.
Chen L, Bao S, Lockard J, Kim J, Thompson R (1996) Impaired classical eyeblink conditioning in cerebellar-lesioned and Purkinje cell degeneration (pcd) mutant mice. J Neurosci 16:2829–2838 Available at: http://www.jneurosci.org/lookup/doi/10.1523/JNEUROSCI.16-08-02829.1996.
Chen S, Augustine GJ, Chadderton P (2016) The cerebellum linearly encodes whisker position during voluntary movement. Elife 5:e10509 Available at: http://elifesciences.org/lookup/doi/10.7554/eLife.10509.
Coesmans M, Weber JT, De Zeeuw CI, Hansel C (2004) Bidirectional parallel fiber plasticity in the cerebellum under climbing fiber control. Neuron 44:691–700 Available at: http://www.ncbi.nlm.nih.gov/pubmed/15541316 [Accessed February 3, 2015].
Coombes SA, Misra G (2016) Pain and motor processing in the human cerebellum. Pain 157:117–127 Available at: http://content.wkhealth.com/linkback/openurl?sid=WKPTLP:landingpage&an=00006396-201601000-00012.
Côté M-P, Murray LM, Knikou M (2018) Spinal Control of Locomotion: Individual Neurons, Their Circuits and Functions. Front Physiol 9:1–27 Available at: https://www.frontiersin.org/article/10.3389/fphys.2018.00784/full.

Crepel F, Mariani J, Delhaye-Bouchaud N (1976) Evidence for a multiple innervation of purkinje cells by climbing fibers in the immature rat cerebellum. J Neurobiol 7:567–578 Available at: http://www.ncbi.nlm.nih.gov/pubmed/1003202.
Cullen KE (2011) The neural encoding of self-motion. Curr Opin Neurobiol 21:587–595 Available at: http://dx.doi.org/10.1016/j.conb.2011.05.022.
Cullen KE, Brooks JX (2015) Neural Correlates of Sensory Prediction Errors in Monkeys: Evidence for Internal Models of Voluntary Self-Motion in the Cerebellum. The Cerebellum 14:31–34 Available at: http://link.springer.com/10.1007/s12311-014-0608-x.
Czubayko U, Sultan F, Thier P, Schwarz C (2001) Two Types of Neurons in the Rat Cerebellar Nuclei as Distinguished by Membrane Potentials and Intracellular Fillings. J Neurophysiol 85:2017–2029 Available at: http://www.physiology.org/doi/10.1152/jn.2001.85.5.2017.
D'Angelo E, Casali S (2012) Seeking a unified framework for cerebellar function and dysfunction: from circuit operations to cognition. Front Neural Circuits 6:116 Available at: http://www.pubmedcentral.nih.gov/articlerender.fcgi?artid=3541516&tool=pmcentrez&rendertype=abstract.
Darmohray DM, Jacobs JR, Marques HG, Carey MR (2019) Spatial and Temporal Locomotor Learning in Mouse Cerebellum. Neuron 102:217-231.e4 Available at: https://doi.org/10.1016/j.neuron.2019.01.038.
de Solages C, Szapiro G, Brunel N, Hakim V, Isope P, Buisseret P, Rousseau C, Barbour B, Léna C (2008) High-Frequency Organization and Synchrony of Activity in the Purkinje Cell Layer of the Cerebellum. Neuron 58:775–788.
De Zeeuw CI, Hoogland TM (2015) Reappraisal of Bergmann glial cells as modulators of cerebellar circuit function. Front Cell Neurosci 9:1–8.
Dean I, Robertson SJ, Edwards FA (2003) Serotonin Drives a Novel GABAergic Synaptic Current Recorded in Rat Cerebellar Purkinje Cells: A Lugaro Cell to Purkinje Cell Synapse. J Neurosci 23:4457–4469 Available at: http://www.jneurosci.org/lookup/doi/10.1523/JNEUROSCI.23-11-04457.2003.
Dean P, Porrill J, Ekerot C-F, Jörntell H (2010) The cerebellar microcircuit as an adaptive filter: experimental and computational evidence. Nat Rev Neurosci 11:30–43 Available at: http://dx.doi.org/10.1038/nrn2756.
Dehnes Y, Chaudhry FA, Ullensvang K, Lehre KP, Storm-Mathisen J, Danbolt NC (1998) The Glutamate Transporter EAAT4 in Rat Cerebellar Purkinje Cells: A Glutamate-Gated Chloride Channel Concentrated near the Synapse in Parts of the Dendritic Membrane Facing Astroglia. J Neurosci 18:3606–3619 Available at: http://www.jneurosci.org/lookup/doi/10.1523/JNEUROSCI.18-10-03606.1998.
Delmaire C, Vidailhet M, Elbaz A, Bourdain F, Bleton JP, Sangla S, Meunier S, Terrier A, Lehéricy S (2007) Structural abnormalities in the cerebellum and sensorimotor circuit in writer's cramp. Neurology 69:376–380.
Demsar J, Curk T, Erjavec A, Gorup C, Hocevar T (2013) Orange: Data Mining Toolbox in Python. J Mach Learn Res 14:2349–2353.
Desmond JE, Fiez JA (1998) Neuroimaging studies of the cerebellum: language, learning and memory. Trends Cogn Sci 2:355–362 Available at: https://linkinghub.elsevier.com/retrieve/pii/S136466139801211X.
Dieudonné S (1998) Submillisecond kinetics and low efficacy of parallel fibre-Golgi cell synaptic currents in the rat cerebellum. J Physiol 510:845–866 Available at: http://doi.wiley.com/10.1111/j.1469-7793.1998.845bj.x.
Dieudonné S (2001) Book Review: Serotonergic Neuromodulation in the Cerebellar Cortex: Cellular, Synaptic, and Molecular Basis. Neurosci 7:207–219 Available at: http://journals.sagepub.com/doi/10.1177/107385840100700306.
Dieudonné S, Dumoulin A (2000) Serotonin-Driven Long-Range Inhibitory Connections in the Cerebellar Cortex. J Neurosci 20:1837–1848 Available at: http://www.jneurosci.org/lookup/doi/10.1523/JNEUROSCI.20-05-01837.2000.
DiGregorio DA, Nusser Z, Silver RA (2002) Spillover of Glutamate onto Synaptic AMPA

Receptors Enhances Fast Transmission at a Cerebellar Synapse. Neuron 35:521–533 Available at: https://linkinghub.elsevier.com/retrieve/pii/S0896627302007870.
Dorgans K, Demais V, Bailly Y, Poulain B, Isope P, Doussau F (2019) Short-term plasticity at cerebellar granule cell to molecular layer interneuron synapses expands information processing. Elife 8:1–24 Available at: https://elifesciences.org/articles/41586.
Doya K (1999) What are the computations of the cerebellum, the basal ganglia and the cerebral cortex? Neural Networks 12:961–974 Available at: https://linkinghub.elsevier.com/retrieve/pii/S0893608099000465.
Drew T, Marigold DS (2015) Taking the next step: cortical contributions to the control of locomotion. Curr Opin Neurobiol 33:25–33 Available at: http://dx.doi.org/10.1016/j.conb.2015.01.011.
Dugué GP, Brunel N, Hakim V, Schwartz E, Chat M, Lévesque M, Courtemanche R, Léna C, Dieudonné S (2009) Electrical Coupling Mediates Tunable Low-Frequency Oscillations and Resonance in the Cerebellar Golgi Cell Network. Neuron 61:126–139 Available at: http://www.ncbi.nlm.nih.gov/pubmed/19146818 [Accessed January 3, 2014].
Eccles JC, Llinás R, Sasaki K (1966) The excitatory synaptic action of climbing fibres on the Purkinje cells of the cerebellum. J Physiol 182:268–296.
Eccles JC, Sasaki K, Strata P (1967) Interpretation of the potential fields generated in the cerebellar cortex by a mossy fibre volley. Exp Brain Res 3 Available at: http://link.springer.com/10.1007/BF00234470.
Ekerot C-F, Larson B (1979) The dorsal spino-olivocerebellar system in the cat. Exp Brain Res 36:201–217 Available at: http://link.springer.com/10.1007/BF00238905.
Ekerot C, Jörntell H (2001) Parallel fibre receptive fields of Purkinje cells and interneurons are climbing fibre-specific. Eur J Neurosci 13:1303–1310 Available at: http://doi.wiley.com/10.1046/j.0953-816x.2001.01499.x [Accessed February 3, 2015].
Ekerot CF, Jörntell H, Garwicz M (1995) Functional relation between corticonuclear input and movements evoked on microstimulation in cerebellar nucleus interpositus anterior in the cat. Exp Brain Res 106:365–376 Available at: http://www.ncbi.nlm.nih.gov/pubmed/8983981.
Eshra A, Hirrlinger P, Hallermann S (2019) Enriched Environment Shortens the Duration of Action Potentials in Cerebellar Granule Cells. Front Cell Neurosci 13:1–9 Available at: https://www.frontiersin.org/article/10.3389/fncel.2019.00289/full.
Esposito MS, Capelli P, Arber S (2014) Brainstem nucleus MdV mediates skilled forelimb motor tasks. Nature 508:351–356 Available at: http://dx.doi.org/10.1038/nature13023.
Fares RP, Belmeguenai A, Sanchez PE, Kouchi HY, Bodennec J, Morales A, Georges B, Bonnet C, Bouvard S, Sloviter RS, Bezin L (2013) Standardized Environmental Enrichment Supports Enhanced Brain Plasticity in Healthy Rats and Prevents Cognitive Impairment in Epileptic Rats Lei S, ed. PLoS One 8:e53888 Available at: http://dx.plos.org/10.1371/journal.pone.0053888.
Ferreira-Pinto MJ, Ruder L, Capelli P, Arber S (2018) Connecting Circuits for Supraspinal Control of Locomotion. Neuron 100:361–374 Available at: https://doi.org/10.1016/j.neuron.2018.09.015.
Fino E, Araya R, Peterka DS, Salierno M, Etchenique R, Yuste R (2009) RuBi-Glutamate: Two-Photon and Visible-Light Photoactivation of Neurons and Dendritic spines. Front Neural Circuits 3:2 Available at: http://www.pubmedcentral.nih.gov/articlerender.fcgi?artid=2691658&tool=pmcentrez&rendertype=abstract [Accessed February 3, 2015].
Friede RL (1973) Dating the development of human cerebellum. Acta Neuropathol 23:48–58.
Fujita H, Aoki H, Ajioka I, Yamazaki M, Abe M, Oh-Nishi A, Sakimura K, Sugihara I (2014) Detailed expression pattern of aldolase C (Aldoc) in the cerebellum, retina and other areas of the CNS studied in Aldoc-Venus knock-in mice. PLoS One 9:e86679 Available at: http://www.pubmedcentral.nih.gov/articlerender.fcgi?artid=3903578&tool=pmcentrez&rendertype=abstract [Accessed March 19, 2015].
Fung WKW, Peall KJ (2019) What is the role of the cerebellum in the pathophysiology of

dystonia? J Neurol 266:1549–1551 Available at: https://doi.org/10.1007/s00415-019-09344-7.
Gao Z, Davis C, Thomas AM, Economo MN, Abrego AM, Svoboda K, De Zeeuw CI, Li N (2018) A cortico-cerebellar loop for motor planning. Nature 563:113–116 Available at: http://www.nature.com/articles/s41586-018-0633-x.
Gao Z, van Beugen BJ, De Zeeuw CI (2012) Distributed synergistic plasticity and cerebellar learning. Nat Rev Neurosci 13:619–635 Available at: http://www.ncbi.nlm.nih.gov/pubmed/22895474 [Accessed January 10, 2015].
Garcia S, Fourcaud-Trocmé N (2009) OpenElectrophy: An Electrophysiological Data- and Analysis-Sharing Framework. Front Neuroinform 3:14 Available at: http://www.pubmedcentral.nih.gov/articlerender.fcgi?artid=2694696&tool=pmcentrez&rendertype=abstract [Accessed May 22, 2015].
Garwicz M, Ekerot C-F, Schouenborg J (1992) Distribution of Cutaneous Nociceptive and Tactile Climbing Fibre Input to Sagittal Zones in Cat Cerebellar Anterior Lobe. Eur J Neurosci 4:289–295 Available at: http://doi.wiley.com/10.1111/j.1460-9568.1992.tb00876.x.
Garwicz M, Ekerot CF (1994) Topographical organization of the cerebellar cortical projection to nucleus interpositus anterior in the cat. J Physiol 474:245–260 Available at: http://doi.wiley.com/10.1113/jphysiol.1994.sp020017.
Garwicz M, Jörntell H, Ekerot C-F (1998a) Cutaneous receptive fields and topography of mossy fibres and climbing fibres projecting to cat cerebellar C3 zone. J Physiol 512:277–293 Available at: http://doi.wiley.com/10.1111/j.1469-7793.1998.277bf.x [Accessed February 3, 2015].
Garwicz M, Jörntell H, Ekerot CF (1998b) Cutaneous receptive fields and topography of mossy fibres and climbing fibres projecting to cat cerebellar C3 zone. J Physiol 512:277–293.
Gauck V, Jaeger D (2000) The Control of Rate and Timing of Spikes in the Deep Cerebellar Nuclei by Inhibition. J Neurosci 20:3006–3016 Available at: http://www.jneurosci.org/lookup/doi/10.1523/JNEUROSCI.20-08-03006.2000.
Glickstein M, Strata P, Voogd J (2009) Cerebellum: history. Neuroscience 162:549–559 Available at: http://www.ncbi.nlm.nih.gov/pubmed/19272426 [Accessed July 16, 2012].
Glickstein M, Sultan F, Voogd J (2011) Functional localization in the cerebellum. Cortex 47:59–80 Available at: http://www.ncbi.nlm.nih.gov/pubmed/19833328 [Accessed November 6, 2012].
Goodlett CR, Mittleman G (2017) The Cerebellum. In: Conn's Translational Neuroscience, pp 191–212. Elsevier. Available at: http://www.sciencedirect.com/science/article/pii/B9780128023815000166.
Grangeray-Vilmint A, Valera AM, Kumar A, Isope P (2018) Short-Term Plasticity Combines with Excitation–Inhibition Balance to Expand Cerebellar Purkinje Cell Dynamic Range. J Neurosci 38:5153–5167.
Grillner S, Jessell TM (2009) Measured motion: searching for simplicity in spinal locomotor networks. Curr Opin Neurobiol 19:572–586 Available at: https://linkinghub.elsevier.com/retrieve/pii/S0959438809001482.
Groenewegen HJ, Voogd J (1977) The parasagittal zonation within the olivocerebellar projection. I. Climbing fiber distribution in the vermis of cat cerebellum. J Comp Neurol 174:417–488 Available at: http://doi.wiley.com/10.1002/cne.901740304.
Gundappa-Sulur G, De Schutter E, Bower JM (1999) Ascending granule cell axon: An important component of cerebellar cortical circuitry. J Comp Neurol 408:580–596 Available at: http://doi.wiley.com/10.1002/%28SICI%291096-9861%2819990614%29408%3A4%3C580%3A%3AAID-CNE11%3E3.0.CO%3B2-O.
Gutierrez-Castellanos N, Da Silva-Matos CM, Zhou K, Canto CB, Renner MC, Koene LMC, Ozyildirim O, Sprengel R, Kessels HW, De Zeeuw CI (2017) Motor Learning Requires Purkinje Cell Synaptic Potentiation through Activation of AMPA-Receptor Subunit GluA3. Neuron 93:409–424 Available at: http://dx.doi.org/10.1016/j.neuron.2016.11.046.

Hartell NA (1996) Strong Activation of Parallel Fibers Produces Localized Calcium Transients and a Form of LTD That Spreads to Distant Synapses. Neuron 16:601–610 Available at: http://www.ncbi.nlm.nih.gov/pubmed/8785057 [Accessed February 13, 2014].
Harvey RJ, Napper RM (1988) Quantitative study of granule and Purkinje cells in the cerebellar cortex of the rat. J Comp Neurol 274:151–157 Available at: http://www.ncbi.nlm.nih.gov/pubmed/3209738.
Harvey RJ, Napper RM (1991) Quantitative studies on the mammalian cerebellum. Prog Neurobiol 36:437–463 Available at: http://www.ncbi.nlm.nih.gov/pubmed/1947173.
Hashimoto K, Kano M (2005) Postnatal development and synapse elimination of climbing fiber to Purkinje cell projection in the cerebellum. Neurosci Res 53:221–228 Available at: https://linkinghub.elsevier.com/retrieve/pii/S0168010205002105.
Hashimoto M, Mikoshiba K (2003) Mediolateral Compartmentalization of the Cerebellum Is Determined on the “Birth Date” of Purkinje Cells. J Neurosci 23:11342–11351 Available at: http://www.jneurosci.org/lookup/doi/10.1523/JNEUROSCI.23-36-11342.2003.
Häusser M, Clark BA (1997) Tonic Synaptic Inhibition Modulates Neuronal Output Pattern and Spatiotemporal Synaptic Integration. Neuron 19:665–678 Available at: https://linkinghub.elsevier.com/retrieve/pii/S0896627300803797.
Hawkes R, Colonnier M, Leclerc N (1985) Monoclonal antibodies reveal sagittal banding in the rodent cerebellar cortex. Brain Res 333:359–365 Available at: https://linkinghub.elsevier.com/retrieve/pii/0006899385915938.
Hawkes R, Herrup K (1995) Aldolase C/zebrin II and the regionalization of the cerebellum. J Mol Neurosci 6:147–158 Available at: http://link.springer.com/10.1007/BF02736761.
Hawkes R, Leclerc N (1989) Purkinje cell axon collateral distribution reflect the chemical compartmentation of the rat cerebellar cortex. Brain Res 476:279–290 Available at: https://linkinghub.elsevier.com/retrieve/pii/0006899389912481.
Hazrati LN, Parent A (1992) Projection from the deep cerebellar nuclei to the pedunculopontine nucleus in the squirrel monkey. Brain Res 585:267–271.
Hensch TK (2005) Critical period plasticity in local cortical circuits. Nat Rev Neurosci 6:877–888 Available at: http://www.nature.com/articles/nrn1787.
Hirono M, Saitow F, Kudo M, Suzuki H, Yanagawa Y, Yamada M, Nagao S, Konishi S, Obata K (2012) Cerebellar Globular Cells Receive Monoaminergic Excitation and Monosynaptic Inhibition from Purkinje Cells Sugihara I, ed. PLoS One 7:e29663 Available at: https://dx.plos.org/10.1371/journal.pone.0029663.
Hodos W (2009) Evolution of Cerebellum. In: Encyclopedia of Neuroscience, Springer,. (Binder M.D., Hirokawa N. WU, ed).
Holmes G (1918) The Symptoms of Acute Cerebellar Injuries Due. J Nerv Ment Dis 48:485–488 Available at: https://insights.ovid.com/crossref?an=00005053-191812000-00023.
Horn KM, Pong M, Gibson AR (2010) Functional Relations of Cerebellar Modules of the Cat. J Neurosci 30:9411–9423 Available at: http://www.jneurosci.org/cgi/doi/10.1523/JNEUROSCI.0440-10.2010.
Hoy JL, Niell CM (2015) Layer-Specific Refinement of Visual Cortex Function after Eye Opening in the Awake Mouse. J Neurosci 35:3370–3383 Available at: http://www.jneurosci.org/cgi/doi/10.1523/JNEUROSCI.3174-14.2015.
Huang C-C, Sugino K, Shima Y, Guo C, Bai S, Mensh BD, Nelson SB, Hantman AW (2013) Convergence of pontine and proprioceptive streams onto multimodal cerebellar granule cells. Elife 2:e00400 Available at: http://www.ncbi.nlm.nih.gov/pubmed/23467508.
Hull C, Regehr WG (2012) Identification of an Inhibitory Circuit that Regulates Cerebellar Golgi Cell Activity. Neuron 73:149–158 Available at: https://linkinghub.elsevier.com/retrieve/pii/S0896627311009949.
Husson Z, Rousseau C V., Broll I, Zeilhofer HU, Dieudonne S (2014) Differential GABAergic and Glycinergic Inputs of Inhibitory Interneurons and Purkinje Cells to Principal Cells of the Cerebellar Nuclei. J Neurosci 34:9418–9431 Available at: http://www.jneurosci.org/cgi/doi/10.1523/JNEUROSCI.0401-14.2014.
H&#xfffd;mori J (1981) Synaptic input to the axon hillock and initial segment of inhibitory

interneurons in the cerebellar cortex of the rat. Cell Tissue Res 217 Available at: http://link.springer.com/10.1007/BF00219363.
Isope P, Barbour B (2002) Properties of unitary granule cell-->Purkinje cell synapses in adult rat cerebellar slices. J Neurosci 22:9668–9678 Available at: http://www.ncbi.nlm.nih.gov/pubmed/12427822 [Accessed February 3, 2015].
Isope P, Hildebrand ME, Snutch TP (2012) Contributions of T-type voltage-gated calcium channels to postsynaptic calcium signaling within purkinje neurons. Cerebellum 11:651–665.
Isope P, Murphy TH (2005) Low threshold calcium currents in rat cerebellar Purkinje cell dendritic spines are mediated by T-type calcium channels. J Physiol 562:257–269 Available at: http://www.ncbi.nlm.nih.gov/pubmed/15513942 [Accessed March 1, 2011].
Ito M (1984) The Cerebellum and Neural Control (Press R, ed).
Ito M (2001) Cerebellar long-term depression: characterization, signal transduction, and functional roles. Physiol Rev 81:1143–1195 Available at: http://www.ncbi.nlm.nih.gov/pubmed/11427694 [Accessed February 3, 2015].
Ito M (2006) Cerebellar circuitry as a neuronal machine. Prog Neurobiol 78:272–303 Available at: https://linkinghub.elsevier.com/retrieve/pii/S0301008206000232.
Ito M, Kano M (1982) Long-lasting depression of parallel fiber-Purkinje cell transmission induced by conjunctive stimulation of parallel fibers and climbing fibers in the cerebellar cortex. Neurosci Lett 33:253–258 Available at: https://linkinghub.elsevier.com/retrieve/pii/0304394082903809.
Ito M, Sakurai M, Tongroach P (1982) Climbing fibre induced depression of both mossy fibre responsiveness and glutamate sensitivity of cerebellar Purkinje cells. J Physiol 324:113–134 Available at: http://jp.physoc.org/content/324/1/113.short.
Ito M, Yoshida M, Obata K (1964) Monosynaptic inhibition of the intracerebellar nuclei induced from the cerebellar cortex. Experientia 20:575–576 Available at: http://link.springer.com/10.1007/BF02150304.
Iwakura A, Uchigashima M, Miyazaki T, Yamasaki M, Watanabe M (2012) Lack of Molecular-Anatomical Evidence for GABAergic Influence on Axon Initial Segment of Cerebellar Purkinje Cells by the Pinceau Formation. J Neurosci 32:9438–9448 Available at: http://www.jneurosci.org/cgi/doi/10.1523/JNEUROSCI.1651-12.2012.
Jansen J, Brodal A (1940) Experimental studies on the intrinsic fibers of the cerebellum. II. The cortico-nuclear projection. J Comp Neurol 73:267–321 Available at: http://doi.wiley.com/10.1002/cne.900730204.
Jayabal S, Watt A (2019) Development of Physiological Activity in the Cerebellum. Handb Cerebellum Cerebellar Disord:1–30.
Jelitai M, Puggioni P, Ishikawa T, Rinaldi A, Duguid I (2016) Dendritic excitation-inhibition balance shapes cerebellar output during motor behaviour. Nat Commun 7:13722 Available at: http://dx.doi.org/10.1038/ncomms13722.
Ji Z, Hawkes R (1994) Topography of Purkinje cell compartments and mossy fiber terminal fields in lobules II and III of the rat cerebellar cortex: spinocerebellar and cuneocerebellar projections. Neuroscience 61:935–954 Available at: http://www.ncbi.nlm.nih.gov/pubmed/7530818 [Accessed May 19, 2015].
Ji Z, Hawkes R (1995) Developing mossy fiber terminal fields in the rat cerebellar cortex may segregate because of Purkinje cell compartmentation and not competition. J Comp Neurol 359:197–212 Available at: http://www.ncbi.nlm.nih.gov/pubmed/7499524 [Accessed May 19, 2015].
Jorntell H, Ekerot C-F (2006) Properties of Somatosensory Synaptic Integration in Cerebellar Granule Cells In Vivo. J Neurosci 26:11786–11797 Available at: http://www.jneurosci.org/cgi/doi/10.1523/JNEUROSCI.2939-06.2006.
Jörntell H, Ekerot C-F (2003) Receptive field plasticity profoundly alters the cutaneous parallel fiber synaptic input to cerebellar interneurons in vivo. J Neurosci 23:9620–9631.
Jörntell H, Ekerot C-F, Garwicz M, Luo XL (2000) Functional organization of climbing fibre projection to the cerebellar anterior lobe of the rat. J Physiol 522 Pt 2:297–309 Available at: http://doi.wiley.com/10.1111/j.1469-7793.2000.00297.x [Accessed

February 3, 2015].
Jörntell H, Ekerot CF (2002) Reciprocal bidirectional plasticity of parallel fiber receptive fields in cerebellar Purkinje cells and their afferent interneurons. Neuron 34:797–806 Available at: http://www.sciencedirect.com/science/article/pii/S0896627302007134 [Accessed February 3, 2015].
Jörntell H, Hansel C (2006) Synaptic memories upside down: bidirectional plasticity at cerebellar parallel fiber-Purkinje cell synapses. Neuron 52:227–238 Available at: http://www.ncbi.nlm.nih.gov/pubmed/17046686 [Accessed February 3, 2015].
Kanichay RT, Silver RA (2008) Synaptic and Cellular Properties of the Feedforward Inhibitory Circuit within the Input Layer of the Cerebellar Cortex. J Neurosci 28:8955–8967 Available at: http://www.jneurosci.org/cgi/doi/10.1523/JNEUROSCI.5469-07.2008.
Kelly RM, Strick PL (2003) Cerebellar Loops with Motor Cortex and Prefrontal Cortex of a Nonhuman Primate. J Neurosci 23:8432–8444 Available at: http://www.jneurosci.org/lookup/doi/10.1523/JNEUROSCI.23-23-08432.2003.
Kiehn O (2016) Decoding the organization of spinal circuits that control locomotion. Nat Rev Neurosci 17:224–238 Available at: http://dx.doi.org/10.1038/nrn.2016.9.
Kitai ST, DeFrance JF, Hatada K, Kennedy DT (1974) Electrophysiological properties of lateral reticular nucleus cells: II. Synaptic activation. Exp Brain Res 21:403–418 Available at: http://link.springer.com/10.1007/BF00237904.
Knogler LD, Markov DA, Dragomir EI, Štih V, Portugues R (2017) Sensorimotor Representations in Cerebellar Granule Cells in Larval Zebrafish Are Dense, Spatially Organized, and Non-temporally Patterned. Curr Biol 27:1288–1302.
Kooy (1916) The inferior olive in vertebrates.
Kostadinov D, Beau M, Pozo MB, Häusser M (2019) Predictive and reactive reward signals conveyed by climbing fiber inputs to cerebellar Purkinje cells. Nat Neurosci 22:950–962 Available at: http://www.nature.com/articles/s41593-019-0381-8.
Kratochwil CF, Maheshwari U, Rijli FM (2017) The Long Journey of Pontine Nuclei Neurons: From Rhombic Lip to Cortico-Ponto-Cerebellar Circuitry. Front Neural Circuits 11 Available at: http://journal.frontiersin.org/article/10.3389/fncir.2017.00033/full.
Lackey EP, Heck DH, Sillitoe R V. (2018) Recent advances in understanding the mechanisms of cerebellar granule cell development and function and their contribution to behavior. F1000Research 7:1142.
Lainé J, Axelrad H (1998) Lugaro cells target basket and stellate cells in the cerebellar cortex. Neuroreport 9:2399–2403 Available at: https://insights.ovid.com/crossref?an=00001756-199807130-00045.
Lê S, Josse J, Husson F (2008) FactoMineR: An R Package for Multivariate Analysis. J Stat Softw 25:1–18.
Lee S, Yoon B-E, Berglund K, Oh S-J, Park H, Shin H-S, Augustine GJ, Lee CJ (2010) Channel-Mediated Tonic GABA Release from Glia. Science (80-) 330:790–796 Available at: http://www.sciencemag.org/cgi/doi/10.1126/science.1184334.
Lefler Y, Yarom Y, Uusisaari M (2014) Cerebellar Inhibitory Input to the Inferior Olive Decreases Electrical Coupling and Blocks Subthreshold Oscillations. Neuron 81:1389–1400 Available at: http://dx.doi.org/10.1016/j.neuron.2014.02.032.
Lemkey-Johnston N, Larramendi LMH (1968) Types and distribution of synapses upon basket and stellate cells of the mouse cerebellum: An electron microscopic study. J Comp Neurol 134:73–111 Available at: http://doi.wiley.com/10.1002/cne.901340106.
Leto K et al. (2016) Consensus Paper: Cerebellar Development. Cerebellum 15:789–828 Available at: http://link.springer.com/10.1007/s12311-015-0724-2.
Llano I, Gerschenfeld HM (1993) Inhibitory synaptic currents in stellate cells of rat cerebellar slices. J Physiol 468:177–200 Available at: http://doi.wiley.com/10.1113/jphysiol.1993.sp019766.
Luo Y, Patel RP, Sarpong GA, Sasamura K, Sugihara I (2017) Single axonal morphology and termination to cerebellar aldolase C stripes characterize distinct spinocerebellar projection systems originating from the thoracic spinal cord in the mouse. J Comp Neurol 520:633–655 Available at: http://www.ncbi.nlm.nih.gov/pubmed/21858823.

Ly R, Bouvier G, Schonewille M, Arabo A, Rondi-Reig L, Lena C, Casado M, De Zeeuw CI, Feltz A (2013) T-type channel blockade impairs long-term potentiation at the parallel fiber-Purkinje cell synapse and cerebellar learning. Proc Natl Acad Sci 110:20302–20307 Available at: http://www.pubmedcentral.nih.gov/articlerender.fcgi?artid=3864350&tool=pmcentrez&rendertype=abstract [Accessed February 3, 2015].
Mann-Metzerand P, Yarom Y (2000) Electrotonic coupling synchronizes interneuron activity in the cerebellar cortex. In, pp 115–122 Available at: https://linkinghub.elsevier.com/retrieve/pii/S0079612300240120.
Manni E, Petrosini L (1997) Luciani's work on the cerebellum a century later. Trends Neurosci 20:112–116.
Mariani J, Changeux J-P (1980) Multiple innervation of purkinje cells by climbing fibers in the cerebellum of the adult staggerer mutant mouse. J Neurobiol 11:41–50 Available at: http://doi.wiley.com/10.1002/neu.480110106.
Marr BYD (1969) A THEORY OF CEREBELLAR CORTEX (mossy fibers en purkinje cell). :437–470.
Matsushita M, Hosoya Y (1982) Spinocerebellar projections to lobules III to V of the anterior lobe in the cat, as studied by retrograde transport of horseradish peroxidase. J Comp Neurol 208:127–143 Available at: http://doi.wiley.com/10.1002/cne.902080203.
Matsushita M, Hosoya Y, Ikeda M (1979) Anatomical organization of the spinocerebellar system in the cat, as studied by retrograde transport of horseradish peroxidase. J Comp Neurol 184:81–105 Available at: http://doi.wiley.com/10.1002/cne.901840106.
Matsushita M, Wang CL (1987) Projection pattern of vestibulocerebellar fibers in the anterior vermis of the cat: an anterograde wheat germ agglutinin-horseradish peroxidase study. Neurosci Lett 74:25–30 Available at: https://linkinghub.elsevier.com/retrieve/pii/0304394087900450.
Mauk MD, Donegan NH (n.d.) A model of Pavlovian eyelid conditioning based on the synaptic organization of the cerebellum. Learn Mem 4:130–158 Available at: http://www.ncbi.nlm.nih.gov/pubmed/10456059.
Medina JF, Nores WL, Mauk MD (2002) Inhibition of climbing fibres is a signal for the extinction of conditioned eyelid responses. Nature 416:330–333 Available at: http://www.nature.com/articles/416330a.
Medrano MC, Dhanasobhon D, Yalcin I, Schlichter R, Cordero-Erausquin M (2016) Loss of inhibitory tone on spinal cord dorsal horn spontaneously and nonspontaneously active neurons in a mouse model of neuropathic pain. Pain 157:1432–1442 Available at: http://insights.ovid.com/crossref?an=00006396-201607000-00009.
Meera P, Pulst SM, Otis TS (2016) Cellular and circuit mechanisms underlying spinocerebellar ataxias. J Physiol 594:4653–4660 Available at: http://doi.wiley.com/10.1113/JP271897.
Mendes CS, Bartos I, Márka Z, Akay T, Márka S, Mann RS (2015) Quantification of gait parameters in freely walking rodents. BMC Biol 13:50 Available at: http://dx.doi.org/10.1186/s12915-015-0154-0.
Mendoza J. (2011) Spinocerebellar Tracts (Kreutzer JS, DeLuca J, Caplan B, eds). New York, NY: Springer New York. Available at: http://link.springer.com/10.1007/978-0-387-79948-3.
Merchant RE (2011) Vestibular Nuclei. In: Encyclopedia of Clinical Neuropsychology, pp 2610–2611. New York, NY: Springer New York. Available at: http://link.springer.com/10.1007/978-0-387-79948-3_376.
Miles FA, Lisberger SG (1981) Plasticity in the Vestibulo-Ocular Reflex: A New Hypothesis. Annu Rev Neurosci 4:273–299 Available at: http://www.annualreviews.org/doi/10.1146/annurev.ne.04.030181.001421.
Miller S, Nezlina N, Oscarsson O (1969a) Projection and convergence patterns in climbing fibre paths to cerebellar anterior lobe activated from cerebral cortex and spinal cord. Brain Res 14:230–233 Available at: https://linkinghub.elsevier.com/retrieve/pii/0006899369900456.

Miller S, Nezlina N, Oscarsson O (1969b) Climbing fibre projection to cerebellar anterior lobe activated from structures in midbrain and from spinal cord. Brain Res 14:234–236 Available at: https://linkinghub.elsevier.com/retrieve/pii/0006899369900468.
Mittmann W, Koch U, Häusser M (2005) Feed-forward inhibition shapes the spike output of cerebellar Purkinje cells. J Physiol 563:369–378 Available at: http://doi.wiley.com/10.1113/jphysiol.2004.075028.
Mori S, Matsui T, Kuze B, Asanome M, Nakajima K, Matsuyama K (1999) Stimulation of a Restricted Region in the Midline Cerebellar White Matter Evokes Coordinated Quadrupedal Locomotion in the Decerebrate Cat. J Neurophysiol 82:290–300 Available at: http://www.physiology.org/doi/10.1152/jn.1999.82.1.290.
Morton SM, Bastian AJ (2004) Cerebellar control of balance and locomotion. Neuroscientist 10:247–259.
Morton SM, Bastian AJ (2006) Cerebellar Contributions to Locomotor Adaptations during Splitbelt Treadmill Walking. J Neurosci 26:9107–9116 Available at: http://www.jneurosci.org/cgi/doi/10.1523/JNEUROSCI.2622-06.2006.
Murray AJ, Croce K, Belton T, Akay T, Jessell TM (2018) Balance Control Mediated by Vestibular Circuits Directing Limb Extension or Antagonist Muscle Co-activation. Cell Rep 22:1325–1338 Available at: https://doi.org/10.1016/j.celrep.2018.01.009.
Muzzu T, Mitolo S, Gava GP, Schultz SR (2018) Encoding of locomotion kinematics in the mouse cerebellum Sugihara I, ed. PLoS One 13:e0203900 Available at: http://dx.plos.org/10.1371/journal.pone.0203900.
Najac M, Raman IM (2015) Integration of Purkinje Cell Inhibition by Cerebellar Nucleo-Olivary Neurons. J Neurosci 35:544–549 Available at: http://www.jneurosci.org/lookup/doi/10.1523/JNEUROSCI.3583-14.2015.
Nedelescu H, Abdelhack M (2013) Comparative Morphology of Dendritic Arbors in Populations of Purkinje Cells in Mouse Sulcus and Apex. Neural Plast 2013:1–12 Available at: http://www.hindawi.com/journals/np/2013/948587/.
Nikolov P, Hassan SS, Aytulun A, Hartmann CJ, Kohlhase J, Schnitzler A, Albrecht P, Minnerop M, Groiss SJ (2019) Cerebellar Involvement in DYT-THAP1 Dystonia. The Cerebellum:19–21 Available at: http://link.springer.com/10.1007/s12311-019-01062-0.
Nunes MLA, Sotelo C, Wehrlé R (1988) Organization of spinocerebellar projection map in three types of agranular cerebellum: Purkinje cells vs. granule cells as organizer element. J Comp Neurol 273:120–136.
O'Brien J, Unwin N (2006) Organization of spines on the dendrites of Purkinje cells. Proc Natl Acad Sci 103:1575–1580 Available at: http://www.pnas.org/cgi/doi/10.1073/pnas.0507884103.
Ohmae S, Medina JF (2015) Climbing fibers encode a temporal-difference prediction error during cerebellar learning in mice. Nat Neurosci 18:1798–1803 Available at: http://www.nature.com/articles/nbt.3301.
Oscarsson O (1979) Functionnal units of the cerbellum - saggital zones and microzones. Trends Neurosci:143–145.
Ozden I, Sullivan MR, Lee HM, Wang SS-H (2009) Reliable coding emerges from coactivation of climbing fibers in microbands of cerebellar Purkinje neurons. J Neurosci 29:10463–10473 Available at: http://www.pubmedcentral.nih.gov/articlerender.fcgi?artid=2783593&tool=pmcentrez&rendertype=abstract [Accessed February 3, 2015].
Palay SL, Chan-Palay V (1974) Cerebellar Cortex. Berlin, Heidelberg: Springer Berlin Heidelberg. Available at: http://link.springer.com/10.1007/978-3-642-65581-4.
Palkovits M, Magyar P, Szentágothai J (1971) Quantitative histological analysis of the cerebellar cortex in the cat. Brain Res 32:15–30 Available at: https://linkinghub.elsevier.com/retrieve/pii/0006899371901521.
Patel VR, Zee DS (2015) The cerebellum in eye movement control: nystagmus, coordinate frames and disconjugacy. Eye 29:191–195 Available at: http://dx.doi.org/10.1038/eye.2014.271.
Paukert M, Huang YH, Tanaka K, Rothstein JD, Bergles DE (2010) Zones of Enhanced

Glutamate Release from Climbing Fibers in the Mammalian Cerebellum. J Neurosci 30:7290–7299 Available at: http://www.pubmedcentral.nih.gov/articlerender.fcgi?artid=2894469&tool=pmcentrez&rendertype=abstract [Accessed October 1, 2012].
Pichitpornchai C, Rawson JA, Rees S (1994) Morphology of parallel fibres in the cerebellar cortex of the rat: An experimental light and electron microscopic study with biocytin. J Comp Neurol 342:206–220 Available at: http://doi.wiley.com/10.1002/cne.903420205.
Pijpers A, Apps R, Pardoe J, Voogd J, Ruigrok TJH (2006) Precise Spatial Relationships between Mossy Fibers and Climbing Fibers in Rat Cerebellar Cortical Zones. J Neurosci 26:12067–12080 Available at: http://www.ncbi.nlm.nih.gov/pubmed/17108180 [Accessed February 3, 2015].
Pijpers A, Winkelman BHJ, Bronsing R, Ruigrok TJH (2008) Selective impairment of the cerebellar C1 module involved in rat hind limb control reduces step-dependent modulation of cutaneous reflexes. J Neurosci 28:2179–2189 Available at: http://www.ncbi.nlm.nih.gov/pubmed/18305251 [Accessed January 4, 2014].
Piochon C, Levenes C, Ohtsuki G, Hansel C (2010) Purkinje Cell NMDA Receptors Assume a Key Role in Synaptic Gain Control in the Mature Cerebellum. J Neurosci 30:15330–15335 Available at: http://www.jneurosci.org/cgi/doi/10.1523/JNEUROSCI.4344-10.2010.
Pisotta I, Molinari M (2014) Cerebellar contribution to feedforward control of locomotion. Front Hum Neurosci 8:1–5 Available at: http://journal.frontiersin.org/article/10.3389/fnhum.2014.00475/abstract.
Popa LS, Ebner TJ (2019) Cerebellum, Predictions and Errors. Front Cell Neurosci 12:1–13 Available at: https://www.frontiersin.org/article/10.3389/fncel.2018.00524/full.
Powell K, Mathy A, Duguid I, Häusser M (2015) Synaptic representation of locomotion in single cerebellar granule cells. Elife 4:1–18 Available at: https://elifesciences.org/articles/07290.
Proville RD, Spolidoro M, Guyon N, Dugué GP, Selimi F, Isope P, Popa D, Léna C (2014) Cerebellum involvement in cortical sensorimotor circuits for the control of voluntary movements. Nat Neurosci 17:1233–1239 Available at: http://www.nature.com/articles/nn.3773.
Quy PN, Fujita H, Sakamoto Y, Na J, Sugihara I (2011) Projection patterns of single mossy fiber axons originating from the dorsal column nuclei mapped on the aldolase C compartments in the rat cerebellar cortex. J Comp Neurol 519:874–899.
Rahimi-Balaei M, Bergen H, Kong J, Marzban H (2018) Neuronal Migration During Development of the Cerebellum. Front Cell Neurosci 12:1–16 Available at: https://www.frontiersin.org/article/10.3389/fncel.2018.00484/full.
Raman IM, Bean BP (1999) Ionic currents underlying spontaneous action potentials in isolated cerebellar Purkinje neurons. J Neurosci 19:1663–1674 Available at: http://www.ncbi.nlm.nih.gov/pubmed/10024353.
Ramnani N (2006) The primate cortico-cerebellar system: anatomy and function. Nat Rev Neurosci 7:511–522 Available at: http://www.nature.com/articles/nrn1953.
Rancillac A, Crépel F (2004) Synapses between parallel fibres and stellate cells express long-term changes in synaptic efficacy in rat cerebellum. J Physiol 554:707–720 Available at: http://doi.wiley.com/10.1113/jphysiol.2003.055871.
Rancz EA, Ishikawa T, Duguid I, Chadderton P, Mahon S, Häusser M (2007) High-fidelity transmission of sensory information by single cerebellar mossy fibre boutons. Nature 450:1245–1248 Available at: http://www.nature.com/articles/nature05995.
Raymond JL (2018) Yet another reason to walk instead of drive. Nat Neurosci 21:648–653 Available at: http://dx.doi.org/10.1038/s41593-018-0142-0.
Raymond JL, Medina JF (2018) Computational Principles of Supervised Learning in the Cerebellum. Annu Rev Neurosci 41:233–253 Available at: https://www.annualreviews.org/doi/10.1146/annurev-neuro-080317-061948.
Ritzau-Jost A, Delvendahl I, Rings A, Byczkowicz N, Harada H, Shigemoto R, Hirrlinger J, Eilers J, Hallermann S (2014) Ultrafast Action Potentials Mediate Kilohertz Signaling at

a Central Synapse. Neuron 84:152–163 Available at: https://linkinghub.elsevier.com/retrieve/pii/S0896627314007375.
Roseberry TK, Lee AM, Lalive AL, Wilbrecht L, Bonci A, Kreitzer AC (2016) Cell-Type-Specific Control of Brainstem Locomotor Circuits by Basal Ganglia. Cell 164:526–537 Available at: http://dx.doi.org/10.1016/j.cell.2015.12.037.
Rosenblatt F (1958) The perceptron: a probabilistic model for information storage and organization in the brain. Psychol Rev 65:386–408 Available at: http://www.ncbi.nlm.nih.gov/pubmed/13602029.
Rowland NC, Jaeger D (2005) Coding of tactile response properties in the rat deep cerebellar nuclei. J Neurophysiol 94:1236–1251.
Ruigrok TJH (1997) Chapter 10 Cerebellar nuclei: the olivary connection. In, pp 167–192 Available at: https://linkinghub.elsevier.com/retrieve/pii/S0079612308633646.
Ruigrok TJH (2011) Ins and outs of cerebellar modules. Cerebellum 10:464–474 Available at: http://www.pubmedcentral.nih.gov/articlerender.fcgi?artid=3169761&tool=pmcentrez&rendertype=abstract [Accessed February 3, 2015].
Ruigrok TJH, Pijpers A, Goedknegt-Sabel E, Coulon P (2008) Multiple cerebellar zones are involved in the control of individual muscles: A retrograde transneuronal tracing study with rabies virus in the rat. Eur J Neurosci 28:181–200 Available at: http://www.ncbi.nlm.nih.gov/pubmed/18662342 [Accessed October 31, 2012].
Safo P, Regehr WG (2008) Timing dependence of the induction of cerebellar LTD. Neuropharmacology 54:213–218 Available at: https://linkinghub.elsevier.com/retrieve/pii/S0028390807001724.
Sarnaik R, Raman IM (2018) Control of voluntary and optogenetically perturbed locomotion by spike rate and timing of neurons of the mouse cerebellar nuclei. Elife 7:1–31 Available at: http://www.ncbi.nlm.nih.gov/pubmed/29659351%0Ahttp://www.pubmedcentral.nih.gov/articlerender.fcgi?artid=PMC5902160.
Scelfo B, Strata P (2005) Correlation between multiple climbing fibre regression and parallel fibre response development in the postnatal mouse cerebellum. Eur J Neurosci 21:971–978 Available at: http://doi.wiley.com/10.1111/j.1460-9568.2005.03933.x.
Schmahmann JD (2019) The cerebellum and cognition. Neurosci Lett 688:62–75 Available at: https://doi.org/10.1016/j.neulet.2018.07.005.
Schmahmann JD, Pandya DN (1997) Anatomic organization of the basilar pontine projections from prefrontal cortices in rhesus monkey. J Neurosci 17:438–458.
Schonewille M, Belmeguenai A, Koekkoek SK, Houtman SH, Boele HJ, van Beugen BJ, Gao Z, Badura A, Ohtsuki G, Amerika WE, Hosy E, Hoebeek FE, Elgersma Y, Hansel C, De Zeeuw CI (2010) Purkinje Cell-Specific Knockout of the Protein Phosphatase PP2B Impairs Potentiation and Cerebellar Motor Learning. Neuron 67:618–628 Available at: http://dx.doi.org/10.1016/j.neuron.2010.07.009.
Schonewille M, Gao Z, Boele H-J, Vinueza Veloz MF, Amerika WE, Šimek AAM, De Jeu MT, Steinberg JP, Takamiya K, Hoebeek FE, Linden DJ, Huganir RL, De Zeeuw CI (2011) Reevaluating the Role of LTD in Cerebellar Motor Learning. Neuron 70:43–50 Available at: https://linkinghub.elsevier.com/retrieve/pii/S0896627311001991.
Schonewille M, Luo C, Ruigrok TJH, Voogd J, Schmolesky MT, Rutteman M, Hoebeek FE, De Jeu MTG, De Zeeuw CI (2006) Zonal organization of the mouse flocculus: Physiology, input, and output. J Comp Neurol 497:670–682 Available at: http://doi.wiley.com/10.1002/cne.21036.
Schultz SR, Kitamura K, Post-Uiterweer A, Krupic J, Hausser M (2009) Spatial Pattern Coding of Sensory Information by Climbing Fiber-Evoked Calcium Signals in Networks of Neighboring Cerebellar Purkinje Cells. J Neurosci 29:8005–8015 Available at: http://www.jneurosci.org/cgi/doi/10.1523/JNEUROSCI.4919-08.2009.
Schwartz EJ, Rothman JS, Dugue GP, Diana M, Rousseau C, Silver RA, Dieudonne S (2012) NMDA Receptors with Incomplete Mg2+ Block Enable Low-Frequency Transmission through the Cerebellar Cortex. J Neurosci 32:6878–6893 Available at:

http://www.jneurosci.org/cgi/doi/10.1523/JNEUROSCI.5736-11.2012.
Scott TG (1965) THE SPECIFICITY OF 5'-NUCLEOTIDASE IN THE BRAIN OF THE MOUSE. J Histochem Cytochem 13:657–667 Available at: http://journals.sagepub.com/doi/10.1177/13.8.657.
Sellmeijer J, Mathis V, Hugel S, Li X-H, Song Q, Chen Q-Y, Barthas F, Lutz P-E, Karatas M, Luthi A, Veinante P, Aertsen A, Barrot M, Zhuo M, Yalcin I (2018) Hyperactivity of Anterior Cingulate Cortex Areas 24a/24b Drives Chronic Pain-Induced Anxiodepressive-like Consequences. J Neurosci 38:3102–3115 Available at: http://www.jneurosci.org/lookup/doi/10.1523/JNEUROSCI.3195-17.2018.
Serapide MF, Pantó MR, Parenti R, Zappalá A, Cicirata F (2001) Multiple zonal projections of the basilar pontine nuclei to the cerebellar cortex of the rat. J Comp Neurol 430:471–484.
Sgaier SK, Millet S, Villanueva MP, Berenshteyn F, Song C, Joyner AL (2005) Morphogenetic and cellular movements that shape the mouse cerebellum: Insights from genetic fate mapping. Neuron 45:27–40.
Shambes GM, Gibson JM, Welker W (1978) Fractured Somatotopy in Granule Cell Tactile Areas of Rat Cerebellar Hemispheres Revealed by Micromapping; pp. 94–105. Brain Behav Evol 15:94–105 Available at: https://www.karger.com/Article/FullText/123774.
Shen J, Colonnese MT (2016) Development of Activity in the Mouse Visual Cortex. J Neurosci 36:12259–12275 Available at: http://www.jneurosci.org/cgi/doi/10.1523/JNEUROSCI.1903-16.2016.
Shepherd GMG (2012) Circuit Mapping by Ultraviolet Uncaging of Glutamate. Cold Spring Harb Protoc 2012:pdb.prot070664-pdb.prot070664 Available at: http://www.cshprotocols.org/cgi/doi/10.1101/pdb.prot070664.
Shibuki K, Gomi H, Chen L, Bao S, Kim JJ, Wakatsuki H, Fujisaki T, Fujimoto K, Katoh A, Ikeda T, Chen C, Thompson RF, Itohara S (1996) Deficient cerebellar long-term depression, impaired eyeblink conditioning, and normal motor coordination in GFAP mutant mice. Neuron 16:587–599.
Shik ML, Orlovsky GN (1976) Neurophysiology of locomotor automatism. Physiol Rev 56:465–501 Available at: http://www.physiology.org/doi/10.1152/physrev.1976.56.3.465.
Sierra H, Cordova M, Chen C-SJ, Rajadhyaksha M (2015) Confocal Imaging–Guided Laser Ablation of Basal Cell Carcinomas: An Ex Vivo Study. J Invest Dermatol 135:612–615 Available at: https://linkinghub.elsevier.com/retrieve/pii/S0022202X15370834.
Sillitoe R V. (2015) Mossy Fibers Terminate Directly Within Purkinje Cell Zones During Mouse Development. The Cerebellum 15:14–17 Available at: http://link.springer.com/10.1007/s12311-015-0712-6.
Sillitoe R V., Chung S-H, Fritschy J-M, Hoy M, Hawkes R (2008) Golgi Cell Dendrites Are Restricted by Purkinje Cell Stripe Boundaries in the Adult Mouse Cerebellar Cortex. J Neurosci 28:2820–2826 Available at: http://www.jneurosci.org/cgi/doi/10.1523/JNEUROSCI.4145-07.2008.
Sillitoe R V., Marzban H, Larouche M, Zahedi S, Affanni J, Hawkes R (2005) Conservation of the architecture of the anterior lobe vermis of the cerebellum across mammalian species. In: Progress in Brain Research, pp 283–297 Available at: https://linkinghub.elsevier.com/retrieve/pii/S0079612304480224.
Simat M, Parpan F, Fritschy J-M (2007) Heterogeneity of glycinergic and gabaergic interneurons in the granule cell layer of mouse cerebellum. J Comp Neurol 500:71–83 Available at: http://doi.wiley.com/10.1002/cne.21142.
Sims RE (2005) Differences in Transmission Properties and Susceptibility to Long-Term Depression Reveal Functional Specialization of Ascending Axon and Parallel Fiber Synapses to Purkinje Cells. J Neurosci 25:3246–3257 Available at: http://www.jneurosci.org/cgi/doi/10.1523/JNEUROSCI.0073-05.2005.
Sotelo C (2004) Cellular and genetic regulation of the development of the cerebellar system. Prog Neurobiol 72:295–339.
Sotelo C, Bourrat F, Triller A (1984) Postnatal development of the inferior olivary complex in

the rat. II. Topographic organization of the immature olivocerebellar projection. J Comp Neurol 222:177–199.
Sotelo C, Llinas R, Baker R (1974) Structural study of inferior olivary nucleus of the cat: morphological correlates of electrotonic coupling. J Neurophysiol 37:541–559.
Stecina K, Fedirchuk B, Hultborn H (2013) Information to cerebellum on spinal motor networks mediated by the dorsal spinocerebellar tract. J Physiol 591:5433–5443.
Steuber V, Jaeger D (2013) Modeling the generation of output by the cerebellar nuclei. Neural Networks 47:112–119 Available at: https://linkinghub.elsevier.com/retrieve/pii/S0893608012002833.
Sugihara I, Bailly Y, Mariani J (2000) Olivocerebellar Climbing Fibers in the Granuloprival Cerebellum: Morphological Study of Individual Axonal Projections in the X-Irradiated Rat. J Neurosci 20:3745–3760 Available at: http://www.jneurosci.org/lookup/doi/10.1523/JNEUROSCI.20-10-03745.2000.
Sugihara I, Quy PN (2007) Identification of aldolase C compartments in the mouse cerebellar cortex by olivocerebellar labeling. J Comp Neurol 500:1076–1092 Available at: http://onlinelibrary.wiley.com/doi/10.1002/cne.21219/full [Accessed November 21, 2014].
Sugihara I, Shinoda Y (2004) Molecular, topographic, and functional organization of the cerebellar cortex: a study with combined aldolase C and olivocerebellar labeling. J Neurosci 24:8771–8785 Available at: http://www.ncbi.nlm.nih.gov/pubmed/15470143 [Accessed March 25, 2015].
Sultan F, Bower JM (1998) Quantitative Golgi study of the rat cerebellar molecular layer interneurons using principal component analysis. J Comp Neurol 393:353–373 Available at: http://doi.wiley.com/10.1002/%28SICI%291096-9861%2819980413%29393%3A3%3C353%3A%3AAID-CNE7%3E3.0.CO%3B2-0.
Suvrathan A, Payne HL, Raymond JL (2016) Timing Rules for Synaptic Plasticity Matched to Behavioral Function. Neuron:1–9 Available at: http://linkinghub.elsevier.com/retrieve/pii/S0896627316307231.
Szapiro G, Barbour B (2007) Multiple climbing fibers signal to molecular layer interneurons exclusively via glutamate spillover. Nat Neurosci 10:735–742 Available at: http://www.nature.com/articles/nn1907.
Tadayonnejad R, Anderson D, Molineux ML, Mehaffey WH, Jayasuriya K, Turner RW (2010) Rebound Discharge in Deep Cerebellar Nuclear Neurons In Vitro. The Cerebellum 9:352–374 Available at: http://www.pubmedcentral.nih.gov/articlerender.fcgi?artid=2949560&tool=pmcentrez&rendertype=abstract [Accessed June 24, 2013].
Takahashi M, Sugiuchi Y, Shinoda Y (2014) Convergent synaptic inputs from the caudal fastigial nucleus and the superior colliculus onto pontine and pontomedullary reticulospinal neurons. J Neurophysiol 111:849–867 Available at: http://www.physiology.org/doi/10.1152/jn.00634.2013.
Takakusaki K (2017) Functional Neuroanatomy for Posture and Gait Control. J Mov Disord 10:1–17 Available at: http://e-jmd.org/journal/view.php?doi=10.14802/jmd.16062.
Takakusaki K, Chiba R, Nozu T, Okumura T (2016) Brainstem control of locomotion and muscle tone with special reference to the role of the mesopontine tegmentum and medullary reticulospinal systems. J Neural Transm 123:695–729.
Takechi H, Eilers J, Konnerth A (1998) A new class of synaptic response involving calcium release in dendritic spines. Nature 396:757–760 Available at: http://www.nature.com/articles/25547.
Tan J, Epema AH, Voogd J (1995) Zonal organization of the flocculovestibular nucleus projection in the rabbit: A combined axonal tracing and acetylcholinesterase histochemical study. J Comp Neurol 356:51–71 Available at: http://doi.wiley.com/10.1002/cne.903560104.
Teune TM, van der Burg J, van der Moer J, Voogd J, Ruigrok TJH (2000) Topography of cerebellar nuclear projections to the brain stem in the rat. In, pp 141–172 Available at: https://linkinghub.elsevier.com/retrieve/pii/S0079612300240144.

Thach WT (1968) Discharge of Purkinje and cerebellar nuclear neurons during rapidly alternating arm movements in the monkey. J Neurophysiol 31:785–797 Available at: http://www.physiology.org/doi/10.1152/jn.1968.31.5.785.
Thach WT, Goodkin HP, Keating JG (1992) The cerebellum and the adaptive coordination of movement. Annu Rev Neurosci 15:403–442 Available at: http://www.ncbi.nlm.nih.gov/pubmed/1575449 [Accessed February 2, 2015].
Toth LA, Kregel K, Leon L, Musch TI (2011) Environmental enrichment in laboratory rodents. Comp Med 61:314–321.
Tran-Van-Minh A, Abrahamsson T, Cathala L, DiGregorio DA (2016) Differential Dendritic Integration of Synaptic Potentials and Calcium in Cerebellar Interneurons. Neuron 91:837–850 Available at: http://linkinghub.elsevier.com/retrieve/pii/S0896627316304147.
Trott JR, Apps R, Armstrong DM (1998a) Zonal organization of cortico-nuclear and nucleo-cortical projections of the paramedian lobule of the cat cerebellum. 2. The C 2 zone. Exp Brain Res 118:316–330 Available at: http://link.springer.com/10.1007/s002210050286.
Trott JR, Apps R, Armstrong DM (1998b) Zonal organization of cortico-nuclear and nucleo-cortical projections of the paramedian lobule of the cat cerebellum. 1. The C 1 zone. Exp Brain Res 118:298–315 Available at: http://link.springer.com/10.1007/s002210050286.
Tsai S-F, Liu Y-W, Kuo Y-M (2019) Acute and long-term treadmill running differentially induce c-Fos expression in region- and time-dependent manners in mouse brain. Brain Struct Funct Available at: http://link.springer.com/10.1007/s00429-019-01926-5.
Tsujimoto T, Gemba H, Sasaki K (1993) Effect of cooling the dentate nucleus of the cerebellum on hand movement of the monkey. Brain Res 629:1–9 Available at: http://linkinghub.elsevier.com/retrieve/pii/000689939390473Z.
Tsutsumi S, Yamazaki M, Miyazaki T, Watanabe M, Sakimura K, Kano M, Kitamura K (2015) Structure–Function Relationships between Aldolase C/Zebrin II Expression and Complex Spike Synchrony in the Cerebellum. J Neurosci 35:843–852 Available at: http://www.jneurosci.org/cgi/doi/10.1523/JNEUROSCI.2170-14.2015.
Uusisaari M, De Schutter E (2011) The mysterious microcircuitry of the cerebellar nuclei. J Physiol 589:3441–3457 Available at: http://doi.wiley.com/10.1113/jphysiol.2010.201582.
Uusisaari M, Knöpfel T (2008) GABAergic synaptic communication in the GABAergic and non-GABAergic cells in the deep cerebellar nuclei. Neuroscience 156:537–549 Available at: http://www.ncbi.nlm.nih.gov/pubmed/18755250 [Accessed September 27, 2011].
Uusisaari M, Knöpfel T (2011) Functional Classification of Neurons in the Mouse Lateral Cerebellar Nuclei. The Cerebellum 10:637–646 Available at: http://www.pubmedcentral.nih.gov/articlerender.fcgi?artid=3215887&tool=pmcentrez&rendertype=abstract [Accessed April 5, 2013].
Uusisaari M, Obata K, Knöpfel T (2007) Morphological and Electrophysiological Properties of GABAergic and Non-GABAergic Cells in the Deep Cerebellar Nuclei. J Neurophysiol 97:901–911 Available at: http://www.physiology.org/doi/10.1152/jn.00974.2006.
Valera AM, Binda F, Pawlowski SA, Dupont J-L, Casella J-F, Rothstein JD, Poulain B, Isope P (2016) Stereotyped spatial patterns of functional synaptic connectivity in the cerebellar cortex. Elife 5:1–22 Available at: http://elifesciences.org/lookup/doi/10.7554/eLife.09862.
Valera AM, Doussau F, Poulain B, Barbour B, Isope P (2012) Adaptation of Granule Cell to Purkinje Cell Synapses to High-Frequency Transmission. J Neurosci 32:3267–3280 Available at: http://www.jneurosci.org/content/32/9/3267.
Van Der Giessen RS, Maxeiner S, French PJ, Willecke K, De Zeeuw CI (2006) Spatiotemporal distribution of Connexin45 in the olivocerebellar system. J Comp Neurol 495:173–184 Available at: http://doi.wiley.com/10.1002/cne.20873.
van der Want JJL, Wiklund L, Guegan M, Ruigrok T, Voogd J (1989) Anterograde tracing of

the rat olivocerebellar system with phaseolus vulgaris leucoagglutinin (PHA-L). Demonstration of climbing fiber collateral innervation of the cerebellar nuclei. J Comp Neurol 288:1–18 Available at: http://doi.wiley.com/10.1002/cne.902880102.
Vincent P, Marty A (1996) Fluctuations of inhibitory postsynaptic currents in Purkinje cells from rat cerebellar slices. J Physiol 494:183–199 Available at: http://doi.wiley.com/10.1113/jphysiol.1996.sp021484.
Voogd J (1967) Comparative Aspects of the Structure and Fibre Connexions of the Mammalian Cerebellum. In, pp 94–134 Available at: https://linkinghub.elsevier.com/retrieve/pii/S0079612308609632.
Voogd J (2011) Cerebellar Zones: A Personal History. The Cerebellum 10:334–350 Available at: http://link.springer.com/10.1007/s12311-010-0221-6.
Voogd J (2016) Deiters' Nucleus. Its Role in Cerebellar Ideogenesis. The Cerebellum 15:54–66 Available at: http://link.springer.com/10.1007/s12311-015-0681-9.
Voogd J, Broere G, van Rossum J (1969) The medio-lateral distribution of the spinocerebellar projection in the anterior lobe and the simple lobule in the cat and a comparison with some other afferent fibre systems. Psychiatr Neurol Neurochir 72:137–151 Available at: http://www.ncbi.nlm.nih.gov/pubmed/5250288.
VOOGD J, GERRITS NM, RUIGROK TJH (1996) Organization of the Vestibulocerebellum. Ann N Y Acad Sci 781:553–579 Available at: http://doi.wiley.com/10.1111/j.1749-6632.1996.tb15728.x.
Voogd J, Glickstein M (1998) The anatomy of the cerebellum. Trends Neurosci 21:370–375 Available at: http://www.ncbi.nlm.nih.gov/pubmed/9735944.
Voogd J, Pardoe J, Ruigrok TJH, Apps R (2003) The Distribution of Climbing and Mossy Fiber Collateral Branches from the Copula Pyramidis and the Paramedian Lobule: Congruence of Climbing Fiber Cortical Zones and the Pattern of Zebrin Banding within the Rat Cerebellum. J Neurosci 23:4645–4656 Available at: http://www.ncbi.nlm.nih.gov/pubmed/12805304 [Accessed March 25, 2015].
Voogd J, Ruigrok TJH (2004) The organization of the corticonuclear and olivocerebellar climbing fiber projections to the rat cerebellar vermis: the congruence of projection zones and the zebrin pattern. J Neurocytol 33:5–21 Available at: http://www.ncbi.nlm.nih.gov/pubmed/15173629.
Voogd J, Ruigrok TJH (2012) Cerebellum and Precerebellar Nuclei. In: The Human Nervous System, Third Edit., pp 471–545. Elsevier. Available at: http://dx.doi.org/10.1016/B978-0-12-374236-0.10015-X.
Wadiche JI, Jahr CE (2005) Patterned expression of Purkinje cell glutamate transporters controls synaptic plasticity. Nat Neurosci 8:1329–1334 Available at: http://www.nature.com/articles/nn1539.
Wagner MJ, Kim TH, Kadmon J, Nguyen ND, Ganguli S, Schnitzer MJ, Luo L (2019) Shared Cortex-Cerebellum Dynamics in the Execution and Learning of a Motor Task. Cell 177:669-682.e24 Available at: https://doi.org/10.1016/j.cell.2019.02.019.
Wagner MJ, Kim TH, Savall J, Schnitzer MJ, Luo L (2017) Cerebellar granule cells encode the expectation of reward. Nature 544:96–100 Available at: http://dx.doi.org/10.1038/nature21726.
Walter JT, Alviña K, Womack MD, Chevez C, Khodakhah K (2006) Decreases in the precision of Purkinje cell pacemaking cause cerebellar dysfunction and ataxia. Nat Neurosci 9:389–397 Available at: http://www.nature.com/articles/nn1648.
Walter JT, Dizon M-J, Khodakhah K (2009) The Functional Equivalence of Ascending and Parallel Fiber Inputs in Cerebellar Computation. J Neurosci 29:8462–8473 Available at: http://www.ncbi.nlm.nih.gov/pubmed/19571137 [Accessed October 16, 2013].
Wang SS-H, Denk W, Häusser M (2000) Coincidence detection in single dendritic spines mediated by calcium release. Nat Neurosci 3:1266–1273 Available at: http://www.ncbi.nlm.nih.gov/pubmed/11100147 [Accessed December 9, 2012].
Wang SS-H, Kloth AD, Badura A (2014) The Cerebellum, Sensitive Periods, and Autism. Neuron 83:518–532 Available at: http://dx.doi.org/10.1016/j.neuron.2014.07.016.
Wang X, Chen G, Gao W, Ebner TJ (2011) Parasagittally aligned, mGluR 1 -dependent

patches are evoked at long latencies by parallel fiber stimulation in the mouse cerebellar cortex in vivo. J Neurophysiol 105:1732–1746 Available at: http://www.physiology.org/doi/10.1152/jn.00717.2010.
Wang YT, Linden DJ (2000) Expression of Cerebellar Long-Term Depression Requires Postsynaptic Clathrin-Mediated Endocytosis. Neuron 25:635–647 Available at: https://linkinghub.elsevier.com/retrieve/pii/S0896627300810661.
Witter L, Rudolph S, Pressler RT, Lahlaf SI, Regehr WG (2016) Purkinje Cell Collaterals Enable Output Signals from the Cerebellar Cortex to Feed Back to Purkinje Cells and Interneurons. Neuron 91:312–319 Available at: http://dx.doi.org/10.1016/j.neuron.2016.05.037.
Wolpert DM, Miall RC, Kawato M (1998) Internal models in the cerebellum. Trends Cogn Sci 2:338–347 Available at: http://www.ncbi.nlm.nih.gov/pubmed/21227230 [Accessed January 29, 2014].
Wu HS, Sugihara I, Shinoda Y (1999) Projection patterns of single mossy fibers originating from the lateral reticular nucleus in the rat cerebellar cortex and nuclei. J Comp Neurol 411:97–118 Available at: http://www.ncbi.nlm.nih.gov/pubmed/10404110 [Accessed September 24, 2013].
Wulff P, Schonewille M, Renzi M, Viltono L, Sassoè-Pognetto M, Badura A, Gao Z, Hoebeek FE, van Dorp S, Wisden W, Farrant M, De Zeeuw CI (2009) Synaptic inhibition of Purkinje cells mediates consolidation of vestibulo-cerebellar motor learning. Nat Neurosci 12:1042–1049 Available at: http://www.nature.com/articles/nn.2348.
Xiao J, Cerminara NL, Kotsurovskyy Y, Aoki H, Burroughs A, Wise AK, Luo Y, Marshall SP, Sugihara I, Apps R, Lang EJ (2014) Systematic Regional Variations in Purkinje Cell Spiking Patterns Chédotal A, ed. PLoS One 9:e105633 Available at: https://dx.plos.org/10.1371/journal.pone.0105633.
Xiao L, Scheiffele P (2018) Local and long-range circuit elements for cerebellar function. Curr Opin Neurobiol 48:146–152 Available at: http://dx.doi.org/10.1016/j.conb.2017.12.016.
Yaginuma H, Matsushita M (1989) Spinocerebellar projections from the upper lumbar segments in the cat, as studied by anterograde transport of wheat germ agglutinin-horseradish peroxidase. J Comp Neurol 281:298–319 Available at: http://doi.wiley.com/10.1002/cne.902810211.
Yalcin I, Bohren Y, Waltisperger E, Sage-Ciocca D, Yin JC, Freund-Mercier M-J, Barrot M (2011) A Time-Dependent History of Mood Disorders in a Murine Model of Neuropathic Pain. Biol Psychiatry 70:946–953 Available at: http://dx.doi.org/10.1016/j.biopsych.2011.07.017.
Yalcin I, Megat S, Barthas F, Waltisperger E, Kremer M, Salvat E, Barrot M (2014) The sciatic nerve cuffing model of neuropathic pain in mice. J Vis Exp:1–7 Available at: http://www.jove.com/video/51608/the-sciatic-nerve-cuffing-model-of-neuropathic-pain-in-mice.
Yamaguchi K, Itohara S, Ito M (2016) Reassessment of long-term depression in cerebellar Purkinje cells in mice carrying mutated GluA2 C terminus. Proc Natl Acad Sci 113:10192–10197 Available at: http://www.pnas.org/lookup/doi/10.1073/pnas.1609957113.
Yamazaki T, Lennon W (2019) Revisiting a theory of cerebellar cortex. Neurosci Res Available at: https://www.sciencedirect.com/science/article/pii/S0168010218305091?dgcid=rss_sd_all.
YEO CH (1991) Cerebellum and Classical Conditioning of Motor Responses. Ann N Y Acad Sci 627:292–304 Available at: http://doi.wiley.com/10.1111/j.1365-2214.2007.00793.x.
Yeo CH, Hesslow G (1998) Cerebellum and conditioned reflexes. Trends Cogn Sci 2:322–330 Available at: https://linkinghub.elsevier.com/retrieve/pii/S1364661398012194.
Zheng N, Raman IM (2010) Synaptic Inhibition, Excitation, and Plasticity in Neurons of the Cerebellar Nuclei. The Cerebellum 9:56–66 Available at: http://link.springer.com/10.1007/s12311-009-0140-6.

Zhou H, Lin Z, Voges K, Ju C, Gao Z, Bosman LW, Ruigrok TJ, Hoebeek FE, De Zeeuw CI, Schonewille M (2014) Cerebellar modules operate at different frequencies. Elife 3:e02536 Available at: http://www.pubmedcentral.nih.gov/articlerender.fcgi?artid=4049173&tool=pmcentrez&rendertype=abstract [Accessed October 15, 2014].

APPENDIX

List of content:

1. Tables

manip	condition	P2mCL	P2mCM	P2pC	P1mCL	P1mCM	P1p	P1mIM	P1mIL	P2pI	P2mIM	P2mIL
T_140416(	WT	0	45,61815	23,00323	44,72588	31,24869	57,83693	40,70453	58,95202	30,87092	47,50808	0
T_310516(	WT	12,36963	41,63635	18,44826	15,33322	24,53473	12,93899	21,72982	14,61822	25,57277	25,57401	13,13324
T_070616(	WT	8,248772	50,71411	24,78798	16,24976	26,00887	30,376	34,88716	55,64007	53,2223	61,53458	27,00975
T_070616(	WT	42,75564	45,91796	34,94596	32,19757	25,82301	15,8274	76,7942	31,70618	8,96579	8,543561	7,182732
T_080616(	WT	24,20203	10,80292	9,444646	31,06186	82,54312	184,3089	195,8725	67,48258	36,60961	23,65841	9,762812
T_090616(	WT	44,14944	22,49591	23,01321	18,20324	63,94694	0	125,8636	27,45155	14,73876	17,43779	8,064424
T_181116(	WT	14,42637	18,31448	18,17595	33,58506	87,98848	48,23537	25,53158	34,01544	23,73449	29,14984	27,1347
T_140416(	WT	24,35291	22,97542	10,2348	24,54893	21,41222	26,06787	40,23773	24,58563	26,44254	39,64507	16,2336
T_080616(	WT	0	34,78473	58,56126	68,54983	31,35128	17,06884	47,93377	45,66518	20,40413	43,96408	44,79941
T_090616(	WT	12,61021	9,880944	32,30211	9,284591	33,22321	49,77799	25,10409	16,36189	13,22288	11,42654	8,810474
160517(3)	ENR	22,68594	14,53029	28,65274	23,42841	13,85793	31,49638	72,97692	32,50712	13,60773	15,47248	10,54079
170517(1)	ENR	0	11,91167	13,04971	9,193057	12,72586	127,2404	69,5007	40,6523	11,28359	12,62019	11,12054
180517(3)	ENR	0	7,005968	26,70118	15,94688	8,824002	8,979089	56,71987	13,48865	6,5681	24,48514	12,94093
190517(2)	ENR	8,414612	12,33582	21,85464	71,33195	90,41774	0	107,124	45,9871	15,32362	7,57633	6,844119
210319(2)	ENR	4,227185	7,40841	13,07818	57,81159	46,37214	135,3006	74,16801	32,84812	14,8802	19,23024	12,00335
190517(1)	ENR	0	72,70534	47,76148	22,55117	91,21081	169,1722	402,241	92,79594	116,8129	55,90227	17,75639
220319(2)	ENR	0	29,90438	37,65346	55,56331	18,78911	22,88584	22,20478	66,51127	72,66886	38,01663	65,89472
160517(2)	ENR	0	8,924148	63,48727	22,34223	36,17232	57,40226	42,91496	54,52854	21,16441	10,34054	0
180517(1)	ENR	0	44,52158	134,3801	64,59746	124,4489	127,3851	299,3481	85,35762	122,8503	90,96623	55,50704
230319(2)	ENR	20,74748	24,79596	95,12176	65,33714	149,0172	95,62654	152,6903	68,13407	27,20837	57,44703	27,29304
90318-A2(	CUFF_1_MONTH	0	39,36594	72,39265	39,77157	63,22006	62,88506	154,209	123,644	92,82665	63,56696	21,438
10318-A3(	CUFF_1_MONTH	0	15,44132	42,10812	41,34307	43,02692	151,0745	163,2538	96,28735	45,60831	61,03182	17,12351
50318-D2(	CUFF_1_MONTH	0	21,31786	17,02684	17,45654	67,65067	70,97018	129,2794	26,51488	39,68486	26,54751	0
70218-D3(	CUFF_1_MONTH	0	22,56063	18,25682	42,67063	66,58156	24,22154	79,06713	60,44271	21,27671	11,25059	8,292115
80218-D4(	CUFF_1_MONTH	0	14,92294	7,966077	19,70126	23,24911	54,55948	185,0207	128,1474	42,70328	21,2583	9,676442
80318-B1(	CUFF_1_MONTH	0	55,79319	19,92307	34,18509	58,21216	54,31382	64,73617	78,95151	64,04708	46,70878	29,15801
00318-B3(	CUFF_1_MONTH	0	11,36819	21,31721	59,5183	67,95324	44,91217	195,7561	79,39903	84,95474	48,95769	32,76051
70318-B4(	CUFF_1_MONTH	11,67907	21,65265	40,39137	66,64997	65,41385	123,1641	150,9939	78,85225	54,63075	38,04039	0
70218-D3(	CUFF_1_MONTH	0	24,65966	11,13677	22,30827	40,92392	14,62544	48,78257	48,10389	27,07767	15,91034	15,96196
10318-A3(	CUFF_1_MONTH	49,73975	78,25105	92,59798	74,41432	200,8405	171,3413	218,9427	172,2341	179,9289	71,95125	20,8008
90318-B2(	CUFF_1_MONTH	0	0	37,05592	26,88129	44,45731	27,33719	32,56939	80,65094	38,43133	41,54664	33,33719
50318-D2(	CUFF_1_MONTH	0	19,76498	49,38855	28,81797	57,67856	111,4501	92,71851	21,9499	31,12119	19,35618	22,61119
80218-D4(	CUFF_1_MONTH	0	19,67871	45,64342	56,25371	67,39261	116,6797	163,2707	152,6363	59,40785	67,60486	48,73888
80318-B1(	CUFF_1_MONTH	0	20,76363	30,63115	46,89796	46,79084	74,65657	115,1956	65,17158	34,73051	24,16913	0
70318-B4(	CUFF_1_MONTH	38,02288	40,37096	233,161	95,65006	163,1307	70,2107	259,6239	136,8	48,60257	67,33859	29,68343
50318-D2(	CUFF_1_MONTH	0	18,64436	42,81439	65,72234	47,71877	63,63898	130,9569	65,80846	66,09493	30,78962	17,3153
00318-A1(	SHAM_1_MONTH	0	9,719434	11,65875	16,62772	18,31077	22,41101	12,29847	56,51457	12,55923	12,28492	11,9545
20318-C1(	SHAM_1_MONTH	0	12,75967	10,36994	22,67345	22,02869	18,26359	14,35265	19,38628	42,15411	27,75559	11,17522
30318-C3(	SHAM_1_MONTH	0	21,66226	52,29501	32,02354	22,42221	13,80728	17,98732	61,04421	12,29136	19,78918	16,8786
60218-D5(	SHAM_1_MONTH	0	57,67923	30,65977	67,10955	81,20422	106,2383	130,1019	74,1905	70,68142	46,89133	74,20411
00318-A1(	SHAM_1_MONTH	0	9,775462	11,48069	34,23933	20,25572	13,56705	53,40247	91,35208	18,45352	31,91704	16,98963
10318-C2(	SHAM_1_MONTH	0	16,07415	17,02493	10,40054	16,914	56,8878	34,9077	52,35138	41,34659	34,67646	11,98282
10318-C4(	SHAM_1_MONTH	0	22,87571	13,76286	54,81402	42,3624	11,25339	60,27877	27,00412	23,62238	23,70607	0
60218-D5(	SHAM_1_MONTH	9,624268	15,88357	31,0701	82,52511	125,9962	90,29393	162,1209	38,89941	14,21439	11,54945	11,85682
20318-C1(	SHAM_1_MONTH	0	19,06386	20,72683	39,68798	24,89023	79,3358	41,84392	26,02519	14,50744	20,93306	27,601
ff_181016	CUFF_15_DAYS	0	55,6572	59,56146	52,67458	97,83443	30,27243	50,52254	69,24433	90,66617	44,43312	79,81971
ff_201016	CUFF_15_DAYS	0	0	30,91478	17,29651	20,94215	37,40399	46,22166	41,29528	59,69013	20,27791	48,26353
ff_080617	CUFF_15_DAYS	0	11,41961	75,55007	72,2526	114,3552	60,18257	113,5979	70,13844	79,35884	11,98072	0
ff_120717	CUFF_15_DAYS	14,92598	8,562909	16,68739	39,75312	58,70264	36,03653	61,47686	18,01671	60,37441	12,03627	9,886491
ff_120717	CUFF_15_DAYS	8,299745	10,85566	12,21507	6,393485	14,7307	12,84034	24,55818	15,67266	19,68236	32,30202	16,42088
ff_130717	CUFF_15_DAYS	0	25,2372	57,02168	63,28726	106,8818	162,0075	92,62757	121,1077	92,95334	55,29312	43,32064
ff_171016	CUFF_15_DAYS	0	0	126,6251	46,15407	109,7935	204,8147	71,84284	100,0994	185,9052	65,05173	18,49765
ff_161016	CUFF_15_DAYS	0	0	135,6224	71,67877	50,12489	125,2742	412,7938	162,4377	110,6503	166,6849	81,60622
ff_181016	CUFF_15_DAYS	16,47509	15,06933	9,413092	48,75792	31,08314	45,44512	32,55068	36,36452	25,67589	40,91766	32,21327
ff_181016	CUFF_15_DAYS	0	0	84,26337	88,88111	43,99759	16,97135	26,10338	133,6805	110,419	40,34793	50,88843
ff_110717	CUFF_15_DAYS	0	15,69179	13,65074	36,01909	81,86061	32,79157	101,2348	154,4577	133,9885	18,75429	12,66207
ff_141016	CUFF_15_DAYS	0	0	7,688223	11,40274	32,27869	36,08212	19,5989	37,46389	49,44898	13,35468	13,45298
ff_141016	CUFF_15_DAYS	71,8394	46,86276	114,3314	22,09153	17,97711	39,11797	92,08878	60,61247	16,89676	46,21983	40,52048
ff_161016	CUFF_15_DAYS	0	0	34,42428	46,78024	46,14538	75,80812	65,52877	7,13914	22,4156	10,92919	9,53181
ff_080717	CUFF_15_DAYS	0	12,4679	14,76981	18,62237	27,56101	38,8327	27,19695	29,52713	61,69944	64,41745	29,60897
ff_090717	CUFF_15_DAYS	0	23,04861	21,07374	15,00758	19,6105	30,91989	67,35632	44,1795	13,16223	18,37061	7,484346
ff_201016	CUFF_15_DAYS	0	0	7,190762	30,06568	126,3627	194,3236	265,0943	99,04282	61,01334	51,15767	48,90068
ff_191016	CUFF_15_DAYS	0	0	10,46625	18,06117	36,96303	91,94241	133,269	52,49664	11,49915	30,68597	11,54231
ff_211016	CUFF_15_DAYS	0	0	13,47426	38,07437	23,81317	44,45268	17,55671	16,27279	19,55041	37,21519	0
ff_171016	CUFF_15_DAYS	0	0	32,90645	26,66928	57,11583	49,06667	66,83803	28,7579	24,52139	10,40446	12,69186
ff_191016	CUFF_15_DAYS	8,960329	7,874565	10,64787	16,75085	24,21958	56,22086	122,1164	50,78114	27,36853	26,59199	22,82162
ff_211016	CUFF_15_DAYS	0	0	15,06282	12,66844	9,342607	31,1836	16,98922	31,00733	12,54562	13,43258	15,91525
ff_070717	CUFF_15_DAYS	0	6,669228	28,20095	33,25202	47,51775	64,28337	117,3816	74,89982	9,321533	5,961397	0
ff_110717	CUFF_15_DAYS	11,44571	25,31594	47,38406	44,34946	89,06677	62,88138	344,7971	37,91738	65,23332	73,36614	64,20931
ff_130717	CUFF_15_DAYS	0	20,72634	39,87847	60,19449	72,22299	123,7155	183,6721	54,96998	61,58345	30,75606	0
am_030617	SHAM_15_DAYS	0	7,877542	11,77598	17,23595	17,06559	17,27497	26,86875	38,38822	25,65964	48,26901	14,62706
am_030617	SHAM_15_DAYS	0	17,8539	15,92355	20,81735	28,12589	10,54126	20,09649	34,0244	27,81204	20,95424	0
am_040617	SHAM_15_DAYS	0	15,9758	27,45316	24,3112	62,59701	125,6559	94,95799	63,31818	40,38675	16,30061	0
am_040617	SHAM_15_DAYS	0	0	0	19,1704	28,9014	115,0932	94,42756	91,55768	22,09192	29,09624	60,67652
am_050617	SHAM_15_DAYS	0	0	0	28,3031	15,89214	47,17758	222,3694	112,015	40,08009	38,49005	10,08708
am_050617	SHAM_15_DAYS	0	12,43472	11,7108	22,94332	27,05695	34,18887	57,7694	74,36767	18,25878	24,28978	0
am_030617	SHAM_15_DAYS	0	15,94559	20,6541	13,92098	18,82531	16,3658	72,99046	57,9001	18,62018	13,57415	12,14966
am_050617	SHAM_15_DAYS	0	9,969262	28,32888	16,44808	38,77075	66,27326	94,25122	104,9829	31,74775	30,19776	0

Table 1 : Average synaptic amplitudes per Zebrin band

	P2m_contra_	P2m_contra_	P2p_contra	P1m_contra_	P1m_contra_	P1p	P1m_ipsi_me	P1m_ipsi_la	P2p_ipsi	P2m_ipsi_me	P2m_ipsi_lat
PC1	0.0163686	0.0487832	0.205869	0.104536	0.260366	0.340015	0.787659	0.24439	0.225622	0.156874	0.0706532
PC2	0.016259	0.0809517	0.384447	0.19495	0.333339	0.17036	-0.575492	0.312435	0.466549	0.102271	0.101498
PC3	0.0774374	0.0965331	0.377419	0.123396	-0.0580027	-0.854608	0.171028	0.142179	0.0231862	0.158883	0.134334
PC4	0.178754	0.0961232	0.366735	0.193853	0.541291	0.0193645	0.00623887	-0.56398	-0.340357	-0.199526	-0.139935
PC5	-0.0388176	0.099368	-0.580273	0.0798936	0.518341	-0.324844	0.0661532	0.146447	0.283039	-0.345826	-0.213962
PC6	0.0460748	-0.191243	0.16703	0.0925887	0.0287559	0.0497198	-0.0395236	0.660781	-0.539757	-0.287523	-0.330577
PC7	0.149121	0.0991052	0.31367	-0.483352	-0.191768	-0.023017	0.0611856	-0.0788183	0.378912	-0.212314	-0.632453
PC8	0.41074	0.755556	-0.129675	-0.315484	0.0604972	0.0749725	-0.0594581	0.190259	-0.237541	0.110485	0.162101
PC9	0.0969771	-0.469324	0.053621	-0.697367	0.386155	-0.0858179	-0.0202163	0.058889	-0.0625598	0.0214426	0.340959
PC10	0.0384757	0.0898949	0.156476	0.0320185	-0.224004	0.0517108	0.0740494	0.00385765	0.13715	-0.798943	0.499381
PC11	0.869423	-0.3417	-0.160261	0.250537	-0.124492	0.0212269	0.00104708	-0.018682	0.144263	0.038941	-0.00672809

Table 2 : Correlation indexes of variables in principal components

condition	P2-contra / P2+ipsi	P1-ipsi / P2-ipsi	P1- ipsi / P1- contra	P1-contra / P2-ipsi
WT	0,73	0,75	-0,07	-0,19
ENR	0,88	0,83	0,84	0,89
LATE_CUFF	-0,15	-0,19	0,61	0,8
LATE_SHAM	0,64	0,24	0,24	0,1

Table 3 : Correlation indexes between synaptic amplitudes coming from distant microzones

Map	Condition	B_contra	Ax_Contra	A_lat_contr	_med_cont	A_med_ips	A_lat_ipsi	Ax_ipsi	B_ipsi
WT_070616(1)	WT	-1,159185	-0,825899	-0,7895	-1,06955	-1,643292	-2,104158	-1,981573	-1,009393
WT_070616(2)	WT	-2,038823	-2,80369	-1,202231	-1,619396	-2,456972	-1,028789	-0,664814	-0,647655
WT_080616(1)	WT	-1,335649	-2,791627	-1,982614	-0,649557	-2,040169	-0,877842	-1,442936	-0,982113
WT_080616(2)	WT	-0,699434	-0,68988	-1,431556	-3,220062	-2,35161	-1,076288	-0,508311	-0,492127
WT_090616(1)	WT	-1,355687	-1,005377	-1,307448	-2,987168	-1,5243	-1,315268	-1,383052	-1,093925
WT_090616(2)	WT	-0,870636	-0,827792	-0,706195	-2,386658	-3,920425	-0,851763	-1,100918	-0,730594
WT_140416(1)	WT	-1,220493	-0,758108	-1,168905	-1,033098	-0,981415	-2,422812	-1,046661	-1,408948
WT_140416(2)	WT	-1,092352	-1,016794	-1,62518	-2,353572	-2,0384	-1,686846	-1,711649	-2,117123
WT_161116(1)	WT	nan	nan	nan	nan	-1,816873	-2,13939	-1,369458	-1,019193
WT_171116(1)	WT	nan	nan	nan	-1,50606	-1,719482	-1,366171	-0,408425	-0,68937
WT_181116(1)	WT	nan	nan	-1,316083	-3,058264	-1,495147	-1,309353	-0,835916	-0,775093
WT_181116(2)	WT	nan	nan	-1,71354	-2,351677	-1,469126	-1,241883	-1,228494	-1,004897
WT_250516(1)	WT	nan	nan	-1,065961	-1,748834	-1,76539	-2,103102	-0,739053	-0,759189
WT_310516(1)	WT	-1,975178	-2,402356	-1,303843	-1,7626	-1,710455	-1,316459	-2,357017	-1,535027
Sham_020617(1)	SHAM15	-0,60596	-0,711742	-0,80887	-1,660505	-1,503505	nan	nan	nan
Sham_030617(1)	SHAM15	-1,013614	-0,626657	-1,125784	-1,078478	-3,579028	-1,801328	-0,876128	-0,864619
Sham_030617(2)	SHAM15	-0,841931	-0,767073	-1,336914	-1,228867	-1,731097	-2,136677	-3,942765	-2,332556
Sham_030617(3)	SHAM15	-1,331673	-1,670783	-1,544823	-1,665041	-1,72438	-2,127593	-1,342782	-1,503037
Sham_050617(1)	SHAM15	-0,622789	-0,80193	-0,530888	-1,232618	-2,443683	-2,079343	-0,926375	-0,78694
Sham_050617(2)	SHAM15	-0,40157	-0,891769	-0,518052	-3,058066	-2,60989	-1,134947	-1,614142	-0,354161
Sham_050617(3)	SHAM15	-0,644558	-0,874249	-1,174515	-1,259413	-2,164422	-2,222164	-1,115249	-0,972623
010318-C2(1)	SHAM1	nan	nan	nan	-2,05191	-1,392504	-1,238801	-1,104531	-0,961606
010318-C2(2)	SHAM1	-0,872838	-1,021386	-0,77269	-1,663672	-1,980636	-2,101034	-1,800347	-1,377635
200318-A1(1)	SHAM1	-0,83193	-1,50258	-1,641034	-0,874608	-3,39321	-1,901641	-1,044374	-1,430193
210318-C4(1)	SHAM1	nan	nan	nan	-1,305909	-1,456736	-1,70921	-1,033292	-0,716157
210318-C4(2)	SHAM1	-1,219962	-2,011259	-2,494009	-1,187442	-1,703114	-1,12685	-1,280715	-1,146008
220318-C1(1)	SHAM1	-1,43101	-2,56756	-0,950213	-2,259405	-1,222274	-1,312309	-1,20611	-1,117395
220318-C1(2)	SHAM1	-1,049064	-2,024541	-1,259436	-1,504837	-1,423756	-1,729123	-2,348644	-1,51958
230318-C3(1)	SHAM1	nan	nan	-1,277247	-0,996583	-2,970722	-1,173507	-0,905937	-0,701724
230318-C3(2)	SHAM1	-1,738113	-1,702331	-1,238779	-1,033216	-3,147284	-0,991561	-1,123309	-1,022603
260218-D5(1)	SHAM1	-0,980374	-1,191674	-1,74318	-2,12732	-1,067641	-1,04395	-0,874046	-1,192272
260218-D5(2)	SHAM1	nan	nan	nan	nan	-1,596184	-2,316705	-0,991	-1,104366
260218-D5(3)	SHAM1	-0,566139	-0,584644	-1,634779	-2,948718	-3,330679	-0,681173	-0,742261	-0,479584
160517(2)	ENR	0	-2,39491	-1,742813	-2,409201	-2,425607	-2,422518	-1,401455	-1,429377
170517(1)	ENR	-0,984804	-0,769177	-0,884254	-2,56366	-3,050282	-1,18804	-1,116424	-0,841633
170517(2)	ENR	-0,904052	-1,552204	-2,707764	-1,161481	-0,874387	nan	nan	nan
180517(1)	ENR	-1,221025	-0,636009	-1,200408	-1,832805	-1,020956	-1,254878	-0,775455	-0,766802
180517(2)	ENR	-1,338474	-0,658173	-1,012979	-1,363111	-2,464122	-1,021158	-0,900068	-0,72775
180517(3)	ENR	-1,240914	-1,206658	-1,028768	-3,27889	-1,253959	-1,125433	-1,451863	-1,71772
190517(1)	ENR	-0,938237	-0,36779	-0,576369	-2,531966	-2,21114	-0,929533	-0,925868	-0,505326
190517(2)	ENR	-0,428758	-0,951515	-1,764965	-2,618177	-2,166467	-0,984347	-0,535445	-0,356508
210319(2)	ENR	-0,536679	-0,617835	-2,055107	-2,380941	-2,375278	-0,873705	-0,711257	-0,914761
210319(3)	ENR	-0,902496	-1,149317	-1,103378	-1,775139	-1,896959	-2,086374	nan	nan
220319(1)	ENR	nan	nan	nan	nan	-1,429691	-1,104052	nan	nan
220319(2)	ENR	-1,180653	-2,530581	-1,187914	-0,814602	-1,780343	-2,425117	-1,324996	-1,863243
230319(1)	ENR	nan	nan	nan	nan	-1,696126	-0,845964	nan	nan
230319(2)	ENR	-0,575636	-1,407323	-1,102707	-2,280863	-2,573289	-1,288789	-0,622111	-0,923244
Cuff_070717(1)	CUFF15	-0,273647	-0,869937	-1,239565	-1,200668	-2,656019	-0,977014	-0,289087	-0,282068
Cuff_080617(1)	CUFF15	-0,358305	-1,114982	-1,866453	-2,404051	-1,620348	-1,234718	-1,086301	-0,376515
Cuff_080717(1)	CUFF15	-0,994469	-1,096979	-1,14243	-1,35672	-1,569765	-1,690715	-2,562343	-2,194885
Cuff_090717(1)	CUFF15	-1,46579	-0,734387	-0,796098	-1,580503	-2,978245	-1,477418	-0,720066	-0,999726
Cuff_110717(1)	CUFF15	0	-8,79277	-4,825177	-9,393044	-34,23347	0	-6,118523	-17,27645
Cuff_110717(2)	CUFF15	0	-2,324943	-5,416928	-3,534201	-7,608326	-8,773594	-6,83034	0
Cuff_120717(1)	CUFF15	0	0	-5,088279	-2,36248	-6,253571	0	-7,129899	0
Cuff_130717(1)	CUFF15	-7,582027	-20,45588	-6,716728	-11,94387	-17,85559	-5,939058	-10,05132	-4,26513
Cuff_130717(2)	CUFF15	-2,842534	-4,23237	-3,326831	-3,994214	-4,182743	-5,510065	-4,781297	-3,396677
Cuff_141016(1)	CUFF15	-0,831656	-0,906475	-1,804866	-1,422469	-2,237454	-2,225813	-1,019606	-0,899855
Cuff_141016(2)	CUFF15	-1,780599	-3,267565	-0,851847	-0,776541	-2,413476	-1,019585	-0,684152	-1,090432
Cuff_161016(1)	CUFF15	-1,02223	-2,911838	-1,993313	-1,955166	-2,116854	-0,788972	-1,143253	-0,708256
Cuff_161016(2)	CUFF15	-1,109552	-1,077592	-0,445856	-0,685034	-2,141053	-1,330504	-1,062138	-1,199417
Cuff_171016(1)	CUFF15	-1,74547	-0,874512	-1,099152	-1,731445	-1,078995	-2,156608	-1,824184	-0,404343
Cuff_171016(2)	CUFF15	-1,171771	-1,124907	-1,956735	-1,855939	-2,039192	-1,245255	-0,770564	-0,659722
Cuff_181016(1)	CUFF15	-1,159306	-0,42101	-1,80549	-1,268479	-1,132818	-1,380794	-0,799956	-1,181243
Cuff_181016(2)	CUFF15	-0,690236	-0,519672	-2,141393	-1,291281	-1,691556	-1,267115	-1,300581	-1,747299
Cuff_181016(3)	CUFF15	-1,307467	-1,834432	-0,875036	-0,530434	-2,406006	-1,478854	-0,868637	-0,694173
Cuff_191016(1)	CUFF15	-0,719874	-0,634652	-1,504824	-2,827517	-2,720513	-0,71432	-0,553294	-1,161974
Cuff_191016(2)	CUFF15	-0,662796	-0,59294	-0,777998	-1,359408	-4,303162	-1,976989	-1,40068	-0,998546
Cuff_201016(1)	CUFF15	-0,295395	-0,478338	-1,497264	-2,919594	-3,65577	-1,140798	-1,552443	-0,952568
Cuff_201016(3)	CUFF15	-1,786622	-1,560468	-0,821677	-1,188722	-1,664023	-2,153679	-1,34624	-1,549024
Cuff_211016(1)	CUFF15	-1,401001	-1,046205	-1,237164	-1,574843	-1,799575	-1,789334	-1,610572	-1,318633
Cuff_211016(2)	CUFF15	-1,43985	-1,737699	-2,088549	-1,518681	-0,842243	-1,456748	-1,717332	-0,866435
050318-D2(1)	CUFF1	-1,16273	-2,055118	-1,005656	-1,88968	-2,2643	-1,436502	-0,871001	-0,81382
050318-D2(2)	CUFF1	-1,043863	-0,96352	-1,217268	-2,895153	-1,313711	-0,629541	-0,774889	-0,937042
050318-D2(3)	CUFF1	-0,707957	-0,740125	-0,710337	-2,028019	-2,960183	-0,909905	-0,85989	-0,979278
060318-D1(2)	CUFF1	-1,147505	-1,68136	-2,167456	-2,471783	-1,131975	-1,337077	nan	nan
070318-B4(1)	CUFF1	-0,520631	-1,898793	-1,003447	-1,877874	-1,963825	-1,066168	-0,60589	-0,653654
070318-B4(2)	CUFF1	-0,412681	-0,676553	-1,239897	-1,677471	-2,383076	-1,063276	-0,868606	-0,774919
080318-B1(1)	CUFF1	-0,668049	-0,79157	-1,446926	-1,224843	-2,061294	-1,612147	-0,505996	-0,676384
080318-B1(2)	CUFF1	-1,098353	-1,608115	-0,657318	-1,676398	-1,623172	-1,71923	-1,285305	-1,058777
090318-B2(1)	CUFF1	-1,186736	-0,883523	-1,283347	-1,029361	-1,747021	-2,390086	-1,228311	-1,246014
100318-B3(1)	CUFF1	-0,554344	-0,731121	-1,466702	-1,803135	-1,991869	-1,008313	-0,908986	-0,932051
110318-A3(1)	CUFF1	-0,756615	-1,079882	-0,826482	-2,052615	-1,871794	-1,394682	-1,546685	-0,732499
110318-A3(2)	CUFF1	-0,78633	-1,127249	-0,990082	-1,94025	-2,937309	-1,404107	-1,067847	-1,11722
110318-A3(3)	CUFF1	-0,824613	-0,462345	-1,181499	-2,863428	-1,740399	-1,322758	-0,679367	-1,367741
190318-A2(1)	CUFF1	-1,002143	-1,149729	-0,812478	-1,650618	-2,115895	-1,628111	-1,383966	-1,054047
190318-A2(2)	CUFF1	-1,189244	-0,829401	-1,690568	-2,251784	-1,886396	-1,146355	-1,192296	-1,262377
270218-D3(1)	CUFF1	-0,848756	-1,279457	-2,70965	-1,643697	-2,705792	-0,982398	-0,393711	-0,593306
270218-D3(2)	CUFF1	-1,146765	-1,409829	-1,667923	-1,261059	-2,452007	-1,661506	-1,326882	-0,907639
280218-D4(1)	CUFF1	-0,794836	-0,55332	-0,951669	-1,78006	-2,767185	-1,1535	-1,31196	-0,84591
280218-D4(2)	CUFF1	-0,660744	-0,493394	-1,043799	-1,104739	-4,912982	-2,41965	-1,672908	-0,757295

Table 4 : Centered synaptic amplitudes used for microzone correlation

condition	B_contravsB_contra	B_contravsAx_Contra	B_contravsA_lat_contra	B_contravsA_med_contra	B_contravsA_med_ipsi	B_contravsA_lat_ipsi	B_contravsAx_ipsi	B_contravsB_ipsi	Ax_ContravsB_contra
WT	0	0,792544496	0,104194471	0,368828442	0,268889493	0,082585941	0,301155814	0,139923469	0,792544496
CUFF_1_MONTH	0	0,385697504	0,186466883	0,11853885	0,38241008	0,25079494	0,273237361	0,493887585	0,385697504
SHAM_1_MONTH	0	0,704630181	0,139551477	0,42775391	0,190247895	0,163978657	0,076462156	0,13828216	0,704630181
ENR	0	0,307657638	0,436109402	0,325149242	0,381880427	0,217754443	0,159180895	0,118637978	0,307657638
CUFF_15_DAYS	0	0,814353544	0,357888455	0,574246778	0,183404544	0,442454414	0,460137509	0,056786907	0,814353544
SHAM_15_DAYS	0	0,626388274	0,833191	0,445907559	0,027684141	0,491846008	0,003179235	0,513040804	0,626388274

condition	Ax_ContravsAx_Contra	Ax_ContravsA_lat_contra	Ax_ContravsA_med_con	Ax_ContravsA_med_ipsi	Ax_ContravsA_lat_ipsi	Ax_ContravsAx_ipsi	Ax_ContravsB_ipsi	A_lat_contravsB_contra	A_lat_contravsAx_Contra
WT	0	0,459833135	0,462229562	0,008489386	0,473946955	0,134738969	0,069943559	0,104194471	0,459833135
CUFF_1_MONTH	0	0,102644255	0,020618082	0,346033504	0,044403914	0,145281673	0,27642066	0,186466883	0,102644255
SHAM_1_MONTH	0	0,036458738	0,369780002	0,473423385	0,141719538	0,342399793	0,42781642	0,139551477	0,036458738
ENR	0	0,286341445	0,355364616	0,127756887	0,87438515	0,579679184	0,769557749	0,436109402	0,286341445
CUFF_15_DAYS	0	0,679572879	0,905525073	0,679481352	0,41201948	0,721209212	0,501836159	0,357888455	0,679572879
SHAM_15_DAYS	0	0,5072953	0,184260167	0,387716107	0,194248202	0,112140015	0,189121101	0,833191	0,5072953

condition	lat_contravsA_lat_cont	lat_contravsA_med_cor	lat_contravsA_med_ip	A_lat_contravsA_lat_ipsi	A_lat_contravsAx_ipsi	A_lat_contravsB_ipsi	A_med_contravsB_contra	A_med_contravsAx_Contra	A_med_contravsA_lat_contra
WT	0	0,002830536	0,323290067	0,323139091	0,041454398	0,263828429	0,368828442	0,462229562	0,002830536
CUFF_1_MONTH	0	0,016811456	0,143686321	0,170861044	0,452339594	0,21427371	0,11853885	0,020618082	0,016811456
SHAM_1_MONTH	0	0,10371524	0,010280278	0,417723083	0,329792525	0,121493425	0,42775391	0,369780002	0,10371524
ENR	0	0,245455075	0,352644087	0,105080618	0,216653516	0,037554184	0,325149242	0,355364616	0,245455075
CUFF_15_DAYS	0	0,803017497	0,670575405	0,518226783	0,94106343	0,409728876	0,574246778	0,905525073	0,803017497
SHAM_15_DAYS	0	0,465443674	0,253885381	0,608529842	0,313927783	0,735575134	0,445907559	0,184260167	0,465443674

condition	hed_contravsA_med_co	med_contravsA_med_i	med_contravsA_lat_ip	A_med_contravsAx_ipsi	A_med_contravsB_ipsi	A_med_ipsivsB_contra	A_med_ipsivsAx_Contra	A_med_ipsivsA_lat_contra	A_med_ipsivsA_med_contra
WT	0	0,189274448	0,340394949	0,238574867	0,143060512	0,268889493	0,008489386	0,323290067	0,189274448
CUFF_1_MONTH	0	0,496285326	0,674153779	0,302714943	0,337512407	0,38241008	0,346033504	0,143686321	0,496285326
SHAM_1_MONTH	0	0,240284589	0,43687337	0,185714559	0,333845858	0,190247895	0,473423385	0,010280278	0,240284589
ENR	0	0,273414584	0,479092654	0,014240249	0,167722352	0,381880427	0,127756887	0,352644087	0,273414584
CUFF_15_DAYS	0	0,852287138	0,361777713	0,804463398	0,681860462	0,183404544	0,679481352	0,670575405	0,852287138
SHAM_15_DAYS	0	0,033309394	0,85812337	0,016737799	0,47720446	0,027684141	0,387716107	0,253885381	0,033309394

condition	A_med_ipsivsA_med_ip	A_med_ipsivsA_lat_ips	A_med_ipsivsAx_ipsi	A_med_ipsivsB_ipsi	A_lat_ipsivsB_contra	A_lat_ipsivsAx_Contra	A_lat_ipsivsA_lat_contra	A_lat_ipsivsA_med_contra	A_lat_ipsivsA_med_ipsi
WT	0	0,577327944	0,145093361	0,305625706	0,082585941	0,473946955	0,323139091	0,340394949	0,577327944
CUFF_1_MONTH	0	0,355804792	0,329153067	0,30704534	0,25079494	0,044403914	0,170861044	0,674153779	0,355804792
SHAM_1_MONTH	0	0,234019973	0,313569401	0,290647817	0,163978657	0,141719538	0,417723083	0,43687337	0,234019973
ENR	0	0,003112725	0,178717448	0,322669306	0,217754443	0,87438515	0,105080618	0,479092654	0,003112725
CUFF_15_DAYS	0	0,100383535	0,668570616	0,911963571	0,442454414	0,41201948	0,518226783	0,361777713	0,100383535
SHAM_15_DAYS	0	0,462585642	0,535611869	0,629931082	0,491846008	0,194248202	0,608529842	0,85812337	0,462585642

condition	A_lat_ipsivsA_lat_ipsi	A_lat_ipsivsAx_ipsi	A_lat_ipsivsB_ipsi	Ax_ipsivsB_contra	Ax_ipsivsAx_Contra	Ax_ipsivsA_lat_contra	Ax_ipsivsA_med_contra	Ax_ipsivsA_med_ipsi	Ax_ipsivsA_lat_ipsi
WT	0	0,16993331	0,350328856	0,301155814	0,134738969	0,041454398	0,238574867	0,145093361	0,16993331
CUFF_1_MONTH	0	0,573564685	0,168476221	0,273237361	0,145281673	0,452339594	0,302714943	0,329153067	0,573564685
SHAM_1_MONTH	0	0,412359975	0,551963577	0,076462156	0,342399793	0,329792525	0,185714559	0,313569401	0,412359975
ENR	0	0,621034068	0,705376565	0,159180895	0,579679184	0,216653516	0,014240249	0,178717448	0,621034068
CUFF_15_DAYS	0	0,562729886	0,097362331	0,460137509	0,721209212	0,94106343	0,804463398	0,668570616	0,562729886
SHAM_15_DAYS	0	0,115971566	0,618373886	0,003179235	0,112140015	0,313927783	0,016737799	0,535611869	0,115971566

condition	Ax_ipsivsAx_ipsi	Ax_ipsivsB_ipsi	B_ipsivsB_contra	B_ipsivsAx_Contra	B_ipsivsA_lat_contra	B_ipsivsA_med_contra	B_ipsivsA_med_ipsi	B_ipsivsA_lat_ipsi	B_ipsivsAx_ipsi	_ipsivsB_ipsi
WT	0	0,692382931	0,139923469	0,069943559	0,263828429	0,143060512	0,305625706	0,350328856	0,692382931	0
CUFF_1_MONTH	0	0,219054648	0,493887585	0,27642066	0,21427371	0,337512407	0,30704534	0,168476221	0,219054648	0
SHAM_1_MONTH	0	0,687429172	0,13828216	0,42781642	0,121493425	0,333845858	0,290647817	0,551963577	0,687429172	0
ENR	0	0,82091129	0,118637978	0,769557749	0,037554184	0,167722352	0,322669306	0,705376565	0,82091129	0
CUFF_15_DAYS	0	0,413234431	0,056786907	0,501836159	0,409728876	0,681860462	0,911963571	0,097362331	0,413234431	0
SHAM_15_DAYS	0	0,796629614	0,513040804	0,189121101	0,735575134	0,47720446	0,629931082	0,618373886	0,796629614	0

Table 5 : Individual correlation indexes between microzones

2. Indivual plots of synaptic amplitude correlations

CUFF_1_MONTH dataset : average amplitude in cluster correlation

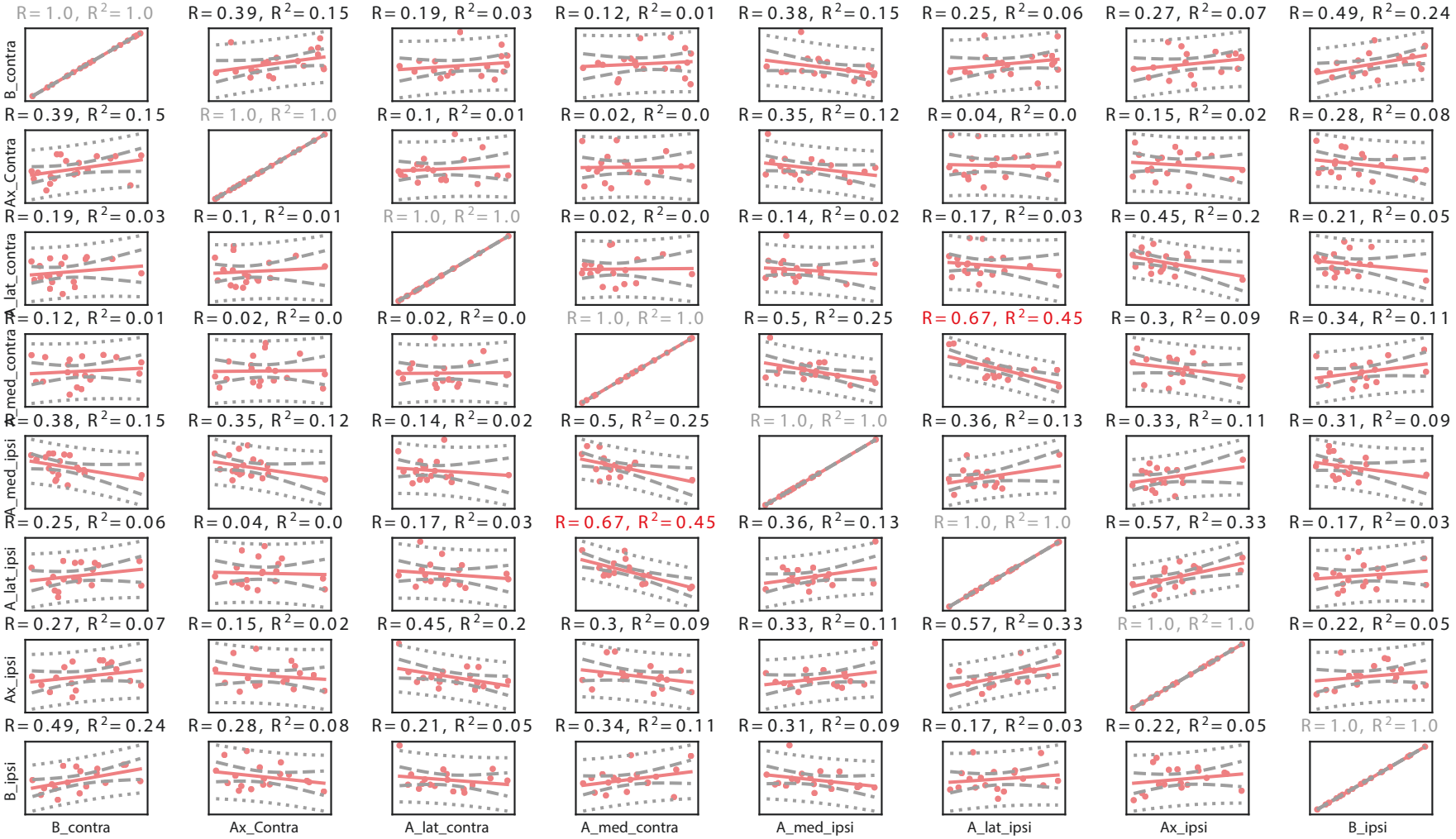

CUFF_15_DAYS dataset : average amplitude in cluster correlation

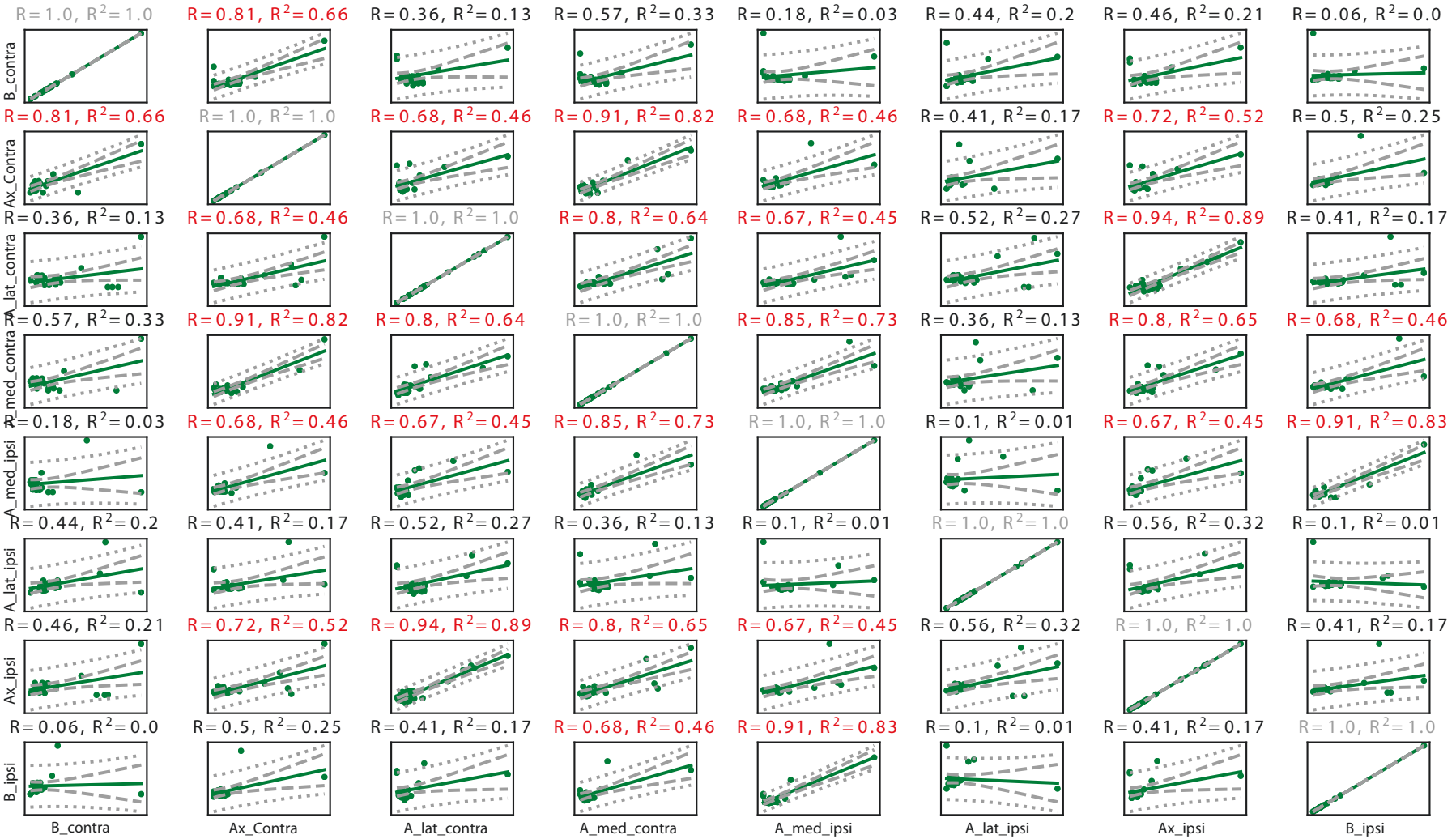

ENR dataset : average amplitude in cluster correlation

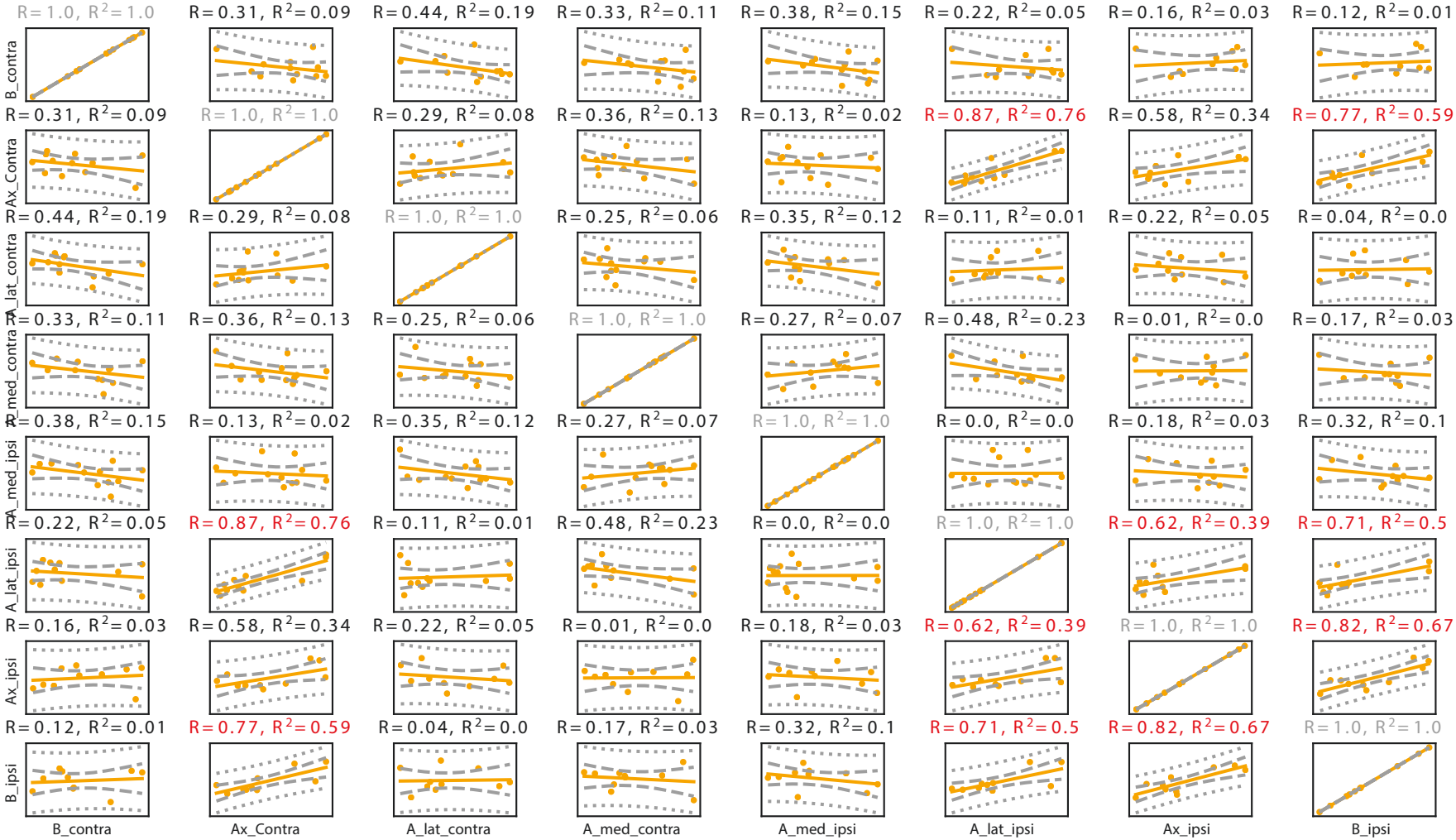

SHAM_1_MONTH dataset : average amplitude in cluster correlation

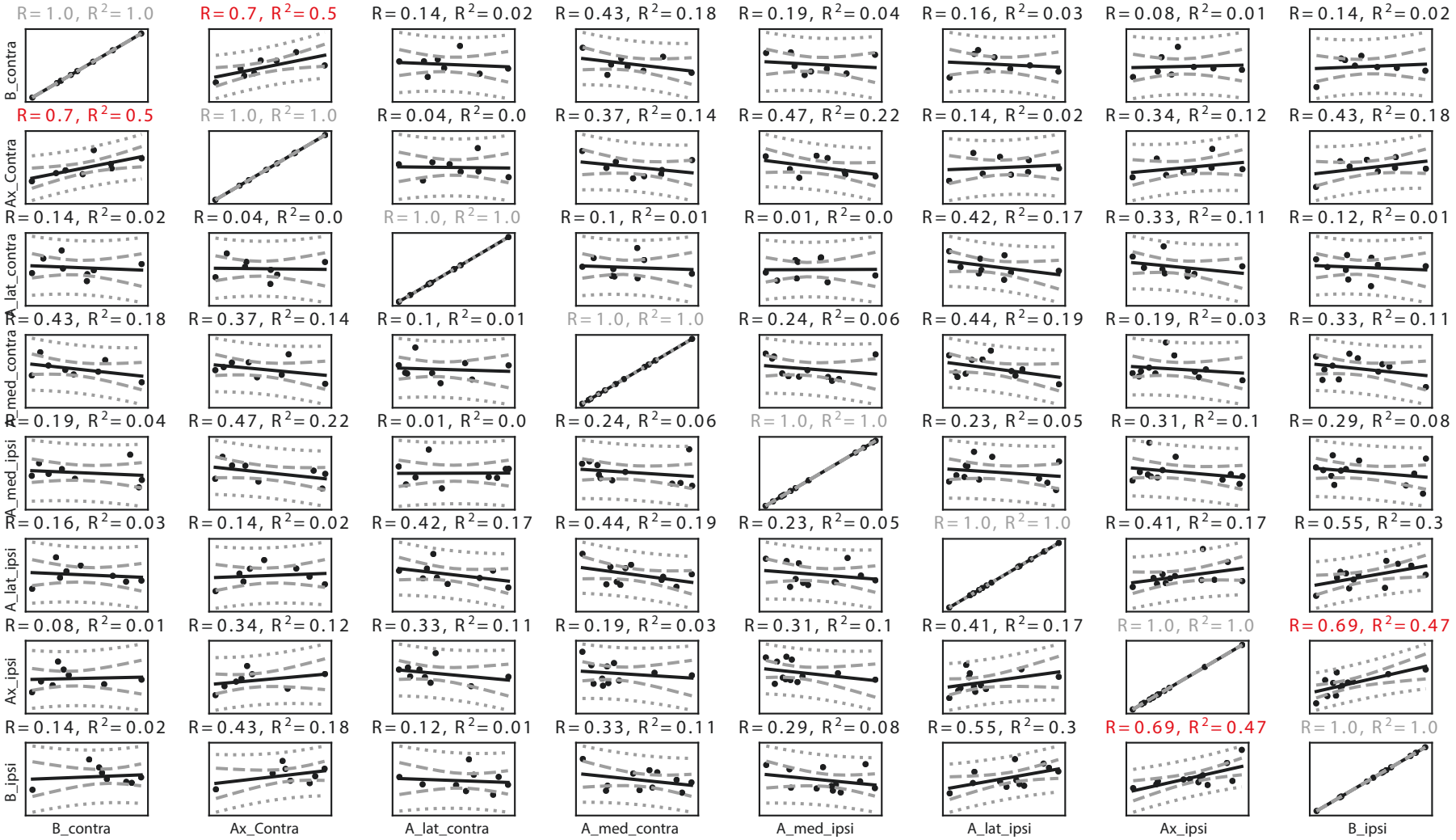

SHAM_15_DAYS dataset : average amplitude in cluster correlation

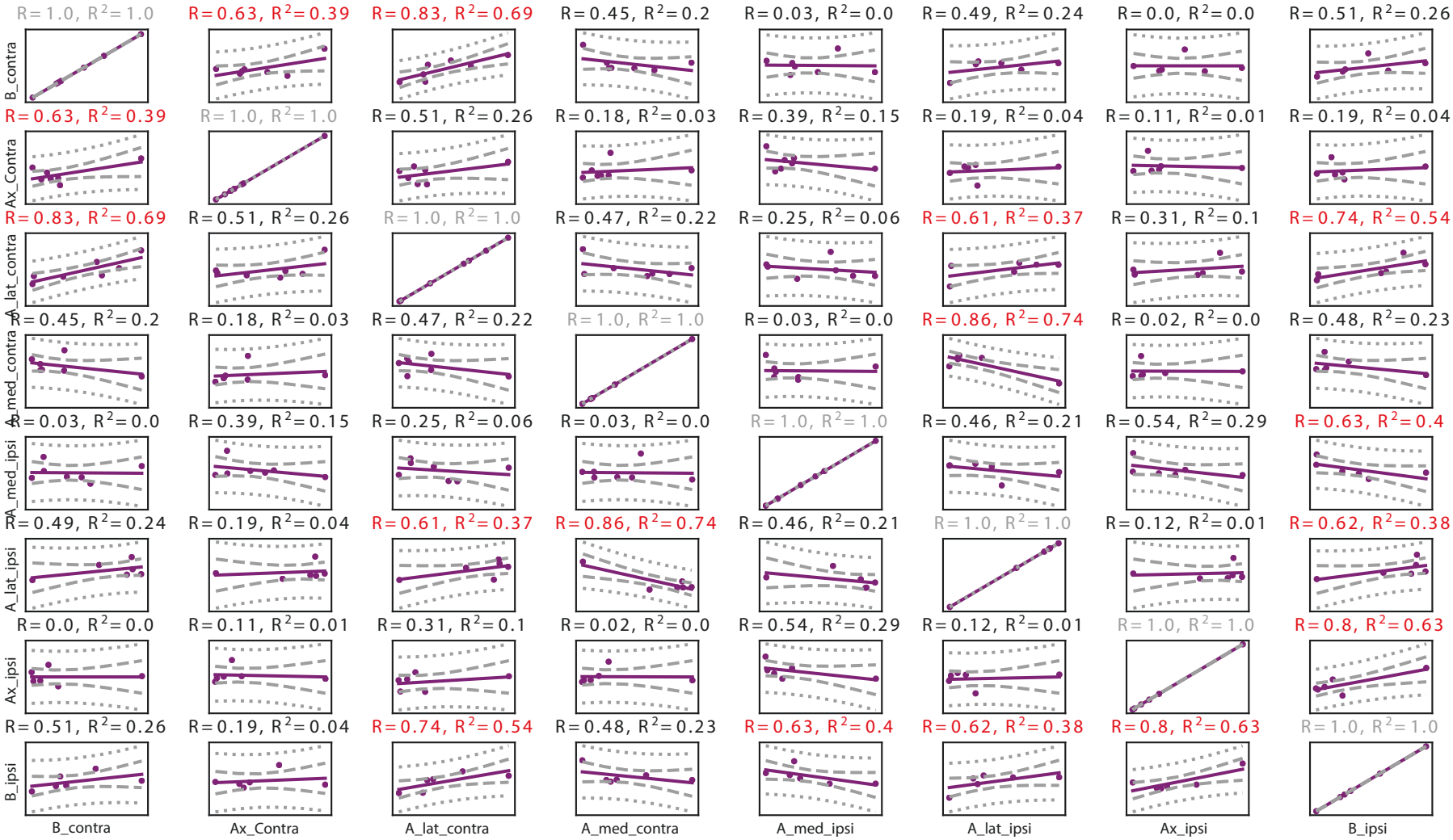

WT dataset : average amplitude in cluster correlation

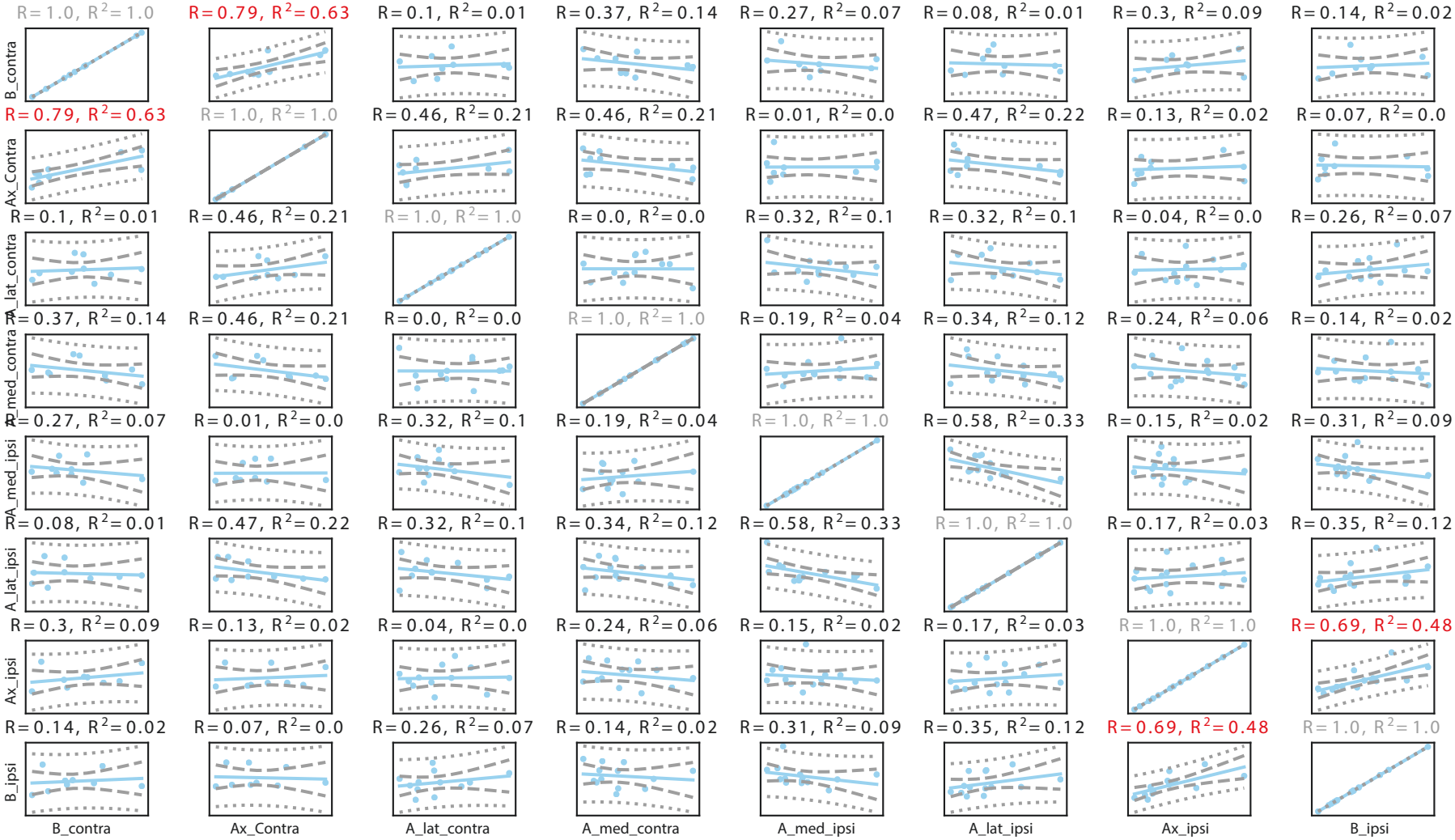

3. Functional Purkinje cell cluster in EAAT4 and ALDOC mice

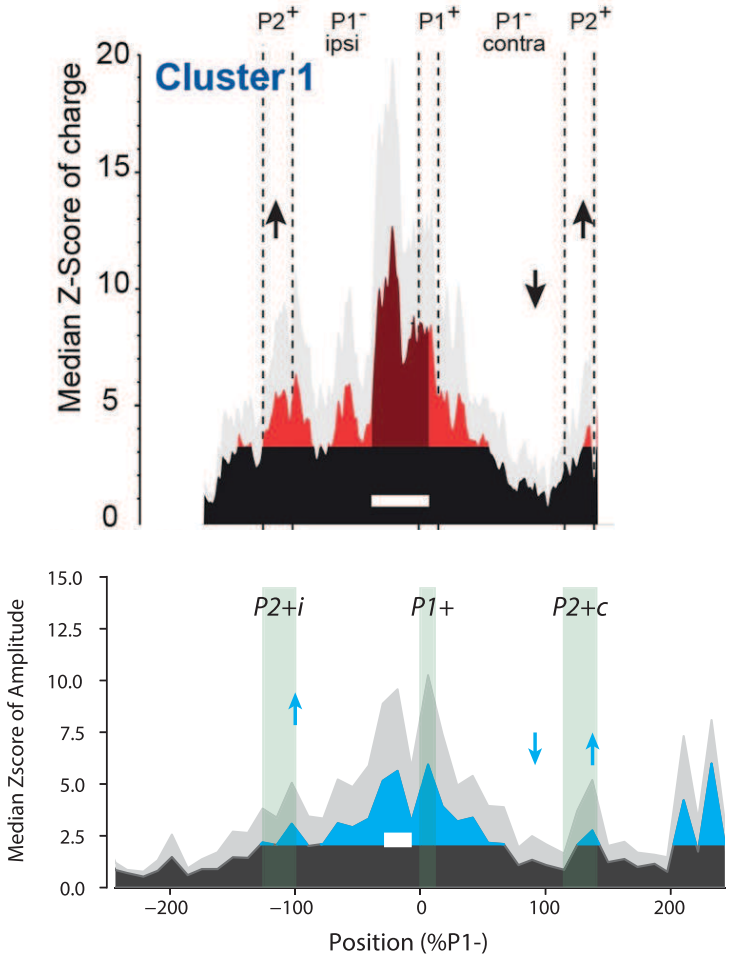

Annex 3 : Stereotyped spatial patterns of functional synaptic connectivity across mouse lines

Median input pattern (Z-score of charge) obtained by Valera et al; 2016 (top) and by myself (Z-score of amplitude, down). Black filled curve represent non connected granule cells (i.e. Zscore < 3.09 or Z-score < 2.0). Coloured-filled curve represent functionnal connected granule cells. They gray filled curve represents median absolute deviation.

4. Building a homemade CatWalk

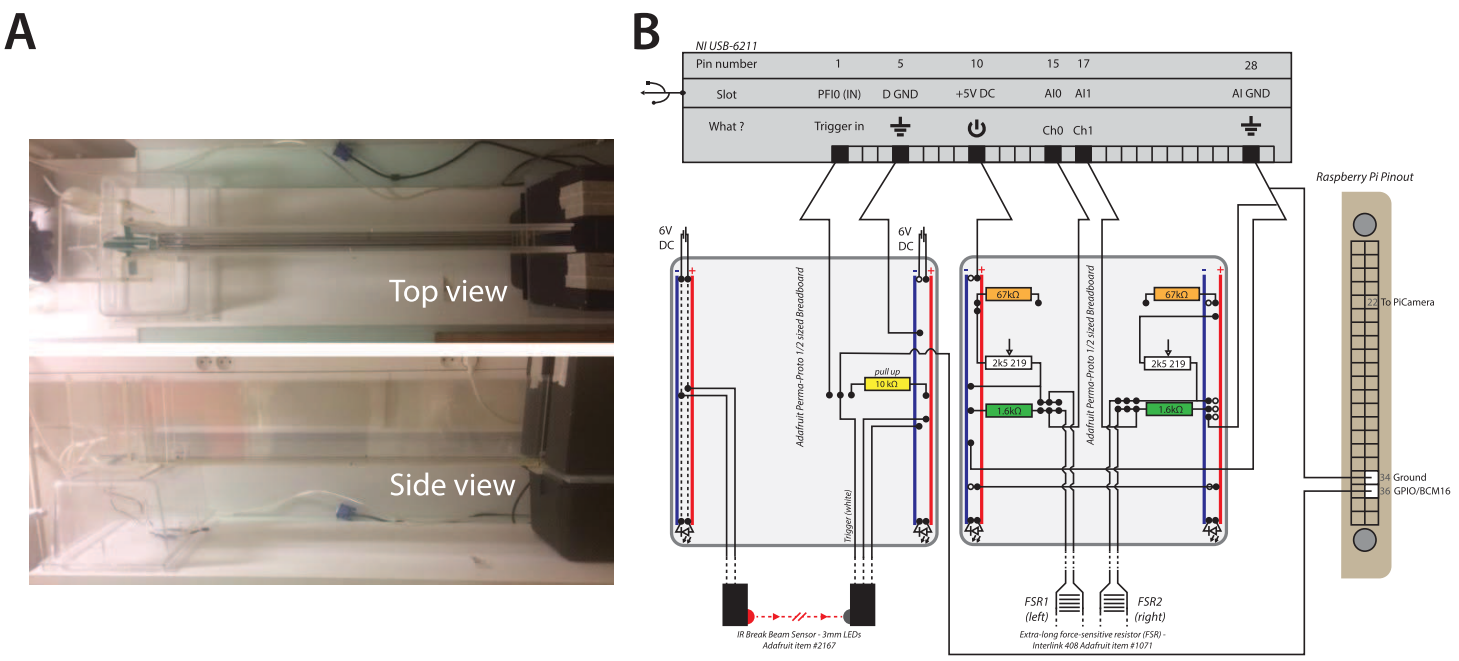

Appendix 4: building a homemade Catwalk

(A) Top and side view of the general apparatus. Mice are trained to cross a surrelevated corridor. Mice are placed in the starting transparent box (black arrows). A gentle air puff can be delivered in the box to encourage mice to rush in the corridor, up to the terminal area (black box on the left symbolized with a white asterix).

(B) Diagram wiring for data and video synchronisation. As mice enter the corridor, they break an IR barrier that triggers both pressure and video acquisition. A digital camera (PyCamera), the pressure sensors (Interlink FSR, Adafruits) and an analog digital interface (Ni DAQMX USB, Texas Instruments) converge towards 2 homemade breadboards to be synchronised via a Python Script hosted on a Raspberry 2 microcomputer.

(C, left) Schematic illustration of the apparatus. Pressure from left and right side of the body are acquired independently and simultaneously. Pressure sensors are ribbon-shaped polymer thick film devices that exhibit a decrease in resistance with increase in force applied to the surface of the sensor.

(C, right) Diagram and equation describing force-to-voltage conversion: FSR devices is tied to a measuring resistor in a voltage divider configuration. Therefore, FSR output voltage increases with increasing force, and is recorded via WinWCP (4.2.5) software (John Dempster, University of Strathclyde, UK).

5. Decorrelated excitation and inhibition in the cerebellar cortex

Binda F; **Spaeth L**; Pawlowski S; Grangeray-Vilmint A; Pouain B & Isope P (*in prep*)

Decorrelated excitation and inhibition in the cerebellar cortex

Francesca Binda, Ludovic Spaeth, Sophie Pawlowski, Anais Grangeray-Vilmint, Bernard Poulain and Philippe Isope

Institut des Neurosciences Cellulaires et Intégratives, CNRS, Université de Strasbourg, 67084, Strasbourg, France

Abstract

The cerebellar cortex is organized in heterogeneous modules that compute sensorimotor information from many brain areas including the cerebral cortex, brainstem nuclei and the spinal cord. Our recent work (Valera et al., 2016) showed that granule cells, the input stage of the cerebellar cortex, underlie modular communication through a specific functional synaptic organization at the granule cell – molecular interneuron and granule cell – Purkinje cell connections. This study predicts that different groups of granule cells may drive excitation and inhibition in Purkinje cells extending the classical organization of feedforward inhibition in the cerebellar cortex. We show using *in vitro* optogenetic stimulation of specific mossy fibers that inhibitory and excitatory synaptic inputs on Purkinje cells are dissociated and display a wide range of temporal delays between EPSC and IPSC onset. Our findings suggest that mossy fiber inputs may be temporally encoded by the specific interplay between excitation and inhibition in Purkinje cells.

Introduction

In Valera et al. (2016) we have demonstrated that the spatial organization of the synaptic connections between granule cells (GCs) and the other cell types of the cerebellar cortex - Purkinje cells (PCs), molecular interneurons (MLIs) and Golgi cells – is stereotyped in the anterior vermis. Clusters of GCs make active synaptic connections with specific groups of PC and MLIs independently as a result of activity dependent processes. We showed that PCs and MLIs from a given cluster (for example between the midline and ~100 μm in the mediolateral axis) display some non-overlapping GC input maps, suggesting that GCs may contact either MLIs or PCs at a given location. These findings predict that PCs may combine separate excitatory and inhibitory synaptic inputs originating from distinct GC clusters. Since specific temporal patterns of integration at the mossy fiber (MF) – GC connection has been observed (Chabrol et al., 2015), our findings suggest that excitation (E) and inhibition (I) may reach PCs with a wide range of latencies (***Figure 1A, two scenarii***). This prediction challenges previous observation showing that the GC-MLI-PC feedforward inhibitory pathway (FFI) is characterized by a reliable E/I sequence with a very low jitter (Eccles et al., 1967; Brunel et al., 2004; Mittmann et al., 2005; Grangeray-Vilmint et al., 2018). It has been suggested that FFI may sharpen the temporal window for spike discharge, prevent the saturation of PC discharge and promote long term potentiation at the GC-PC synapses, thus extending the dynamic range for rate coding of the stimulus (Eccles et al., 1967; Barbour, 1993; Brunel et al., 2004; Mittmann et al., 2005; Isaacson and Scanziani, 2011; Binda et al., 2016). However, in these studies, FFI has been evoked by using stimulation of the molecular layer or GCs but not via MF activation, the physiological pathway. Individual MF give off numerous collaterals that can contact many GC clusters in the same lobule (Shinoda et al., 2000; Quy et al., 2011) and may lead to temporally dispersed GC activation. Therefore, in combination with our results in Valera et al (2016), it is unclear whether MF inputs can induce E/I sequences with a fixed short delay. We

addressed this question by stimulating MFs from a single precerebellar nucleus and monitored the resulting E/I sequence in PCs.

Results

Optogenetic MF stimulation evokes excitation and inhibition in PCs.

To mimic MF natural inputs, we injected rAAV 9/2 in precerebellar nuclei in order to express Channelrhodopsin2 (ChRd2(H134R)-YFP) in individual MFs (***Figure 1B***). Since different synaptic properties have been described at the MF-GC connection from different origins (Chabrol et al., 2015) we chose to target a unique pre-cerebellar nucleus, the cuneate (number or recordings n= 57, number of cells n_c = 15 and number of mice N = 4) which convey proprioceptive and exteroceptive information from the upper limb. Also, several studies have demonstrated that MF originating in the cuneate nucleus send collaterals at different location in the same lobule (Quy et al., 2011; Valera et al., 2016). First, we assessed whether individual fluorescent MF rosettes could be photostimulated in acute cerebellar transverse slices. Fluorescent MF rosettes were recorded in loose cell-attached mode (Barbour and Isope, 2000) while pulses (10-100 ms length) of blue light were elicited. In all the fluorescent rosettes, illumination triggered a unique or a short burst of action potentials (mean spike number = 3.9 ± 2.5 n = 6; ***Figure 1C)***. Using a confocal-based laser scanning approach, we then systematically illuminated small zones (83 x 83 µm) of the GC layer from a given lobule (Lobule III to VIII) to stimulate MF rosettes while EPSCs and IPSCs were monitored in a PC (n=15) recorded in whole cell mode (***Figure 1D***).

Stimulating specific MFs induced a wide range of temporal EPSC/IPSC profiles in PCs

EPSCs and IPSCs (or synaptic charges, EPSQ and IPSQ, Materials and Methods) elicited in PCs by MFs illumination (50 ms pulses) were recorded at V_m = -60 mV and V_m = 0 mV respectively (***Figure 1D;*** EPSQ: - 3.5 ± 3.4 pC; IPSQ: 13.8 ± 11.5 pC, mean ± SD). Although we observed excitation followed by inhibition in 45/57 recordings, in 6/57 inhibition preceded

77 excitation and in 6 recordings only inhibition was observed. Furthermore, consistent with our
78 prediction we observed a large temporal spread of the onset of excitatory and inhibitory synaptic
79 inputs elicited by MFs from a given area. This temporal spread was quantified by measuring
80 the differences between IPSC and EPSC latencies from the beginning of illumination (ΔLat =
81 latency I – latency E). ΔLat ranged from negative to positive values that can exceed ±5 ms
82 (from – 11.8 to 13.21 ms; mean = 3.6 ± 4.55 ms, mean ± SD; ***Figure 2A***). We compared this
83 distribution with ΔLat measured following direct electrical stimulation of GC clusters
84 (GC_ΔLat; ***Figure 2B***). As opposed to MF stimulation, GC stimulation systematically lead to
85 short ΔLat (mean GC_ΔLat = 2 ± 0.74 ms, mean ± SD, n = 23; ***Figure 2B***) as previously shown
86 (Vincent and Marty, 1996; Brunel et al., 2004; Mittmann et al., 2005; Grangeray-Vilmint et al.,
87 2018). We then used GC_ΔLat as a proxy for the classical FFI in the GC-MLI-PC pathway
88 evoked by one GC cluster. Since in this dataset 0< GC_ΔLat <5 ms (***Figure 2B***), we separated
89 the ΔLat measurement from the MFs illumination experiment in two groups (***Figure 2C***): a
90 putative FFI-ΔLat (group 1; n = 27/57; 47.5%) with 0 < ΔLat <5 ms and a second group (group
91 2; n = 30/57) aggregating the other measurements, including ΔLat > 5ms (31.5%) or negative
92 (10.5%) and MF stimulation eliciting only inhibition (10,5%). Therefore, the ΔLat spread can
93 solely be explained by a dissociation between a direct GC-evoked excitation and an indirect
94 GC-evoked inhibition mediated by different cluster of GCs. Thus, these findings suggest that
95 the burst of action potentials elicited by blue light in MF rosettes is propagated in MF collaterals
96 that target different GC clusters in the GC layer, including distant subsets of GCs targeting local
97 MLIs but not PCs. Indeed, high positive values of ΔLat are always the result of long latency of
98 inhibitory inputs (Pearson r = 0.76, r^2 = 0.58, p < 0.00001, n = 51. ***Figure 2 – Figure supplement***
99 ***1***). These results are in agreement with previous findings (Chabrol et al., 2015) demonstrating
100 that long temporal integration delays may occur at the MF-GC connection. The combination of

an excitation propagated in several MF branches with long integration delays at the MF-GC synapses (>10 ms) may then explain the ΔLat spread.

Correlation and decorrelation between excitation and inhibition

Because it has been shown that excitation-inhibition (E/I) ratios could be equalized (Xue et al., 2014; but see Grangeray-Vilmint et al., s2018), we then evaluated the correlation between EPSQ and IPSQ in both groups. In group 1 the excitatory synaptic charges (EPSQs) were linearly correlated with the inhibitory synaptic charges (IPSQs; Pearson r = 0.77; $r^2 = 0.6$, $p < 0.00001$, n = 27; ***Figure 3***, ***left***) while in group 2, no correlation was observed (Pearson r = 0.17; $r^2 = 0.0275$, p = 0.43, n = 24; ***Figure 3, right***). Thus, for individual cluster of GCs targeted by the same MFs, the excitatory and inhibitory synaptic weights evoked in PCs are controlled together and lead to a similar E/I balance as described in the cerebral cortex (Xue et al., 2014) . Conversely, group 2 measurements showed that MFs from a given precerebellar nucleus (e.g. the cuneate nucleus) can activate independent GC clusters and lead to specific E/I balance with specific ΔLat.

These findings demonstrate that the non-overlapping synaptic maps described in Valera et al (2016) lead to a dissociation between GC-driven E and I inputs in PCs. This organization defines a specific temporal code given by MF-driven GCs activation. Indeed, Chabrol et al. (2015) demonstrated that pathway specific short-term plasticity at the MF-GC synapses permit temporal coding of multimodal MF inputs by GCs. Therefore, our two studies suggest that the activity dependent spatial organization of synaptic information processing in the cerebellar cortex might determine temporal processing. Furthermore, we recently demonstrated that long term potentiation (LTP) at the GC-PC synapses is gated by MLI (Binda et al., 2016). We then postulate that the independent regulation of GC-MLI-PC synapses can influence LTP induction from specific cluster of GCs. These features may underlie cerebellar module communication and motor coordination (Apps et al., 2018).

Materials and Methods

Pre-cerebellar nuclei rAAVs-mediated transduction

In vivo stereotaxic injections of rAVVs viral particles were performed as previously described (Valera et al. 2016). CD1 male mice (P 21) were anesthetized by a brief exposure to isoflurane 4 % and anesthesia was maintained by intraperitoneal injections of a mixture of ketamine (100 mg/kg), medetomidine (1 mg/kg) and acepromazine (3 mg/kg). rAAVs 9/2 particles carrying the cDNA for ChRd2(H134R)-YFP under the hSyn promoter (3.38 10^{13} GC/ml; Penn Vector Core, Pennsylvania) were unilaterally injected in the cuneate nucleus at an approximate speed of 250 nl/min via a graduated pipette equipped with a piston for manual injections. A final volume of 1.5 µl was delivered by two injections (0.75 µl/injection) separated by 0.2 mm in the antero-posterior direction; after that half of the virus volume was delivered, the pipette was raised up 0.2 mm and maintained in place until the end of the injection. For effective virus diffusion, the pipette was left in place at least 5 minutes following injection. Injections coordinates were determined from The Mouse Brain Atlas (Franklin and Paxinos, 2007) and corrections based on tissue markers were applied to counterbalance the variability of the CD1 outbred background (from lambda, starting point: AP 2.73 ± 0.14, Lat 1.36 ± 0.08, DV: 5.1 ± 0.09, mean ± SEM). At the end of the injection, antipamezole (1 mg/kg) were administered to the mice via intraperitoneal injection to favor recovery from anesthesia.

Slice preparation

Acute cerebellar transverse slices were prepared from injected mice three weeks after injection. Mice were anesthetized by a brief exposure to isoflurane 4 %, decapitated and the cerebellum rapidly dissected in ice-cold artificial cerebrospinal fluid (aCSF) bubbled with carbogen (95% O_2, 5% CO_2) and containing (in mM): NaCl 120, KCl 3, $NaHCO_3$ 26, NaH_2PO_4 1.25, $CaCl_2$ 2,

$MgCl_2$ 1 and glucose 16. 300 µm-thick transverse slices were cut (Microm HM 650V, Microm, Germany) in ice-cold sucrose-based cutting solution bubbled with carbogen (95% O_2, 5% CO_2) and containing (in mM): sucrose 246, KCl 4, $NaHCO_3$ 26, $CaCl_2$ 1, $MgCl_2$ 5, glucose 10 and kynurenic acid 1. Slices were then transferred in bubbled aCSF at 34° C and they were allowed to recovery for at least 30 minutes before starting experiments. Following recovery, slices were maintained at room temperature for the rest of the day.

Electrophysiology

Electrophysiology experiments were performed at room temperature in a recording chamber continuously perfused with bubbled aCSF supplemented with (in mM): strychnine 0.001, D-APV 0.05, DPCPX 0.0005. AM251 0.001, CGP52432 0.001 and JNJ16259685 0.002. To allow the full illumination of the surface, slices were rapidly mounted on glass coverslips coated with poly-L-lysine (1 mg/ml) right before transferring them to the recording chamber.

Patch clamp pipettes were pulled from borosilicate glass to a final resistance of 3-4 MΩ when filled with the following solution (in mM): cesium methanesulfonate 135, NaCl 6, $MgCl_2$ 1, HEPES 10, MgATP 4, Na2GTP 0.4, EGTA 1.5, QX314Cl 5, pH 7.3. Lucifer yellow CH was added to the internal solution (1 mg/ml) for later patched cell identification.

Whole-cell patch clamp recordings were performed with a Multiclamp 700B amplifier (Molecular Devices, USA) and acquired with WinWCP 4.2.1 freeware (John Dempster, SIPBS, University of Strathclyde, UK); whole-cell currents from PCs were filtered at 2 kHz and digitized at 50 kHz; series resistance were monitored during the experiments and compensated by 70-80%.

Loose cell-attached recordings were obtained using a Multiclamp 700B amplifier (Molecular Devices, USA) and acquired with WinWCP 4.2.1 freeware (John Dempster, SIPBS, University of Strathclyde, UK). Rosettes were recorded with 5 MΩ glass pipettes (borosilicate) and potential was held at 0mV for all recordings. The internal pipette solution contained (in mM):

NaCl 120, KCl 3, HEPES 10, NaH_2PO_4 1.25, $CaCl_2$ 2, $MgCl_2$ 1 and glucose 10 (Sigma- Aldrich, USA). Osmolarity and pH were respectively set at 295 mOsm and 7.3. Recordings were low-pass filtered at 2.6 kHz then sampled at 20-50 kHz. All experiments were performed at room temperature (23°C) using the same bubbled aCSF than for slices preparation. For controls, NBQX (20 µM, Sigma-Aldrich, USA) and lidocaine (1mM, Sigma-Aldrich, USA) were bath-applied respectively to block AMPA receptor transmission and action potential propagation.

For GC stimulation, a glass pipette (borosilicate) containing (in mM) : NaCl 120, KCl 3, HEPES 10, NaH_2PO_4 1.25, $CaCl_2$ 2, $MgCl_2$ 1 and glucose 10 (Sigma- Aldrich, USA) was inserted in the deepness of the GC layer. GCs were electrically stimulated (3-5µA, 100µs) using a constant current delivered by an isolated stimulator (model DS3, Digitimer Ltd, England).

Photostimulation

Mossy fibers blue light-mediated activation was obtained by a two dimension-scan mode of a confocal microscope (FV300, Olympus, Japan) equipped with a diode-pumped solid-state blue laser (473 nm, CrystalLaser, USA); stimulation (50 ms blue light pulses through a 20X objective, 83x83 µm scan area) was driven by a Programmable Acquisition Protocol Processor (PAPP, Fluoview 300) at successive positions along the longitudinal axis. The stimulation protocol was repeated between 3 and 7 times and average traces used for analysis. MFs-dependent EPSCs and IPSCs were isolated by clamping Purkinje cells at – 60 mV and 0 mV respectively.

Illumination of loose cell-attached MF rosettes was elicited using a 460nm blue LED (Prizmatix, Israel). The illuminated area was restricted to the recorded rosette using a DMD-array (Mosaïc, Andor Technology, Northern Ireland) through a 40x objective (Olympus, Japan). Steady illumination power was set at 2-4mW/mm².

Data Analysis

EPSC and IPSC average traces were obtained and synaptic charges were calculated for a 150 ms window. The latency was defined as the crossing point between the baseline and the linear fit of the MFs-induced response calculated between the 20 % and 80 % of the rising phase. Statistics are indicated in the text. For the ΔLat measurement following direct GC stimulation, the dataset recorded for this experiment has been combined with the dataset from Grangeray-Vilmint et al. (2018).

Figure Legends

Figure 1. Optogenetic stimulation of MFs from the cuneate nucleus

A, diagram of the cerebellar cortex illustrating MF collaterals in the granule cell layer. Results from Valera et al. (2016) suggest that GC clusters may lead to independent excitatory (E) and inhibitory (I) synaptic inputs. If true, MF stimulation should induce two types of E/I sequences in PCs: *1.* a typical FFI with a short delay (ΔLat) when a single GC cluster provide both a direct excitatory input and an indirect GC-MLI input; *2.* A spread ΔLat when several GC clusters lead to independent E/I sequences. **B**, *Left,* rAAVs 9/2 injection in the cuneate nucleus. *Right*, confocal image of YFP fluorescence in MF rosettes in a transverse cerebellar slice after fixation (see Figure 1 – Figure supplement 2 from Valera et al, 2016). **C**, *Left,* YFP fluorescence in MF rosettes in an acute cerebellar slice. The pipette used for loose cell-attached recording of a rosette is highlighted in grey. *Right*, example of burst of action potential recorded in a rosette and elicited by blue light illumination. *Bottom right*, light activated action potentials are blocked by lidocaine but not by NBQX. **D**, *Left,* diagram of the illumination protocol. The data were obtained by confocal-based laser scanning of identified surface of the GC layer (83x83µm). *Left,* representative traces of EPSC and IPSC induced by light-mediated stimulation of MFs in one area of the GC layer. MF, mossy fibers; PC, Purkinje cell; GC, granule cell; MLI, molecular interneurons.

Figure 2. A wide range of E/I temporal profiles recorded in PCs after MF stimulation

A, histogram of the ΔLat following MF illumination. **B**, histogram of the ΔLat following GC electrical stimulation. *Inset*, diagram illustrating FFI. **C**, Two groups and 4 types of E/I temporal profiles were distinguished during MFs illumination. Group 1 corresponds to $0 < \Delta Lat < 5$ ms. Group 2 correspond to $\Delta Lat < 5$ ms, negative (Inhibition first) and GC clusters eliciting only inhibition (No excitation). Red and Blue triangle identify the onset of the excitatory and inhibitory current, respectively. *Inset*, highlight of the onset of EPSC and IPSC superimposed.

Bottom, the 4 potential scenarios explaining the profiles. *Excitation first (0 < ΔLat < 5 ms)* corresponds to classical FFI, i.e. the same GCs contact both MLIs and PCs. *Excitation first (ΔLat < 5 ms)* and *inhibition first* illustrate that several clusters of GC have been excited (two GC clusters are represented in the diagram below) which elicit excitation and inhibition independently. *No excitation*, only inhibition has been observed.

Figure 3. Correlated group 1 ΔLat, uncorrelated group 2 ΔLat.

Scatter plot of the inhibitory synaptic charge (IPSQ) against the excitatory synaptic charge (EPSQ) recorded following MF illumination for the 2 groups. Group 1, $0 < \Delta Lat < 5$ ms; group 2, $|\Delta Lat| > 5$ ms. IPSQs; Pearson $r = 0.77$; $r^2 = 0.6$, $p < 0.00001$, $n = 27$. Pearson $r = 0.17$; $r^2 = 0.0275$, $p = 0.43$, $n = 24$.

248

249 **References**

250

251 Apps R et al. (2018) Cerebellar Modules and Their Role as Operational Cerebellar Processing
252 Units. Cerebellum.

253 Barbour B (1993) Synaptic currents evoked in Purkinje cells by stimulating individual granule
254 cells. Neuron 11:759–769.

255 Binda F, Dorgans K, Reibel S, Sakimura K, Kano M, Poulain B, Isope P (2016) Inhibition
256 promotes long-term potentiation at cerebellar excitatory synapses. Sci Rep 6:33561.

257 Brunel N, Hakim V, Isope P, Nadal J-P, Barbour B (2004) Optimal information storage and
258 the distribution of synaptic weights: perceptron versus Purkinje cell. Neuron 43:745–
259 757.

260 Chabrol FP, Arenz A, Wiechert MT, Margrie TW, DiGregorio DA (2015) Synaptic diversity
261 enables temporal coding of coincident multisensory inputs in single neurons. Nat
262 Neurosci 18:718–727.

263 Eccles JC, Ito M, Szentagotai J (1967) The cerebellum as neuronal machine. Berlin: Springer-
264 verlag.

265 Franklin K, Paxinos G (2007) The Mouse Brain in Stereotaxic coordinates, 3rd ed. Academic
266 Press, San Diego.

267 Grangeray-Vilmint A, Valera AM, Kumar A, Isope P (2018) Short-Term Plasticity Combines
268 with Excitation-Inhibition Balance to Expand Cerebellar Purkinje Cell Dynamic Range. J
269 Neurosci 38:5153–5167.

270 Isaacson JS, Scanziani M (2011) How inhibition shapes cortical activity. Neuron 72:231–243.

271 Mittmann W, Koch U, Häusser M (2005) Feed-forward inhibition shapes the spike output of
272 cerebellar Purkinje cells. J Physiol 563:369–378.

273 Quy PN, Fujita H, Sakamoto Y, Na J, Sugihara I (2011) Projection patterns of single mossy
274 fiber axons originating from the dorsal column nuclei mapped on the aldolase C
275 compartments in the rat cerebellar cortex. J Comp Neurol 519:874–899.

276 Shinoda Y, Sugihara I, Wu HS, Sugiuchi Y (2000) The entire trajectory of single climbing
277 and mossy fibers in the cerebellar nuclei and cortex. Prog Brain Res 124:173–186.

278 Valera AM, Binda F, Pawlowski SA, Dupont J-L, Casella J-F, Rothstein JD, Poulain B, Isope
279 P (2016) Stereotyped spatial patterns of functional synaptic connectivity in the cerebellar
280 cortex. Elife 5:e09862.

281 Vincent P, Marty A (1996) Fluctuations of inhibitory postsynaptic currents in Purkinje cells
282 from rat cerebellar slices. J Physiol 494 (Pt 1):183–199.

283 Xue M, Atallah B V., Scanziani M (2014) Equalizing excitation-inhibition ratios across visual
284 cortical neurons. Nature 511:596–600.

285

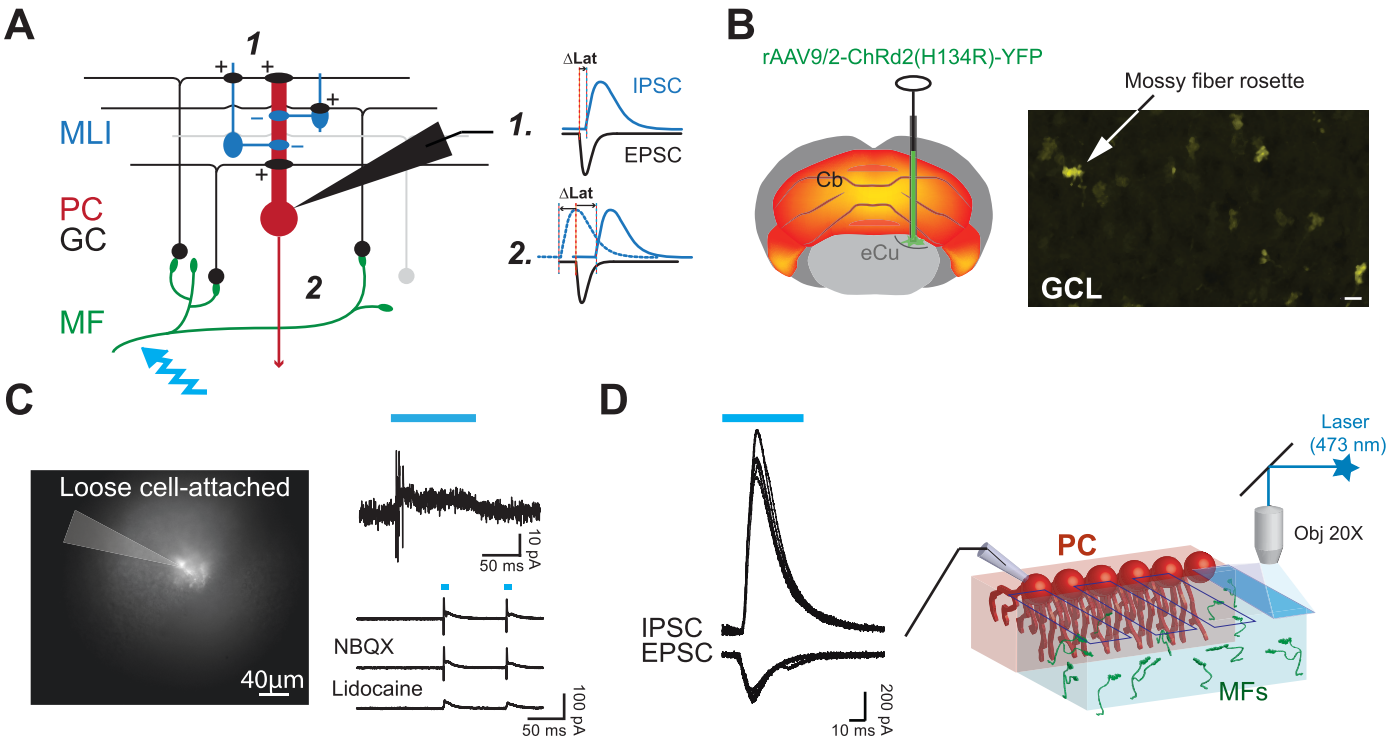
A
1
MLI
PC
GC
MF
2
1.
ΔLat
IPSC
EPSC
2.
ΔLat
B
rAAV9/2-ChRd2(H134R)-YFP
Cb
eCu
Mossy fiber rosette
GCL
C
Loose cell-attached
40µm
10 pA
50 ms
NBQX
Lidocaine
100 pA
50 ms
D
IPSC
EPSC
200 pA
10 ms
Laser
(473 nm)
Obj 20X
PC
MFs

Figure 1

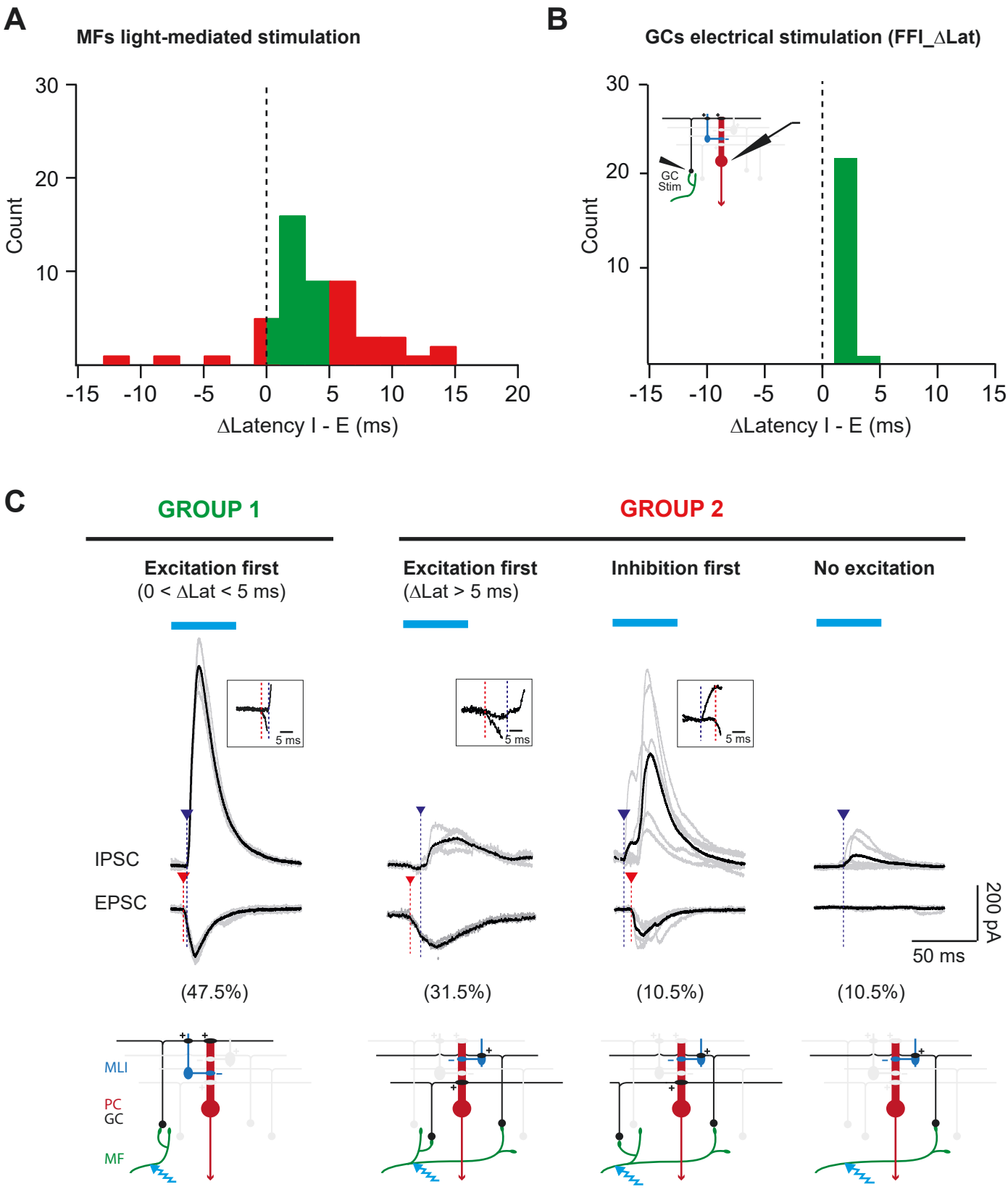
A
MFs light-mediated stimulation
Count
ΔLatency I - E (ms)
B
GCs electrical stimulation (FFI_ΔLat)
GC Stim
Count
ΔLatency I - E (ms)
C
GROUP 1
GROUP 2
Excitation first
(0 < ΔLat < 5 ms)
Excitation first
(ΔLat > 5 ms)
Inhibition first
No excitation
5 ms
IPSC
EPSC
200 pA
50 ms
(47.5%)
(31.5%)
(10.5%)
(10.5%)
MLI
PC
GC
MF

Figure 2

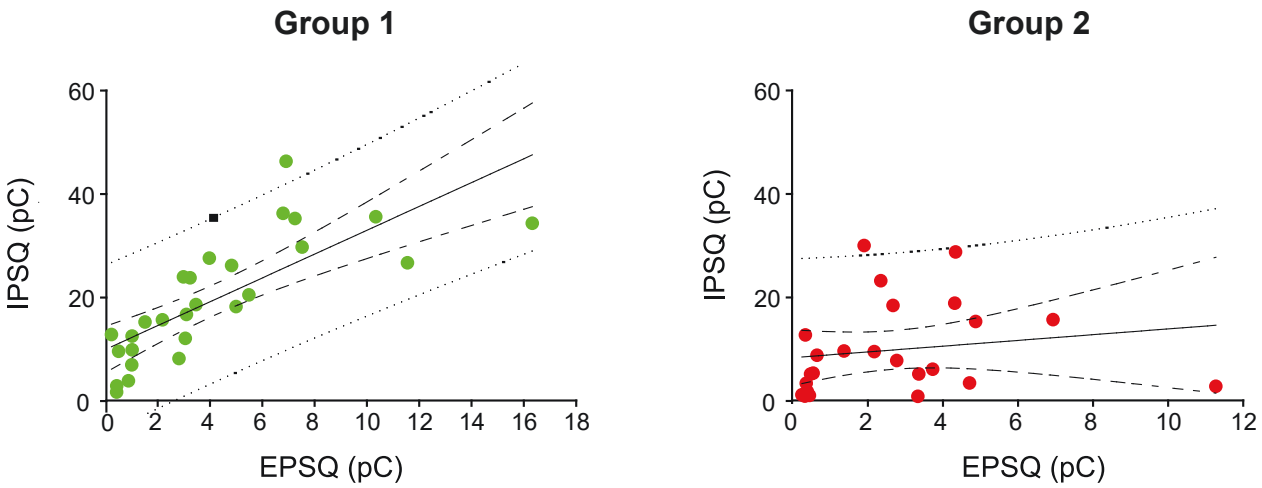

Figure 3

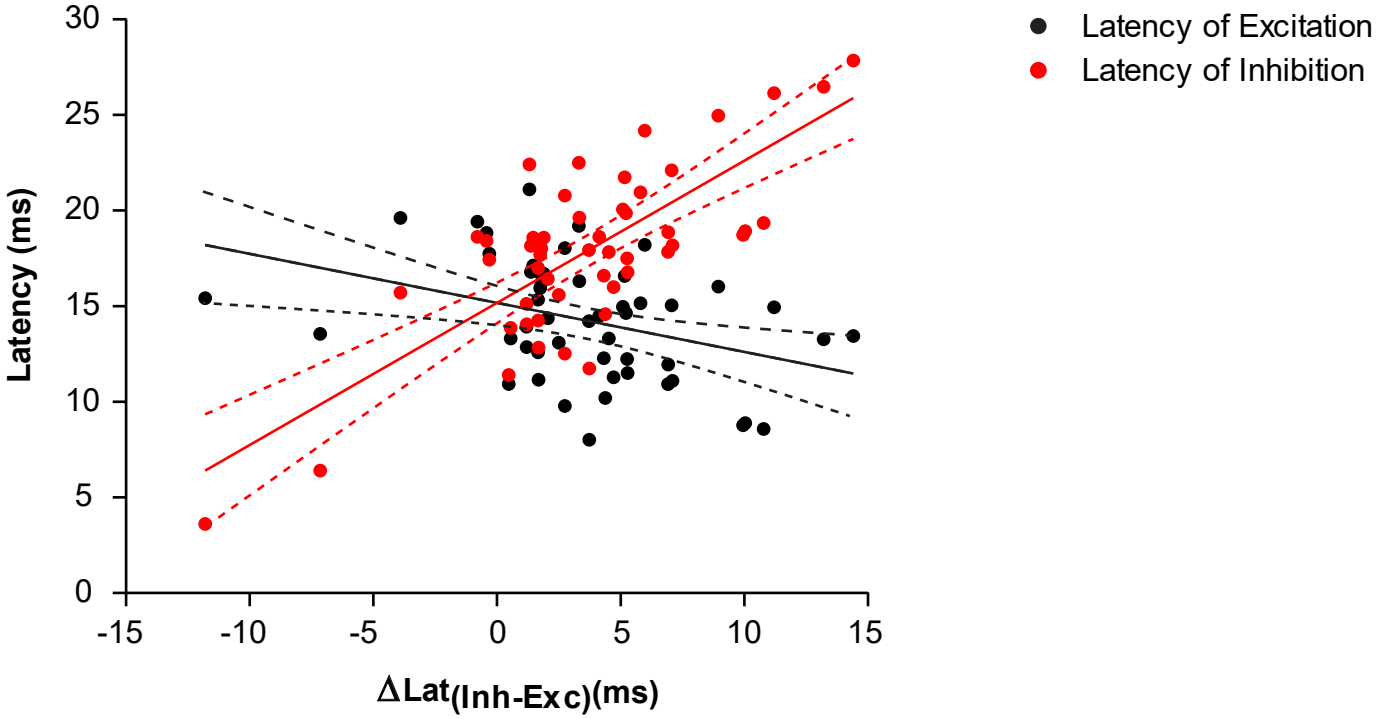

Figure 2 - Figure supplement 1

Scatter plot of the EPSC and IPSC latencies (from the beginning of the illumination) related to ΔLat. Linear regression line and confidence bands are superimposed (Inhibition: Pearson r = 0.76, r^2 = 0.58, p < 0.00001. Excitation: Pearson r = -0.37, r^2 = 0.14, p = 0.007)

6. Cerebellar modules and their role as operational cerebellar processing units

Apps R; Hawkes R; Aoki S: Bengtsson F [...]; **Spaeth L**; Sugihara I; Valera A; Voogd J; Wylie RD & Ruigrok TJH

The Cerebellum (2018) 17:654-682

The Cerebellum (2018) 17:654–682
https://doi.org/10.1007/s12311-018-0952-3

CONSENSUS PAPER

Cerebellar Modules and Their Role as Operational Cerebellar Processing Units

Richard Apps[1] · Richard Hawkes[2] · Sho Aoki[3,4] · Fredrik Bengtsson[5] · Amanda M. Brown[6,7,8] · Gang Chen[9] · Timothy J. Ebner[9] · Philippe Isope[10] · Henrik Jörntell[5] · Elizabeth P. Lackey[6,7,8] · Charlotte Lawrenson[1] · Bridget Lumb[1] · Martijn Schonewille[4] · Roy V. Sillitoe[6,7,8,11] · Ludovic Spaeth[10] · Izumi Sugihara[12] · Antoine Valera[10] · Jan Voogd[4] · Douglas R. Wylie[13] · Tom J. H. Ruigrok[4]

Published online: 6 June 2018

Abstract

The compartmentalization of the cerebellum into modules is often used to discuss its function. What, exactly, can be considered a module, how do they operate, can they be subdivided and do they act individually or in concert are only some of the key questions discussed in this consensus paper. Experts studying cerebellar compartmentalization give their insights on the structure and function of cerebellar modules, with the aim of providing an up-to-date review of the extensive literature on this subject. Starting with an historical perspective indicating that the basis of the modular organization is formed by matching olivocorticonuclear connectivity, this is followed by consideration of anatomical and chemical modular boundaries, revealing a relation between anatomical, chemical, and physiological borders. In addition, the question is asked what the smallest operational unit of the cerebellum might be. Furthermore, it has become clear that chemical diversity of Purkinje cells also results in diversity of information processing between cerebellar modules. An additional important consideration is the relation between modular compartmentalization and the organization of the mossy fiber system, resulting in the concept of modular plasticity. Finally,

✉ Tom J. H. Ruigrok
t.ruigrok@erasmusmc.nl

Richard Apps
r.apps@bristol.ac.uk

Richard Hawkes
rhawkes@ucalgary.ca

Sho Aoki
ktsky1020@yahoo.co.jp

Fredrik Bengtsson
fredrik.bengtsson@med.lu.se

Amanda M. Brown
amanda.brown@bcm.edu

Gang Chen
chenx007@umn.edu

Timothy J. Ebner
ebner001@umn.edu

Philippe Isope
philippe.isope@inci-cnrs.unistra.fr

Henrik Jörntell
henrik.jorntell@med.lu.se

Elizabeth P. Lackey
elizabeth.lackey@bcm.edu

Charlotte Lawrenson
pycll@bristol.ac.uk

Bridget Lumb
b.m.lumb@bristol.ac.uk

Martijn Schonewille
m.schonewille@erasmusmc.nl

Roy V. Sillitoe
sillitoe@bcm.edu

Ludovic Spaeth
lspaeth@inci-cnrs.unistra.fr

Izumi Sugihara
isugihara.phy1@tmd.ac.jp

Antoine Valera
antoine.valera@etu.unistra.fr

Jan Voogd
janvoogd@bart.nl

Douglas R. Wylie
dwylie@ualberta.ca

Extended author information available on the last page of the article

examination of cerebellar output patterns suggesting cooperation between modules and recent work on modular aspects of emotional behavior are discussed. Despite the general consensus that the cerebellum has a modular organization, many questions remain. The authors hope that this joint review will inspire future cerebellar research so that we are better able to understand how this brain structure makes its vital contribution to behavior in its most general form.

Keywords Cerebellum · Purkinje cells · Compartments · Climbing fibers · Mossy fibers · Zebrin · Aldolase C · Functional organization · Longitudinal stripes · Microzones

Introduction

> It is difficult to give a consensus of informed opinion because, although there is much informed opinion, there is rather little consensus. David Colquhoun (1971) Lectures on Biostatistics. Oxford, UK: Clarendon Press.

The cerebellum has long been considered as a uniform structure with well-organized in- and output relations that ultimately serves a particular adaptive control function that is mainly, if not completely, used for coordinating, modifying, adapting, and learning motor functions [1, 2]. By now, we have learned that the idea of an operational uniform cerebellar cortex needs to be revised [3]. In addition, the functional extent of cerebellar influence extends to cognitive, affective, and autonomic domains [4, 5]. Yet, although not completely resolved, one consideration that is generally accepted is that the basic operational unit is the cerebellar module. Each cerebellar module includes a longitudinal, i.e., (para-)sagittally organized, zone of Purkinje cells (PCs) in the cerebellar cortex that receives common climbing fiber input from a particular region of the inferior olive, and in turn, the same PCs target a discrete part of the cerebellar nuclei. This part of the nuclei is also targeted by collaterals of the same olivocerebellar axons that provide the climbing fibers to the zone of PCs, and harbors a population of small GABAergic neurons that project back to the same part of the inferior olive. This precise olivo-cortico-nuclear circuitry forms the core of individual cerebellar modules (Fig. 1). The basic cerebellar modules, A, B, C, and D, as defined by Voogd [7] have now each been subdivided into several smaller entities and in some cases, based on similar peripheral receptive fields, these have been shown to comprise yet smaller units, termed microzones, which are the cortical component of micromodules [6, 8–12].

Several decades ago, it became clear that the apparent uniformity of the cerebellar cortex masked underlying differences in the expression of a multitude of genetic markers in a broad transverse and finer parasagittally organized patterns, which are commonly referred to as stripes [8]. Much work has been devoted to describe the organization of the anatomically defined zones in relation to these biochemically defined stripes [13]. This interest has gained new impetus given the additional finding that differences in physiological properties can be related to this biochemical heterogeneity [14–17]. Such a finding raises the important possibility that individual cerebellar modules may not be uniform in their operation [3]. The current paper brings together up-to-date views on cerebellar modules. The general approach is at a systems level in order to understand the neural circuit basis of cerebellar modules and to establish to what extent they are functional entities and can fulfill functions that are independent of other modules.

Jan Voogd, who first used the term “cerebellar module” to describe the basic operational unit of the cerebellum, provides an historical synopsis. Izumi Sugihara subsequently reviews

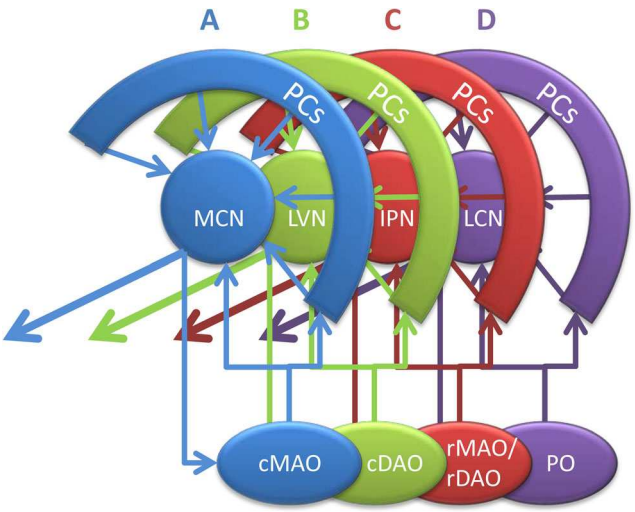

Fig. 1 Simplified diagram illustrating the four main modules of the right cerebellum seen from medial. The elementary modular connections are based on the projection of longitudinally arranged strips of Purkinje cells (PCs) to four main target nuclei and their olivocerebellar input from selective inferior olivary subnuclei. As such two vermal Purkinje cell zones (A and B) are recognized, together with their respective targets, the medial cerebellar nucleus (MCN) and lateral vestibular nucleus (LVN) and their sources of climbing fibers, caudal parts of the medial accessory (cMAO) and dorsal accessory (cDAO) olives, respectively. The C zones of the paravermis targets the interposed nuclei (IPN) and receives climbing fibers from the rostral (r) MAO and rDAO, while the D zones targets the lateral cerebellar nucleus (LCN) and receive from the principal olive (PO). Note that olivary subnuclei are also reciprocally connected according the same scheme. The interconnected olivocorticonuclear entity is referred to as module and each have a specific output. All modules (apart from the B module) have been further subdivided. Note that the modules of the vestibulocerebellum are not indicated in this diagram. Modified after Ruigrok [6]

his work on the relation between modules and several biochemical markers. His detailed scheme of the relation of olivocerebellar organization and the aldolase C (zebrin II) pattern is now widely used, but he also points to the shortcomings of the aldolase C pattern and the great potential that additional markers may have in studying both the development and the adult organization of cerebellar modules. Doug Wylie uses the vestibulocerebellum system in the pigeon to examine sagittally organized zones of PCs and how they modulate their activity in response to optic flow. Although these zones are present in lobule IXcd and in lobule X, their relation to the zebrin pattern of stripes differs, as there is no distinctive pattern in lobule X, whereas the same functional zones cover adjacent stripes of zebrin II-positive (ZII+) and zebrin II-negative (ZII-) PCs in lobule IX. This raises the important issue that zebrin alone is insufficient as a marker to describe the functional heterogeneity of PCs. Richard Hawkes subsequently explores the extent to which cerebellar modules can be divisible into their smallest processing units, leading to the idea of the "cerebellar quantum." As such, the cerebellar cortex may be made up of short strips or microzones (i.e., positioned within an anatomically defined zone or biochemically defined stripe) or, maybe, elongated patches, which, together, may comprise several thousands of individual processing units. Parallel processing power, positional coding, improving signal-to-noise ratios, and functional processing diversity are potential advantages of such modular processing. The question of what constitutes the basic functional unit of the cerebellum is also asked by Fredrik Bengtsson and Henrik Jörntell. However, they address this important question from a systems level physiological perspective and propose that the fundamental unit of the cerebellar cortex is a population of PCs located within a given microzone, working together as a "super PC." In pinpointing the cerebellar quantum (Hawkes) or the super PC (Bengtsson and Jörntell), both sections touch upon the role of mossy fiber afferents that show a more prominent transverse orientation but also adhere to modular organizational principles. This aspect is further discussed by Roy Sillitoe and colleagues who explore the relation between the organization of the mossy fiber systems, granule cells, and cortical interneurons.

These initial sections mostly deal with the anatomical foundations of the cerebellar modular functionality and are followed by sections that concentrate on their physiological properties. Martijn Schonewille reviews differences in several physiological properties of PCs with different molecular signatures. This significant recent development in cerebellar physiology is also highlighted by Gang Chen and Tim Ebner, who further explore the physiological and functional differences of modules based on ZII+ and ZII− stripes. Philippe Isope, Ludovic Spaeth, and Antoine Valera, on the other hand, return to the effect of mossy fiber input on plasticity within modular circuits and propose that modular identity may not be rigid but adaptable.

Exploring the fate of cerebellar modular output, Sho Aoki and Tom Ruigrok survey how this output is distributed and used by other areas—does the output from individual modules remain separated or can the outputs of different modules converge to be jointly processed in common receiving areas? Finally, Richard Apps and colleagues review recent developments on cerebellar involvement in emotional behavior. In line with the ideas developed in the previous section, they call attention to a body of evidence that the various modular constituents of the vermal A zone are connected to widespread brainstem and diencephalic (limbic) areas. They suggest that different components of the A module (possibly relating to micromodules) may carry out different, but orchestrated, aspects of an integrated emotional response.

Defining Cerebellar Modules (J. Voogd)

The term "modules" was first used for Purkinje cell zones defined by their cerebellar and vestibular target nuclei and their climbing fiber afferents by Voogd and Bigaré [18] in a paper read at a meeting in Montreal. Our paper was based on the work of Groenewegen et al. [19] and Bigaré [20]. Cerebellar modules, however, were recognized before this term was used by us. In Brodal's [21] study of the olivocerebellar projection in the cat and Jansen and Brodal's [22, 23] studies of the corticonuclear projection, the lobules were the units or modules in their description. As a byproduct, they described an intermediate zone, located in the anterior lobe hemisphere, lateral to the vermis, that, like the vermis, received an olivocerebellar projection from the accessory olives but projected to the interposed nucleus. This was the first definition of a longitudinal Purkinje cell zone as we know it today. Attempts to extrapolate the intermediate zone to more posterior parts of the cerebellum failed, because the authors did not recognize the loops in the folial chains in the posterior cerebellum (Fig. 2(a1)).

My contribution to the distinction of longitudinal Purkinje cell zones was based on the following considerations [26, 28]. Bolk's [25] description of the cerebellar vermis and hemisphere as folial chains with ansiform and (para-) floccular loops defined the topography of the Purkinje cell zones (Fig. 2(a2)). The distinction of anterior and posterior subdivisions in Brunner's [29] interposed nucleus and of dorsal and ventral subdivisions of the lateral cerebellar nucleus as target nuclei of the zones was based on the localization of the relatively small myelinated fibers from the posterior interposed nucleus in the medial one-third and of the larger fibers from the anterior interposed and the dorsal part of the lateral cerebellar nucleus in the lateral two-thirds of the brachium conjunctivum [30] (Fig. 2(b)). Finally, the observation of compartments in the white matter that channeled the

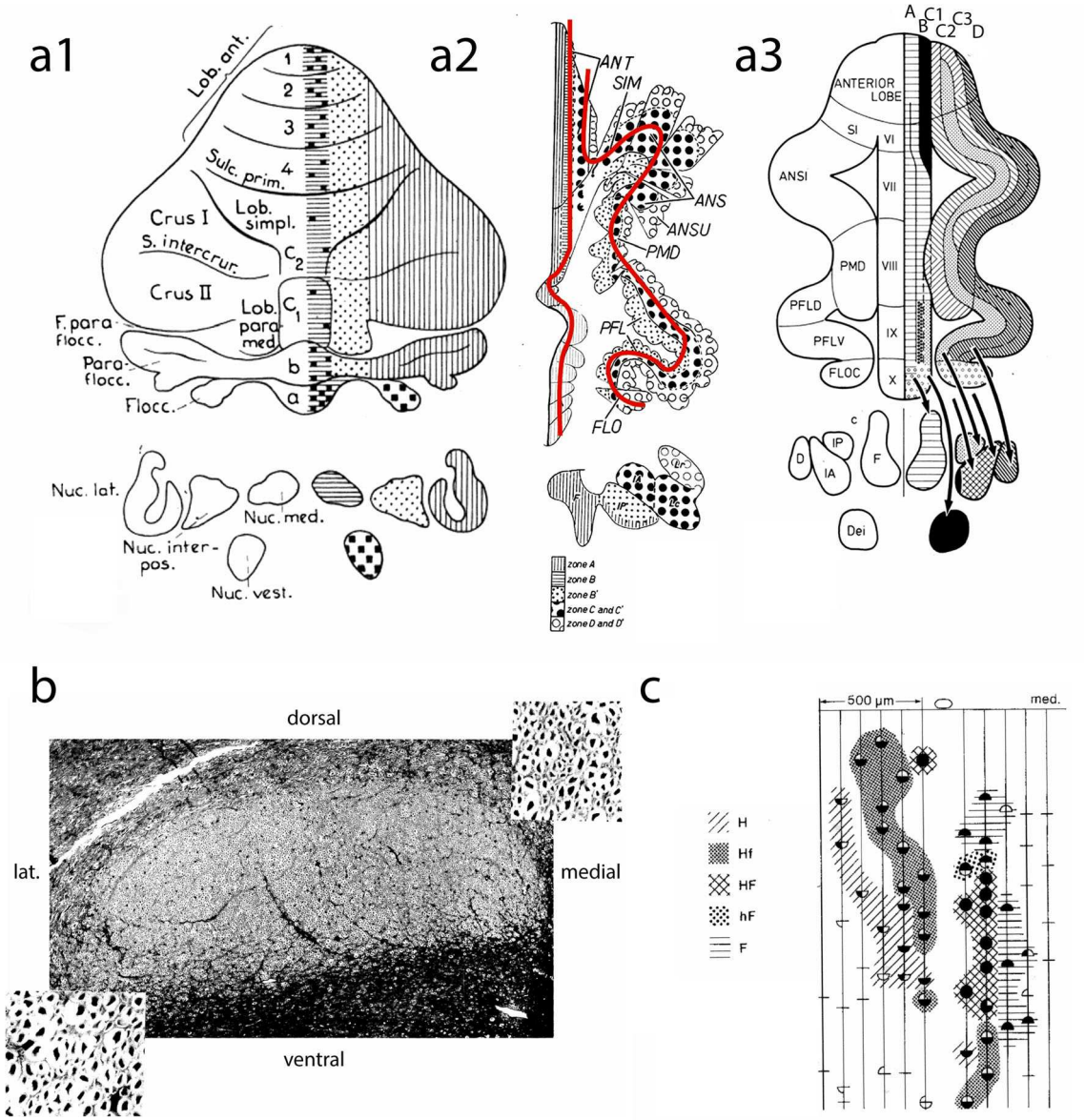

Fig. 2 **a1** Diagram of the corticonuclear projection of the cerebellum, showing the vermal, intermediate, and lateral zones of Jansen and Brodal [24]. Nomenclature of the lobules according to Bolk [25]. **a2** Diagram of the flattened cerebellar cortex of the cat showing the corticonuclear projection (after Voogd [26]). The red lines indicate the direction of the folial chains of vermis and hemisphere. **a3** Corticonuclear projection shown in diagrams of the flattened cerebellar cortex of the cat from Groenewegen et al. [19]. **b** Superior cerebellar peduncle of the cat, Häggqvist stain. Note small myelinated fibers in the medial third and coarse fibers in lateral two-thirds [after 24]. **c** Microzones with different climbing fiber inputs in the B zone of the cerebellum of the cat. Stimulation of the ipsilateral and contralateral ulnar and sciatic nerves results in Purkinje cells with similar responses in microzones as indicated by different hatching and stippling: H (hindlimb), Hf (mainly hindlimb), HF (hind- and forelimb), hF (mainly forelimb), F (forelimb), after Andersson and Oscarsson [27]. *ANS*, *ANSI* ansiform lobule; *ANSU* ansula; *D* dentate nucleus; *Dei* Deiters nucleus; *F* fastigial nucleus; *F. parafloc* parafloccular fissure; *FLO*, *FLOC* flocculus; *IA* anterior interposed nucleus; *IP* posterior interposed nucleus; *Lc. Lateral nucleus* pars convexa; *Lob. Paramed* paramedian lobule; *Lob.ant*, *ANT* anterior lobe; *Lob.simpl* simple lobule; *Lr*, *lateral nucleus* pars rotunda; *Nuc.interpos* interposed nucleus; *Nuc.lat* lateral nucleus; *Nuc.med*. medial nucleus; *Nuc.vest*. vestibular nucleus; *Parafloc* paraflocculus; *PFL*(D,V) paraflocculus (dorsalis, ventralis); *PMD* paramedian lobule; *S.intercrur* intercrural sulcus; *SIM*, *SI* primary fissure simplex lobul; *Sulc.prim*

Purkinje cell axons to their target nuclei provided an intrinsic coordinate system for the zones. The innervation of Purkinje cell zones by specific subdivisions of the inferior olive followed from the localization of their olivocerebellar fibers in the corresponding white matter compartments [7]. Their termination as longitudinal zones of climbing fibers was first shown by Courville et al. [31], the organizer of the Montreal meeting. As a consequence, seven zones were distinguished (Fig. 2(a3)). Two were located in the vermis. The medial A zone projecting to the fastigial nucleus, the lateral B zone to Deiters'

nucleus. In the hemisphere, the C1 and C3 zones that connect with the anterior interposed nucleus and C2 that projects to the posterior interposed nucleus replaced Brodal and Jansen's intermediate zone. The hemisphere was found to be composed of the two D zones that project to different parts of the dentate nucleus.

This simple zonal pattern was found to be inadequate after Hawkes and Leclerc's [32] discovery of the "stripy"' distribution of ZII+ and ZII− PCs. Apart from the identification of the B, C1, and C3 Purkinje cell zones as being positioned within ZII− stripes and the C2, D1, and D2 zones within ZII+ stripes, a number of narrow, ZII+ "satellite bands" were found to be present. These narrow bands, like their broad counterparts, are characterized by their climbing fiber afferents and, presumably, also by their corticonuclear projection [10, 33, 34]. The reconstruction of this more complicated map now serves as the standard reference for the description of zonal organization of the cerebellum [13].

Where the history of the Purkinje cell zones goes back to the early twentieth century [35], microzones made their appearance much later. They were first identified in the B zone of the cerebellum of the cat by Andersson and Oscarsson [27]. They consist of 50-mm-long and at least 200-μm-wide strips of PCs sharing the same climbing fiber receptive fields. The five microzones distinguished in the B zone differ in their input from forelimb or hindlimb nerves or a mixture of these nerves and the short or long latency of the response (Fig. 2(c)). The somatotopical localization in the B zone with the forelimb medially and the hindlimb laterally earlier was described by Oscarsson and Uddenberg [36]. Evoked potentials from the dorsal spino-olivary climbing fiber system [37] and the exteroceptive component of the cuneocerebellar mossy fiber system [38] are distributed in a similar, but more detailed microzonal pattern in the anterior lobe C3 zone of the cerebellum of the cat [39]. Overall, mossy fibers innervating these microzones had receptive fields resembling the climbing fiber receptive field defining that microzone [40].

What is the morphological basis for the microzones? The termination of mossy fibers in narrow longitudinal aggregates of rosettes in the granular layer was already described by Scheibel [41]. A similar, microzone-like distribution of individual climbing fibers was reported by Sugihara et al. [42]. The significance of the termination of mossy fibers in multiple longitudinal strips of mossy fiber terminals is difficult to understand, because this pattern would be erased by the parallel fibers [43]. Microzones, defined by their cutaneous receptive field of olivary mediated complex spike responses, thus far, only have been identified in the C1 and C3 zones of the anterior lobe. The microzone-like terminations of single or small groups of climbing and mossy fibers are present in the entire cerebellum. It would be interesting to know what these thousands or even millions of microzones in other parts of the cerebellum represent.

Molecular Labeling of Cerebellar Topographic Modules (I. Sugihara)

Correlation Between Molecular Expression and the Cerebellar Modular Structure

Cerebellar modules are basically defined by topographic axonal connections between subareas of the three major structures of the cerebellar system: cerebellar cortex, cerebellar nuclei, and inferior olive [6, 18]. Thus, the cerebellar system is compartmentalized into multiple modules, which are supposed to be the bases of different functional localization. These compartments, particularly those in the cerebellar cortex, are often characterized by the presence of a different profile of molecular expression, which can conversely be used to label compartments specifically.

Heterogeneous expression of some molecules, cell adhesion molecules in particular, has a significant role in the control of the aggregation and rearrangement of Purkinje cell subsets, and target specification and synaptic formation of afferent and efferent axons, which are essential for cerebellar module formation. However, the functional significance of the heterogeneous expression of many other molecules has not been clarified yet. The heterogeneous expression of molecules in cerebellar modules persists until adulthood in some cases, or newly emerges during the postnatal developmental stages and stays until adulthood in other cases. The correlation between the molecular expression pattern and the functional cerebellar modular organization is highly variable among molecules but usually conserved among individual animals for each molecule. Therefore, molecular expression pattern can be a useful genetic and histological tool to examine the anatomy and physiology of cerebellar modules. Its positional correlation to the cerebellar modular organization has been clarified for several molecules.

Zebrin (Aldolase C) Expression in Cerebellar Modules

A clear immunostaining pattern with high contrast between negative-positive longitudinal stripes was reported with a monoclonal antibody that recognizes originally unidentified antigen "zebrin II" (ZII) [44], which was later identified as the isozyme of glycolytic enzyme aldolase C. ZII (aldolase C) expression pattern is clearly correlated with cerebellar modules. Conventional modules A, B, C1, C2, C3, D0, D1, D2 and later added modules such as X, CX, X-CX [45] are located in identified ZII expression stripes in the rat [10, 34, 46] (Fig. 3, Table 1). Therefore, the ZII-striped pattern is very useful as a landmark structure for the cerebellar modules. However, ZII+ stripes are less useful as a modular boundary marker in a few areas in which ZII+ stripes are neighboring with themselves, as well as in neighboring ZII− stripes. For example, B, C1, CX, and C3 modules, which are generally ZII

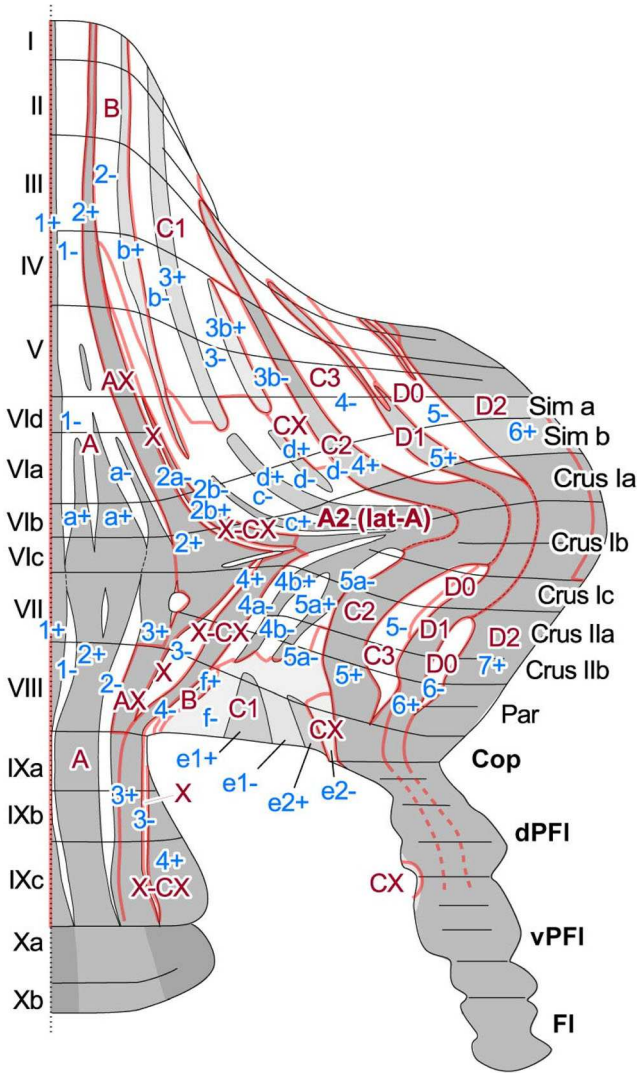

Fig. 3 Schematic of positional correlation between zebrin II (aldolase C) striped pattern and the cerebellar module mapped on the unfolded rat cerebellar cortex in the rat. Based on Sugihara and Shinoda [10]

−, are neighboring in the paravermal area in the anterior lobules and in lobule VIII (and its lateral extension copula pyramidis or copular part of the paramedian lobule). C2, D1, and D2 modules, which are generally ZII+, are neighboring in crus I and paraflocculus.

Expression of Other Molecules in Cerebellar Modules

Some molecules, such as excitatory amino acid transporter 4 (EAAT4) and phospholipase Cbeta3 (PLCβ 3), are expressed in the same striped pattern as ZII. Other molecules, such as PLCβ4, are expressed in a striped pattern that is completely complementary to the ZII pattern. Thus, the expression patterns of these molecules are correlated with cerebellar modules in a similar or complementary way to that of the ZII expression pattern.

Recently, the expression pattern of protocadherin 10 (Pcdh10) has been examined in the embryonic and postnatal mice [48]. This molecule is expressed strongly in four particular subareas in the embryonic cerebellum. In the later stages until adulthood, these subareas are integrated into the zonal organization of the cerebellar cortex. While the three medial Pcdh10-positive subareas are located within the A module and lateral A module in the adult cerebellar cortex, the most lateral Pcdh10-positive subarea (named "mid-lateral") is transformed exclusively into the complete C2 module in the paravermis. Thus, Pcdh10 is a specific marker for the C2 module in the paravermal cerebellum.

Visualization of the Modular Organization by the Molecular Expression Pattern

By labeling the molecule that is expressed in correlation with cerebellar modules, the morphological entity of cerebellar modules can be directly visualized, thereby facilitating analysis of the detailed spatial organization of modules. ZII stripes are generally shifted laterally in lobules VI–VII and crus I and negative stripes are absent in the apex of crus I. These characteristics of the ZII-striped pattern reconfirmed the proposed morphology of cerebellar modules in crus I, where modules are shifted laterally and C1, C3, or D0 modules are absent [46].

Module A, which covers nearly the whole vermis, is large. Lateral module A covers the paravermal area of simple lobule, crus I, crus II, and paramedian lobule. These modules contain both ZII+ and ZII− stripes. We proposed that within module A, the pattern of ZII stripes represent an organization of cerebellar compartments that is distinct in functional localization to some extent, and classified the stripes into three groups [10]. In other words, we proposed that the ZII-striped pattern within module A and lateral module A indicates submodular organization in these areas.

The modular organization makes an intricate complex in the paravermal cerebellar cortex. The composite of three main modules (C1, C2, and C3) and later-reported modules (X, CX, and X-CX) [45] has been confirmed in ZII stripes [47]. Within C1 module, several "lightly" ZII+ and ZII− stripes are recognized such as 3+ and 3b+ in the anterior lobe and e1+ and e2+ in lobule VIII. The Purkinje cells of these stripes are not as strongly labeled with ZII+ as the other zones, but nevertheless stand out within the ZII− stripes on either side of them. These lightly ZII+ stripes of the C1 module have specific topographic connections with slightly different areas in the cerebellar nuclei and the inferior olive [9]. Thus, these ZII stripes may represent a submodular organization as well.

Table 1 Simplified correlation between the cerebellar module and zebrin stripes. This table is based on studies in the rat [6, 10, 34, 46, 47]. See Sugihara et al. [47] for a more detailed description

Module (cortical zone)	Zebrin II (aldolase C) stripe		Topographic connection	
	lobules I–VI	lobules VII–IX	CN	IO
A	1+, 1−, a+, a−	1+, 1−, 2+, 2−	MN	cMAO
AX	2+	3+	MN	cMAO
A2	c+, c−, d+, d−	4b+, 4b−,5a+, 5a−	DLP	cMAO
B	2−	4−	LVN	dDAO
X	2a−	3−	ICG	cMAO
CX	3b−	e2−	PIN	cMAO
X-CX	2b+	4+	PIN	DMCC
C1	b+, b−, 3+, 3−	f+, f−, e1+, e−	AIN	vDAO
C2	4+	5+	PIN	rMAO
C3	4−	5−	AIN	vDAO
D1	5+	6+	LN	vPO
D0	5−	6-	DLH	DM
D2	6+	7+	LN	dPO

Experiments in Animal Models in Which Modules Are Visualized

Immunostaining of the cerebellar cortex after physiological recording or axonal labeling enables identification of the location of recording sites and axonal terminals into identified cerebellar modules. By this technique, synchronous complex spike activity in PCs within a module has been clarified [49]. Some different properties of PCs belonging to different modules have also become evident [50], as described in other sections of this article. Module-specific climbing and mossy fiber axonal projections have been revealed [10, 51].

Animals in which one of these molecules is visualized can be used in experiments of modules. We developed Aldoc-Venus mice in which mutated green fluorescent protein, Venus, is visualized in cells in which aldolase C (ZII) is expressed. The expression pattern of Venus accurately reproduces aldolase C expression. The striped pattern of aldolase C is not altered in Aldoc-Venus mice heterozygotes or homozygotes. Experiments about identified cerebellar modules are in progress by using aldoc-Venus heterozygous mice in vivo and in vitro. Tsutsumi et al. [52] used similar aldoc-tdTomato mice and recorded calcium signals, the rise of which is equivalent to a complex spike, from all PCs in multiple identified aldolase C stripes in the apex of crus II.

Conclusion

Identification of the positional correlation between the cerebellar modules and molecular expression patterns has clarified the morphological entity of the cerebellar module. Labeling of these molecules facilitates studies of module-specific axonal connections, neuronal activities, and developmental mechanisms. Thus, although the mechanisms or functional consequences of module-related molecular expression have not been fully clarified, an understanding of the functional significance of cerebellar modules has been advanced recently.

Optic Flow Modules in the Vestibulocerebellum of Pigeons (D.R. Wylie)

Self-motion of an organism through a world cluttered with visual stimuli results in “optic flow” across the entire retina [53]. This visual information is analyzed by retinal-recipient nuclei in the pretectum [54] and accessory optic system (AOS) [55], and reaches the vestibulocerebellum (VbC) via particular subnuclei in the inferior olive [56]. The VbC includes the flocculus, nodulus, and uvula, and is a site of visual-vestibular integration important for the generation of compensatory eye movements and the analysis of self-motion [57–59].

In birds, where the cerebellum essentially appears as a vermis without hemispheres [60], the VbC includes folia IXcd and X [61]. The optic flow information to the VbC originates in the pretectal nucleus lentiformis mesencephali (LM) and the nucleus of the basal optic root (nBOR) of the AOS [62–65]. The pigeon VbC shows many aspects of the classic modular organization of the cerebellum [18] as shown in Fig. 4a. The complex spike activity (CSA) of Purkinje cells (PCs) in the pigeon VbC responds best to particular patterns of optic flow resulting from self-translation or self-rotation through space, and these PCs are organized into sagittal zones across folia IXcd and X. As in mammals, CSA in the flocculus is modulated by rotational optic flow about either the vertical axis (VA neurons) or an horizontal axis oriented 45° to the

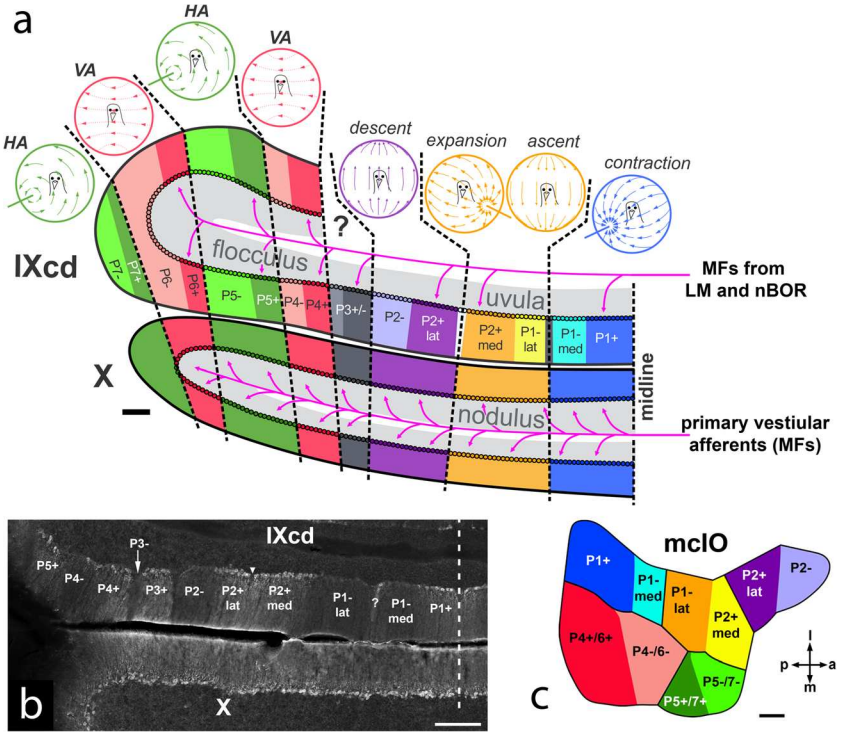

Fig. 4 **a** Diagram of the optic flow modules in the pigeon vestibulocerebellum (VbC; folia IXcd and X) (based on data from [66–69]. The lateral half of the VbC is the flocculus, the medial half is the uvula (IXcd)/nodulus (X). Each module is represented by a depiction of the optic flowfield that maximally excites the complex spike activity (CSA) of the Purkinje cells (PCs). The ZII+ and ZII− stripes in IXcd are also indicated. (All PCs in X are uniformly ZII+). There are seven optic flow modules, each spanning a ZII+/− stripe pair (see text for details). P3+/− PCs do not respond to optic flow. The magenta arrows indicate the primary vestibular afferents, which project as mossy fibers (MFs) to X. Magenta arrows also show the optic flow MF inputs from the nucleus of the basal optic root (nBOR) and pretectal nucleus lentiformis mesencephali (LM) to the ZII+ stripes in IXcd. **b** Coronal section through ventral IXcd and dorsal X, showing the ZII expression. The inverted triangle indicates the "notch" where PCs are absent, and bisects the P2+ stripe in to medial and lateral halves (P2+med, P2+lat). The "?" indicates a ZII+ stripe, 1 to 3 PCs in width, which similarly divides the P1−stripe (P1−med, P1−lat). The vertical dashed line indicates the midline. **c** Dorsal view of the medial column of the inferior olive (mcIO) and is color-coded to match the ZII stripes in (**a**), to indicate the topography of the climbing fiber projections (based on data from [32, 33]). *a* anterior, *p* posterior, *m* medial, *l* lateral. Scale bars: 200 μm in (**a**), 300 μm in (**b**), 100 μm in (**c**)

midline (HA neurons) [70–72]. In pigeon, there are two VA zones interdigitated with two HA zones [73]. In the uvula/nodulus, the CSA responds best to optic flow resulting from self-translation [66]. There are four response types organized into three sagittal zones. In the most medial zone, CSA responds best to optic flow resulting from translation backwards along an horizontal axis 45° to the midline such that there is a focus of contraction at 45° contralateral azimuth. Medial to this is a zone where the CSA responds best to optic flow resulting from either (i) forward translation along an horizontal axis 45° to the midline such that there is a focus of expansion at 45° ipsilateral azimuth, or (ii) upward translation along the vertical axis. Lateral to this is a zone where the CSA responds to the optic flow resulting from downward translation along the vertical axis [66]. A sagittal organization is also apparent with respect to the projection of PCs in the VbC: PCs in each of the optic flow zones project to particular regions in the vestibular and cerebellar nuclei [74–76]. Also, each of the optic flow zones receives climbing fiber (CF) input from particular regions of the medial column of the inferior olive (mcIO) [77, 78] (see also Fig. 4c).

A sagittal organization in IXcd is apparent with respect to the expression of Zebrin II (ZII; a.k.a. aldolase C [79]. As in mammals [44], ZII is heterogeneously expressed such that there are sagittal stripes of PCs exhibiting high ZII expression (ZII+) alternating with sagittal stripes of PCs that show little or no ZII expression (ZII−) [80]. In the VbC, there are seven stripe pairs (Fig. 4a). The most medial ZII− stripe, P1−, is bisected by a thin ZII+ stipe, such that P1− is divided into medial and lateral region (P1−med, P1−lat) (Fig. 4b). Similarly, the P2+ stripe is bisected by a notch that contains no PCs, effectively dividing the stripe in two halves (P2+med, P2+lat) (Fig. 4b). Using electrophysiological recordings combined with immunochemistry, we showed that the optic flow zones spans a ZII+/− stripe pair (Fig. 4a) [66, 67]. For example, the contraction zone spans P1+ and P1−med. As such, we consider that a ZII+/− pair represents a functional unit in the VbC, but what are the differences between the ZII+ and ZII−

stripes within the unit? We have shown that they receive CF input from separate, but adjacent areas of the mcIO (Fig. 4c) [81, 82], and there is some suggestion that the ZII+ and ZII− PCs have differential projections [76]. We have some evidence that the CSA of ZII+ PCs shows a greater depth of modulation to optic flow stimuli, compared to the ZII− PCs within the same functional unit [83]. This applies if one compares ZII− and ZII+ PCs in IXcd, and if one compares the ZII− PCs in IXcd with the PCs in X (all ZII+). The depth of modulation of ZII+ PCs in IXcd is not different to that of PCs in X [83]. Moreover, the ZII+ and ZII− stripes likely receive different mossy fiber (MF) inputs. Both nBOR and LM project directly to IXcd as MFs [62, 63], and the majority (~ 85%) of these terminate adjacent to the ZII+ stripes [68] (Fig. 4a). It is not known if other MF afferents target the ZII− stripes.

Note that the optic flow zones span folia IXcd and X, but the ZII stripes do not. Rather, all the PCs in X are uniformly ZII+ [80]. Folia IXcd and X also differ with respect to MF inputs. The optic flow MFs from nBOR and LM mentioned above innervate IXcd, but not X. In contrast, there is a primary vestibular projection to folium X, but not IXcd [69] (see Fig. 4a).

In summary, the pigeon VbC contains optic flow modules that are sagittally oriented and span folia IXcd and X. The classic sagittal zonal organization is apparent with respect to PC response properties, CF inputs, and PC projections. However, there is clearly a transverse component to the modules as well, since IXcd and X receive discrete MF inputs carrying optic flow and vestibular information, respectively. Finally, the modules clearly contain subregions defined by neurochemistry, as each module encompasses a ZII+/− stripe pair. Whether this type of modular organization applies to other parts of the cerebellum, or the VbC in other vertebrate classes, remains unknown.

The Cerebellum Quantum (R. Hawkes)

The modular nature of the cerebellar cortex suggests that it represents a map or family of maps, although what exactly is being "mapped" is less evident. The afferent topography is perhaps the simplest answer, in which case the map is fundamentally discontinuous in the sense that neighboring representations of body regions are neither anatomically nor physiologically continuous. What is the cerebellar "quantum"? In this context, the central idea is topographical equivalence: all cells in the "quantum" share a common chemistry, receive statistically identical inputs, project to the same target field(s), and have equivalent interneuron connectivity. Such a quantum would represent the smallest unitary processing unit.

Cerebellar modular architecture arose early in vertebrate evolution as the ground plan across birds and mammals is generally conserved. The largest cerebellar cortical compartments are the transverse zones (note that these are distinct from the sagittally oriented zones defined by olivocorticonuclear connectivity). In the mammalian vermis, four transverse zones are found in all species studied—the anterior zone (AZ), central zone (CZ), posterior zone (PZ), and the nodular zone (NZ) [84, 85] (in mouse a subdivision of the CZ has been identified—[86]: in birds, the ground plan has an additional transverse zone—the LZ [80]). Transverse zones evolve independently in response to different lifestyles (mosaic evolution). For example, in bats the echolocation centers in lobules VI/VII are accommodated by an expansion of the CZ—[87], and in the blind star-nosed mole, the CZ and NZ (visual receiving areas) are reduced and the trigeminal (star)-receiving areas (NZ and crus I/II) are expanded [88]. In sum, the cerebellar cortex comprises of the order ~ 10^1 transverse zones: in a mouse each of ~ 10^4 Purkinje cells (PCs).

Transverse zones are further divided into parasagittal stripes. How these stripes relate to the microzones identified by Oscarsson and his group [for review, see 88] is not certain: a tentative common framework is provided by the group of Voogd and Sugihara [10, 11, 13]. Stripes are discontinuous across transverse zone boundaries [85], suggesting that the earliest parcellation of the cerebellum during development is into transverse zones and subsequently these further subdivide into stripes. As is the case for zones, the number and variety of PC stripes is also not properly understood. The problem of how many stripes are present is exacerbated because many stripes revealed by ZII expression are, in fact, composite (e.g., heat shock protein-HSP25+/− subtypes within the ZII+ population [84]; PLCβ4+ sub-stripes within the ZII− population [89] etc.). As a consequence, the absolute number of stripes remains uncertain. Secondly, when molecular markers and mutant phenotypes are used in combination, some 10 PC subtypes can reliably be identified: this is likely an underestimate. By way of estimate, 5 transverse zones, each duplicated on either side of the midline, and 20 stripes per zone (based on connectivity plus chemistry) yields ~ 200 stripes per cerebellum, each comprising < 10^3 PCs in the mouse. This is almost certainly an underestimate.

Stripes are further subdivided into strings of patches. For example, tactile receptive field mapping of trigeminal representations reveals an elaborate mosaic of somatosensory patches (so-called fractured somatotopy: [90–92], which in some cases have been shown to align with ZII+/− stripe boundaries [93, 94]. A complementary heterogeneity was also revealed by Garwicz et al. [43], further dividing microzones in the anterior paravermis (C3) of the cat into multiple rostrocaudal patches. Possible anatomical correlates of patches—blebs (e.g., [95] and expression markers, such as NOS [96] and dystrophin [97]—confirm an elaborate parcellation of the granular layer. The upshot is the dicing of stripes into several thousand functional patches, each comprising ~ 10^2 PCs [98].

The cerebellar cortex is close to a pure feed-forward structure with little or no cross talk between neighboring stripes, so their proximity would seem irrelevant. However, this simplistic view may be wrong. Functional aggregates—limb inputs to the AZ, eye inputs to the flocculonodular lobes, trigeminal inputs to crus II, etc.—are found throughout the cerebellar cortex: indeed, this is the reality beneath the long-outdated idea of cerebellar homunculi. Such "neighborhoods" may be functionally critical due to MF data sharing via parallel fiber innervation.

So why does the cerebellum need a modular structure? We can suggest three reasons. First is the requirement for parallel processing. It is mandatory for the motor system to respond in a timely fashion and where there are so many degrees of freedom to control in an integrated manner serial processing is a non-starter. Hence, a highly parallel modular architecture has evolved to serve real-time motor control.

Secondly, the cerebellar cortex may exploit positional coding by assigning particular inputs to specific anatomical loci (limb inputs to stripes in the AZ; vibrissal inputs to patches in crus I/II, etc.). This re-encodes input modality as position (e.g., activation of a particular patch of crus II *ipso facto* implies ipsilateral vibrissal stimulation, etc.). Such positional coding ensures that minor sensory inputs are not dispersed and lost in the background noise. Positional coding also provides a substrate for the customization of the biochemistry once different patterns of gene expression are associated with particular zones, stripes, etc.; the door is open to regional specialization, tuning a stripe to its specific input/output requirements. Dozens of molecules are co-expressed differentially in stripes, both in the embryo and the adult. The question is—are the differences in stripe chemistry no more than genetic drift between paralogous PC populations or are they functionally significant? Evidence from several sources suggests that the latter option might be true (see the section by Chen and Ebner where the evidence is reviewed).

Thirdly, topographically equivalent quanta are a means to manage cerebellar signal-to-noise problems by exploiting the internal redundancy afforded by multiple, statistically identical PCs as a filter to generate a smoothed, more reliable output. The number of PCs needed—and hence the minimum quantum size—depends on how noisy each input is and how reliable the output needs to be.

In conclusion, the speculations above suggest that the cerebellar quantum is either a stripe (several hundred per cerebellum, each $< 10^3$ PCs in mouse) or a patch (several thousand per cerebellum, each $< 10^2$ PCs). This is not to imply that multiple quanta do not work in tandem to generate specific behaviors. First, perhaps cerebellar neighborhoods reflect a higher functional order—functionally related stripes/patches arrayed mediolaterally within a transverse zone and innervated by a common set of parallel fibers: stripes in the AZ processing forelimb signals also having access to hind limb information; vibrissal patches in crus I/II receiving contextual data about the lips and teeth, etc. Secondly, stripes may work as pairs—for example, ZII+/− stripe pairs in the pigeon NZ respond in concert to optic flow [79; and above]. Finally, multiple stripes may cooperate. Support for this view comes from data showing that networks of patches are linked by common MF inputs (see section by Spaeth et al.) and evidence that multiple stripes cooperate to control single muscles [99].

Is the Micromodule the Minimal Functional Unit of Cerebellar Processing? (F. Bengtsson and H. Jörntell)

Based on anatomical and physiological mapping studies, there are some indications to support this view, but also some caveats that prevent us from drawing a definite conclusion.

First of all, one needs to define the terms used to describe functional units of the cerebellum. The terms modules and micromodules have historically been used in a confusing non-conformative way and here we try to disentangle the terminology. The relationship between a module and a micromodule is that a module is a sagittal zone of cerebellar cortex, the parts of the inferior olive (IO) that supplies that zone with climbing fibers (CFs), and the subdivision of the cerebellar nuclei (CN) that the sagittal zone sends its Purkinje cell (PC) axons to. A micromodule, or what members of our lab originally referred to as a microcomplex, consists of a microzone within the sagittal zone (each sagittal zone may contain several 10's of microzones [100] and its associated subdivisions of the IO and CN [12, 40, 101]. The PCs of each microzone predominantly contact a small group of neurons in a specific CN subdivision, and here we refer to this set of neurons as a "micro-group." Similarly, the PCs of each microzone receive CFs from a small part of a specific subdivision of the IO, and we refer to this set of IO neuron as a "micro-part" [101].

To date, there is no evidence to support that different PCs of the microzone control specific CN cells within the micro-group. Rather, individual PCs diverge extensively in their projection to the CN and each CN cell receives a wide convergence of PC inputs [102]. The lack of differential CN cell control within the micro-group is the rationale for assuming that it is acting as one unit, which consequently has one functional contribution. Caveat to this assumption is if separate PCs within the microzone are eventually shown to have differential control of these CNs, or if the mossy fibers that drive the CN cells [103] split this group into smaller functional units. Notably, there is a specific relationship between the receptive fields of the mossy fiber input and of the PC-mediated CF input to the individual CN cell [103], which suggests that the mossy fiber input to the CN cell is defined by learning and can therefore be expected to be homogenous

for CN cells within the same micro-group. However, in the adult animal, the mossy fiber to CN plasticity do not seem highly active or easily induced [104], which of course does not contradict the possibility that it exists or that it might be highly active under development.

Although not included in the original concept of a micromodule, recent findings suggest that the inhibitory nucleo-olivary pathway should be included [105]. As the name suggests, the pathway originates in the CN and is under control of the PC output. A decreased PC firing will result in a disinhibition of the IO, thus forming a closed inhibitory feedback loop between the IO and the cerebellar circuit. The pathway seems to be zonally specific [106]. The spontaneous activity in the PCs is controlled by the level of IO input [107, 108]. Given that the assumption of a uniform micro-group of CN cells above applies, the total level of nucleo-olivary inhibition within a micromodule would be expected to be uniform and most of its PCs would have the same set point for their spontaneous firing activity. Different micromodules, however, may well have different levels of total nucleo-olivary inhibition and hence different levels of spontaneous PC activity. This scenario could work as an explanatory model for multiple reports that there are overall differences in the PC and CF activity between zebrin stripes [16, 17], as these appear to have a large degree of congruence with the functionally defined microzones [8].

The general idea that the modules of the cerebellum are functionally specific is supported by inactivation of specific areas of the IO, which results in functionally specific deficits in motor control [109]. The functional effects of the olivary inactivation can readily be explained as different modules predominantly project to different motor systems, i.e., vestibulospinal, tectospinal, reticulospinal, or rubrospinal systems as well as the corticospinal system [110]. For each micromodule, each CN micro-group can be expected to activate specific aspects of the function of the specific motor system for the module, which would be the cause of functional differences between micromodules. On the output side, each micro-group is divergent and contact strongly divergent upper motor neurons that in turn contact divergent spinal interneurons [111]. Yet, some center of gravity for which combinations of muscles each micromodule controls exists [99].

As every microzone has a specific function, assuming that it is the control of a specific set of muscles, for example, the PCs of the microzone will learn or potentiate specific mossy-/parallel fiber input that relates (sensory, motor, or sensorimotor) to the activation of that particular set of muscles. Depending on the specifics of a particular movement, different parallel fiber inputs will be active to a different degree and perhaps with a different temporal relationship to the CN output of the micromodule. Depending on the degree of correlation with the output effect of the CN group, subsets of parallel fiber inputs to PCs within a given microzone will be either potentiated or depressed. If the micromodule indeed is the minimal functional unit of the cerebellar circuitry, then the consequence is that the population of PCs in the microzone effectively is combined into one "super PC," which operates with the same micro-group of CN neurons. The advantage of a super PC would be that it provides the possibility to sample a much higher total number of mossy fibers, from which the mossy fibers with the highest possible correlations with the micromodule activity functions can be selected, to the control function of the micromodule than a single PC alone would be capable of.

Zonal Patterning of Mossy Fibers and Interneurons (A.M. Brown, E.P. Lackey, and R.V. Sillitoe)

Sagittal zones originate during early cerebellar development, and nearly all major cell types in the cerebellum respect the boundaries of zones [8, 112]. The zonal patterns of developing and adult Purkinje cells (PCs) have been extensively studied, but we are far from fully understanding how mossy fibers and the various types of interneurons are restricted within the zonal framework. This is an intriguing problem to consider from a circuit perspective because mossy fibers form mono- and disynaptic connections to each class of interneurons in the cerebellar cortex.

Mossy fibers project from over two-dozen brainstem and spinal cord nuclei. Functionally similar mossy fibers terminate on granule cells within the same transverse domains in the cerebellar cortex. Within these transverse domains, mossy fiber terminal fields organize into parasagittal zones that have a reproducible anatomical relationship with olivo-cortico-nuclear modules. In contrast to climbing fibers, which terminate on just one or two contralateral zones of PCs, mossy fibers branch to terminate in multiple bilateral zones [113]. Furthermore, sensory information from different mossy fiber sources can converge onto single granule cells [114]. Cues derived from Purkinje cell clusters are thought to provide the organizational scaffold for the zonal distribution of both climbing fibers and mossy fibers. Purkinje cell clusters initially express transient parasagittal molecular markers as early as E14 in mice. Although Purkinje cell and climbing fiber patterning starts early, mossy fiber arrival in the cerebellum spans mid-embryonic and postnatal development [115]. This suggests that a protracted relationship might exist for module patterning to occur. Indeed, mossy fibers directly contact PCs through the second postnatal week in mice [116]. This idea is consistent with data showing that mossy fibers do not exhibit clear-cut zones until after birth [117]. Despite the clear heterogeneity of mossy fiber terminal field domains, their zones are generally broader and not as sharply defined as those of climbing fiber projections or the PCs [6]. Adding to

this complexity is that mossy fiber receptive fields, mapped by recording granule cell responses to tactile stimuli, reveal multiple sensory representations of body parts in mosaic patches that form a "fractured somatotopy" [91, 93]. This complexity is mirrored in the organization of the mossy fiber targets, the granule cells. Granule cells are also restricted to transverse and parasagittal patterns of gene expression and these patterns are reflected by abnormalities detected after various experimental manipulations [96, 118–120]. Granule cell progenitors arise from the rhombic lip and proliferate in the external granular layer (EGL). Despite potential molecular differences in the progenitor populations, it is not clear how lineage influences the final patterning of granule cells. However, it seems that temporal mechanisms may distinguish broad transverse domains such that specific granule cells are fated to specific lobules [121]. It is also possible that interactions between the EGL progenitors and/or recently differentiated granule cells and Purkinje cell signals may direct parasagittal granule cell patterning. Between E11 and E14 in mice, cells arising from the rhombic lip travel to the EGL where, under the control of Purkinje cell signals, the EGL expands through progenitor proliferation. Granule cells must then traverse past the Purkinje cell dendrites and somata in order to reach what will become the granule cell layer [112]. During this time, Purkinje cell parasagittal zones could influence granule cell molecular phenotypes. It has also been suggested that mossy fibers might play an active role in patterning granule cell zones [120]. Interestingly, granule cell parallel fiber projections are also patterned relative to the Purkinje cell map (see section by Isope, Spaeth, and Valera).

Similar to granule cells, the excitatory unipolar brush cells also exhibit transverse and parasagittal zonal restriction. After they are born, unipolar brush cells migrate through the white matter en route to lobules IX and X, and by adult they localize to the granule cell layer [122]. Differential molecular expression distinguishes them into three subtypes, calretinin+, mGlrR1α+, and PLCβ4+, and mGlrR1α− and PLCβ4+, which all respect the parasagittal Purkinje cell zones [123]. There is compelling evidence to suggest that PCs have a large impact on the distribution of unipolar brush cells. For instance, unipolar brush cells lose their restriction to lobules IX and X when normal Purkinje cell patterning is disrupted by genetic lesions (e.g., via the deletion of *Ebf2*: [124]).

Much less is known about the zonal patterning of the inhibitory interneurons. Golgi cells, for example, exhibit molecular restriction in the anterior-posterior axis with some degree of morphological restriction to parasagittal zones. There are multiple molecular subtypes of Golgi cells, but so far, only the subtype expressing ZAC1 is known to be restricted to the posterior zone [125]. Golgi cell apical dendrites, which ascend into the molecular layer and contact parallel fibers, respect the borders of Purkinje cell parasagittal zones. Fewer than 3% of Golgi cell dendrites cross the borders of Purkinje cell zones and, though mechanisms have been suggested for this restriction, it is not clear how this relationship develops or is maintained [126].

Least is known about the patterning of basket and stellate cells in the molecular layer. Like Golgi cells, basket and stellate cells could exhibit a morphological restriction to zones wherein, particularly for basket cells and less so for stellate cells, their axons extend in the parasagittal plane. This may result in restriction of the inhibitory influence of the basket or stellate cells to specific zones [127, 128].

To achieve this restriction, it is possible that the parasagittal orientation of basket and stellate cell axons could have followed the spreading of Purkinje cell clusters into zones during cerebellar development. This argument is supported by the idea that modules might have their origins in the earliest stages of cerebellar development and therefore cells that are born later in cerebellar development, such as interneurons, develop within a circuit that is already committed to a zonal map. The outcome of these multicellular rearrangements plus the targeting of mossy fibers to the cerebellar input layer is thought to be modulation of Purkinje cell simple spikes via parallel fiber projections [129]. Both the frequency and regularity of simple spikes are dynamic during postnatal development and consistent with the maturation of parallel fiber synapses and establishment of mature Purkinje cell zonal expression patterns [129]. The maturation process of zones is mediated by spontaneous activity and sensory experience, which may intersect with genetic programs to integrate or sculpt mossy fibers into modules [112]. Ultimately, however, the formation and function of an operational module may depend on several factors including regional variations in Purkinje cell morphology, Purkinje cell packing density, granule cell packing density, neuronal soma size, intrinsic Purkinje cell firing properties, synaptic plasticity, the positions of mossy and climbing fiber synapses within their target layers, the distributions of the various cerebellar interneurons, and perhaps even glia [3].

Modular Gene Expression Relates to Physiological Properties and Information Processing (M. Schonewille)

A wealth of anatomical and immunohistochemical data has revealed the modular organization of the cerebellum and its chemical landmarks, as described above. The efforts to understand the physiological and functional features of this organization have thus far not matched that. This section will discuss the progress made so far in analyzing the differences at the physiological level between modules in relation to the differential gene expression patterns.

Module-Related Differences in Purkinje Cell Physiology

One of the first proteins to receive attention in this respect was excitatory amino acid transporter 4, EAAT4, which is expressed in Purkinje cells (PCs) in pattern similar to zebrin II (ZII) [130]. In ZII+ PCs, the synaptic transport current is several fold larger than in ZII− PCs [14]. Due to the absence of EAAT4, mGluR1 (metabotropic glutamate receptor 1) currents are larger and mGluR1-dependent long-term depression (LTD) is more likely to occur in ZII− PCs. Conversely, long-term potentiation (LTP) could be induced selectively in patches of ZII+ PCs using high-frequency stimulation of parallel fibers in vivo [15], which will be described in the next section. Interestingly, in another dataset, the climbing fiber evoked EPSCs and complex spikes in ZII+ PCs were found to be larger despite the presence of more EAAT4, suggesting that climbing fibers also participate in the modular differentiation [131].

Not only plasticity, but also the most basic physiological cell property, firing rate, appeared to differ between cerebellar regions in vitro [132]. Indeed, in vivo, ZII− PCs in mice fire simple spikes at ~95 Hz, while ZII+ PCs on average fire at ~60 Hz during quiet wakefulness [17, 133] (Fig. 5a, b). This difference in firing rate is largely intrinsic to PCs and could be significantly reduced by blocking TRPC3 [17] (Fig. 5d, e). TRP channels are known to be the effector channels of mGluR1 [cf. 87, 134] and are part of a pathway including PLC, PKC, and IP3R1, which all have zebrin-related expression patterns. Similar experiments comparing ZII− and ZII+ areas in anesthetized rats confirmed the higher simple spike firing rate in ZII− PCs [16]. In this study, Xiao et al. observed a higher coefficient of variation (CV) for simple spikes in ZII− PCs. However, the use of anesthetics affects the regularity of PC firing [135], potentially explaining why the opposite result, higher regularity in ZII+ PCs, was found in awake mice [133]. Common finding in both studies is that some variations in other parameters are not related to zebrin patterning, suggesting further heterogeneity in PCs [50, 133, 136]. Overall, these results confirm a module-related differentiation of PCs, the sole output of the cerebellar cortex.

Climbing fiber input from the IO affects simple spike activity, both on longer and shorter timescales [137, 138]. In anesthetized rats, the impact of a complex spike was similar in both ZII+ and ZII−, but the effects were more prominent in ZII+ PCs [50]. In mice during quiet wakefulness, the effects appear to be related to the cerebellar modules. ZII+ PCs display changes in all directions, while ZII− PCs only show suppression or no change [17]. When TRPC3 is blocked, this restriction is removed and ZII− PCs show all types as well, suggesting that TRPC3 is also involve in post-complex spike effects on simple spikes [17].

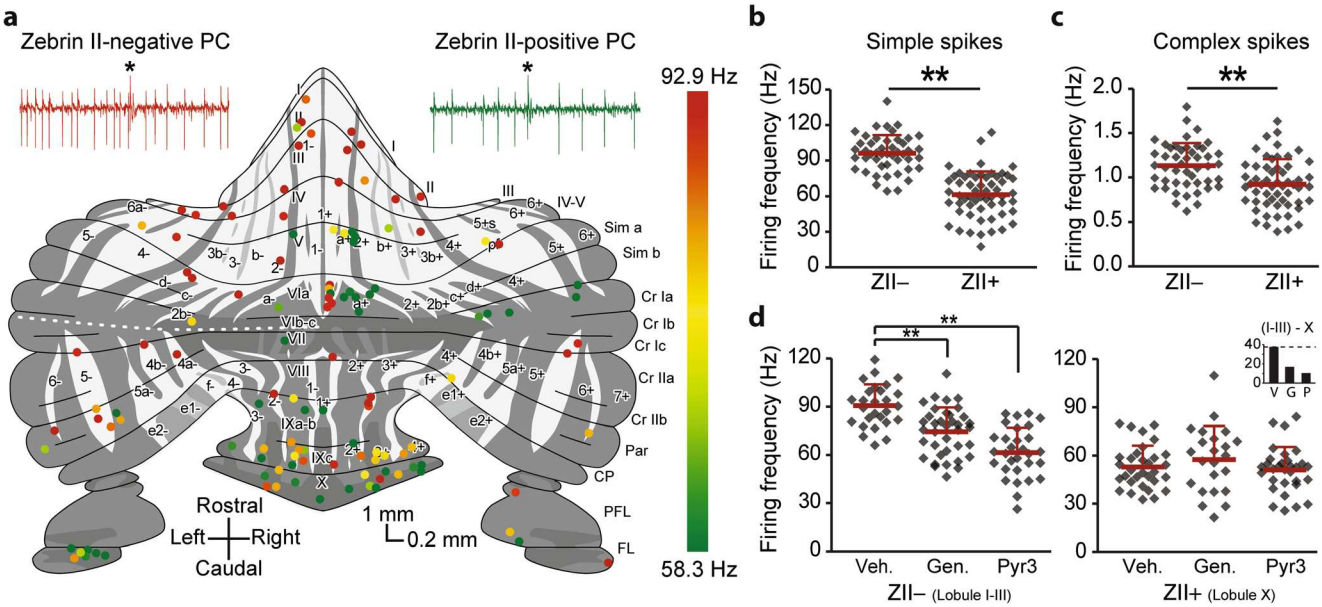

Fig. 5 Physiological difference between zebrin-identified cerebellar modules. **a** Schematic drawing of unfolded cerebellar surface, adapted from [66–69], depicting post-mortem immunohistochemically determined recording locations of PC, with color-coded simple spike firing rate. Note the higher firing rate in ZII− PCs and the consistent presence of the difference, even in nearby pairs. **b** Summary of (**a**) demonstrating the significant difference in average simple spike firing rate between ZII+ and ZII− PCs, recorded in vivo. **c** Complex spike firing rates show a similar difference, with higher firing rates in ZII- than in ZII+ PCs. **d** Pharmacological block of TRPC3 with two difference blockers, genestein, and pyr3, selectively affects PC simple spike activity in ZII− PCs, indicating the contribution of TRPC3 to creating this difference

Module-Related Differences in Other Parts of the Olivocerebellar Circuit

Other parts of the olivocerebellar circuit also show zebrin-related differences. Complex spikes directly reflect the activity in the inferior olive. Theoretically, the higher simple spike rate in ZII− modules should provide stronger inhibition of the CN [139, 140], which would then disinhibit the IO [141–144], although the effects of this inhibition appear more complex [145, 146]. The prediction holds, as the complex spike rate is indeed higher in ZII− PC in awake mice [17] (Fig. 5c), although this was not confirmed in anesthetized rats [16]. Traditionally, the complex spike was considered to be an all-or-none phenomenon with a fixed underlying composition [147, 148], but there are functionally relevant temporal and spatial variations in its properties and consequences [149–151]. Some variations can be linked to the zebrin-based subdivision: the number of spikelets, for instance, correlates selectively in ZII− PCs with the simple spike firing rate, in rat [50]. The absence of this correlation in monkeys [152] could be due to species differences or related to the population with mixed zebrin identity. Together, these data suggest that the differentiation of physiological activity is present in at least two out of three nodes in the olivocerebellar circuit.

The question remains if the differentiation underlies fundamental differences in information processing and ultimately in function. The higher firing rate and preference for LTD [14] in ZII− PCs [16, 17] versus the lower rate with preferred LTP [15] in ZII+ PCs suggest this is indeed the case. In fact, some experimental evidence is in line with this concept. Eyeblink conditioning has been linked to ZII− PCs [153] that have a high resting rate, which is suppressed during the conditional blink [154–156]. In contrast, compensatory eye movement adaptation depends on ZII+ PCs in the flocculus (see, e.g., Fig. 3) that have a low resting rate and show potentiated activity during the adapted response [157].

Taken together, the current literature demonstrates that two out of three elements in the olivocerebellar circuit, the inferior olivary neurons and PCs, have distinct physiological properties that correlate with the zebrin-identified cerebellar modules. The differences are present at the level of cellular activity and interaction between inputs, both in the form of direct interactions and prolonged plastic changes. Future experiment should clarify the differentiation at the level of the cerebellar nuclei and determine the computational and ultimately functional relevance of this differentiation.

Physiological Correlates of Zebrin II Parasagittal Zones (G. Chen and T.J. Ebner)

As detailed in the contributions to this consensus paper by Voogd, Sugihara, and Hawkes, a dominant feature of the cerebellum is its longitudinal architecture as defined by the parasagittal organization of its afferent and efferent projections and by the molecular compartmentalization of these parasagittal zones (see Figs. 2 and 3). Although highlighted by the expression of zebrin II/aldolase C (ZII), the parasagittal organization involves a host of other molecules, expressed on PCs in either a ZII+ or ZII− banding pattern of stripes [8, 158] [8, 158]. Importantly, many of these molecules control neuronal excitability, for example EAAT4 and mGluR1 subtypes.

The contribution by Schonewille describes recent studies on the differential firing characteristics of PCs in ZII+/− stripes, with the key observations that the spontaneous simple spike and complex spike firing rates are higher in ZII− than in ZII+ stripes (see Fig. 5 and Table 2) [16, 17]. Several of the firing differences are intrinsic to PCs as they persist when synaptic inputs are blocked, either pharmacologically or genetically [17]. The mGluR1 signaling pathway associated with ZII− PCs plays a role. However, neither EAAT4 nor aldolase C contributes to the intrinsic differences in firing rates, both of which are expressed in a ZII+ pattern. Building on the Schonewille review, this section focuses on two additional aspects of the physiological properties of ZII+/− stripes: responses to afferent inputs and synaptic plasticity.

Zebrin II+/− Stripes Respond Differentially to Various Inputs

Spinocerebellar and olivocerebellar afferent pathways activate parasagittally oriented responses in the cerebellar cortex [94, 159, 163, 164]. Simultaneous recordings reveal that climbing fiber input activates PCs in parasagittal zones with a rhythmicity of 6–10 Hz [165–167]. Optical imaging shows that inferior olive or peripheral stimulation evokes a marked parasagittal banding pattern that aligns precisely with the underlying ZII+ stripes (Table 2) [159, 160]. The bands are primarily due to climbing fiber input as they are optimally activated by 6–10 Hz peripheral stimuli and blocked by silencing the inferior olive. Two-photon imaging examining the relationship between ZII expression and synchrony at the single cell level observed that greater complex spike synchrony occurs among neighboring ZII+ or ZII− PCs but not across these two populations [52]. However, the stripes are not static, as sensory input increases the synchrony across ZII+/− boundaries in the awake animal.

Several factors contribute to the parasagittal responses including differences in (1) topography of climbing fiber and mossy fiber inputs to the cerebellar cortex and (2) intrinsic properties of the afferents, PCs, and molecular layer interneurons. Here, we concentrate on the intrinsic properties. Climbing fiber inputs to ZII+ stripes release more glutamate and generate larger, longer-duration AMPA-mediated excitatory currents in PCs than in ZII−

Table 2 Functional difference between zebrin banding architectures

	Zebrin II+	Zebrin II−
Spatial pattern of activation	1. Parasagittal bands evoked by peripheral and inferior olive stimulation [159, 160] 2.Off-beam inhibitory bands evoked by PF stimulation [128] 3. mGluR1 mediated long latency patches by PF stimulation [15]	1. Less off-beam inhibition [128] 2. Peripheral stimulation evoked patches between EAAT4 bands [161]
CF-PC synaptic transmission	More glutamate released per CF action potential and longer EPSC [131]	
PC firing properties	1. Lower SS and CS firing rates [17] 2. Greater SS firing variability [16] 3. Higher incidence of SS suppression and oscillations following CS [17] 4. SS firing correlates with CS spikelets [50]	1. Higher SS and CS firing rates [16, 17] 2. More regular SS firing [16] 3. Greater relative SS pause following CS [16, 50]
Synaptic plasticity	1. No LTD [14] 2. LTP of mGluR1 mediated long latency patches [15, 162]	1. Robust LTD [14]

stripes (Table 2) [131]. These differences in climbing fiber responses are largely presynaptic in origin and due to a larger pool of release competent vesicles and enhanced multi-vesicular release. In addition to the differences in climbing fiber afferents, the molecular specialization of PCs contributes to the parasagittal response pattern. In Crus II, the patch-like responses to peripheral stimuli are closely aligned to bands that express lower levels of EAAT4 (Table 2) [161], suggesting that PC responsiveness is controlled by the degree of glutamate uptake. Differences in EAAT4 expression also contribute to whether mossy fiber input evokes beam-like or patch-like responses [161]. Furthermore, several of the differences in PC simple spike firing, including the greater kurtosis and positive skewness in ZII stripes, appear input-driven [50].

Parallel fibers (PFs), the bifurcated axons of granule cells in the molecular layer, extend for 3–5 mm along the long axis of a folium and make glutamatergic synapses with the dendrites of PCs and cerebellar interneurons. In many folia, PFs cross several parasagittal bands and it is generally assumed that PFs provide for relatively uniform, short-latency activation of their postsynaptic targets [168]. However, PCs in ZII+/− stripes respond differently to PF input (Table 2) [15, 128]. Flavoprotein and Ca^{2+} imaging show that PF stimulation evokes an excitatory on-beam response and a compartmentalized off-beam response consisting of parasagittal bands of decreased fluorescence [128]. These off-beam bands are in register with ZII+ stripes, blocked by $GABA_A$ receptor antagonists, associated with inhibition of PCs and spatially modulate the response to peripheral inputs. Also, PF stimulation evokes mGluR1-dependent patches of increased fluorescence at very long latencies that are aligned with ZII+ stripes [15, 162]. Therefore, the ZII striping pattern modulates the responses to both peripheral and PF inputs.

Zebrin II+/− Purkinje Cells Have Different Synaptic Plasticity

PCs in Z+/− stripes exhibit different levels of synaptic plasticity. Conjunctive stimulation of PF and climbing fiber inputs results in long-term depression (LTD) of PF synapses on PCs and LTD plays important roles in motor learning [169]. Intriguingly, LTD was not observed in lobule X that uniformly expresses ZII+ and a high level of EAAT4 (Table 2) [14]. Conversely, robust LTD occurs in lobule III that is primarily ZII− and has low levels of EAAT4. The zonal expression patterns of mGluR subtypes and EAAT4 act to reduce the mGluR1 responses in PCs and prevent the induction of LTD. Increased EAAT4 levels in ZII+ stripes enable faster clearance and limit glutamate diffusion [14, 131]. Also, long-term potentiation (LTP) of PF synapses on PCs can be evoked by several induction protocols [15, 170, 171]. While less well studied than LTD, one difference has been reported for the LTP of the long-latency patches evoked by PF stimulation [15]. In response to theta burst PF stimulation, the long-latency patches, which are aligned with ZII+ bands, show dramatic LTP that is both mGluR1 and PLCβ dependent [15, 162].

In summary, the parasagittal compartmentalization of PCs has strong counterparts in physiological function that includes differential responsiveness to inputs, intrinsic excitability, and synaptic plasticity. Of the possible PC signaling pathways, to date mGluR1s and EAAT4 have been shown to have the more prominent roles in shaping the physiological differences between ZII+/− stripes. However, lacking is a unifying hypothesis on what functions these intrinsic differences play in the cerebellum's role in motor and non-motor functioning. What is needed are studies that identify the specialized information processing occurring in ZII+/− stripes during behavior and determine how those unique computations are used by the cerebellum.

Toward a Description of the Functional Modular Organization of the Cerebellar Cortex (P. Isope, L. Spaeth, and A. Valera)

In this section, we will review how the interplay between the mossy-fiber (MF)/granule cell (GC)/Purkinje cell (PC) pathway and the olivo-cerebellar system determines a functional modular organization.

Cerebellar Modules and MF Projections in the Cerebellar Cortex

Previous sections have established that cerebellar modules are essentially defined by the olivo-cerebellar loop. The cerebellar cortex is divided into a large number of parasagittal bands subdivided into 100–200-μm-wide "microzones" that contain PCs excited by CFs driven by the same peripheral inputs [11, 172–174]. Since the stimulation of restricted areas of the cerebellar cortex [175] or the cerebellar nuclei [176] evokes movements of the receptive fields from which sensory inputs originated, a segregated information processing is potentially maintained throughout the olivo-cerebellar system [12]. Furthermore, CFs gate long-term plasticity induction at the GC-PC synapses [177, 178], a major site for information storage in the cerebellum suggesting that microzones may work as paralleled processing units for motor learning [179]. However, a pure parallel processing is unlikely for several reasons. First, individual microzones project on different targets (see section by Aoki and Ruigrok) suggesting that a given body area receives information from many microzones. Secondly, the anatomical organization of the MF-GC-PC pathway [2], which convey the afferent copy of the motor command or the planned action (from the cerebral motor, premotor and frontal cortices via the pontine nuclei) and the current status of the body (from the spinal cord), compromises a strict parallel information processing [180–184]. Indeed, MFs project onto GCs that contact hundreds of PCs in the same lobule via their parallel fibers (PFs) [185, 186] and transmit the information to several microzones in the transverse plane. Also, a wealth of tracing studies have demonstrated that in many areas of the cerebellum, MFs send a high number of collaterals in the GC layer both in the transverse (e.g., projection from the lateral reticular nucleus, dorsal column nuclei, and pontine nuclei) [187, 188] and in the sagittal orientation (e.g., collaterals of the dorsal spino-cerebellar tract targeting both lobule I–III and VIII) [189], suggesting that a given input is heavily redundant in the cerebellar cortex. Moreover, in a given GC layer area, MF from different sources overlap even at the level of individual GCs [114, 190, 191]. For example, in the anterior lobe of the vermis, MF inputs from the dorsal spino-cerebellar tract (hindlimb), the external cuneate (forelimb/shoulder), the cervix (forelimb, neck, and upper trunk), and from the pontine nuclei, overlap [113, 123]. The MF-GC pathway is therefore highly divergent and favors combinatorial processing and pattern discrimination as suggested by Marr and Albus, and Ito [2, 192, 193]. This organization must promote the communication between cortical microzones via the PFs and might determine a coordinated PC output to the cerebellar nuclei. Because adjacent microzones can express different zebrin markers leading to specific physiological properties and/or plasticity (see sections by Hawkes, Chen and Ebner, Schonewille), we can postulate that PFs multiplex modules are involved in specific tasks.

The Functional Cortical Module: a Spatial Code

Paradoxically, although MF projections are redundant and overlapping, several groups demonstrated that microzones have the same MF and CF receptive fields (i.e., from the same body area) [174, 194, 195], some of them even suggested that local MF inputs represent the major and unique input to PCs through the ascending GC axon [195]. On the contrary, in vitro and in vivo studies have identified dense and localized distant synaptic connections between PCs from a given microzone and the MF-GC pathway belonging to another microzone [161, 196–199]. In fact, all these results can be reconciled by the fact that 85% of the GC-PC synapses are silent [197], that a limited number of GC layer sites are heavily connected to a given microzone [196, 199], and that PCs are always contacted by local GCs as a non-conditional input [195, 199, 200]. Furthermore, zebrin stripe identity may also account for local vs. distant communication [161] through the level of glutamate transporter (see section by Chen and Ebner). Strikingly, in the anterior vermis, the functional synaptic organization between microzones at the GC-PC and GC-molecular interneurons (MLIs) synapses is conserved among mice [199]. Bands of neighboring PCs (60 to 120 μm width) display the same GC input maps with local and distant clusters of GCs densely connected (dense clusters of GCs have been also observed recently in vivo [201–203]). These conserved networks define functional modules (with super PCs as proposed in the section by Bengtsson and Jörntell) in the cerebellar cortex that do not necessary match anatomical CF and MF input boundaries and zebrin stripes (Fig. 6). Activity-dependent mechanisms can also modify these maps through the awakening or the depression of GC-PC synapses [199]. Therefore, functional modules adapt under behavioral control. Altogether, these findings highlight the specificity of the MF/GC/PC functional maps and the communication between identified microzones, which define a spatial code of related modules. In this context, we should then refine our definition of the cerebellar modules and consider microzones as the anatomical modules while specific combinations of GC, MLI, and PC groups distributed in several location of the cerebellar cortex define the functional correlate of these modules (Fig. 6).

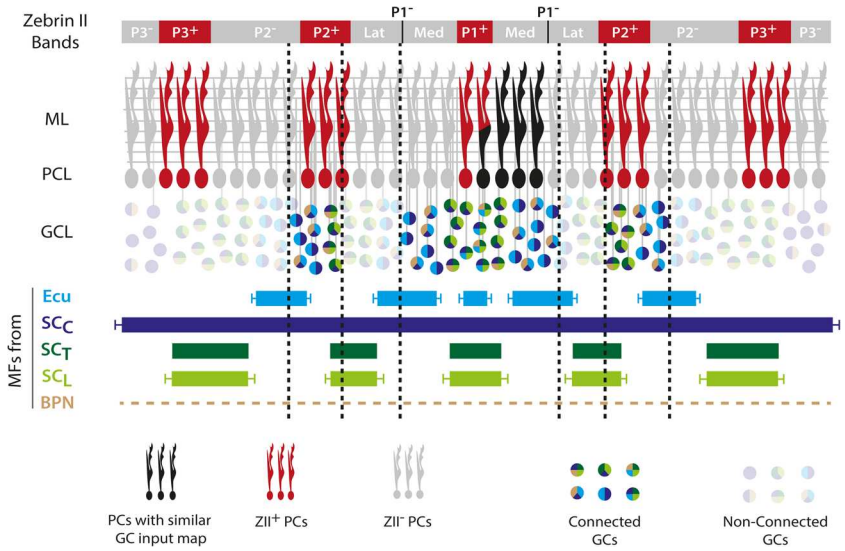

Fig. 6 An example of a functional Purkinje cell module in the lobule III–IV of the cerebellar cortex. GC clusters belonging to different microzones (identified by the zebrin band pattern in red and gray) communicate with specific groups of PCs (one example in black). In this example, a group of PCs (120 μm width spanning P1− and P1+ zebrin stripes) close to the midline receives GC inputs from ipsilateral and contralateral P2+, ipsilateral and contralateral median P1− and P1+ microzones. This organization is conserved across mice. Each GC cluster receives specific MF inputs from different precerebellar nuclei and modalities (identified by the color in the GC pie chart). MFs projections in the GCL are complex and redundant. The other GCs remain silent or unconnected (shaded pie chart). This functional module does not necessarily fit with the anatomical boundaries given by the CF and MF inputs. *ML* molecular layer, *PCL* Purkinje cell layer, *GCL* granule cell layer, *MFs* Mossy fibers, *Ecu* external cuneate, *SCL* lumbar part of the spinocerebellar tract, *SCT* thoracic part of the spinocerebellar tract, *SCC* cervical part of the spinocerebellar tract, *BPN* basal pontine nuclei, *CFs* climbing fibers, *MFs* mossy fibers, *PCs* Purkinje cells, *GCs* granule cells. Adapted from [113, 199]

The Functional Cortical Module: a Temporal Code

This functional spatial modular organization of the MF/GC/PC pathway might influence temporal coding in PCs. Indeed, the temporal organization of the MF discharges, which span a wide range of frequencies in different cerebellar lobules, strongly influences the output of the GC layer [190, 204–210]. During high-frequency bursts of MF inputs, temporal summation may favor an explosive integration and a high signal-to-noise ratio as GCs may be excited by only one or two different MFs [205, 209]. Several studies have also demonstrated that burst of stimulation at frequency up to a kHz are reliably decoded both at the MF-GC and at the GC-PC synapses [211–213]. At lower frequencies, for example in the vestibular cerebellum, the combination of several sources of MFs with pathway-specific short-term synaptic plasticity leads to a precise temporal code in targeted GCs [190]. Finally, GC discharges in the clustered GC groups are gated by the Golgi cells through a double mechanism: (1) a feedback inhibition through the ascending axon of the GCs [214] as a gain control mechanism and (2) a feed-forward inhibition through the MF-Golgi cell pathway that increases the saliency of the MF signaling by improving the reproducibility of the GC firing [207]. Therefore, there is strong evidence that clusters of GCs at a given location respond to a specific spatio-temporal configuration of MF inputs. Since GC clusters are specifically connected to bands of PCs, this arrangement may control and broadly synchronize identified modules.

In conclusion, recent advances have described adaptive functional modular information processing in the cerebellar cortex. Combinations of MF inputs that activate local or distant clusters of GC in specific sequences are selected by groups of neighboring PCs that define a functional cortical module (Fig. 6). The selection process is gated by the CF inputs targeting these PCs. The dynamical interactions between these functional modules determine the collective pattern of discharge at the PC output layer and define a population code of a given behavioral component [215].

Output of Cerebellar Modules (S. Aoki and T.J.H. Ruigrok)

Although exhaustive research has provided many details of the anatomical, chemical, and physiological characteristics of cerebellar modules, it is still not clear how these modules contribute to improved learning and execution of all kinds of movement [3, 6, 12]. In particular, it is not simple to envision the precise function of a given module and to understand how, or to what extent, different modules operate independently or need to cooperate for optimal behavioral output. If, as is generally assumed, individual modules can be seen as operational entities, each module is expected to participate in a different

functional aspect of cerebellar control [4, 12, 216]. Indeed, the output of every cerebellar cortical zone of Purkinje cells (PCs), or microzone, by way of its converging projections to a specific location in the cerebellar or vestibular nuclei, is subsequently fed into a specific array of different nuclei in the brainstem and diencephalon [217, 218]. However, tracing studies also indicate that projection patterns of different cerebellar nuclei can have the same target area or that different regions of the same cerebellar nucleus can select rather different goals [218, 219].

Furthermore, although it seems quite clear that the nucleo-olivary projection stems from a class of small GABAergic cerebellar nuclear neurons that are mostly intermingled with the other projection neurons [220, 221], the latter neurons project and collateralize to functionally rather diverse areas ranging from upper spinal cord to diencephalon [222, 223]. From these projection targets, it can be surmised that an important part of the cerebellar output is fed back into the cerebellum by way of a multitude of feedback circuits. Not only can cerebellar output directly impact the cerebellar cortex by way of nucleo-cortical collaterals [224–226], but reverberating loops are also found by projections to precerebellar centers such as the magnocellular red nucleus (involving the cerebellar nuclei), the basal pontine nuclei (involving mostly the cerebellar cortex), or the reticulotegmental nucleus of the pons (involving both nuclei and cerebellar cortex) [227–230]. Moreover, both direct (i.e., nucleo-olivary projection) and indirect circuits (involving midbrain nuclei) link cerebellar output to the inferior olive [141, 145, 231]. Different modules make use of different or different combinations of these feedback reentrance circuits. For example, the GABAergic output of all modules is directed to their respective part of the inferior olivary complex [141, 232], whereas especially the ZII+ stripes seem to make use of an excitatory olivary connection by way of midbrain nuclei such as the parvicellular red nucleus and the nuclei of Bechterew and Darkschewitsch [13]. More elaborate circuitry involving the thalamus, cerebral cortex, and basal pontine nuclei also seems to operate [233, 234]. Between all these different targets, such as thalamus and medullary reticular formation, profuse collateralization of nuclear efferents is observed [222, 223]. In this respect, it is hard to understand how this system of diverging and partly converging connections is being used in an integrated way to result in coordinated learning and execution of movements, cognitive and affective behavior, or visceral functions [4, 235].

Best-known examples of the functional properties of cerebellar modules are illustrated by the ample bulk of research studying the adaptive control of reflexive eye and head movements. Here, individual floccular modules control movements around a particular visual axis [82, 236, 237]. However, it should be noted that also in the vestibulocerebellum, several non-adjacent zones seem to be present with basically the same function [71]. Furthermore, apart from floccular control of eye movements, cerebellar control of saccades stems from the flocculus, quite different cerebellar regions control saccades and voluntary eye movements [238, 239]. This would inevitably result in a multimodular control of individual eye muscles, with each module dealing with a certain aspect of control.

This aspect was also demonstrated in a study in rat in which several hind- or forelimb muscles were injected with a transneuronally transported rabies virus (RABV). Retrograde RABV infection of PCs occurred by way of initial infection of reticulospinal, vestibulospinal, and rubrospinal pathways. In this way, it was shown that several cerebellar modules contribute to the control of individual muscles. For example, injection of the anterior tibial muscle of the rat initially resulted in infection of PCs that control the lateral vestibular nucleus (B zone, Fig. 7a), but subsequent zonal infection of PCs that contact the medial cerebellar nucleus, anterior interposed nucleus, and dorsolateral hump established that all these zones (and modules) all seem to be involved in the control of this muscle. Injecting its antagonist (e.g., anterior tibial muscle), to some extent, resulted in infection of the same PCs, although differences were also observed [99]. As the transneuronal transport of RABV depends on the number (and strength) of the synaptic steps within a particular pathway, the cerebellar impact on other routes than the rubro-, vestibulo-, and reticulospinal pathways, such as the corticospinal pathways, on these muscles could not be studied [99].

For this reason, we have recently made RABV injections in different places of the sensorimotor cortex of the rat, with the intention of studying the cerebellar modular involvement in processes that take place in the cerebral cortex. The survival time was carefully chosen to not exceed third-order labeling. In this way, after first-order RABV infection of the thalamic relay, and second-order infection of cerebellar nuclear neurons, third-order RABV infection of PCs was identified in various places of the cerebellar cortex (Fig. 7b). The main result here was that injections centered in either primary (M1), or secondary (M2) motor cortex or primary somatosensory cortex (S1), all resulted in multiple, zonally arranged, aggregates of RABV-infected PCs [241]. As these aggregates were observed in vermal, paravermal, and hemispheral regions of the cerebellum, it was concluded that the information from different cerebellar modules converges to a particular cerebral domain, suggesting that cerebellar modules cooperate not only through controlling several descending bulbospinal systems but also through interactively impacting cortical sensorimotor processing (Fig. 7c).

The Cerebellar A Module and Emotional Behavior (C. Lawrenson, B. Lumb and R. Apps)

The cerebellum is typically recognized for its role in movement coordination and motor learning, but increasing

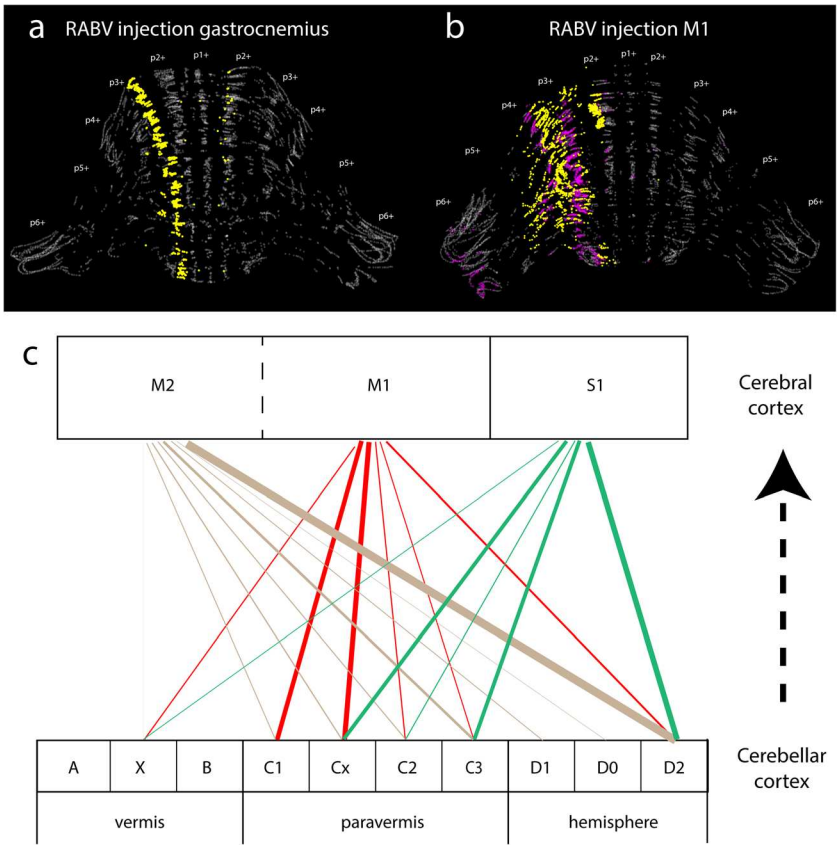

Fig. 7 Multiple modules collaborate in sensorimotor processing. **a** Superimposed stack of plots of 10 serial (1 out of 4), 40-μm-thick sections showing RABV−/ZII+ Purkinje cells (gray), RABV+/ZII− (yellow), and RABV+/ZII+ (magenta) Purkinje cells in the rat anterior lobe 120 h after injection of RABV in the gastrocnemius muscle (case 1010). Note that a prominent band of RABV+/ZII− Purkinje cells is seen between the P1+ and P2+ zebrin stripes, which mostly is territory of the B zone [240]. The main zebrin+ stripes (p1+ to p6+) are indicated. **b** Similar superimposed stack of 12 plotted sections 70 h after injection in M1 (case 1151). Note that three separated clusters of RABV infected Purkinje cells are recognized: a vermal one just lateral of P2+, a large paravermal cluster that encompasses P3+, P3−, P4+, P4− zebrin stripes and a hemispheral cluster lateral within the P6+ strip. **c** Diagram showing multimodular impact of cerebellar zones on three sensorimotor regions. Line thickness is shown relative to 100% of total number of RABV labeled Purkinje cells in the anterior part of the cerebellum (modified after [241]). Modular identity is inferred from its relation with the zebrin pattern [11, 99]

evidence suggests it may also be involved in higher-order functions, including emotional behavior [4, 242, 243]. As described in the previous section, anatomical pathway tracing studies in animals have found that the cerebellum projects to an extensive list of brainstem and diencephalon nuclei, including a number of limbic structures [244–247]. In humans, structural and functional abnormalities can sometimes lead to impaired mood regulation and anxiety disorders (the cerebellar cognitive affect syndrome) [248–252]. In addition, neuroimaging studies have found changes in BOLD signal in the human cerebellum during fear learning paradigms [for review see 253]. In many cases, such changes are associated with the midline cerebellar vermis [249, 254, 255], and experimental studies in animals have found that lesions and other interventions of this cerebellar compartment have effects on defensive behaviors evoked by emotionally salient events [256–264].

The cerebellar vermis primarily consists of the "A" module. Individual modules are defined by their olivo-cortico-nuclear projections. In the case of the A module, the cortical parasagittal zonal component receives olivocerebellar (climbing fiber) input from the caudal medial accessory olive, and the Purkinje cells (PCs) located within this region of cortex have a corticonuclear output to the medial (fastigial) cerebellar nucleus [8, 45, 265]. This medial nucleus has widespread connections to midbrain and cerebral cortical regions including the amygdala, hypothalamus, periaqueductal gray (PAG), striatum, prefrontal cortex, parietal cortex, and hippocampus [218, 245–247]. Other cerebellar modules (notably the lateral vermal B and paravermal C3 modules) have been shown to be subdivided into smaller units, the cortical component of which are termed microzones [9, 27, 100, 101]. As discussed in previous sections, microzones and their micromodular connections are thought to represent the basic functional units of the cerebellum. Given that a finer grain olivocerebellar topography is present within the broader A module [266], this suggests a micromodular organization may also be present in this region of the cerebellum (see also section by Sugihara). Since emotional behaviors involve an

integration of cognitive, somatomotor, and autonomic activity, this raises the possibility that different parts of the A module (possibly corresponding to micromodules) may be associated with different aspects of a coordinated emotional response.

To date, most studies have not attempted to explore cerebellar contributions to emotional behaviors at the modular (or micromodular) level of resolution. However, large cerebellar lesions involving vermal lobules III–VIII have shown various behavioral changes in relation to fearful or predator-prey interactions in rats. These include (i) fewer signs of fear when animals were placed in a brightly lit arena versus a dimly lit arena; (ii) decreases in freezing behavior and other signs of fear in the presence of a cat; (iii) faster recovery time than controls to the neophobic response to a novel taste test; and (v) attenuated spontaneous predation of mice [261, 264].

Some evidence for a lobular organization has also been found. For example, lesions of the anterior cerebellar vermis (lobules III–VI), but not the hemispheres resulted in impaired acquisition and retention of fear-conditioned bradycardia [256, 257]. Moreover, a subpopulation of PCs was found to respond to the conditioned stimulus, and in some cases this activity was correlated with the magnitude of the conditioned bradycardia response [267]. However, Supple et al. [267] did not investigate the possibility of correlated activity with other aspects of defensive behaviors, which might be expected if a finer grain localization of function was present.

In relation to human studies, a meta-analysis of fMRI mapping of the cerebellum supports a role for the human anterior lobe (vermal lobules IV and V) in fear learning and affective state [see review by 251]. And Sacchetti and colleagues found that reversible inactivation of a similar region in rats impairs the consolidation of fear memories [259, 263, 268]. By comparison, regions of the posterior lobe vermis appear to be involved in different aspects of behavior. In particular, it has long been known that vermal lobules VI and VII are important in the control of saccadic eye and head movements in a range of species including humans (the oculomotor vermis) [239, 269–273], while lesions of vermal lobule VIII in rats results in deficits in innate and conditioned fear induced freezing behavior but no detectable changes in general motor activity [258, 274]. By contrast, vermal lobules IX and X are related to autonomic functions including regulation of blood pressure, heart rate, respiration, and the baroreceptor reflex [275, 276].

Thus, different cerebellar vermal lobules (that may relate to different components of the A module) appear to be associated with different aspects of an integrated array of behaviors. From rostral to caudal: lobules IV–VI with fear memory and affective state; lobule VI–VII with orientation of gaze; lobule VIII with fear-induced freezing behavior; and lobule IX and X with cardiorespiratory control (Fig. 8). Different parts of the A module, possibly relating to individual micromodules, could therefore regulate and integrate the cognitive, motor, and autonomic aspects of fear-related behavior.

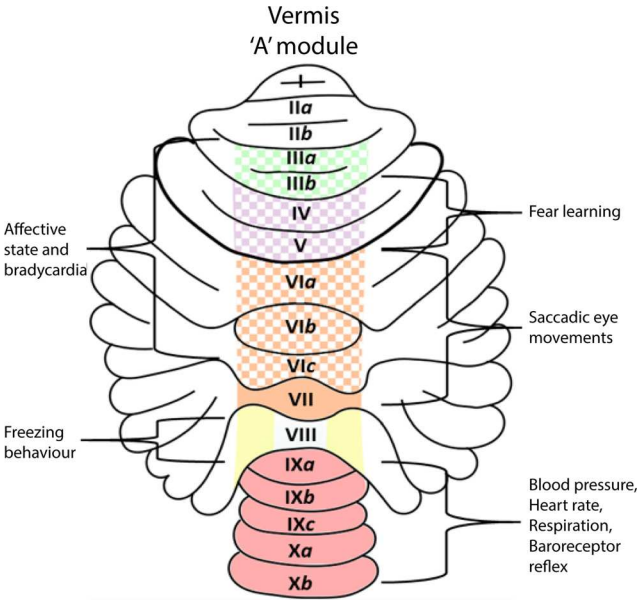

Fig. 8 The "A" module of the cerebellar vermis can be separated into several different rostrocaudally arranged regions, in some cases corresponding to specific lobules, that are associated with a variety of cognitive, motor and autonomic functions relating to defensive behaviors

General Conclusions

The present collection of views on the anatomical and functional organization of the cerebellum has resulted in the realization that as a first requirement for a general consensus would be to agree to a general terminology. In this review, the authors agreed to use the following definitions of terms.

- Module: interconnected longitudinal zone of PCs (a sagittal zone), (large part of) cerebellar nucleus, and (large part) of olivary subnucleus generally referred by a letter and number of the participating sagittal zone (see next item)
- Sagittal zone: (para-)sagittal band of Purkinje cells with similar anatomical connections to a particular cerebellar or vestibular (sub-) nucleus and identified by a capital letter and number according to Voogd
- Microzone: PC zone with similar olivary receptive fields
- Micromodule/microcomplex: a microzone with its (potentially) interconnected small parts of a cerebellar nucleus and olivary subnucleus
- Quantum/super PC: smallest interconnected olivo-cortico-nuclear entity (with a similar function?)
- Stripe: chemically identified banding pattern of cerebellar cortex (usually identifying zebrin II/aldolase c bands)
- Strip/band/patch: array of PCs or mossy fibers within a zone or stripe or without a reference
- Transverse zone: one of four antero-posterior zebrin domains as defined by Hawkes

There is broad consensus that this battery of terms reflects different ways of describing and identifying the same complex modular architecture. First, there is the olivocerebellar projection pattern—separated into the cortical climbing fibers and their nuclear collaterals—which matches the corticonuclear projections of the targeted PCs. Matching nucleo-olivary projections close the modular loop, while the bulbar projections of the other nuclear neurons form the executive branch of such a module (Sugihara, Voogd: Fig. 1). Beyond this, cerebellar architecture at higher resolution is the topic of intense debate.

Although it is evident that there is generally a good correspondence between the chemical signature of Purkinje cells and their anatomical connections, the level of chemical complexity surpasses that of our current anatomical knowledge. To what extent are modules subdivided into smaller anatomical entities and can these really be seen as micromodules (Apps, Wylie)? What is the smallest operational unit in which the modular connectivity pattern can be recognized (Hawkes, Jörntell) and could this be different for different cerebellar modules (Hawkes, Apps)? Would such a cerebellar quantum or super PC require an anatomically fully closed integrated circuit between the incorporated inferior olivary cells, Purkinje cells, and nuclear cells? Another aspect that is still not fully understood is the anatomical incorporation of the nucleo-cortical connections into the modular circuitry [224, 277–279].

Questions concerning the anatomical equivalency of the relation between olivocorticonuclear connections and chemical identity of Purkinje cells also relate to the much more difficult question concerning the functional interpretation of cerebellar modules, as it is far from settled to what extent the olivocorticonuclear circuitry (as modules or micromodules) represent functional entities. This will necessitate a better understanding of how the organization of mossy fibers fits in the modular scheme (Hawkes, Sillitoe, Isope)? Questions of how the distributed mossy fiber-parallel fiber system functionally and adaptively interacts with individual (micro-)modules are far from answered (Ebner, Isope)? Likewise, it remains to be determined to what extent information processing in modules with different chemical signatures fundamentally differs (Schonewille, Ebner) and how this subsequently may be used in the same functional setting (Wylie, Ruigrok)? What, really, is the function of individual (micro) modules? Do modules cooperate both within and outside of the cerebellum and in what way? Are the different modules with the same basic connectivity (e.g., C1 and C3) signs of redundancy (Hawkes, Isope)? To what extent do cerebellar modules serve multiple but integrated functions (Apps)?

Although, these and other questions cannot yet be readily answered, hypotheses have been formulated and a host of new and innovative techniques are at hand to begin to explore them all. For now, it should be clear that the cerebellum cannot be seen as a single operational machine, but that its basic modular organization has the potential to serve a great many functions in both individual and integrated ways.

Acknowledgements RH thanks Boris Barbour and Chris Yeo for advice on an earlier draft.

Funding Information Sugihara was supported by JSPS KAKENHI research grant (16K070025). Wylie was supported by funding from the Canadian Institutes for Health Research (CIHR) and the Natural Sciences and Engineering Research Council of Canada (NSERC). Sillitoe was supported by funds from Baylor College of Medicine (BCM) and Texas Children's Hospital (TCH). R.V.S. received support from BCM IDDRC grant U54HD083092 (Neurovisualization Core), the National Institutes of Neurological Disorders and Stroke (NINDS) R01NS089664, and the Hamill Foundation. A.M.B. received support from NINDS F31NS101891. Schonewille was supported by the Erasmus MC Rotterdam, the Dutch Scientific Organization Veni (NWO-ALW Veni), and the European Research Counsil Starting Grant (ERC-Stg, 680235). Ebner was supported in part by NIH grant R01 NS18338. Isope was supported by the CNRS, Université de Strasbourg, the Agence Nationale de la Recherche (Grant N°ANR-15-CE37-0001-01), and by the Fondation pour la Recherche Medicale (Grant N° DEQ20140329514). Ruigrok was supported by the Erasmus MC Rotterdam and the Dutch Ministry of Health, Welfare and Sports (T.R.), and JSPS Institutional Program for Young Researcher Overseas Visits (S.A.). Apps was supported by the Biotechnology and Biological Sciences Research Council (BBSRC, UK).

Compliance with Ethical Standards

Conflict of Interest The authors declare that they have no conflict of interest.

References

1. Glickstein M, Doron K. Cerebellum: connections and functions. Cerebellum. 2008;7:589–94. https://doi.org/10.1007/s12311-008-0074-4.
2. Ito M. The cerebellum and neural control. Raven Press; 1984.
3. Cerminara NL, Lang EJ, Sillitoe RV, Apps R. Redefining the cerebellar cortex as an assembly of non-uniform Purkinje cell microcircuits. Nat Rev Neurosci. 2015;16:79–93. https://doi.org/10.1038/nrn3886.
4. Apps R, Strata P. Neuronal circuits for fear and anxiety—the missing link. Nat Rev Neurosci. 2015;16:642. https://doi.org/10.1038/nrn4028.
5. Koziol LF, Budding D, Andreasen N, D'Arrigo S, Bulgheroni S, Imamizu H, et al. Consensus paper: the cerebellum's role in movement and cognition. Cerebellum. 2014;13:151–77. https://doi.org/10.1007/s12311-013-0511-x.
6. Ruigrok TJ. Ins and outs of cerebellar modules. Cerebellum. 2011;10:464–74. https://doi.org/10.1007/s12311-010-0164-y.

7. Voogd J. The importance of fiber connections in the comparative anatomy of the mammalian cerebellum. In: Llinas R, editor. Neurobiology of cerebellar evolution and development. Chicago: AMA; 1969. p. 8771–85.
8. Apps R, Hawkes R. Cerebellar cortical organization: a one-map hypothesis. Nat Rev Neurosci. 2009;10:670–81.
9. Cerminara NL, Aoki H, Loft M, Sugihara I, Apps R. Structural basis of cerebellar microcircuits in the rat. J Neurosci. 2013;33:16427–42. https://doi.org/10.1523/JNEUROSCI.0861-13.2013.
10. Sugihara I, Shinoda Y. Molecular, topographic, and functional organization of the cerebellar cortex: a study with combined aldolase C and olivocerebellar labeling. J Neurosci. 2004;24:8771–85.
11. Voogd J, Ruigrok TJ. The organization of the corticonuclear and olivocerebellar climbing fiber projections to the rat cerebellar vermis: the congruence of projection zones and the zebrin pattern. J Neurocytol. 2004;33:5–21. https://doi.org/10.1023/B:NEUR.0000029645.72074.2b.
12. Apps R, Garwicz M. Anatomical and physiological foundations of cerebellar information processing. Nat Rev Neurosci. 2005;6:297–311.
13. Voogd J, Shinoda Y, Ruigrok TJ, Sugihara I. Cerebellar nuclei and the inferior olivary nuclei: organization and connections. Handbook of the cerebellum and cerebellar disorders. Dordrecht: Springer Science; 2013. p. 377–436.
14. Wadiche JI, Jahr CE. Patterned expression of Purkinje cell glutamate transporters controls synaptic plasticity. Nat Neurosci. 2005;8:1329–34. https://doi.org/10.1038/nn1539.
15. Wang X, Chen G, Gao W, Ebner TJ. Parasagittally aligned, mGluR1-dependent patches are evoked at long latencies by parallel fiber stimulation in the mouse cerebellar cortex in vivo. J Neurophysiol. 2011;105:1732–46. https://doi.org/10.1152/jn.00717.2010.
16. Xiao J, Cerminara NL, Kotsurovskyy Y, Aoki H, Burroughs A, Wise AK, et al. Systematic regional variations in Purkinje cell spiking patterns. PLoS One. 2014;9:e105633. https://doi.org/10.1371/journal.pone.0105633.
17. Zhou H, Lin Z, Voges K, Ju C, Gao Z, Bosman LW, et al. Cerebellar modules operate at different frequencies. Elife. 2014;3:e02536. https://doi.org/10.7554/eLife.02536.
18. Voogd J, Bigaré F. Topographical distribution of olivary and cortico nuclear fibers in the cerebellum: a review. In: Courville J, de Montigny C, Lamarre Y, editors. The inferior olivary nucleus anatomy and physiology. New York: Raven Press; 1980. p. 207–34.
19. Groenewegen HJ, Voogd J, Freedman SL. The parasagittal zonation within the olivocerebellar projection. II. Climbing fiber distribution in the intermediate and hemispheric parts of cat cerebellum. J Comp Neurol. 1979;183:551–602.
20. Bigaré F. De efferente verbindingen van de cerebellaire schors van de kat. Anatomy. Leiden: University of Leiden; 1980.
21. Brodal A. Experimentelle Untersuchungen uber die Olivo-Cerebellaren Lokalization. Z Neurol. 1940;169:1–53.
22. Jansen J, Brodal A. Experimental studies on the intrinsic fibers of the cerebellum. II. The corticonuclear projection. J Comp Neurol. 1940;73:267–321.
23. Jansen J, Brodal A. Experimental studies on the intrinsic fibres of the cerebellum. III. The cortico-nuclear projection in the rabbit and the monkey (Macacus rhesus). Norske Vid Akad Avh I Math Nat KI. 1942;3(3):1–50.
24. Jansen J, Brodal A. Aspects of cerebellar anatomy. Oslo: Johan Grundt Tanum; 1954.
25. Bolk L. Das cerebellum der Saugetiere. Jena: Bohn-Fischer; 1906.
26. Voogd J. The cerebellum of the cat: structure and fiber connections. Assen: Van Gorcum; 1964.
27. Andersson G, Oscarsson O. Climbing fiber microzones in cerebellar vermis and their projection to different groups of cells in the lateral vestibular nucleus. Exp Brain Res. 1978;32:565–79.
28. Voogd J. Cerebellar zones: a personal history. Cerebellum. 2011;10:334–50. https://doi.org/10.1007/s12311-010-0221-6.
29. Brunner H. Die zentrale kleinhirnkerne bei den Saugetieren. Arb Neurol Inst Wiener Univ. 1919;22:200–72.
30. Verhaart WJ. The fibrecontent of the superior cerebellar peduncle in the pons and the mesencephalon. Acta Morphol Neerl Scand. 1956;1:21–9.
31. Courville J, Faraco-Cantin F, Diakiw N. A functionally important feature of the distribution of the olivo-cerebellar climbing fibers. Can J Physiol Pharmacol. 1974;52:1212–7.
32. Hawkes R, Leclerc N. Antigenic map of the rat cerebellar cortex: the distribution of parasagittal bands as revealed by monoclonal anti-Purkinje cell antibody mabQ113. J Comp Neurol. 1987;256:29–41.
33. Pijpers A, Apps R, Pardoe J, Voogd J, Ruigrok TJ. Precise spatial relationships between mossy fibers and climbing fibers in rat cerebellar cortical zones. J Neurosci. 2006;26:12067–80.
34. Voogd J, Pardoe J, Ruigrok TJ, Apps R. The distribution of climbing and mossy fiber collateral branches from the copula pyramidis and the paramedian lobule: congruence of climbing fiber cortical zones and the pattern of zebrin banding within the rat cerebellum. J Neurosci. 2003;23:4645–56.
35. Manto M, Haines D. Cerebellar research: two centuries of discoveries. Cerebellum. 2012;11:446–8. https://doi.org/10.1007/s12311-011-0336-4.
36. Oscarsson O, Uddenberg N. Somatotopic termination of spino-olivocerebellar path. Brain Res. 1966;3:204–7.
37. Ekerot CF, Larson B. The dorsal spino-olivocerebellar system in the cat. I. Functional organization and termination in the anterior lobe. Exp Brain Res. 1979;36:201–17.
38. Ekerot CF, Larson B. Termination in overlapping sagittal zones in cerebellar anterior lobe of mossy and climbing fiber paths activated from dorsal funiculus. Exp Brain Res. 1980;38:163–72.
39. Ekerot CF, Larson B. The dorsal spino-olivocerebellar system in the cat. II Somatotopical organization. Exp Brain Res. 1979;36:219–32.
40. Garwicz M, Ekerot C-F. Topographical organization of the cerebellar cortical projection to nucleus interpositus anterior in the cat. J Physiol. 1994;474:245–60.
41. Scheibel AB. Sagittal organization of mossy fiber terminal systems in the cerebellum of the rat: a Golgi study. Exp Neurol. 1977;57:1067–70.
42. Sugihara I, Wu H, Shinoda Y. Morphology of single olivocerebellar axons labeled with biotinylated dextran amine in the rat. J Comp Neurol. 1999;414:131–48. https://doi.org/10.1002/(SICI)1096-9861(19991115)414:2<131::AID-CNE1>3.0.CO;2-F. [pii]
43. Garwicz M, Ekerot CF, Jörntell H. Organizational principles of cerebellar neuronal circuitry. News Physiol Sci. 1998;13:26–32.
44. Brochu G, Maler L, Hawkes R. Zebrin II: a polypeptide antigen expressed selectively by Purkinje cells reveals compartments in rat and fish cerebellum. J Comp Neurol. 1990;291:538–52. https://doi.org/10.1002/cne.902910405.
45. Buisseret-Delmas C, Angaut P. The cerebellar olivo-corticonuclear connections in the rat. Prog Neurobiol. 1993;40:63–87.
46. Sugihara I, Shinoda Y. Molecular, topographic, and functional organization of the cerebellar nuclei: analysis by three-dimensional mapping of the olivonuclear projection and aldolase C labeling. J Neurosci. 2007;27:9696–710. https://doi.org/10.1523/JNEUROSCI.1579-07.2007.
47. Sugihara I, Fujita H, Na J, Quy PN, Li BY, Ikeda D. Projection of reconstructed single Purkinje cell axons in relation to the cortical and nuclear aldolase C compartments of the rat cerebellum. J Comp Neurol. 2009;512:282–304. https://doi.org/10.1002/cne.21889.

48. Vibulyaseck S, Fujita H, Luo Y, Tran AK, Oh-Nishi A, Ono Y, et al. Spatial rearrangement of Purkinje cell subsets forms the transverse and longitudinal compartmentalization in the mouse embryonic cerebellum. J Comp Neurol. 2017;525:2971–90. https://doi.org/10.1002/cne.24250.
49. Sugihara I, Marshall SP, Lang EJ. Relationship of complex spike synchrony bands and climbing fiber projection determined by reference to aldolase C compartments in crus IIa of the rat cerebellar cortex. J Comp Neurol. 2007;501:13–29. https://doi.org/10.1002/cne.21223.
50. Tang T, Xiao J, Suh CY, Burroughs A, Cerminara NL, Jia L, et al. Heterogeneity of Purkinje cell simple spike-complex spike interactions: zebrin- and non-zebrin-related variations. J Physiol. 2017;595:5341–57. https://doi.org/10.1113/JP274252.
51. Luo Y, Patel RP, Sarpong GA, Sasamura K, Sugihara I. Single axonal morphology and termination to cerebellar aldolase C stripes characterize distinct spinocerebellar projection systems originating from the thoracic spinal cord in the mouse. J Comp Neurol. 2018;526:681–706. https://doi.org/10.1002/cne.24360.
52. Tsutsumi S, Yamazaki M, Miyazaki T, Watanabe M, Sakimura K, Kano M, et al. Structure-function relationships between aldolase C/zebrin II expression and complex spike synchrony in the cerebellum. J Neurosci. 2015;35:843–52. https://doi.org/10.1523/JNEUROSCI.2170-14.2015.
53. Gibson JJ. The visual perception of objective motion and subjective movement. Psychol Rev. 1954;61:304–14.
54. Gamlin PD. The pretectum: connections and oculomotor-related roles. Prog Brain Res. 2006;151:379–405. https://doi.org/10.1016/S0079-6123(05)51012-4.
55. Simpson JI. The accessory optic system. Annu Rev Neurosci. 1984;7:13–41. https://doi.org/10.1146/annurev.ne.07.030184.000305.
56. Leonard CS, Simpson JI, Graf W. Spatial organization of visual messages of the rabbit's cerebellar flocculus. I. Typology of inferior olive neurons of the dorsal cap of Kooy. J Neurophysiol. 1988;60:2073–90.
57. Barmack NH, Qian Z, Yoshimura J. Regional and cellular distribution of protein kinase C in rat cerebellar Purkinje cells. J Comp Neurol. 2000;427:235–54.
58. Ito M. Cerebellar learning in the vestibulo-ocular reflex. Trends Cogn Sci. 1998;2:313–21.
59. Yakusheva TA, Shaikh AG, Green AM, Blazquez PM, Dickman JD, Angelaki DE. Purkinje cells in posterior cerebellar vermis encode motion in an inertial reference frame. Neuron. 2007;54:973–85. https://doi.org/10.1016/j.neuron.2007.06.003.
60. Voogd J, Glickstein M. The anatomy of the cerebellum. Trends Cogn Sci. 1998;2:307–13.
61. Larsell O. The comparative anatomy and histology of the cerebellum: from myxinoids through birds. Minneapolis: University of Minnesota Press; 1967.
62. Brecha N, Karten HJ, Hunt SP. Projections of the nucleus of the basal optic root in the pigeon: an autoradiographic and horseradish peroxidase study. J Comp Neurol. 1980;189:615–70. https://doi.org/10.1002/cne.901890404.
63. Clarke PG. Some visual and other connections to the cerebellum of the pigeon. J Comp Neurol. 1977;174:535–52. https://doi.org/10.1002/cne.901740307.
64. Winterson BJ, Brauth SE. Direction-selective single units in the nucleus lentiformis mesencephali of the pigeon (Columba livia). Exp Brain Res. 1985;60:215–26.
65. Wylie DR. Projections from the nucleus of the basal optic root and nucleus lentiformis mesencephali to the inferior olive in pigeons (Columba livia). J Comp Neurol. 2001;429:502–13.
66. Graham DJ, Wylie DR. Zebrin-immunopositive and -immunonegative stripe pairs represent functional units in the pigeon vestibulocerebellum. J Neurosci. 2012;32:12769–79. https://doi.org/10.1523/JNEUROSCI.0197-12.2012.
67. Pakan JM, Graham DJ, Gutierrez-Ibanez C, Wylie DR. Organization of the cerebellum: correlating zebrin immunochemistry with optic flow zones in the pigeon flocculus. Vis Neurosci. 2011;28:163–74. https://doi.org/10.1017/S0952523810000532.
68. Pakan JM, Graham DJ, Wylie DR. Organization of visual mossy fiber projections and zebrin expression in the pigeon vestibulocerebellum. J Comp Neurol. 2010;518:175–98. https://doi.org/10.1002/cne.22192.
69. Schwarz IE, Schwarz DW. The primary vestibular projection to the cerebellar cortex in the pigeon (Columba livia). J Comp Neurol. 1983;216:438–44. https://doi.org/10.1002/cne.902160409.
70. Graf W, Simpson JI, Leonard CS. Spatial organization of visual messages of the rabbit's cerebellar flocculus. II. Complex and simple spike responses of Purkinje cells. J Neurophysiol. 1988;60:2091–121.
71. Voogd J, Wylie DR. Functional and anatomical organization of floccular zones: a preserved feature in vertebrates. J Comp Neurol. 2004;470:107–12. https://doi.org/10.1002/cne.11022.
72. Wylie DR, Frost BJ. Responses of pigeon vestibulocerebellar neurons to optokinetic stimulation. II. The 3-dimensional reference frame of rotation neurons in the flocculus. J Neurophysiol. 1993;70:2647–59.
73. Winship IR, Wylie DR. Zonal organization of the vestibulocerebellum in pigeons (Columba livia): I. Climbing fiber input to the flocculus. J Comp Neurol. 2003;456:127–39. https://doi.org/10.1002/cne.10507.
74. Wylie DR, Brown MR, Barkley RR, Winship IR, Crowder NA, Todd KG. Zonal organization of the vestibulocerebellum in pigeons (Columba livia): II. Projections of the rotation zones of the flocculus. J Comp Neurol. 2003;456:140–53. https://doi.org/10.1002/cne.10508.
75. Wylie DR, Brown MR, Winship IR, Crowder NA, Todd KG. Zonal organization of the vestibulocerebellum in pigeons (Columba livia): III. Projections of the translation zones of the ventral uvula and nodulus. J Comp Neurol. 2003;465:179–94. https://doi.org/10.1002/cne.10857.
76. Wylie DR, Pakan JM, Huynh H, Graham DJ, Iwaniuk AN. Distribution of zebrin-immunoreactive Purkinje cell terminals in the cerebellar and vestibular nuclei of birds. J Comp Neurol. 2012;520:1532–46. https://doi.org/10.1002/cne.22810.
77. Crowder NA, Winship IR, Wylie DR. Topographic organization of inferior olive cells projecting to translational zones in the vestibulocerebellum of pigeons. J Comp Neurol. 2000;419:87–95.
78. Wylie DR, Winship IR, Glover RG. Projections from the medial column of the inferior olive to different classes of rotation-sensitive Purkinje cells in the flocculus of pigeons. Neurosci Lett. 1999;268:97–100.
79. Ahn AH, Dziennis S, Hawkes R, Herrup K. The cloning of zebrin II reveals its identity with aldolase C. Development. 1994;120:2081–90.
80. Pakan JM, Iwaniuk AN, Wylie DR, Hawkes R, Marzban H. Purkinje cell compartmentation as revealed by zebrin II expression in the cerebellar cortex of pigeons (Columba livia). J Comp Neurol. 2007;501:619–30. https://doi.org/10.1002/cne.21266.
81. Craciun I, Gutierrez-Ibanez C, Corfield JR, Hurd PL, Wylie DR. Topographic organization of inferior olive projections to the zebrin II stripes in the pigeon cerebellar uvula. Front Neuroanat. 2018;12:18. https://doi.org/10.3389/fnana.2018.00018.
82. Wylie DR, Gutierrez-Ibanez C, Corfield JR, Craciun I, Graham DJ, Hurd PL. Inferior olivary projection to the zebrin II stripes in lobule IXcd of the pigeon flocculus: a retrograde tracing study. J Comp Neurol. 2017;525:3158–73. https://doi.org/10.1002/cne.24270.

83. Long RM, Pakan JMP, Graham DJ, Hurd PL, Gutierrez-Ibanez C, Wylie DR. Modulation of complex spike activity differs between zebrin positive and negative Purkinje cells in the pigeon cerebellum. J Neurophysiol. 2018; https://doi.org/10.1152/jn.00797.2017.
84. Armstrong CL, Hawkes R. Pattern formation in the cerebellar cortex. Biochem Cell Biol. 2000;78:551–62.
85. Ozol K, Hayden JM, Oberdick J, Hawkes R. Transverse zones in the vermis of the mouse cerebellum. J Comp Neurol. 1999;412: 95–111.
86. Marzban H, Kim CT, Doorn D, Chung SH, Hawkes RA. Novel transverse expression domain in the mouse cerebellum revealed by a neurofilament-associated antigen. Neuroscience. 2008;153: 1190–201.
87. Kim JY, Marzban H, Chung SH, Watanabe M, Eisenman LM, Hawkes R. Purkinje cell compartmentation of the cerebellum of microchiropteran bats. J Comp Neurol. 2009;517:193–209. https://doi.org/10.1002/cne.22147.
88. Marzban H, Hoy N, Buchok M, Catania KC, Hawkes R. Compartmentation of the cerebellar cortex: adaptation to lifestyle in the star-nosed mole Condylura cristata. Cerebellum. 2015;14: 106–18. https://doi.org/10.1007/s12311-014-0618-8.
89. Marzban H, Chung S, Watanabe M, Hawkes R. Phospholipase Cbeta4 expression reveals the continuity of cerebellar topography through development. J Comp Neurol. 2007;502:857–71. https://doi.org/10.1002/cne.21352.
90. Bower JM, Kassel J. Variability in tactile projection patterns to cerebellar folia crus IIA of the Norway rat. J Comp Neurol. 1990;302:768–78.
91. Shambes GM, Gibson JM, Welker W. Fractured somatotopy in granule cell tactile areas of rat cerebellar hemispheres revealed by micromapping. Brain Behav Evol. 1978;15:94–140.
92. Joseph JW, Shambes GM, Gibson JM, Welker W. Tactile projections to granule cells in caudal vermis of the rat's cerebellum. Brain Behav Evol. 1978;15:141–9.
93. Chockkan V, Hawkes R. Functional and antigenic maps in the rat cerebellum: zebrin compartmentation and vibrissal receptive fields in lobule IXa. J Comp Neurol. 1994;345:33–45. https://doi.org/10.1002/cne.903450103.
94. Hallem JS, Thompson JH, Gundappa-Sulur G, Hawkes R, Bjaalie JG, Bower JM. Spatial correspondence between tactile projection patterns and the distribution of the antigenic Purkinje cell markers anti-zebrin I and anti-zebrin II in the cerebellar folium crus IIA of the rat. Neuroscience. 1999;93:1083–94.
95. Hawkes R, Gallagher E, Ozol K. Blebs in the mouse cerebellar granular layer as a sign of structural inhomogeneity. 1. Anterior lobe vermis. Acta Anat (Basel). 1997;158:205–14.
96. Hawkes R, Turner RW. Compartmentation of NADPH-diaphorase activity in the mouse cerebellar cortex. J Comp Neurol. 1994;346: 499–516. https://doi.org/10.1002/cne.903460404.
97. Sillitoe RV, Benson MA, Blake DJ, Hawkes R. Abnormal dysbindin expression in cerebellar mossy fiber synapses in the mdx mouse model of Duchenne muscular dystrophy. J Neurosci. 2003;23:6576–85.
98. Hawkes R. An anatomical model of cerebellar modules. Prog Brain Res. 1997;114:39–52.
99. Ruigrok TJ, Pijpers A, Goedknegt-Sabel E, Coulon P. Multiple cerebellar zones are involved in the control of individual muscles: a retrograde transneuronal tracing study with rabies virus in the rat. Eur J Neurosci. 2008;28:181–200. https://doi.org/10.1111/j.1460-9568.2008.06294.x.
100. Ekerot CF, Garwicz M, Schouenborg J. Topography and nociceptive receptive fields of climbing fibres projecting to the cerebellar anterior lobe in the cat. J Physiol. 1991;441:257–74.
101. Garwicz M, Apps R, Trott JR. Micro-organization of olivocerebellar and corticonuclear connections of the paravermal cerebellum in the cat. Eur J Neurosci. 1996;8:2726–38.
102. Bengtsson F, Ekerot CF, Jörntell H. In vivo analysis of inhibitory synaptic inputs and rebounds in deep cerebellar nuclear neurons. PLoS One. 2011;6:e18822. https://doi.org/10.1371/journal.pone.0018822.
103. Bengtsson F, Jörntell H. Specific relationship between excitatory inputs and climbing fiber receptive fields in deep cerebellar nuclear neurons. PLoS One. 2014;9:e84616. https://doi.org/10.1371/journal.pone.0084616.
104. Mogensen H, Bengtsson F, Jörntell H. No medium-term spinocerebellar input plasticity in deep cerebellar nuclear neurons in vivo? Cerebellum. 2017;16:638–47. https://doi.org/10.1007/s12311-016-0839-0.
105. Bengtsson F, Hesslow G. Cerebellar control of the inferior olive. Cerebellum. 2006;5:7–14.
106. Andersson G, Hesslow G. Activity of Purkinje cells and interpositus neurones during and after periods of high frequency climbing fibre activation in the cat. Exp Brain Res. 1987;67:533–42.
107. Zucca R, Rasmussen A and Bengtsson F. Climbing fiber regulation of spontaneous Purkinje cell activity and cerebellum-dependent blink responses(1,2,3). eNeuro. 2016:3. doi https://doi.org/10.1523/ENEURO.0067-15.2015.
108. Cerminara NL, Rawson JA. Evidence that climbing fibers control an intrinsic spike generator in cerebellar Purkinje cells. J Neurosci. 2004;24:4510–7.
109. Horn KM, Pong M, Gibson AR. Functional relations of cerebellar modules of the cat. J Neurosci. 2010;30:9411–23. https://doi.org/10.1523/JNEUROSCI.0440-10.2010.
110. Jörntell H. Cerebellar physiology: links between microcircuitry properties and sensorimotor functions. J Physiol. 2017;595:11–27. https://doi.org/10.1113/JP272769.
111. Spanne A, Jörntell H. Processing of multi-dimensional sensorimotor information in the spinal and cerebellar neuronal circuitry: a new hypothesis. PLoS Comput Biol. 2013;9:e1002979. https://doi.org/10.1371/journal.pcbi.1002979.
112. Leto K, Arancillo M, Becker EB, Buffo A, Chiang C, Ding B, et al. Consensus paper: cerebellar development. Cerebellum. 2016;15:789–828. https://doi.org/10.1007/s12311-015-0724-2.
113. Ji Z, Hawkes R. Topography of Purkinje cell compartments and mossy fiber terminal fields in lobules II and III of the rat cerebellar cortex: spinocerebellar and cuneocerebellar projections. Neuroscience. 1994;61:935–54.
114. Huang CC, Sugino K, Shima Y, Guo C, Bai S, Mensh BD, et al. Convergence of pontine and proprioceptive streams onto multimodal cerebellar granule cells. Elife. 2013;2:e00400. https://doi.org/10.7554/eLife.00400.
115. Ashwell KW, Zhang LL. Ontogeny of afferents to the fetal rat cerebellum. Acta Anat (Basel). 1992;145:17–23.
116. Kalinovsky A, Boukhtouche F, Blazeski R, Bornmann C, Suzuki N, Mason CA, et al. Development of axon-target specificity of ponto-cerebellar afferents. PLoS Biol. 2011;9:e1001013. https://doi.org/10.1371/journal.pbio.1001013.
117. Arsenio Nunes ML, Sotelo C. Development of the spinocerebellar system in the postnatal rat. J Comp Neurol. 1985;237:291–306. https://doi.org/10.1002/cne.902370302.
118. Hawkes R, Beierbach E, Tan SS. Granule cell dispersion is restricted across transverse boundaries in mouse chimeras. Eur J Neurosci. 1999;11:3800–8.
119. Ozol KO, Hawkes R. Compartmentation of the granular layer of the cerebellum. Histol Histopathol. 1997;12:171–84.
120. Schilling K, Schmidt HH, Baader SL. Nitric oxide synthase expression reveals compartments of cerebellar granule cells and suggests a role for mossy fibers in their development. Neuroscience. 1994;59:893–903.
121. Machold R, Fishell G. Math1 is expressed in temporally discrete pools of cerebellar rhombic-lip neural progenitors. Neuron. 2005;48:17–24. https://doi.org/10.1016/j.neuron.2005.08.028.

122. Dino MR, Willard FH, Mugnaini E. Distribution of unipolar brush cells and other calretinin immunoreactive components in the mammalian cerebellar cortex. J Neurocytol. 1999;28:99–123.
123. Chung SH, Marzban H, Watanabe M, Hawkes R. Phospholipase Cbeta4 expression identifies a novel subset of unipolar brush cells in the adult mouse cerebellum. Cerebellum. 2009;8:267–76. https://doi.org/10.1007/s12311-009-0092-x.
124. Chung SH, Sillitoe RV, Croci L, Badaloni A, Consalez G, Hawkes R. Purkinje cell phenotype restricts the distribution of unipolar brush cells. Neuroscience. 2009;164:1496–508. https://doi.org/10.1016/j.neuroscience.2009.09.080.
125. Chung SH, Marzban H, Aldinger K, Dixit R, Millen K, Schuurmans C, et al. Zac1 plays a key role in the development of specific neuronal subsets in the mouse cerebellum. Neural Dev. 2011;6:25. https://doi.org/10.1186/1749-8104-6-25.
126. Sillitoe RV, Chung SH, Fritschy JM, Hoy M, Hawkes R. Golgi cell dendrites are restricted by Purkinje cell stripe boundaries in the adult mouse cerebellar cortex. J Neurosci. 2008;28:2820–6. https://doi.org/10.1523/JNEUROSCI.4145-07.2008.
127. Dizon MJ, Khodakhah K. The role of interneurons in shaping Purkinje cell responses in the cerebellar cortex. J Neurosci. 2011;31:10463–73. https://doi.org/10.1523/JNEUROSCI.1350-11.2011.
128. Gao W, Chen G, Reinert KC, Ebner TJ. Cerebellar cortical molecular layer inhibition is organized in parasagittal zones. J Neurosci. 2006;26:8377–87. https://doi.org/10.1523/JNEUROSCI.2434-06.2006.
129. Arancillo M, White JJ, Lin T, Stay TL, Sillitoe RV. In vivo analysis of Purkinje cell firing properties during postnatal mouse development. J Neurophysiol. 2015;113:578–91. https://doi.org/10.1152/jn.00586.2014.
130. Dehnes Y, Chaudhry FA, Ullensvang K, Lehre KP, Storm-Mathisen J, Danbolt NC. The glutamate transporter EAAT4 in rat cerebellar Purkinje cells: a glutamate-gated chloride channel concentrated near the synapse in parts of the dendritic membrane facing astroglia. J Neurosci. 1998;18:3606–19.
131. Paukert M, Huang YH, Tanaka K, Rothstein JD, Bergles DE. Zones of enhanced glutamate release from climbing fibers in the mammalian cerebellum. J Neurosci. 2010;30:7290–9.
132. Kim CH, Oh SH, Lee JH, Chang SO, Kim J, Kim SJ. Lobule-specific membrane excitability of cerebellar Purkinje cells. J Physiol. 2012;590:273–88. https://doi.org/10.1113/jphysiol.2011.221846.
133. Zhou H, Voges K, Lin Z, Ju C, Schonewille M. Differential Purkinje cell simple spike activity and pausing behavior related to cerebellar modules. J Neurophysiol. 2015;113:2524–36. https://doi.org/10.1152/jn.00925.2014.
134. Hartmann J, Dragicevic E, Adelsberger H, Henning HA, Sumser M, Abramowitz J, et al. TRPC3 channels are required for synaptic transmission and motor coordination. Neuron. 2008;59:392–8.
135. Schonewille M, Khosrovani S, Winkelman BH, Hoebeek FE, De Jeu MT, Larsen IM, et al. Purkinje cells in awake behaving animals operate at the upstate membrane potential. Nat Neurosci. 2006;9:459–61. https://doi.org/10.1038/nn0406-459. author reply 61
136. Cao Y, Liu Y, Jaeger D, Heck DH. Cerebellar Purkinje cells generate highly correlated spontaneous slow-rate fluctuations. Front Neural Circuits. 2017;11:67. https://doi.org/10.3389/fncir.2017.00067.
137. Badura A, Schonewille M, Voges K, Witter L, Gao Z, Galliano E, et al. Climbing fiber input shapes reciprocity of Purkinje cell firing. Neuron. 2013;78:700–13.
138. Sato Y, Miura A, Fushiki H, Kawasaki T. Short-term modulation of cerebellar Purkinje cell activity after spontaneous climbing fiber input. J Neurophysiol. 1992;68:2051–62.
139. Heiney SA, Kim J, Augustine GJ, Medina JF. Precise control of movement kinematics by optogenetic inhibition of Purkinje cell activity. J Neurosci. 2014;34:2321–30. https://doi.org/10.1523/JNEUROSCI.4547-13.2014.
140. Lee KH, Mathews PJ, Reeves AM, Choe KY, Jami SA, Serrano RE, et al. Circuit mechanisms underlying motor memory formation in the cerebellum. Neuron. 2015;86:529–40.
141. de Zeeuw CI, Holstege JC, Ruigrok TJ, Voogd J. Ultrastructural study of the GABAergic, cerebellar, and mesodiencephalic innervation of the cat medial accessory olive: anterograde tracing combined with immunocytochemistry. J Comp Neurol. 1989;284:12–35. https://doi.org/10.1002/cne.902840103.
142. Angaut P, Sotelo C. Synaptology of the cerebello-olivary pathway. Double labelling with anterograde axonal tracing and GABA immunocytochemistry in the rat. Brain Res. 1989;479:361–5.
143. Chaumont J, Guyon N, Valera AM, Dugue GP, Popa D, Marcaggi P, et al. Clusters of cerebellar Purkinje cells control their afferent climbing fiber discharge. Proc Natl Acad Sci U S A. 2013;110:16223–8.
144. Witter L, Canto CB, Hoogland TM, de Gruijl JR, De Zeeuw CI. Strength and timing of motor responses mediated by rebound firing in the cerebellar nuclei after Purkinje cell activation. Front Neural Circuits. 2013;7:133. https://doi.org/10.3389/fncir.2013.00133.
145. Ruigrok TJ, Voogd J. Cerebellar influence on olivary excitability in the cat. Eur J Neurosci. 1995;7:679–93.
146. Lefler Y, Yarom Y, Uusisaari MY. Cerebellar inhibitory input to the inferior olive decreases electrical coupling and blocks subthreshold oscillations. Neuron. 2014;81:1389–400. https://doi.org/10.1016/j.neuron.2014.02.032.
147. Schmolesky MT, Weber JT, De Zeeuw CI, Hansel C. The making of a complex spike: ionic composition and plasticity. Ann N Y Acad Sci. 2002;978:359–90.
148. Davie JT, Clark BA, Hausser M. The origin of the complex spike in cerebellar Purkinje cells. J Neurosci. 2008;28:7599–609. https://doi.org/10.1523/JNEUROSCI.0559-08.2008.
149. Mathy A, Ho SS, Davie JT, Duguid IC, Clark BA, Hausser M. Encoding of oscillations by axonal bursts in inferior olive neurons. Neuron. 2009;62:388–99. https://doi.org/10.1016/j.neuron.2009.03.023.
150. Najafi F, Giovannucci A, Wang SS, Medina JF. Coding of stimulus strength via analog calcium signals in Purkinje cell dendrites of awake mice. Elife. 2014;3:e03663. https://doi.org/10.7554/eLife.03663.
151. Burroughs A, Wise AK, Xiao J, Houghton C, Tang T, Suh CY, et al. The dynamic relationship between cerebellar Purkinje cell simple spikes and the spikelet number of complex spikes. J Physiol. 2017;595:283–99. https://doi.org/10.1113/JP272259.
152. Warnaar P, Couto J, Negrello M, Junker M, Smilgin A, Ignashchenkova A, et al. Duration of Purkinje cell complex spikes increases with their firing frequency. Front Cell Neurosci. 2015;9:122. https://doi.org/10.3389/fncel.2015.00122.
153. Mostofi A, Holtzman T, Grout AS, Yeo CH, Edgley SA. Electrophysiological localization of eyeblink-related microzones in rabbit cerebellar cortex. J Neurosci. 2010;30:8920–34. https://doi.org/10.1523/JNEUROSCI.6117-09.2010.
154. Ohmae S, Medina JF. Climbing fibers encode a temporal-difference prediction error during cerebellar learning in mice. Nat Neurosci. 2015;18:1798–803. https://doi.org/10.1038/nn.4167.
155. Jirenhed DA, Bengtsson F, Acquisition HG. Extinction, and reacquisition of a cerebellar cortical memory trace. J Neurosci. 2007;27:2493–502.
156. ten Brinke MM, Boele HJ, Spanke JK, Potters JW, Kornysheva K, Wulff P, et al. Evolving models of Pavlovian conditioning:

cerebellar cortical dynamics in awake behaving mice. Cell Rep. 2015;13:1977–88. https://doi.org/10.1016/j.celrep.2015.10.057.
157. Voges K, Wu B, Post L, Schonewille M, De Zeeuw CI. Mechanisms underlying vestibulo-cerebellar motor learning in mice depend on movement direction. J Physiol. 2017;595:5301–26. https://doi.org/10.1113/JP274346.
158. Hawkes R, Herrup K. Aldolase C/zebrin II and the regionalization of the cerebellum. J Mol Neurosci. 1995;6:147–58. https://doi.org/10.1007/BF02736761.
159. Chen G, Hanson CL, Ebner TJ. Functional parasagittal compartments in the rat cerebellar cortex: an in vivo optical imaging study using neutral red. J Neurophysiol. 1996;76:4169–74. https://doi.org/10.1152/jn.1996.76.6.4169.
160. Hanson CL, Chen G, Ebner TJ. Role of climbing fibers in determining the spatial patterns of activation in the cerebellar cortex to peripheral stimulation: an optical imaging study. Neuroscience. 2000;96:317–31.
161. Cramer SW, Gao W, Chen G, Ebner TJ. Reevaluation of the beam and radial hypotheses of parallel fiber action in the cerebellar cortex. J Neurosci. 2013;33:11412–24. https://doi.org/10.1523/JNEUROSCI.0711-13.2013.
162. Armbrust KR, Wang X, Hathorn TJ, Cramer SW, Chen G, Zu T, et al. Mutant beta-III spectrin causes mGluR1alpha mislocalization and functional deficits in a mouse model of spinocerebellar ataxia type 5. J Neurosci. 2014;34:9891–904. https://doi.org/10.1523/JNEUROSCI.0876-14.2014.
163. Ekerot CF, Larson B. Correlation between sagittal projection zones of climbing and mossy fibre paths in cat cerebellar anterior lobe. Brain Res. 1973;64:446–50.
164. Llinas R, Sasaki K. The functional organization of the olivocerebellar system as examined by multiple Purkinje cell recordings. Eur J Neurosci. 1989;1:587–602.
165. Lang EJ, Sugihara I, Llinas R. Olivocerebellar modulation of motor cortex ability to generate vibrissal movements in rat. J Physiol. 2006;571:101–20.
166. Sasaki K, Bower JM, Llinas R. Multiple Purkinje cell recording in rodent cerebellar cortex. Eur J Neurosci. 1989;1:572–86.
167. Welsh JP, Lang EJ, Suglhara I, Llinas R. Dynamic organization of motor control within the olivocerebellar system. Nature. 1995;374:453–7. https://doi.org/10.1038/374453a0.
168. Eccles JC, Ito M, Szentagothai J. The cerebellum as a neuronal machine. Berlin: Springer; 1967.
169. Ito M. Mechanisms of motor learning in the cerebellum. Brain Res. 2000;886:237–45.
170. Belmeguenai A, Hansel CA. Role for protein phosphatases 1, 2A, and 2B in cerebellar long-term potentiation. J Neurosci. 2005, 25:10768–72. https://doi.org/10.1523/JNEUROSCI.2876-05.2005.
171. Lev-Ram V, Wong ST, Storm DR, Tsien RY. A new form of cerebellar long-term potentiation is postsynaptic and depends on nitric oxide but not cAMP. Proc Natl Acad Sci U S A. 2002;99:8389–93. https://doi.org/10.1073/pnas.122206399.
172. Oscarsson O. Functional units of the cerebellum - sagittal zones and microzones. TINS. 1979;2:143–5.
173. Ekerot CF, Garwicz M, Jörntell H. The control of forelimb movements by intermediate cerebellum. Prog Brain Res. 1997;114:423–9.
174. Garwicz M, Jörntell H, Ekerot CF. Cutaneous receptive fields and topography of mossy fibres and climbing fibres projecting to cat cerebellar C3 zone. J Physiol. 1998;512(Pt 1):277–93.
175. Nguyen-Vu TD, Kimpo RR, Rinaldi JM, Kohli A, Zeng H, Deisseroth K, et al. Cerebellar Purkinje cell activity drives motor learning. Nat Neurosci. 2013;16:1734–6.
176. Ekerot CF, Jörntell H, Garwicz M. Functional relation between corticonuclear input and movements evoked on microstimulation in cerebellar nucleus interpositus anterior in the cat. Exp Brain Res. 1995;106:365–76.
177. Ito M. Cerebellar long-term depression: characterization, signal transduction, and functional roles. Physiol Rev. 2001;81:1143–95. https://doi.org/10.1152/physrev.2001.81.3.1143.
178. Jörntell H, Hansel C. Synaptic memories upside down: bidirectional plasticity at cerebellar parallel fiber-Purkinje cell synapses. Neuron. 2006;52:227–38.
179. Rummelhart DE, McClelland JL, Group PR. Parallel distributed processing. Cambridge: The MIT Press; 1986.
180. Billig I, Yatim N, Compoint C, Buisseret-Delmas C, Buisseret P. Cerebellar afferences from the mesencephalic trigeminal nucleus in the rat. Neuroreport. 1995;6:2293–6.
181. Matsushita M. Spinocerebellar projections from the lowest lumbar and sacral-caudal segments in the cat, as studied by anterograde transport of wheat germ agglutinin-horseradish peroxidase. J Comp Neurol. 1988;274:239–54. https://doi.org/10.1002/cne.902740208.
182. Matsushita M. Cerebellar projections of the central cervical nucleus in the rat: an anterograde tracing study. Neurosci Res. 1991;12:201–16.
183. Sengul G, Fu Y, Yu Y, Paxinos G. Spinal cord projections to the cerebellum in the mouse. Brain Struct Funct. 2015;220:2997–3009. https://doi.org/10.1007/s00429-014-0840-7.
184. Yaginuma H, Matsushita M. Spinocerebellar projections from the thoracic cord in the cat, as studied by anterograde transport of wheat germ agglutinin-horseradish peroxidase. J Comp Neurol. 1987;258:1–27. https://doi.org/10.1002/cne.902580102.
185. Harvey RJ, Napper RM. Quantitative studies on the mammalian cerebellum. Prog Neurobiol. 1991;36:437–63.
186. Pichitpornchai C, Rawson JA, Rees S. Morphology of parallel fibres in the cerebellar cortex of the rat: an experimental light and electron microscopic study with biocytin. J Comp Neurol. 1994;342:206–20. https://doi.org/10.1002/cne.903420205.
187. Quy PN, Fujita H, Sakamoto Y, Na J, Sugihara I. Projection patterns of single mossy fiber axons originating from the dorsal column nuclei mapped on the aldolase C compartments in the rat cerebellar cortex. J Comp Neurol. 2011;519:874–99. https://doi.org/10.1002/cne.22555.
188. Shinoda Y, Sugihara I, Wu HS, Sugiuchi Y. The entire trajectory of single climbing and mossy fibers in the cerebellar nuclei and cortex. Prog Brain Res. 2000;124:173–86.
189. Hantman AW, Jessell TM. Clarke's column neurons as the focus of a corticospinal corollary circuit. Nat Neurosci. 2010;13:1233–9. https://doi.org/10.1038/nn.2637.
190. Chabrol FP, Arenz A, Wiechert MT, Margrie TW, DiGregorio DA. Synaptic diversity enables temporal coding of coincident multisensory inputs in single neurons. Nat Neurosci. 2015;18:718–27. https://doi.org/10.1038/nn.3974.
191. Ishikawa T, Shimuta M, Hausser M. Multimodal sensory integration in single cerebellar granule cells in vivo. Elife 2015:4. https://doi.org/10.7554/eLife.12916.
192. Albus JS. A theory of cerebellar function. Math Biosci. 1971;10:25–61.
193. Marr D. A theory of cerebellar cortex. J Physiol. 1969;202:437–70.
194. Bower JM, Woolston DC. Congruence of spatial organization of tactile projections to granule cell and Purkinje cell layers of cerebellar hemispheres of the albino rat: vertical organization of cerebellar cortex. J Neurophysiol. 1983;49:745–66.
195. Brown IE, Bower JM. Congruence of mossy fiber and climbing fiber tactile projections in the lateral hemispheres of the rat cerebellum. J Comp Neurol. 2001;429:59–70.
196. Ekerot CF, Jörntell H. Parallel fibre receptive fields of Purkinje cells and interneurons are climbing fibre-specific. Eur J Neurosci. 2001;13:1303–10.

197. Isope P, Barbour B. Properties of unitary granule cell—Purkinje cell synapses in adult rat cerebellar slices. J Neurosci. 2002;22:9668–78.
198. Jörntell H, Ekerot CF. Reciprocal bidirectional plasticity of parallel fiber receptive fields in cerebellar Purkinje cells and their afferent interneurons. Neuron. 2002;34:797–806.
199. Valera AM, Binda F, Pawlowski SA, Dupont JL, Casella JF, Rothstein JD, Poulain B and Isope P. Stereotyped spatial patterns of functional synaptic connectivity in the cerebellar cortex. Elife. 2016:5. https://doi.org/10.7554/eLife.09862.
200. Walter JT, Dizon MJ, Khodakhah K. The functional equivalence of ascending and parallel fiber inputs in cerebellar computation. J Neurosci. 2009;29:8462–73. https://doi.org/10.1523/JNEUROSCI.5718-08.2009.
201. Giovannucci A, Badura A, Deverett B, Najafi F, Pereira TD, Gao Z, et al. Cerebellar granule cells acquire a widespread predictive feedback signal during motor learning. Nat Neurosci. 2017;20:727–34. https://doi.org/10.1038/nn.4531.
202. Knogler LD, Markov DA, Dragomir EI, Stih V, Portugues R. Sensorimotor representations in cerebellar granule cells in larval zebrafish are dense, spatially organized, and non-temporally patterned. Curr Biol. 2017;27:1288–302. https://doi.org/10.1016/j.cub.2017.03.029.
203. Wagner MJ, Kim TH, Savall J, Schnitzer MJ, Luo L. Cerebellar granule cells encode the expectation of reward. Nature. 2017;544:96–100. https://doi.org/10.1038/nature21726.
204. Arenz A, Silver RA, Schaefer AT, Margrie TW. The contribution of single synapses to sensory representation in vivo. Science. 2008;321:977–80. https://doi.org/10.1126/science.1158391.
205. Bengtsson F, Jorntell H. Sensory transmission in cerebellar granule cells relies on similarly coded mossy fiber inputs. Proc Natl Acad Sci U S A. 2009;106:2389–94. https://doi.org/10.1073/pnas.0808428106.
206. Chadderton P, Margrie TW, Hausser M. Integration of quanta in cerebellar granule cells during sensory processing. Nature. 2004;428:856–60. https://doi.org/10.1038/nature02442.
207. Duguid I, Branco T, Chadderton P, Arlt C, Powell K, Hausser M. Control of cerebellar granule cell output by sensory-evoked Golgi cell inhibition. Proc Natl Acad Sci U S A. 2015;112:13099–104. https://doi.org/10.1073/pnas.1510249112.
208. Jörntell H, Ekerot CF. Properties of somatosensory synaptic integration in cerebellar granule cells in vivo. J Neurosci. 2006;26:11786–97. https://doi.org/10.1523/JNEUROSCI.2939-06.2006.
209. Rancz EA, Ishikawa T, Duguid I, Chadderton P, Mahon S, Hausser M. High-fidelity transmission of sensory information by single cerebellar mossy fibre boutons. Nature. 2007;450:1245–8. https://doi.org/10.1038/nature05995.
210. van Kan PL, Gibson AR, Houk JC. Movement-related inputs to intermediate cerebellum of the monkey. J Neurophysiol. 1993;69:74–94. https://doi.org/10.1152/jn.1993.69.1.74.
211. Hallermann S, Fejtova A, Schmidt H, Weyhersmuller A, Silver RA, Gundelfinger ED, et al. Bassoon speeds vesicle reloading at a central excitatory synapse. Neuron. 2010;68:710–23. https://doi.org/10.1016/j.neuron.2010.10.026.
212. Saviane C, Silver RA. Fast vesicle reloading and a large pool sustain high bandwidth transmission at a central synapse. Nature. 2006;439:983–7. https://doi.org/10.1038/nature04509.
213. Valera AM, Doussau F, Poulain B, Barbour B, Isope P. Adaptation of granule cell to Purkinje cell synapses to high-frequency transmission. J Neurosci. 2012;32:3267–80. https://doi.org/10.1523/JNEUROSCI.3175-11.2012.
214. Cesana E, Pietrajtis K, Bidoret C, Isope P, D'Angelo E, Dieudonne S, et al. Granule cell ascending axon excitatory synapses onto Golgi cells implement a potent feedback circuit in the cerebellar granular layer. J Neurosci. 2013;33:12430–46. https://doi.org/10.1523/JNEUROSCI.4897-11.2013.
215. Thier P, Dicke PW, Haas R, Barash S. Encoding of movement time by populations of cerebellar Purkinje cells. Nature. 2000;405:72–6. https://doi.org/10.1038/35011062.
216. Ruigrok TJH, Sillitoe RV, Voogd J. Cerebellum and cerebellar connections. In: Paxinos G, editor. The rat nervous system. Amsterdam: Elsevier; 2015. p. 133–205.
217. Faull RL, Carman JB. The cerebellofugal projections in the brachium conjunctivum of the rat I. The contralateral ascending pathway. J Comp Neurol. 1978;178:495–517.
218. Teune TM, van der Burg J, van der Moer J, Voogd J, Ruigrok TJ. Topography of cerebellar nuclear projections to the brain stem in the rat. Prog Brain Res. 2000;124:141–72.
219. Dum RP, Strick PL. An unfolded map of the cerebellar dentate nucleus and its projections to the cerebral cortex. J Neurophysiol. 2003;89:634–9. https://doi.org/10.1152/jn.00626.2002.
220. Fredette BJ, Mugnaini E. The GABAergic cerebello-olivary projection in the rat. Anat Embryol (Berl). 1991;184:225–43.
221. Teune TM, van der Burg J, Ruigrok TJ. Cerebellar projections to the red nucleus and inferior olive originate from separate populations of neurons in the rat: a non-fluorescent double labeling study. Brain Res. 1995;673:313–9.
222. Bentivoglio M, Kuypers HG. Divergent axon collaterals from rat cerebellar nuclei to diencephalon, mesencephalon, medulla oblongata and cervical cord. A fluorescent double retrograde labeling study. Exp Brain Res. 1982;46:339–56.
223. Ruigrok TJ, Teune TM. Collateralization of cerebellar output to functionally distinct brainstem areas. A retrograde, non-fluorescent tracing study in the rat. Front Syst Neurosci. 2014;8:23. https://doi.org/10.3389/fnsys.2014.00023.
224. Gao Z, Proietti-Onori M, Lin Z, Ten Brinke MM, Boele HJ, Potters JW, et al. Excitatory cerebellar Nucleocortical circuit provides internal amplification during associative conditioning. Neuron. 2016;89:645–57. https://doi.org/10.1016/j.neuron.2016.01.008.
225. Houck BD, Person AL. Cerebellar premotor output neurons collateralize to innervate the cerebellar cortex. J Comp Neurol. 2015;523:2254–71. https://doi.org/10.1002/cne.23787.
226. Tolbert DL, Bantli H, Bloedel JR. The intracerebellar nucleocortical projection in a primate. Exp Brain Res. 1977;30:425–34.
227. Beitzel CS, Houck BD, Lewis SM, Person AL. Rubrocerebellar feedback loop isolates the interposed nucleus as an independent processor of corollary discharge information in mice. J Neurosci. 2017;37:10085–96.
228. Huisman AM, Kuypers HG, Conde F, Keizer K. Collaterals of rubrospinal neurons to the cerebellum in rat. A retrograde fluorescent double labeling study. Brain Res. 1983;264:181–96.
229. Parenti R, Zappala A, Serapide MF, Panto MR, Cicirata F. Projections of the basilar pontine nuclei and nucleus reticularis tegmenti pontis to the cerebellar nuclei of the rat. J Comp Neurol. 2002;452:115–27. https://doi.org/10.1002/cne.10316.
230. Tsukahara N, Bando T, Murakami F, Oda Y. Properties of cerebello-precerebellar reverberating circuits. Brain Res. 1983;274:249–59.
231. De Zeeuw CI, Ruigrok TJ. Olivary projecting neurons in the nucleus of Darkschewitsch in the cat receive excitatory monosynaptic input from the cerebellar nuclei. Brain Res. 1994;653:345–50.
232. Ruigrok TJ, Voogd J. Cerebellar nucleo-olivary projections in the rat: an anterograde tracing study with Phaseolus vulgaris-leucoagglutinin (PHA-L). J Comp Neurol. 1990;298:315–33. https://doi.org/10.1002/cne.902980305.
233. Kros L, Rooda OH, De Zeeuw CI, Hoebeek FE. Controlling cerebellar output to treat refractory epilepsy. Trends Neurosci. 2015;38:787–99.
234. Proville RD, Spolidoro M, Guyon N, Dugue GP, Selimi F, Isope P, et al. Cerebellum involvement in cortical sensorimotor circuits for

the control of voluntary movements. Nat Neurosci. 2014;17:1233–9.
235. Li B, Zhuang QX, Gao HR, Wang JJ, Zhu JN. Medial cerebellar nucleus projects to feeding-related neurons in the ventromedial hypothalamic nucleus in rats. Brain Struct Funct. 2017;222:957–71. https://doi.org/10.1007/s00429-016-1257-2.
236. Van der Steen J, Simpson JI, Tan J. Functional and anatomic organization of three-dimensional eye movements in rabbit cerebellar flocculus. J Neurophysiol. 1994;72:31–46.
237. Graf W, Gerrits N, Yatim-Dhiba N, Ugolini G. Mapping the oculomotor system: the power of transneuronal labelling with rabies virus. Eur J Neurosci. 2002;15:1557–62.
238. Prevosto V, Graf W, Ugolini G. Cerebellar inputs to intraparietal cortex areas LIP and MIP: functional frameworks for adaptive control of eye movements, reaching, and arm/eye/head movement coordination. Cereb Cortex. 2010;20:214–28.
239. Thier P, Dicke PW, Haas R, Thielert CD, Catz N. The role of the oculomotor vermis in the control of saccadic eye movements. Ann N Y Acad Sci. 2002;978:50–62.
240. Sugihara I, Quy PN. Identification of aldolase C compartments in the mouse cerebellar cortex by olivocerebellar labeling. J Comp Neurol. 2007;500:1076–92. https://doi.org/10.1002/cne.21219.
241. Aoki S, Coulon P, Ruigrok TJH. Multizonal cerebellar influence over sensorimotor areas of the rat cerebral cortex. Cereb Cortex. 2017; https://doi.org/10.1093/cercor/bhx343.
242. Strata P, Scelfo B, Sacchetti B. Involvement of cerebellum in emotional behavior. Physiol Res. 2011;60(Suppl 1):S39–48.
243. Strick PL, Dum RP, Fiez JA. Cerebellum and nonmotor function. Annu Rev Neurosci. 2009;32:413–34. https://doi.org/10.1146/annurev.neuro.31.060407.125606.
244. Anand BK, Malhotra CL, Singh B, Dua S. Cerebellar projections to limbic system. J Neurophysiol. 1959;22:451–7.
245. Heath RG, Harper JW. Ascending projections of the cerebellar fastigial nucleus to the hippocampus, amygdala, and other temporal lobe sites: evoked potential and histological studies in monkeys and cats. Exp Neurol. 1974;45:268–87.
246. Middleton FA, Strick PL. Cerebellar projections to the prefrontal cortex of the primate. J Neurosci. 2001;21:700–12.
247. Snider RS, Maiti A. Cerebellar contributions to the Papez circuit. J Neurosci Res. 1976;2:133–46. https://doi.org/10.1002/jnr.490020204.
248. Turner BM, Paradiso S, Marvel CL, Pierson R, Boles Ponto LL, Hichwa RD, et al. The cerebellum and emotional experience. Neuropsychologia. 2007;45:1331–41. https://doi.org/10.1016/j.neuropsychologia.2006.09.023.
249. Schmahmann JD, Sherman JC. The cerebellar cognitive affective syndrome. Brain. 1998;121(Pt 4):561–79.
250. Parvizi J, Anderson SW, Martin CO, Damasio H, Damasio AR. Pathological laughter and crying: a link to the cerebellum. Brain. 2001;124:1708–19.
251. Greve KW, Stanford MS, Sutton C, Foundas AL. Cognitive and emotional sequelae of cerebellar infarct: a case report. Arch Clin Neuropsychol. 1999;14:455–69.
252. Annoni JM, Ptak R, Caldara-Schnetzer AS, Khateb A, Pollermann BZ. Decoupling of autonomic and cognitive emotional reactions after cerebellar stroke. Ann Neurol. 2003;53:654–8. https://doi.org/10.1002/ana.10549.
253. Lange I, Kasanova Z, Goossens L, Leibold N, De Zeeuw CI, van Amelsvoort T, et al. The anatomy of fear learning in the cerebellum: a systematic meta-analysis. Neurosci Biobehav Rev. 2015;59:83–91. https://doi.org/10.1016/j.neubiorev.2015.09.019.
254. Grossauer S, Koeck K, Kau T, Weber J, Vince GH. Behavioral disorders and cognitive impairment associated with cerebellar lesions. J Mol Psychiatry. 2015;3:5. https://doi.org/10.1186/s40303-015-0009-1.
255. Steinlin M, Imfeld S, Zulauf P, Boltshauser E, Lovblad KO, Ridolfi Luthy A, et al. Neuropsychological long-term sequelae after posterior fossa tumour resection during childhood. Brain. 2003;126:1998–2008. https://doi.org/10.1093/brain/awg195.
256. Supple WF Jr, Leaton RN. Lesions of the cerebellar vermis and cerebellar hemispheres: effects on heart rate conditioning in rats. Behav Neurosci. 1990;104:934–47.
257. Supple WF Jr, Kapp BS. The anterior cerebellar vermis: essential involvement in classically conditioned bradycardia in the rabbit. J Neurosci. 1993;13:3705–11.
258. Koutsikou S, Crook JJ, Earl EV, Leith JL, Watson TC, Lumb BM, et al. Neural substrates underlying fear-evoked freezing: the periaqueductal grey-cerebellar link. J Physiol. 2014;592:2197–213. https://doi.org/10.1113/jphysiol.2013.268714.
259. Sacchetti B, Baldi E, Lorenzini CA, Bucherelli C. Cerebellar role in fear-conditioning consolidation. Proc Natl Acad Sci U S A. 2002;99:8406–11. https://doi.org/10.1073/pnas.112660399.
260. Utz A, Thurling M, Ernst TM, Hermann A, Stark R, Wolf OT, et al. Cerebellar vermis contributes to the extinction of conditioned fear. Neurosci Lett. 2015;604:173–7. https://doi.org/10.1016/j.neulet.2015.07.026.
261. Supple WF Jr, Leaton RN, Fanselow MS. Effects of cerebellar vermal lesions on species-specific fear responses, neophobia, and taste-aversion learning in rats. Physiol Behav. 1987;39:579–86.
262. Bradley DJ, Ghelarducci B, Spyer KM. The role of the posterior cerebellar vermis in cardiovascular control. Neurosci Res. 1991;12:45–56.
263. Sacchetti B, Sacco T, Strata P. Reversible inactivation of amygdala and cerebellum but not perirhinal cortex impairs reactivated fear memories. Eur J Neurosci. 2007;25:2875–84. https://doi.org/10.1111/j.1460-9568.2007.05508.x.
264. Supple WF Jr, Cranney J, Leaton RN. Effects of lesions of the cerebellar vermis on VMH lesion-induced hyperdefensiveness, spontaneous mouse killing, and freezing in rats. Physiol Behav. 1988;42:145–53.
265. Voogd JB. F. The inferior olivary nucleus: anatomy and physiology. New York: Raven; 1980.
266. Apps R. Columnar organisation of the inferior olive projection to the posterior lobe of the rat cerebellum. J Comp Neurol. 1990;302:236–54. https://doi.org/10.1002/cne.903020205.
267. Supple WF Jr, Sebastiani L, Kapp BS. Purkinje cell responses in the anterior cerebellar vermis during Pavlovian fear conditioning in the rabbit. Neuroreport. 1993;4:975–8.
268. Sacchetti B, Scelfo B, Tempia F, Strata P. Long-term synaptic changes induced in the cerebellar cortex by fear conditioning. Neuron. 2004;42:973–82. https://doi.org/10.1016/j.neuron.2004.05.012.
269. Takagi M, Zee DS, Tamargo RJ. Effects of lesions of the oculomotor cerebellar vermis on eye movements in primate: smooth pursuit. J Neurophysiol. 2000;83:2047–62.
270. Llinas R, Wolfe JW. Functional linkage between the electrical activity in the vermal cerebellar cortex and saccadic eye movements. Exp Brain Res. 1977;29:1–14.
271. Noda H, Fujikado T. Topography of the oculomotor area of the cerebellar vermis in macaques as determined by microstimulation. J Neurophysiol. 1987;58:359–78.
272. Fujikado T, Noda H. Saccadic eye movements evoked by microstimulation of lobule VII of the cerebellar vermis of macaque monkeys. J Physiol. 1987;394:573–94.
273. Noda H. Cerebellar control of saccadic eye movements: its neural mechanisms and pathways. Jpn J Physiol. 1991;41:351–68.
274. Watson TC, Koutsikou S, Cerminara NL, Flavell CR, Crook JJ, Lumb BM, et al. The olivo-cerebellar system and its relationship to survival circuits. Front Neural Circuits. 2013;7:72. https://doi.org/10.3389/fncir.2013.00072.

275. Bradley DJ, Pascoe JP, Paton JF, Spyer KM. Cardiovascular and respiratory responses evoked from the posterior cerebellar cortex and fastigial nucleus in the cat. J Physiol. 1987;393:107–21.
276. La Noce A, Bradley DJ, Goring MA, Spyer KM. The influence of lobule IX of the cerebellar posterior vermis on the baroreceptor reflex in the decerebrate rabbit. J Auton Nerv Syst. 1991;32:31–6.
277. Ankri L, Husson Z, Pietrajtis K, Proville R, Lena C, Yarom Y, Dieudonne S, Uusisaari MY. A novel inhibitory nucleo-cortical circuit controls cerebellar Golgi cell activity. elife. 2015:4. https://doi.org/10.7554/eLife.06262.
278. Trott JR, Apps R, Armstrong DM. Zonal organization of cortico-nuclear and nucleo-cortical projections of the paramedian lobule of the cat cerebellum. 2. The C2 zone. Exp Brain Res. 1998;118:316–30.
279. Trott JR, Apps R, Armstrong DM. Zonal organization of cortico-nuclear and nucleo-cortical projections of the paramedian lobule of the cat cerebellum. 1. The C1 zone. Exp Brain Res. 1998;118:298–315.

Affiliations

Richard Apps[1] · Richard Hawkes[2] · Sho Aoki[3,4] · Fredrik Bengtsson[5] · Amanda M. Brown[6,7,8] · Gang Chen[9] · Timothy J. Ebner[9] · Philippe Isope[10] · Henrik Jörntell[5] · Elizabeth P. Lackey[6,7,8] · Charlotte Lawrenson[1] · Bridget Lumb[1] · Martijn Schonewille[4] · Roy V. Sillitoe[6,7,8,11] · Ludovic Spaeth[10] · Izumi Sugihara[12] · Antoine Valera[10] · Jan Voogd[4] · Douglas R. Wylie[13] · Tom J. H. Ruigrok[4]

1 School of Physiology, Pharmacology and Neuroscience, University of Bristol, Bristol, UK
2 Hotchkiss Brain Institute, University of Calgary, Calgary, Canada
3 Neurobiology Research Unit, Okinawa Institute of Science and Technology, Onna, Japan
4 Department of Neuroscience, Erasmus MC Rotterdam, Rotterdam, the Netherlands
5 Department of Experimental Medical Sciences, Lund University, Lund, Sweden
6 Department of Pathology & Immunology, Baylor College of Medicine, Houston, TX, USA
7 Department of Neuroscience, Baylor College of Medicine, Houston, TX, USA
8 Jan and Dan Duncan Neurological Research Institute at Texas Children's Hospital, Houston, TX, USA
9 Department of Neuroscience, University of Minnesota, Minneapolis, MN, USA
10 Institut des Neurosciences Cellulaires et Intégratives, CNRS, Université de Strasbourg, Strasbourg, France
11 Program in Developmental Biology, Baylor College of Medicine, Houston, TX, USA
12 Department of Systems Neurophysiology, Graduate School of Medical and Dental Sciences, Tokyo Medical and Dental University, Tokyo, Japan
13 Neuroscience and Mental Health Institute, University of Alberta, Edmonton, AB, Canada

7. Résumé étendu de la thèse en français

Traitement modulaire de l’information dans le cortex cérébelleux

Par Ludovic Spaeth
Sous la direction de Philippe Isope

Résumé étendue de la thèse en français

1. Contexte scientifique

Le cervelet est une structure du système nerveux central, localisé dans l'encéphale et contenant à lui seul près de la moitié de l’ensemble des neurones du système nerveux. Il est impliqué dans la coordination du mouvement, l’apprentissage moteur ainsi que dans le maintien de la posture et de l’équilibre. Pour se faire, il est en dialogue permanent au sein d’un large réseau nerveux qui comprend la moelle épinière, le tronc cérébral, le thalamus et le cortex cérébral.

L’exécution d’un mouvement volontaire requiert la préparation et la planification d’un ordre moteur au sein des structures corticales. C’est un plan d’action qui permettra la coordination spatiale et temporelle des différents effecteurs nécessaires au mouvement. Cette commande motrice est ensuite envoyée à d’autres structures cérébrales et spinales pour au final conduire à l’accomplissement du mouvement par les muscles. Le cervelet reçoit une copie de cette commande, aussi appelée copie efférente, et va alors agir comme un comparateur : il va confronter l’ordre moteur à une prédiction du retour sensoriel attendu suite à l'exécution du mouvement et ajuster la commande si nécessaire (par exemple, en cas d’imprévu environnemental).

Des études cliniques et fondamentales ont mis en évidence que le cervelet était organisé selon une règle modulaire : les neurones du cervelet sont connectés entre eux sous forme de modules anatomo-fonctionnels. Chacun de ces modules reçoit certains types d’informations, et va en retour contrôler certains éléments moteurs (par exemple, un muscle ou un groupe de muscle). Chez l’Homme comme chez l’animal, des lésions focales du cervelet conduisent des troubles moteurs localisés, par exemple au niveau d’un bras seulement.

Le cervelet est divisé en deux structures majeurs : le cortex cérébelleux et les noyaux cérébelleux profonds. Le cortex cérébelleux est divisé en trois parties selon l'axe médio latéral : le vermis, le para vermis et les hémisphères cérébelleux. Ces deux structures reçoivent une multitudes d'information sensorimotrices provenant de l'ensemble du corps, mais aussi du reste de l'encéphale, et agissent de concert pour permettre l'exécution d'un mouvement fluide et efficace. Le cortex cérébelleux reçoit deux types d'entrées excitatrices glutamatergiques : les fibres grimpantes et les fibres moussues.

Les fibres grimpantes sont issues de l'olive inférieure (aussi appelée olive bulbaire), localisée dans la partie ventrale du bulbe rachidien, et portent au cervelet des informations somato-sensorielles intégrées qui proviennent du reste de l'encéphale. Les fibres grimpantes sont organisées de manière topographique : un groupe localisé de neurones de l'olive inférieure projette sur un groupe bien précis de cellules de Purkinje, neurones inhibiteurs et unique voie de sortie du cortex cérébelleux. Ce même groupe de cellules de Purkinje projette à son tour sur des sous-populations de neurones des noyaux cérébelleux profonds, qui vont envoyer des collatérales sur les neurones originaux localisés dans l'olive inférieure. Cette boucle olivo-cortico-nucléaire est à la base de l'organisation modulaire du cervelet : les modules cérébelleux regroupent ainsi une partie de l'olive inférieure, une partie du cortex cérébelleux et une partie des noyaux cérébelleux profonds. Chacun de ces modules, agencés en parallèles selon l'axe parasagittal, sont responsables du traitement de l'information d'une région du corps. De plus, les frontières de la partie corticale des modules, aussi appelée microzone, sont identifiables grâce à l'expression de certains marqueurs par cellules de Purkinje. Ces neurones expriment des protéines issues de la famille des Zébrines de manière différentielles, entraînant l'alternance de bandes parasagittales tantôt positives et tantôt négatives. Ces bandes Zébrines coïncident avec les frontières des microzones dans le cortex cérébelleux, et permettent ainsi l'identification des modules cérébelleux.

Les fibres moussues sont la deuxième entrée excitatrice majoritaire au cervelet. Elles proviennent de la moelle épinière ainsi que de divers noyaux bulbaires et pontiques (appelés noyaux pré-cérébelleux). Elles portent au cervelet des informations sensorimotrices relatives à l'état de l'organisme (par exemple, la tension des muscles, la position des articulations ou encore les stimuli cutanés). Ces fibres projettent de manière redondante au cervelet : une seule fibre moussue envoie plusieurs collatérales dans différentes régions du cortex cérébelleux ainsi que des collatérales dans les noyaux cérébelleux profonds. Elles réalisent des synapses sur les cellules granulaires, interneurones excitateurs majoritaire du cortex cérébelleux. Les cellules granulaires relaient l'information sensorimotrices dans le cortex cérébelleux via les fibres parallèles : des axones en forme de T qui cheminent selon l'axe

transversal et qui réalisent des synapses *en passant* sur plusieurs centaines de cellules de Purkinje.

Les fibres parallèles contredisent le traitement en parallèle de l'information révélé par l'organisation des modules parasagittaux : l'information sensori-motrice provenant des fibres moussues peut être ainsi envoyé à plusieurs modules parallèles. Une étude préalable issue du laboratoire a montré pour la première fois que les cellules de Purkinje d'une même microzone peuvent être subdivisées en microzones fonctionnelles : des groupes de cellules de Purkinje adjacentes reçoivent des entrées synaptiques fonctionnelles qui proviennent des mêmes groupes de cellules en grains. Ces entrées granulaires sont issues de la même microzone mais également de microzones voisines, mettant en lumière une communication inter-modulaire dans le vermis antérieur du cortex cérébelleux. En outre, l'organisation spatiale de ces entrées est conservée d'un individu à l'autre : parmi les millions de possibilités de connections fonctionnelles, les cellules de Purkinje des lobules III et IV du vermis sélectionnent certaines cellules en grain de manière préférentielle, très probablement au travers de mécanismes de plasticités à long terme qui sont là résultante de l'apprentissage moteur au sein des micro réseaux du cervelet.

2. Objectifs du projet de thèse

Les modules de la partie vermale des lobules III et IV du cortex cérébelleux reçoivent des entrées sensorielles issues des muscles proximaux et distaux. En retour, ils projettent sur plusieurs muscles localisés dans les membres inférieurs, et sont donc impliqués dans la coordination de la locomotion. Les données issues du laboratoire rapportées au contexte scientifique décrit plus haut permettent d'établir l'hypothèse suivante : la coordination des différents muscles nécessaires à l'exécution d'un mouvement nécessite la coordination des modules cérébelleux qui contrôlent ces muscles. Selon cette hypothèse, les cartes synaptiques de connexion entre les cellules en grain et les cellules de Purkinje dans le vermis antérieur sont stéréotypées en raison du caractère stéréotypé de la locomotion chez la souris : différents individus évoluant dans le même environnement adoptent des stratégies similaires pour développer une locomotion efficace.
Mon projet vise donc à étudier les règles synaptiques de la mise en place de la communication inter-modulaire dans les lobules III et IV du cortex cérébelleux, au travers de la réponse à deux questions :

(1) Comment la communication inter-modulaire se met elle en place au cours du développement postnatal chez la souris ?

(2) Est-il possible de corréler les cartes synaptiques fonctionnelles des cellules en grains vers les cellules de Purkinje avec l'adaptation d'un comportement moteur tel que la locomotion ?

Pour répondre à ces questions, les cartes synaptiques de connections cellules en grain-cellules de Purkinje ont été établies à l'aide d'enregistrement électrophysiologiques couplées à la photostimulation de glutamate "*cagé*" dans des tranches aigües de cervelet de souris.
Pour répondre à la question (1), ces tranches ont été réalisées à l'aide de souris âgées de 9 à 40 jours. Pour répondre à la question (2), des modèles murins d'enrichissement ou de perturbation de la locomotion ont été utilisés pour réaliser les tranches.

3. Résultats

3.1. La communication inter-modulaire se met en place progressivement au cours du développement postnatal

En accord avec les données précédentes issues du laboratoire, nous avons ciblé un groupe de cellules de Purkinje localisées au niveau de la ligne médiane dans les lobules III et IV du vermis antérieur (cluster 1). Les entrées granulaires qui convergent vers ces cellules de Purkinje sont conservées entre les individus adultes. Des enregistrements en patch clamp des cellules du cluster 1 couplés au *décageage* de glutamate ont révélé une mise en place progressive des entrées granulaires au cours du développement postnatal.
A 9 jours, seules les entrées dites locales sont présentes : les connexions fonctionnelles sont issues de cellules granulaires localisées au sein de la même microzone que les cellules de Purkinje enregistrées. A partir de 12 jours, des entrées fonctionnelles excitatrices distantes se mettent en place : elles proviennent de cellules en grain qui appartiennent à des micro zones adjacentes, préférentiellement localisées du même côté de la ligne médiane. Ces connexions s'étendent ensuite du côté controlatéral au fur et mesure de la croissance des animaux, rassemblant de plus en plus de cellules granulaires jusqu'à obtenir le patron connexion adulte entre 30 et 40 jours.

Une analyse de variance a montré que les cartes enregistrées chez les souris adolescentes (entre 14 et 18 jours) sont plus variables que les cartes obtenues à l'état adulte, suggérant l'action de mécanismes développementaux ou fonctionnels spécifiques à cette période d'âge. Dès lors, nous postulons qu'il s'agit d'une période critique quant à l'établissement de cartes synaptiques fonctionnelles pérennes dans le cortex cérébelleux.

3.2 Vers la causalité entre l'adaptation locomotrice et la connectivité fonctionnelle dans le cortex cérébelleux

La stéréotypie interindividuelle des entrées granulaires fonctionnelles vers les cellules de Purkinje du vermis antérieur peut être expliquée par (1) un câblage génétique déterministe ou (2) un arrangement adaptatif fonctionnels. Une étude antérieure du laboratoire réalisée *in vitro* suggère une piste fonctionnelle, dès lors nous avons tenté d'en déterminer le corrélat physiologique en établissant des cartes synaptiques entre les cellules en grains et les cellules de Purkinje dans 2 modèles d'adaptation locomotrice.

Le premier modèle, appelée *cuff,* consiste à comprimer la branche principale du nerf sciatique via une approche chirurgicale. Ce procédé entraîne une altération de la balance droite/gauche sévère chez les souris cuff et plus modérée chez les souris témoins. Les cartes synaptiques réalisée avant l'apparition de l'effet maximal de la perturbation locomotrice montrent une altération significative du poids, du nombre et de la distribution des connexions synaptiques fonctionnelles entre les cellules en grain et les cellules de Purkinje du cluster 1 chez les souris cuff et témoin. Dans les deux cas, la perturbation locomotrice est transitoire : les souris récupèrent une balance fonctionnelle environ 3 semaines après la chirurgie. Les cartes synaptiques enregistrées chez les souris témoins après récupération sont comparables à celles obtenues chez les souris contrôles (qui n'ont pas subi de perturbation), contrairement aux souris cuff chez qui les cartes synaptiques apparaissent modifiées en comparaison des cartes obtenues chez des souris naïves.

Le second modèle, dit enrichi, consistait à permettre la pleine expression et le développement du comportement locomoteur des souris. Les souris enrichies ont eu accès à une roue d'entraînement au travers de sessions quotidiennes pendant 20 jours avant l'établissement des cartes synaptiques. Les souris s'adaptent très rapidement à la roue, quadruplant en moyenne leur activité locomotrice au terme de la période d'entraînement. L'apprentissage moteur conduit à une réorganisation des cartes synaptiques fonctionnelles dans le cortex cérébelleux, ce qui suggère que les cellules de Purkinje du cluster 1 sont sensible à la modification des entrées sensori-motrices liées au développement de l'activité locomotrice.

L’analyse de la variance inter individuelle a montré que les cartes synaptiques étaient moins homogènes dans la conditions cuff quand dans les autres conditions. Une analyse en composante principale a permis d’extraire les données de moindre variance : les entrées synaptiques issues de micro zone distantes. Ces micro zones ont été comparée 2 à 2 dans chaque condition, et ont permis de déterminer des patrons d’association caractéristiques de chaque condition expérimentale. En d’autres mots, la communication inter modulaire dans le cortex cérébelleux suit des règles dynamiques qui dépendent de comportement moteur considéré.

L’utilisation des deux modèles montrent un lien causal entre l’adaptation motrice et l’arrangement synaptique fonctionnel dans le cortex cérébelleux.

3.3 Dissociation spatiale et temporelle des entrées excitatrices et inhibitrices

Les cellules de Purkinje reçoivent l’information nerveuse selon deux modalités : (1) l’information excitatrice provenant d’une connexion monosynaptique avec les cellules en grains et (2) l’information inhibitrice via les interneurones de la couche moléculaire. La littérature décrit l’inhibition antérograde : les cellules de Purkinje reçoivent l’information via une séquence d’entrées excitatrices puis inhibitrices séparées par un cours délai et originaire des mêmes cellules en grain. Des cartographies de connexions granulaires vers les cellules de Purkinje ont révélé que les cellules en grain peuvent envoyer l’information de manière dissociée : certaines sont purement inhibitrices, d’autres purement excitatrices. Dans nos données, le cas de l’inhibition antérograde s’avère être minoritaire.
Ces données de cartographie fonctionnelles ont été appuyées par dès la stimulation optogénétiques des fibres moussues, qui représenta la voie naturelle d’activation des cellules en grain. L’étude de la latence des entrées excitatrices et inhibitrices a révélé que les séquences d’excitation-inhibitions suivaient plusieurs règles. Nous avons ainsi pu observer des cas d’inhibition antérograde, ainsi que des cas où l’inhibition est intégrée dans un délai plus long, ou même avant l’excitation. Un dernier cas a révélé la présence d’entrée inhibitrice fonctionnelles uniquement. Ces résultats sont à la fois confirmés et sous tendus par la dissociation spatiale des entrées observées plus haut.

4. Conclusion

Les résultats issus des deux modèles mettent en évidence, et pour la première fois, un lien de causalité direct entre l'adaptation d'un comportement moteur et l'organisation synaptique fonctionnelle des micro réseaux du cervelet. Ils apportent de nouveaux outils de réflexions quant au traitement de l'information sensori-motrice dans le cervelet.

La communication inter-modulaire semble être régie par des lois dynamiques qui associent certaines micro zones corticales en fonction de l'apprentissage moteur. L'identification des microzones impliquées dans l'adaptation de tel ou tel comportement moteur est une première étape d'une stratégie qui pourrait aider à la mise en place de protocoles de stimulations compensatoires dans les cas de troubles moteurs.

Université de Strasbourg

Ludovic SPAETH

Traitement modulaire de l'information dans le cortex cérébelleux

École Doctorale des Sciences de la Vie et de la Santé STRASBOURG

Résumé

Le cervelet est indispensable à la coordination motrice ainsi qu'au maintien de la posture. Le traitement de l'information dans le cortex cérébelleux repose sur une organisation modulaire : chaque module est impliqué dans le contrôle de muscles spécifiques. Des lésions focales du cervelet entrainent des troubles moteurs dans une région précise du corps, conduisant à des pathologies telles que l'ataxie. Ce travail vise à comprendre comment les modules cérébelleux traitent l'information sensorimotrice, communiquent entre eux et leur implication dans la coordination motrice chez la souris. Des approches optiques et électrophysiologiques ont permis d'établir les cartes de connexions synaptiques entre différents modules. L'étude du développement de ces cartes a démontré que la mise en place des synapses entre des modules distants coïncide avec l'émergence de la locomotion. L'emploi de modèles de perturbation de la locomotion a démontré que les cartes synaptiques sont réorganisées suite à l'adaptation de la coordination motrice. Ce projet apporte de nouvelles hypothèses quant au contrôle de la coordination motrice en conditions normales et pathologiques.

Mots-clés : cervelet, cellule de Purkinje, cellule granulaire, carte synaptique, glutamate-cagé

Résumé en anglais

The cerebellum is essential for motor coordination and to learn new motor skills. In the cerebellar cortex, information processing is based on a modular organization: each module is involved in the control of specific motor units. Localized lesions of the cerebellum impair coordinated movements in only one part of the body and lead to movement disorders like ataxia. This project aims to understand how cerebellar modules communicate, process incoming information and how they relate to coordinated movements in mice. We combine optical and electrophysiological approaches in vitro in order to determine the functional synaptic maps between different modules. The development of these maps revealed that the establishment of connections between distant modules coincide with the appearance of motor coordination in mice. Using models of motor alteration, we showed that synaptic maps are reorganized following motor adaptation. The results bring new hypotheses about the control of motor coordination in normal and pathological conditions. Future directions will be to assess how a specific activation of identified modules may compensate for motor impairments.

Keywords: cerebellum, Purkinje cell, granule cell, synaptic map, glutamate uncaging